

Proceedings of the 3rd JTC1 Workshop

Impact of global changes on landslides hazard and risk

7-10 June 2023 at Deichman Bjørvika, Oslo, Norway

Organized by: Norwegian Geotechnical Institute (NGI)

Edited by: Vittoria Capobianco, Laura Rødvand,
Farrokh Nadim, Håkon Heyerdahl, Suzanne
Lacasse

Jointly organised by:

Joint Technical Committee on Natural Slopes and Landslides (JTC1) of FedIGS: Federation of international Geo-Engineering Societies, composed of ISSMGE: International Society for Soil Mechanics and Geotechnical Engineering; ISRM: International Society for Rock Mechanics and Rock Engineering; IAEG: International Association for Engineering Geology and the Environment; IGS: International Geosynthetics Society.

Foreword

The third workshop of the Joint Technical Committee 1 on Natural Slopes and Landslides this year addressed topics related to anthropogenic and climate change impacts on landslide hazard and risk.

The workshop consisted in two lecture days and one/day technical excursion, held in Oslo, Norway.

The third Hutchinson lecture was addressed by Professor Clarence E. Choi (The Hong Kong University) on “Engineered and nature-based solutions against flow-type landslide hazards”.

A diverse and international group of top-level scientists presented **five keynote lectures** on topics related to landslide hazard and risk, covering tools and methods for the assessment of rock and geomorphological instabilities, quantitative assessment of landslide risk and interdisciplinary risk reduction strategies, and how plants and their related chemical processes influence soil properties.

Five themed sessions started with an invited lecture. The advanced topics in focus for the discussions included:

- Impact of Climate-driven perils and climate change on landslide hazard;
- Numerical modelling of landslides; Landslide hazard and risk - Assessment and mitigation;
- Landslide mobility;
- Runout and impact forces;
- Monitoring and early warning systems for landslides.

The poster session was focused on topics including:

- Rock mass degradation and landslide initiation;
- Climate and anthropogenic impacts on landslide risk in different geographic regions, including the Arctic;
- Prediction of landslide mobility and inundation; application of modern remote sensing technologies to landslide risk assessment;
- Landslide risk reduction strategies: risk mitigation including early warning and nature-based solutions.

A fruitful panel discussion at the end of the first technical day orbited around effective landslide risk management under rapid climate change, demographic change and changing societal priorities, highlighting the need for the landslide community to move towards more sustainable landslide risk mitigation strategies that are holistic and system-oriented.

This electronic book includes all the Extended and Short Abstracts accepted for Oral and Poster presentation at the Workshop.

Organisation

Chair

Dr Vittoria Capobianco, NGI Dr Laura Rødvang, NGI

Host

Dr Dominik Lang, Director Natural Hazards, Norwegian Geotechnical Institute (NGI), Oslo, Norway

Organising Committee

Kirsten Helness Haaland, NGI (secretariat)
Maren Kristine Johnsen, NGI (media and communication)
Håkon Heyerdahl, NGI (Excursion Day)
Amanda J. DiBiagio, NGI (website)

Scientific Committee

Chair: Dr Farrokh Nadim, NGI

Dr Amy Oen, NGI
Prof. Dr. Ana Priscilla Paniagua-Lopez, NTNU
Dr Jean-Sébastien L'Heureux, NGI
Dr Zhongqiang Liu, NGI
Dr Rajinder Bhasin, NGI
Dr Luca Piciullo, NGI
Prof Anthony Leung, HKUST

Norwegian Steering Committee

Dr Lars Harald Blikra (Norwegian Water Resources & Energy Directorate, NVE)
Professor Vikas Thakur (NTNU)
Professor Louise Mary Vick (University of Tromsø, UiT)
Professor Reginald L. Hermanns (Norwegian Geological Survey, NGU)
Professor Jens Jahren (University of Oslo, UiO)
Professor Gijs Breedveld (The University Centre in Svalbard, UNIS)
Dr Suzanne Lacasse (Norwegian Geotechnical Institute, NGI)

International Advisory Board

Chair JTCI: Prof. Luciano Picarelli ; Prof. Gonghui Wang (from March 2023)

Vice-Chair: Prof. Giovanni Crosta, Università Milano Bicocca, Italy (ISRM)
Vice-Chair: Dr Eric Leroi, Risques & Développement, France (IAEG)
Vice-chair: Prof. Eduardo Alonso, UPC, Spain (ISSMGE)
Vice-chair: Dr Suzanne Lacasse (NGI)
Vice-chair: Prof. Véronique Merrien, France (CNAM) – Chair ISL 2024

Members:

Dr Raymond Cheung, Dr J. A. Coe, Prof. C. Di Maio, Prof. J. Montero, Prof. A. Take, Prof. Ariane Locat, Prof. Alessandro Tarantino, Prof. Enrique Romero, Prof. M.M. Futai, Dr Chris Massey, Dr Matthew Lato.

Program

Opening – Day 1 – 7th June (Deichman library, 5th floor)	
18:00-20:00	<i>Icebreaker</i>
from 18:00	Registration

Day 2 – 8th June (Deichman library, sous-terrain)			
08:00-09:15	Registration and morning coffee		
09:15-09:45	<table border="1"> <tr> <td>Welcome addresses</td> <td> <p>Dr Lars Andresen <i>Managing Director of NGI</i></p> <p>Prof. Gonghui Wang (video) <i>Chair of the JTC1</i></p> <p>Drs Vittoria Capobianco and Laura Rødvand <i>Organizing committee JTC1 workshop Oslo</i></p> </td> </tr> </table>	Welcome addresses	<p>Dr Lars Andresen <i>Managing Director of NGI</i></p> <p>Prof. Gonghui Wang (video) <i>Chair of the JTC1</i></p> <p>Drs Vittoria Capobianco and Laura Rødvand <i>Organizing committee JTC1 workshop Oslo</i></p>
Welcome addresses	<p>Dr Lars Andresen <i>Managing Director of NGI</i></p> <p>Prof. Gonghui Wang (video) <i>Chair of the JTC1</i></p> <p>Drs Vittoria Capobianco and Laura Rødvand <i>Organizing committee JTC1 workshop Oslo</i></p>		
Session 1			
Keynote session			
Moderator: Prof. Caterina di Maio (University of Basilicata)			
9:45-10:15	<table border="1"> <tr> <td>Keynote address: "Applications of remote sensing techniques to rock slope stability and risk assessment – Building a toolbox of complementary methods"</td> <td>Prof. Jean Hutchinson <i>Queen's University, Canada</i></td> </tr> </table>	Keynote address: "Applications of remote sensing techniques to rock slope stability and risk assessment – Building a toolbox of complementary methods"	Prof. Jean Hutchinson <i>Queen's University, Canada</i>
Keynote address: "Applications of remote sensing techniques to rock slope stability and risk assessment – Building a toolbox of complementary methods"	Prof. Jean Hutchinson <i>Queen's University, Canada</i>		
10:15-10:45	<table border="1"> <tr> <td>Keynote address: "Recent evolution of geomorphological instabilities in the alpine area"</td> <td>Prof. Giovanni Crosta <i>University of Milano-Bicocca, Italy</i></td> </tr> </table>	Keynote address: "Recent evolution of geomorphological instabilities in the alpine area"	Prof. Giovanni Crosta <i>University of Milano-Bicocca, Italy</i>
Keynote address: "Recent evolution of geomorphological instabilities in the alpine area"	Prof. Giovanni Crosta <i>University of Milano-Bicocca, Italy</i>		
10:45-11:15	<i>Coffee break</i>		

Session 2			
Impact of climate-driven perils and climate change on landslide hazard			
Moderator: Dr Vittoria Capobianco (NGI)			
11:20-11:40	<table border="1"> <tr> <td>Invited lecture: "Method and case studies on quantifying changes in landslide hazard as a consequence of climate change in Canada"</td> <td>Prof. Renato Macciotta Pulisci <i>University of Alberta, Canada</i></td> </tr> </table>	Invited lecture: "Method and case studies on quantifying changes in landslide hazard as a consequence of climate change in Canada"	Prof. Renato Macciotta Pulisci <i>University of Alberta, Canada</i>
Invited lecture: "Method and case studies on quantifying changes in landslide hazard as a consequence of climate change in Canada"	Prof. Renato Macciotta Pulisci <i>University of Alberta, Canada</i>		
11:40-12:25	Oral presentations (see detailed program)		
12:25-12:30	Introduction to ISL2024		
12:30-13:25	<i>Lunch</i>		
13:30-14:00	<table border="1"> <tr> <td>Keynote address: "Make soil while the sun shines - how plants influence soil cohesion"</td> <td>Dr Alexia Stokes <i>INRAE, France</i></td> </tr> </table>	Keynote address: "Make soil while the sun shines - how plants influence soil cohesion"	Dr Alexia Stokes <i>INRAE, France</i>
Keynote address: "Make soil while the sun shines - how plants influence soil cohesion"	Dr Alexia Stokes <i>INRAE, France</i>		

Session 3			
Numerical modelling of landslides			
Moderator: Dr Jelke Dijkstra (Chalmers University)			
14:00-14:20	<table border="1"> <tr> <td>Invited lecture: "Potential for remobilization of debris fans"</td> <td>Prof. Thomas Marcher <i>Graz University of Technology, Austria</i></td> </tr> </table>	Invited lecture: "Potential for remobilization of debris fans"	Prof. Thomas Marcher <i>Graz University of Technology, Austria</i>
Invited lecture: "Potential for remobilization of debris fans"	Prof. Thomas Marcher <i>Graz University of Technology, Austria</i>		
14:20-15:20	Oral presentations (see detailed program)		
15:20-15:50	<i>Coffee break</i>		
15:50-17:00	<table border="1"> <tr> <td>Panel discussion</td> <td>Moderator: Dr Farrokh Nadim (NGI)</td> </tr> </table>	Panel discussion	Moderator: Dr Farrokh Nadim (NGI)
Panel discussion	Moderator: Dr Farrokh Nadim (NGI)		

Day 3 – 9th June (Deichman library, sous-terrain)	
Session 4	
Keynote session	
Moderator: Dr Suzanne Lacasse (NGI)	
08:00-08:30	Morning coffee

08:30-09:00	Hutchinson lecture: "Engineered and nature-based solutions against flow-type landslide hazards"	Prof. Clarence Choi <i>University of Hong Kong, Hong Kong</i>
09:00-09:30	Keynote address: "Interdisciplinary investigation of landslides: a path to risk reduction"	Prof. Joseph Wartman <i>University of Washington, USA</i>
09:30-09:55	<i>Coffee break</i>	
09:55-11:00	Poster session (see detailed program)	

Session 5 Landslide hazard and risk - Assessment and mitigation Moderator: Michael Porter (BGC)		
11:00-11:20	Invited lecture: "Diagnosis of the landslide mechanism for the assessment of slow-moving landslide hazard and the risk mitigation design"	Prof. Federica Cotecchia <i>Politecnico di Bari, Italy</i>
11:20-12:30	Oral presentations (see detailed program)	
12:30-13:30	<i>Lunch</i>	
13:30-14:00	Keynote address: "Towards a quantitative assessment of landslide risk: challenges and perspectives"	Dr Zhongqiang Liu <i>NGI, Norway</i>

Session 6 Landslide mobility, runout and impact forces Moderator: Dr Laura Rødvand (NGI)		
14:00-14:20	Invited lecture: "Some remarks and issues linked to the landslide runout distance assessment"	Prof. Michel Jaboyedoff <i>University of Lausanne, Switzerland</i>
14:20-15:00	Oral presentations (see detailed program)	
15:00-15:35	<i>Coffee break</i>	

Session 7 Monitoring and early warning systems for landslides Moderator: Dr Lars Harald Blikra (NVE)		
15:40-16:00	Invited lecture: "IoT-based slope stability analysis as local landslide early warning"	Dr Luca Piciullo <i>NGI, Norway</i>
16:00-16:50	Oral presentations (see detailed program)	
19:00	<i>Gala dinner (Havsmak restaurant, Oslo Opera House) Dress code: cocktail attire</i>	

Day 4 – 10th June, Case study NGI office (Sandakerveien 140)		
08:30-09:30	JTC1 Committee meeting Hybrid - Meeting Room <i>Peck (2nd floor)</i> and Teams	Prof. Gonghui Wang
10:00-11:15	Gjerdrum quick clay landslide: emergency and evacuation Gjerdrum Landslide Investigation	Laura Rødvand, <i>NGI, Norway</i> Luca Agrini, <i>NGI, Norway</i> Bjørn Kalsnes, <i>NGI, Norway</i> Odd Arne Fauskerud, <i>Multiconsult, Norway</i> Inger-Lise Solberg, <i>Landslide Commission and Geological Survey of Norway (NGU), Norway</i>
11:15-11:45	<i>Coffee break</i>	
11:45-13:45	Commission work and remediation measures	Håkon Heyerdahl, <i>NGI, Norway</i> Toril Hofshagen, <i>NVE, Norway</i>
	Visit NGI's soil/rock laboratory and getting acquainted with quick clay.	Pasquale Carotenuto, <i>NGI, Norway</i>
13:45-14:45	<i>Lunch</i>	

Contents

Foreword	2
Organisation	3
Program	4
Hutchinson Lecture	
Prof. Clarence E. Choi	11
Keynote Lectures	
Prof. Jean Hutchinson	12
Prof. Giovanni Crosta	14
Prof. Joseph Wartman	15
Dr Alexia Stokes	16
Dr Zhongquiang Liu	17
Invited Lectures	
Prof. Renato Macciotta Pulisci	18
Prof. Thomas Marcher	19
Prof. Federica Cotecchia	20
Prof. Michel Jaboyedoff	21
Dr Luca Piciullo	22
Extended abstracts	
When Soil Heterogeneity Helps the Geotechnical Design: the Case of Drainage Trenches	23
<i>L. Comegna, M. Pirone, L. Picarelli and G. Urciuoli</i>	
The Effect Of Wildfire Wooden Ember Cover On Hydrological Behaviour And Stability Of Silty Volcanic Slopes	27
<i>L. Coppola, A. Reder, G. Rianna, A. Tarantino and L. Pagano</i>	
Alaska's Unstable Slopes: A Look at Three Examples of Increasing Instability with a Warming Climate	31
<i>M.M. Darrow, D.M. Capps and R.P. Daanen</i>	
In Situ and Satellite Monitoring of a Landslide and of a Drainage System	35
<i>J. De Rosa, C. Di Maio, R. Vassallo, G. Cutrera, R. Murtas, G.V. Pandiscia, F. Trillo and B. Lacovara</i>	
Including the Impact of Climate Change in Quantitative Risk Analysis: an Example From Kaikōura, New Zealand	39
<i>S. de Vilder, C. Massey, M.A. Brideau, B. Lukovic, R. Morgenstern, D. Townsend and B. Rosser</i>	

Time-dependent Shallow Landslide Hazard Mapping Using an Event-based Machine Learning Approach	43
<i>A-K. Edrich, A. Yildiz, R. Roscher and J. Kowalski</i>	
Probabilistic Analysis of the Performance of a Road Network Affected by Slow-Moving Landslides	47
<i>S. Ferlisi, A. Marchese, D. Peduto and P. Gehl</i>	
Effects of Soil Burn Temperature and Organic Content on Post-wildfire Debris Flow Mobility	51
<i>F. Gao and C. E. Choi</i>	
Towards a Generic Methodology to Assess Instabilities and Retreat Rate in Flysch seacliffs	55
<i>L. Guillen, Y. Thiery, T. Dewez, C. Levy, P. Bourbon, S. Caritg, P. Razin, L. Martins, C. Garnier, A. Cuccurullo and D. Gallipoli</i>	
A Massive Rockslide and Debris Flow Linked to Climate Change	59
<i>M. Gutierrez</i>	
Negative Poisson's Ratio Auxetic Structures to Arrest Geophysical Granular Flows: Experimental Insights	63
<i>T. Han, J. Zhang and C.E. Choi</i>	
Rainfall-induced Landslides and Subsequent Debris Flows in Regional-scale Areas	68
<i>S. Jeong and M. Hong</i>	
Earthquake Loading on Submarine Slopes Preconditioned by Marine Gas: Estimating the Triggering Potential Based on Stability analyses	71
<i>P. Kaminski and J. Grabe</i>	
Water Input Changes in the Kulcs Landslide Area	75
<i>C. Király, G. Varga, D. Cseresznyés, G. Jakab, T. Földes, N. Magyar and Z. Szalai</i>	
Risk Before Failure for the Alta and Gjerdrum Landslides in Norway	80
<i>J-S. L'Heureux, S. Lacasse and Z. Liu</i>	
Calibration of Coupled Finite Element Analyses for Early Warning System: the Case of an Unsaturated Slope in Norway	84
<i>V. Mangraviti, V. Capobianco, L. Piciullo and J. Dijkstra</i>	
An Efficient Reliability-Based Design Approach to Reduce Rockfall Risk Below a Target Threshold	88
<i>M. Marchelli and V. De Biagi</i>	
Role of Positive Temperature Variations on Rock Slopes Outcrops (a review)	92
<i>V. Merrien-Soukatchoff and M. Gasc-Barbier</i>	

Runout of Landslides in Quick Clays <i>M. Metral, A. Ferrari, H. Heyerdahl, Z. Liu</i>	97
Combining Distributed Fibre Optic Sensing With Passive Seismic Interferometry for Advanced Monitoring Applications <i>S. Ouellet, J. Dettmer, M. Karrenbach, G. Olivier and M. Lato</i>	101
Predicting Annual Displacement Probability of Slow-Moving Landslides through Markov Chain and Monte Carlo Simulation <i>M. Porter</i>	105
A Simplified Procedure to Assess the Potential Effects of Climate Change on the Mobility of a Slow Active Earthflow in Southern Italy <i>G. Rianna, A. Reder, L. Comegna, G. Urciuoli and L. Picarelli</i>	109
Adaptation to Climate Changes: a Necessary Step Towards the Improvement of Landslide Prediction Models <i>E. Šegina, M.J. Aufferl and T. Peternel</i>	113
Advantages and Challenges of Advanced Slope Stability Analyses <i>C. Sellin, M. Karlsson and M. Karstunen</i>	117
A Pilot Study in the Napf-Region (Central Switzerland) for an Upcoming National Landslide Early Warning System <i>M. Stähli, T. Halter, F. Walter, A. Wicki and P. Lehman</i>	121
Advanced Numerical Model for Landslides: from Quick Clay to Submarine Landslides <i>Q.A. Tran</i>	125
Enhanced Discontinuity Set Extractor (eDSE): An AI Tool for Classifying and Characterising Rock Discontinuities and Rock Masses from 3D Point Cloud Datasets <i>D.H.Y. Wong, S. Millis and W.K. Leung</i>	129
InSARTrac as a Novel Tool for Landslide Monitoring and Failure Mechanism Assessment <i>C. Zambanini and D.S. Kieffe</i>	134
Short abstracts	
Active Layer Detachment Slides, Kluane Ranges, Southwest Yukon <i>C.M. Ackerson, B. Ward and K. Kennedy</i>	137
What Causes Creep Bursts in the Åknes Landslide, Norway <i>A. Aspaas, P. Lacroix, L. Kristensen, B. Etzelmüller and F. Renard</i>	138
Degradation of Hard Clays under Freezing and Thawing Cycles <i>K. Bočková, J. Vaunat and J. Moya</i>	139

Selection of Appropriate Landslide Mitigation Measures – LaRiMiT (Landslide Risk Mitigation Toolbox)	140
<i>V. Capobianco, B. Kalsnes and E.B. Storrrøsten</i>	
Full-Scale Slope Monitoring and Back-Analysis of a Weather-Induced Landslide With and Without the Effect of Vegetation: Preliminary Insights	141
<i>S.E. Donvito, V. Capobianco, Y. Shin, L. Piciullo and V. Tagarelli</i>	
Mechanism of Deep Groundwater Inflow into Landslide Mass based Ground Temperature Monitoring in the Metamorphic Area, Japan	142
<i>G. Furuya, D. Habashita, K. Nawa, A. Suemine and G. Wang</i>	
Preliminary Stages of a Landslide-Generated Tsunami Hazard Assessment of Glacier Bay National Park and Preserve, Alaska USA	143
<i>C. Hults, J. Coe, N. Avdievitch, J.W. Kim, Z. Lu and D. Staley</i>	
A Rock Glacier Inventory of the Central Alaska Range, Alaska	144
<i>K. Kelkar, L. Farquharson, M. Darrow, D. Mann, S. Zwieback and D. Capps</i>	
Numerical Modelling of the Initiation of progressive failure in Eastern Canadian sensitive clay	145
<i>A. Kirstein, A. Locat, G. Grimstad and H.P. Jostad</i>	
Seasonal and Climatic Controls on Unstable Rockslopes in Norway	146
<i>L. Kristensen, I. Skrede, K. Indrevær, I. Penna, A. Aspaas and G. Pless</i>	
Study on the Potential of Nature Based Solutions for the Protection of a Rockfall Site at Artouste (French Pyrenees)	147
<i>C. Lévy, C. Bastien, B. Séverine, A. Pignalosa, F. Pugliese, C. Gerundo, J.C.R. Sánchez, S. Fàbregas and J.A.B Canovas</i>	
Numerical Simulation for Runout Behaviour of Sensitive Clay Landslides Using the Material Point Method	149
<i>Z. Liu, M. Zhou, M. Lu, A.J. DiBiagio and H. Heyerdahl</i>	
The Effect of Rock Fragmentation on Rockfall Barriers	150
<i>G. Matas, J. Gili, N. Lantada and J. Corominas</i>	
Rock Avalanches in Northeastern Baffin Island: Understanding low occurrence in a region with high hazard potential	151
<i>M. Matthew, J. Gosse, R. Hermanns and A. Normandeau</i>	
Geo-Infrastructure Vulnerability to Landslide Hazards and Climate Change in the UK: Predictable Consequences?	152
<i>R. Moore and H. Reeves</i>	
Meteorological Thresholds for Regional Scale Rockfall Early Warning in Norway	153
<i>R.M. Palau, K.G. Gislås, G.L. Gilbert and A. Solheim</i>	

Low-Cost Methods For Monitoring Shallow Landslide Occurrence Along Linear Infrastructures	154
<i>M. Pavanello, M. Bordoni, V. Vivaldi, M. Reguzzoni, A. Tamburini, F. Villa and C. Meisina</i>	
A Methodology To Detect Ground Deformation Events In A-DInSAR Time Series: Application To Slow-Moving Landslides	155
<i>L. Pedretti, M. Bordoni, V. Vivaldi, S. Figini, M. Parnigoni, A. Grossi, L. Lanteri, M. Tararbra, N. Negro and C. Meisina</i>	
NBS Methods for Hydrological Correction in a Glacier Deposit Torrent to Avoid Recurrent Debris Flows into The Urban Area of Erill-La-Vall (Lleida Province-Spain)	156
<i>C. Raimat, J. Trujillo and A.Solheim</i>	
Characteristics of Fluidized Landslides in the Niigata Area, Japan	158
<i>N. Watanabe, N. Aiba and G. Furuya</i>	
Landslides and Hydrological Environment of Sedimentary Rock Slope in north Greenland	159
<i>S. Yamasaki and T. Watanabe</i>	

The 3rd Hutchinson Lecture

The Hutchinson Lecture was created by JTC1 to honour the memory and seminal contributions of Professor John Hutchison of Imperial College, London UK. The Hutchinson Lecture is awarded by JTC1 to a landslide specialist aged 42 years or less, with significant contributions on natural slopes and landslides.

Prof. Clarence E. Choi



Affiliation: University of Hong Kong, Hong Kong, China.

Short biography:

Clarence is a researcher, practitioner, and teacher in the Department of Civil Engineering at the University of Hong Kong. He leads a team of researchers to solve problems related to landslides and ground improvement. His research has contributed to the development of nine technical design guidelines on landslide hazard mitigation in Hong Kong.

Lecture Title: Engineered and nature-based solutions against flow-type landslide hazards.

Keynote Lectures

Prof. Jean Hutchinson



Affiliation: Queen's University, Canada

Short biography:

Dr. D. Jean Hutchinson is a Professor in Geological Sciences and Geological Engineering at Queen's University, is a registered Professional Engineer in Ontario, and is a Fellow of both the Canadian Academy of Engineering and the Engineering Institute of Canada. Jean specializes in rock engineering and engineering geology, site characterisation and risk management for mining and transportation infrastructure, with a focus on slope instability and landslide hazards, and novel monitoring techniques.

Jean's research interests include multi-criteria risk assessment and management for geological engineering projects. With her students, Jean has developed new techniques for site investigation, including applications of terrestrial and aerial LiDAR and photogrammetry, and development of better tools for characterising rock masses for engineering design. She has worked on developing risk-based decision making, using geomatics and monitoring tools for large slopes, and has conducted research on ground subsidence and geomechanics aspects of mine closure planning in the past. In addition to research, Dr. Hutchinson also serves as an expert reviewer, with assignments currently as a member of the Mine Technical Review Team at Bingham Canyon Mine for Rio Tinto Kennecott, and a member of the Due Diligence Committee for the Cariboo Region Road Reconstruction Program in northern British Columbia.

Dr. Hutchinson volunteers for several learned societies including as the President of the Canadian Foundation for Geotechnique and Vice Chair of the Engineering Geology Group of the Transportation

Research Board (US). She recently completed a 4-year term as Vice President, North America for the IAEG, and is currently a member of the IAEG Advisory Board.

Dr. Hutchinson has received several awards, including the Glossop Medal (UK) in 2019, the Canadian Pacific Railway Medal (Canada) in 2017 and the Robert Schuster Medal (Canada / US) in 2016. In recognition of her contributions to engineering research and practice, Dr. Hutchinson was elected as a Fellow of the Canadian Academy of Engineering (2020) and the Engineering Institute of Canada (2011).

Lecture Title: Applications of remote sensing techniques to rock slope stability and risk assessment – Building a toolbox of complementary methods.

Prof. Giovanni Crosta



Affiliation: University of Milano-Bicocca, Italy

Short biography:

Giovanni Crosta is professor of Engineering Geology and Hydrogeology at the Università degli Studi di Milano Bicocca, Dept. of Earth and Environmental Sciences. He has been Chair Professor at Tongji University, Dept. of Geotechnical Engineering (Shanghai, China) and Director of the Master in “Management of Water Resources in International Cooperation”.

Lecture Title: Recent evolution of geomorphological instabilities in the alpine area.

Prof. Joseph Wartman



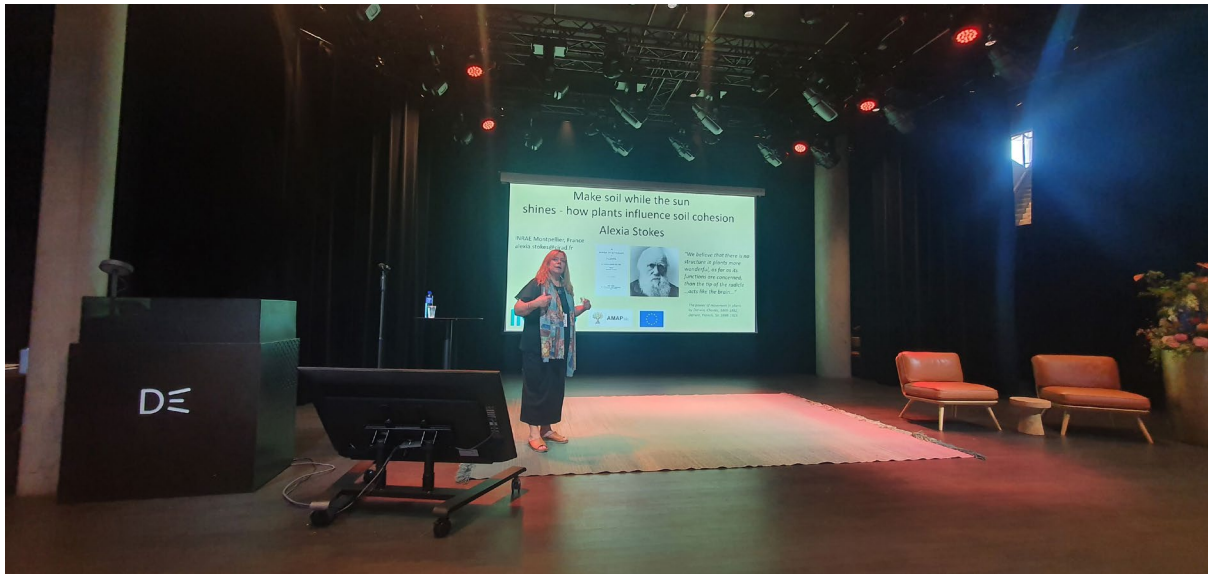
Affiliation: University of Washington, USA

Short biography:

Joe Wartman directs the Natural Hazard and Disaster Reconnaissance (RAPID) Facility, headquartered at the University of Washington (UW), where he is a Professor of Civil and Environmental Engineering. He specializes in geological hazards with a specific interest in landslides and their impacts on communities. Over the past two decades, he has investigated and analyzed major landslide and slope failure events worldwide, including the collapse of the levee system in New Orleans following Hurricane Katrina in 2005; rockfalls triggered the 2010-2011 Canterbury earthquake sequence in New Zealand; the devastating 2014 Oso, Washington, USA landslide; catastrophic flowslides triggered by the 2018 Palu, Indonesia earthquake; and the 2020 Haines, Alaska, USA landslide. Wartman's landslide research appears in the journals *Scientific Advances*, *Geomorphology*, *Journal of Geophysical Research*, *Engineering Geology*, *GeoHealth*, and the *International Journal of Disaster Risk Reduction*, among others. In addition to his scientific publications, Dr. Wartman's prize-winning non-technical writing on landslides has appeared in the *New York Times*, the *Seattle Times*, *EOS*, and other venues. He and his co-investigators received the E. B. Burwell Award from the Geologic Society of America for their investigation of the Oso landslide.

Lecture Title: Interdisciplinary investigation of landslides: a path to risk reduction.

Dr Alexia Stokes



Affiliation: French National Research Institute for Agriculture, Food and Environment - INRAE, France

Short biography:

Studying vegetation in different biomes around the world, Alexia Stokes focuses on plant root growth and biophysical interactions in soil. She uses knowledge to find solutions for stabilizing soil on slopes and improving tree anchorage during storms. More recently working on microbial interactions in soil, Alexia aims to link belowground biodiversity with soil structure and examine the implications for ecosystem services. Alexia has published more than 120 journal papers and edited three books since her PhD at the University of York (UK). She is now a senior scientist at INRAE Montpellier (France).

Lecture Title: Make soil while the sun shines - how plants influence soil cohesion.

Dr Zhongqiang Liu



Affiliation: Norwegian Geotechnical Institute, Norway

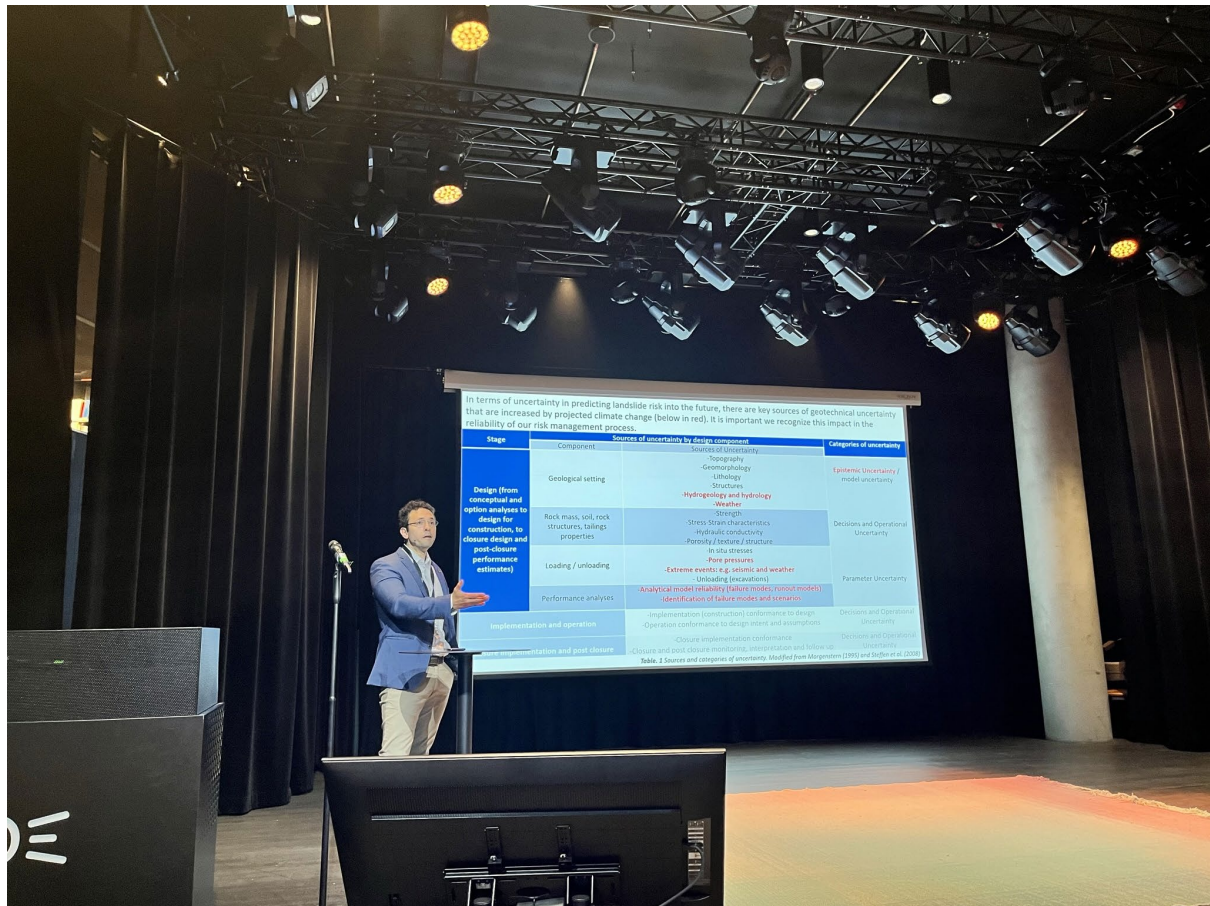
Short biography:

Dr Zhongqiang Liu is Principal Geotechnical Engineer at Norwegian Geotechnical Institute (NGI), Oslo, Norway, with expertise in risk and hazard assessment for geohazards, machine learning in geotechnics. His major fields of work are related to geohazards, assessment of uncertainties, statistical and machine learning methods, risk and reliability analysis, and offshore foundation engineering. He initiated and is now Chair of Technical Committee 309 of ISSMGE: "Machine Learning and Big Data in Geotechnics". He is Chair-Elect of "Geotechnical Safety Network (GEOSNet)" since 2022. Dr Liu is Guest lecturer at Norwegian University of Science and Technology (NTNU) and at University of Oslo (UiO). He is Technical Lead of Research Group – Risk and Reliability at NGI. His research has earned several international recognitions, including Best Paper Award of Journal Georisk in 2015, OTC ASCE Best Paper Award in 2019, GEOSNet Young Researcher Award in 2019 and Best Paper Award of JZUSA in 2023.

Lecture Title: Managing landslide risk: emerging challenges and recent innovations.

Invited Lectures

Prof. Renato Macciotta Pulisci



Affiliation: University of Alberta, Canada

Short biography:

Renato is an Assistant Professor in the department of Civil and Environmental Engineering at the University of Alberta, Edmonton, Canada. He has a BSs in Civil Engineering from the Catholic University of Peru, and a PhD in Geotechnical Engineering from the University of Alberta. Renato’s 15 year research experience and 20 year practical experience cover the areas of natural and engineered slopes, water and tailings dams, and open pit slopes; where he has participated in slope monitoring projects, slope stability evaluation, landslide characterization, qualitative and quantitative risk assessments, sites investigations, amongst others. His work has been published in over 100 technical articles, including 65 journal publications.

Lecture Title: Method and case studies on quantifying changes in landslide hazard as a consequence of climate change in Canada.

Prof. Thomas Marcher



Affiliation: Graz University of Technology, Austria

Short biography:

Specialized civil and geotechnical engineer with over 25 years of experience in the design and construction of underground projects around the world (Europe, Asia, North America, South America).

Lead geotechnical expert, project manager and coordinator in preliminary design, feasibility, design and construction of tunnels, hydroelectric power plants, power transmission and distribution, dams and power plants. In-depth knowledge in design of underground spaces in soil and rock, including deep tunnels (up to 2000 m overburden), large cross-sections and caverns.

Member of the International Society for Rock Mechanics, the Austrian Standards Institute, the German and Austrian Society for Geomechanics.

From 2002 - 2013 Thomas headed the geotechnical department of ILF Consulting Engineers in Austria. Since 2014, Thomas is owner of SKAVA consulting. In 2018, Thomas was appointed full professor and chair at the Institute of Rock Mechanics and Tunneling at Graz University of Technology in Austria. The main research topics are HSSR mechanics (hard soil/soft rock), anisotropy of rock mass, data science and ML in geotechnics, deep tunnelling / cavern storage and rock mass movement.

Lecture Title: Potential for remobilization of debris fans

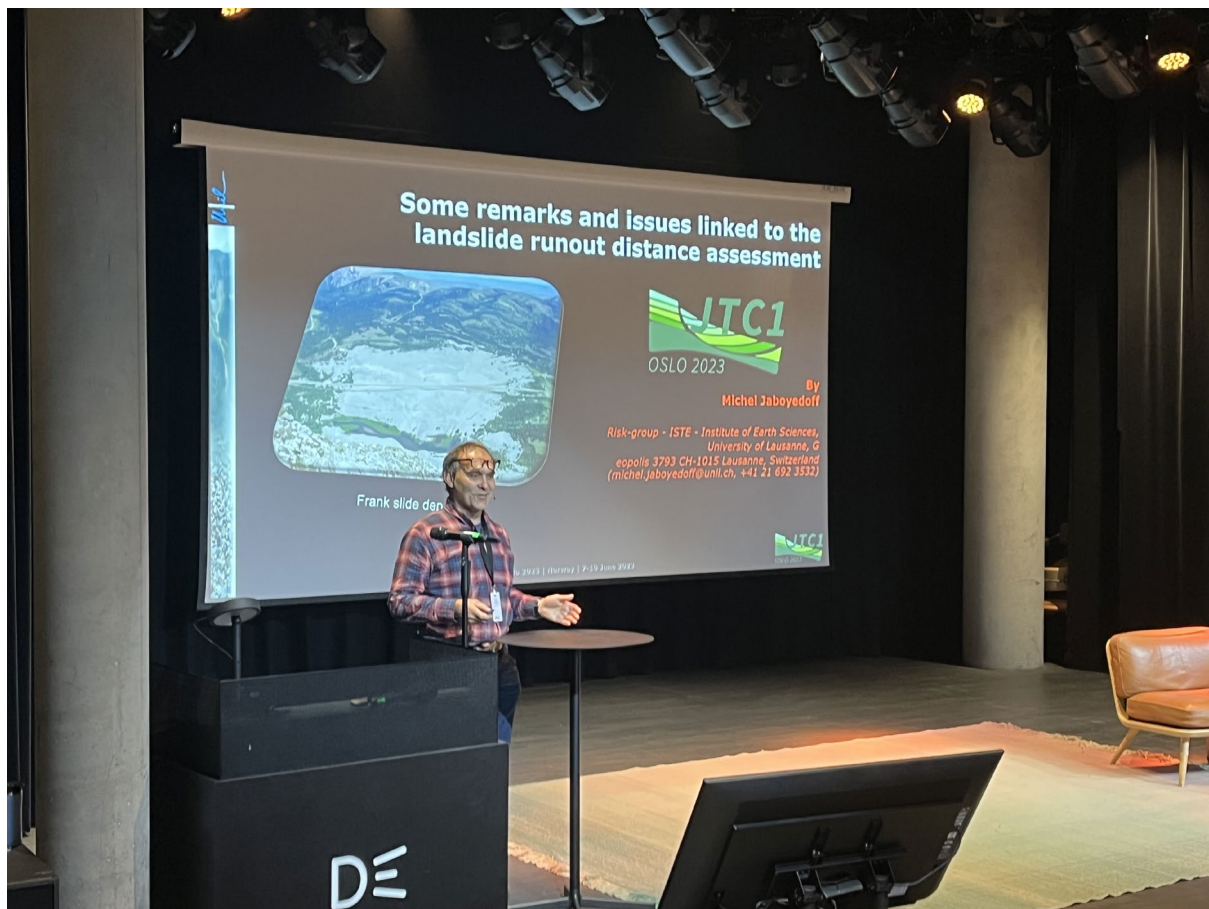


Affiliation: Politecnico di Bari, Italy

Short biography:

Full professor in Geotechnical Engineering at the Technical University of Bari (Politecnico di Bari; Italy). She has conducted experimental research, in the laboratory and the field, and endeavoured the development of theoretical frameworks of hydro-mechanical behaviour of soils and of geotechnical systems. Her work has conveyed knowledge about the influence of micro to meso structure on the behaviour of clays, under either full or partial saturation, in relation to their geological history, of reference for several elasto-plastic hardening constitutive models. With regard to geotechnical systems, she has mostly developed research about the geo-hydro-mechanical modelling of complex natural deposits, in either mountainous areas, or alluvial planes, the mechanics of slopes and landslides, the effects of geotechnical settlements on either ancient or modern structures, the response of contaminated marine sediment deposits. She has studied the processes generating different landslide mechanisms, implementing advanced soil mechanics in the assessment of landslide hazard at the site scale (work subsidized also by MIUR funding). In a recent 'Strategic Project', subsidized by European funds (selection on behalf of Apulia Region), under her coordination the research has resulted in a multi-scalar method for the assessment of landslide hazard based upon geo-hydro-mechanical analyses. She is currently doing research heading towards a framework of geo-hydro-mechanical characterization of landslide classes and on landslide risk sustainable mitigation (drainage systems and smart vegetation). She is author of 176 papers, published, after peer review, in international scientific journals, books and proceedings.

Lecture title: Diagnosis of the landslide mechanism for the assessment of slow-moving landslide hazard and the risk mitigation design.

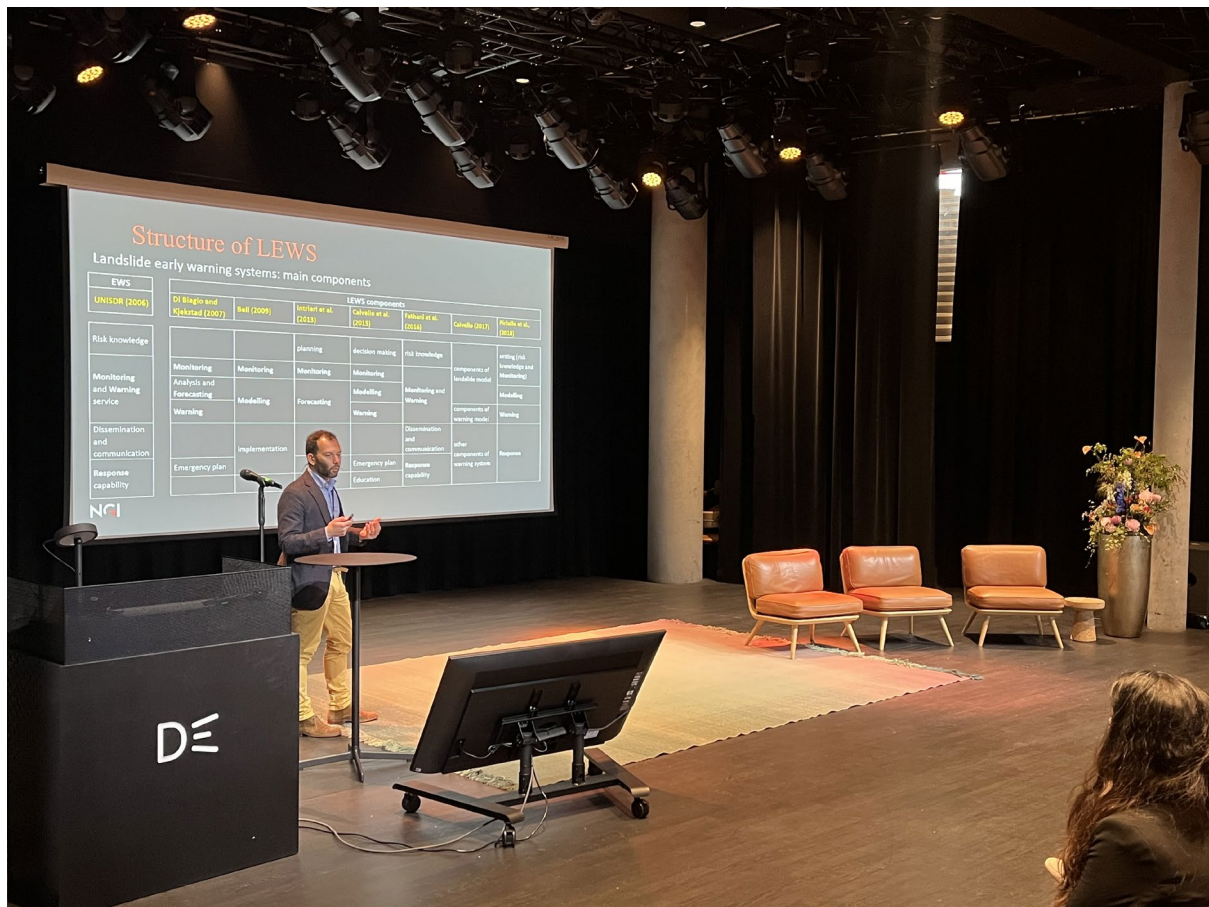


Affiliation: University of Lausanne, Switzerland

Short biography:

Michel Jaboyedoff is a geologist and has a degree in physics and a PhD degree in clay mineralogy. During his PhD, he started doing research on natural hazards, especially on rockfall. In 2017, he received the DPRI Award. Since 2005, he is a full professor at the University of Lausanne, focusing his research on natural hazards and related risks. Many studies are integrating remote sensing techniques such as Lidar and any 3D point clouds, in order to characterise fracturing. He developed among other the COLTOP colour scheme, the sloping base level concept and debris-flow modelling at a regional scale. This has been implemented in different software for hazard and risk analysis. Especially about landslide hazard rating. He is working on integrated risk analysis, and he is involved in several landslide-related risk projects around the world (Argentina, Bolivia, Canada, Italy, Nepal, Norway, Switzerland, USA, ...), and took part in European Projects FP7 (Mountain Risks, Safeland, CHANGES) and he got some Swiss National Science Foundation project. He is also the president of the Quanterra foundation and co-founder of a spin-off of the University of Lausanne (terr@num).

Lecture title: Some remarks and issues linked to the landslide runout distance assessment.



Affiliation: Norwegian Geotechnical Institute, Norway

Short biography:

Luca Piciullo is an Associate Professor at OsloMet and a Senior Researcher at the Norwegian Geotechnical Institute. His scientific pursuits primarily revolve around slope stability analysis, rainfall thresholds, early warning systems, risk assessment, and tailings dam stability analysis. With a portfolio of national and international research endeavors, including significant involvement in EU projects, and over 20 impactful scientific papers, Luca's expertise is highly regarded in the academic community. His contributions extend beyond research as he convenes sessions on landslide early warning and monitoring at renowned conferences like EGU and WLF. Additionally, Luca serves as a distinguished expert adviser for Start FOREWARN and is a member of the executive committee of the International network LANDAWARE. Furthermore, he is a member of the technical committee on Tailing and Mine Wastes of The International Society for Soil Mechanics and Geotechnical Engineering (ISSMGE).

Lecture title: IoT-based slope stability analysis as local landslide early warning.

When Soil Heterogeneity Helps the Geotechnical Design: the Case of Drainage Trenches

Luca Comegna¹, Marianna Pirone², Luciano Picarelli³, Gianfranco Urciuoli²

¹ Università della Campania “Luigi Vanvitelli”, Aversa, Italy

² Università degli Studi di Napoli “Federico II”, Napoli, Italy

³ Centro Euro-Mediterraneo per i Cambiamenti Climatici, Italy

SUMMARY: Experience shows that often even advanced geotechnical models cannot fully match the hydraulic or mechanical soil response due to unexpected variability of both soil structure and properties even within short distances. Engineers are then called to assess the influence of soil variability in the solution of geotechnical problems. This paper shows that in some cases, as in the design of drainage trenches, unforeseen layering favours a better soil response than in homogeneous conditions making the drainage system more efficient than foreseen.

Keywords: soil heterogeneity, soil anisotropy, drainage trenches, Efficiency, Time Factor

Introduction

As it is well known to engineers, a major problem in geotechnical analysis is matching models to reality. In fact, even the most sophisticated models are sometimes of little reliability. Hidden or disregarded heterogeneities, soil anisotropy, randomly distributed discontinuities, or unforeseeable natural stress conditions, can in fact deeply affect the overall soil response. Such situations are quite usual in soils of fluvial and lacustrine origin, which are naturally inhomogeneous, in colluvial deposits, in highly weathered soils or rocks and in landslide bodies, which are destructured and remolded by slope movements. However, there are cases, as the one of drainage trenches for slope stabilization, in which soil heterogeneity can favour a better soil response than foreseen based on results of analyses.

Influence of drainage trenches on flow patterns in homogeneous soils

The use of drainage trenches is a classical system for stabilization of shallow translational landslides in saturated clayey soils. They can in fact strongly modify the flow net, leading to higher effective stresses, thus operative shear strength, than in natural conditions.

Figure 1 shows the flow net that should establish in the long-term (steady state conditions) in between two parallel trenches that are part of a wider set of trenches reaching the slip surface of a hypothetical landslide in homogeneous and isotropic soils. Assuming water level at the ground surface and initial hydrostatic conditions, the flow net is now characterized by seepage vectors oriented in the direction of the trenches and thus by a generalized pore pressure decrease within the entire zone above the base of the trenches where the water flow generates a less than hydrostatic pore pressure distribution: the figure, in particular, shows the final piezometric head profile along the horizontal and vertical boundaries of the investigated soil volume. As it is well known, the time requested to attain the steady-state conditions, which is a function of system geometry and soil properties, is an important factor that strongly conditions the design.

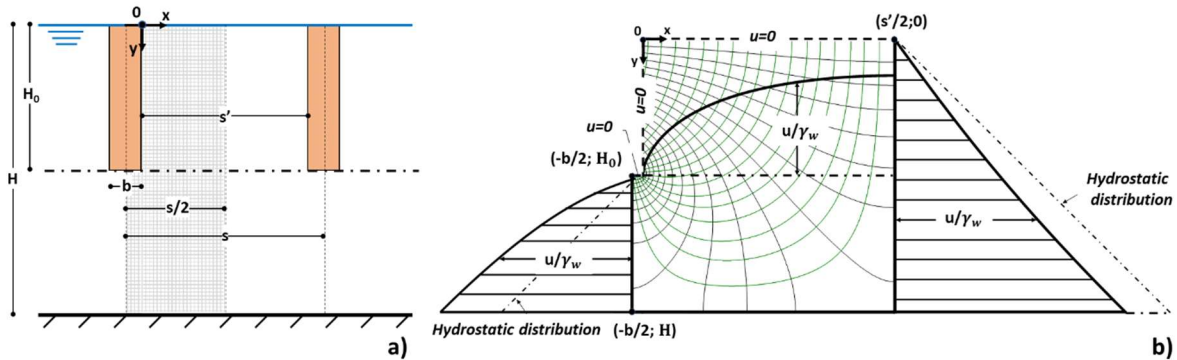


Fig. 1. Flow lines and pore water pressure profiles (b) around a drainage trench in homogeneous soils (a): the horizontal dotted line represents a slip surface (Urciuoli et al., 2020).

The solutions of this problem that are available in the literature (Hutchinson, 1977; Desideri et al., 1997), generally in the form of abacuses, assume full soil homogeneity and isotropy, providing the so-called Efficiency, \bar{E} , and Time Factor, T , of the system, two dimensionless factors that respectively allow to calculate the average effective stress increase and the length of time required to attain such an increase. However, as outlined above, in many cases, as for shallow unstable covers, the soil may display significant heterogeneities due to the presence of thin layers of higher or lower permeability, of open discontinuities or even of shear zones resulting from past slope failures. This problem is dealt with in the following by considering the presence of i) an intermediate soil layer of smaller or higher permeability, and of ii) a shear zone located at the base of trenches.

The influence of a horizontal intermediate layer of different permeability

The presence of thin layers of different permeability above the base of the trenches can deeply affect the flow pattern (Urciuoli et al., 2020) (Fig. 2a). In fact, less pervious layers behave as barriers diverting the flow path towards the trenches; in contrast, more pervious layers force seepage vectors to move vertically towards them. However, in both cases soil layering has a beneficial effect on system effectiveness. As an example, Figures 2b and 2c report the dimensionless results of some numerical analyses providing the long-term average Efficiency, \bar{E}_∞ , along the basal horizontal surface of a system of drainage trenches dug into a homogeneous soil including a horizontal layer of higher or lower permeability at an intermediate depth, and assuming an hydrostatic initial pore pressure distribution with ground level at the ground surface (Fig. 2a). The Efficiency $\bar{E}(T)$ is the average normalized pore pressure decrease along the horizontal line through the base of the trenches that, as in Figure 1a, is assumed to coincide with a slip surface, with respect to the initial value u_0 : $\bar{E}(T) = \frac{u_0 - \bar{u}(T)}{u_0}$. \bar{E} depends on time

through the Time Factor $T = \frac{c_v^{2D} \cdot t}{H_0^2}$, where c_v^{2D} is the 2D coefficient of consolidation. $\bar{E}_\infty = 1$ indicates zeroing of the average pore water pressure. The black solid line in Figures 2b and 2c, which displays the system efficiency into a homogeneous soil as a function of trench spacing, is the lowermost one among all solutions, suggesting that the presence of an intermediate heterogeneous layer entails in any case a higher efficiency. Figures 2b and 2c also show that for the highest contrasts in permeability a higher efficiency is assured; the situation reverses for lower contrasts in permeability that, of course, result in solutions that are closer and closer to that obtained for homogeneous soils. In both cases the beneficial role of an interlayer of

different permeability increases with depth from the ground surface (Fig. 2c). Of course, the efficiency decreases with spacing between trenches (Fig. 2b).

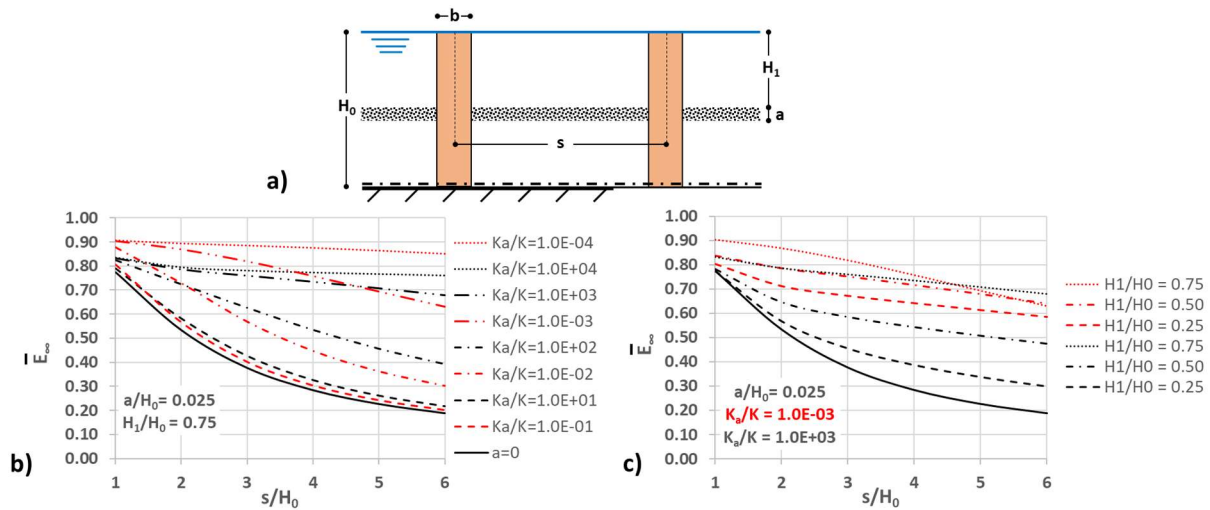


Figure 2. Influence of a heterogeneous layer of permeability k_a (k being the deposit permeability) on the average efficiency of a system of drainage trenches dug until a slip surface (horizontal dotted line).

The influence of a horizontal anisotropic layer located at the trench base

Several Authors (Skempton & Petley, 1967) have shown that the slip surface of landslides is generally surrounded by a thin shear zone, which includes other shorter shear discontinuities (minor shears). Moreover, based on in depth field and laboratory investigations on an earthflow, Comegna & Picarelli (2008) highlighted its lower permeability with respect to that of the uppermost soil body, which includes widespread open discontinuities and cracks, and its high anisotropy due to both the alignment of clay particles and the presence of a network of minor and principal shear surfaces in the direction of shear that lead to a higher parallel hydraulic permeability. Further analyses have then been carried out assuming that a shear zone of thickness $a = 100$ cm (as in the investigated earthflow) is located just at the base of the set of trenches considering the permeability values obtained in that investigation. The results of the analyses are reported in Figure 3. Again, the presence of the shear zone results in a higher efficiency than in the case of homogeneous soil. As suggested by Figure 2b, this effect strongly depends on the contrast in permeability; in the case at hand, it entails an increase of the efficiency of 15-25% depending on trenches spacing. Even though this point is not examined in the paper, soil anisotropy alone plays a minor role.

The Time Factor

As mentioned above, the Time Factor T has a key role in the design of a drainage system since it indicates in what time its potentiality can be fully exploited. The figure 4 reports the value of \bar{E} as function of T only for spacing $s = 6H_0$ and layer depth $H_1 = 0.75 H_0$. As shown, the presence of an intermediate layer of whatever permeability is beneficial also from this point of view. In particular, it shows that the rate of consolidation is much higher for layers of higher permeability.

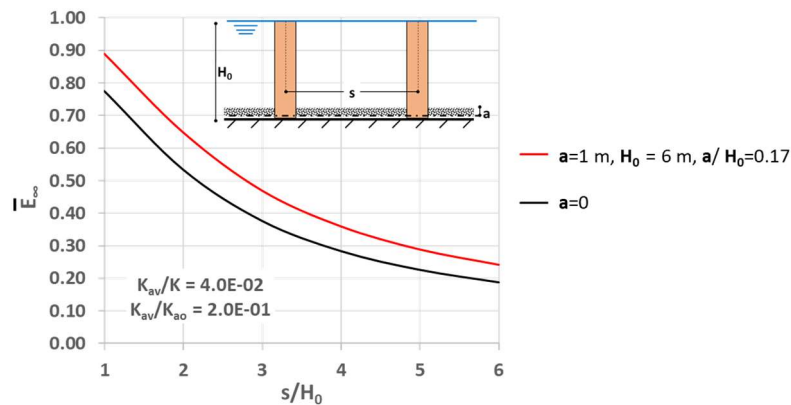


Figure 3. Influence of an anisotropic shear zone located at the base of trenches on the average efficiency of the drainage system (k_{av} and k_{a0} are the vertical and horizontal permeability of the shear zone respectively).

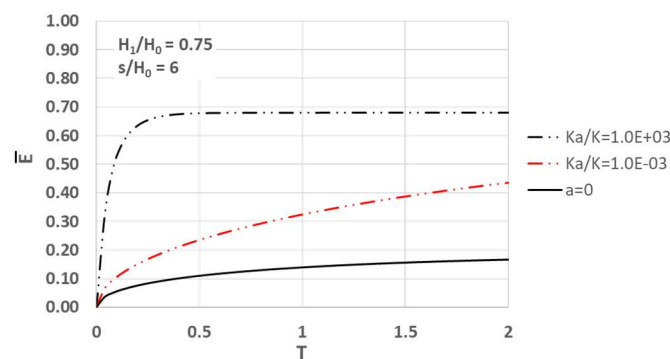


Figure 4. Time Factor for some cases presented in Figure 2.

Conclusions

Drainage trenches are widely used for stabilization of shallow translational landslides. Their design is generally based on the assumption of soil homogeneity and isotropy. This paper has examined the influence of an intermediate soil layer of small thickness located in an intermediate zone between the top and the base of trenches and that of a shear zone located just at the base of trenches, showing that it has always a beneficial role on both Efficiency and Time Factor regardless of its permeability. The designer, of course, should take care of the long-term efficiency of the drainage system preventing the risk of trenches clogging.

References

- Comegna L & Picarelli L (2008) Anisotropy of a shear zone. *Géotechnique* 58, 737–742.
- Desideri A, Miliziano S & Rampello S (1997) *Drenaggi a Gravità per la Stabilizzazione dei Pendii*. Hevelius Edizioni, Benevento.
- Hutchinson JN (1977). Assessment of the effectiveness of corrective measures in relation to geological conditions and types of slope movement. *Bulletin of the International Association of Engineering Geology* 16, 131–155.
- Skempton AW & Petley DJ (1967). The strength along structural discontinuities in stiff clays. *Proceedings of the Geotechnical Conference, Oslo*, 2, 55-69.
- Urciuoli G, Comegna L, Pirone M & Picarelli L (2020). The beneficial role of a natural permeable layer in slope stabilization by drainage trenches. *Hydrology and Earth System Sciences* 24, 1669-1676.

ACKNOWLEDGMENTS

The research has been supported by MIUR PON R&I 2014-2020 (project MITIGO)

The Effect Of Wildfire Wooden Ember Cover On Hydrological Behaviour And Stability Of Silty Volcanic Slopes

L. Coppola¹, A. Reder², G. Rianna², A. Tarantino³, L Pagano¹

¹ Università degli studi di Napoli “Federico II”, Naples, Italy

² REgional Model and geo-Hydrological Impacts-REMHI,
Centro Euro-Mediterraneo sui Cambiamenti Climatici, Caserta, Italy

³ University of Strathclyde, Scotland, United Kingdom

SUMMARY: This work presents an experimental investigation into the hydrological response of a silty volcanic soil covered by a thin layer (5 cm) of wooden ember granular material. This layer simulates the presence of wildland fire ash. The investigation was carried out using an instrumented lysimeter positioned outdoor and subjected to natural climatic loading. The experimental dataset was then compared with those previously collected on the silty layer only under bare and vegetated conditions. The results show that evaporative fluxes are reduced remarkably by the wooden ember covering layer generating higher water content in the silty volcanic soil making slopes more prone to instability.

Keywords: pyroclastic soil, landslide, lysimeter, wooden ember material.

Introduction

Wildfires affecting vegetated hillslopes cause a significant increase of hazard associated with rainfall induced landslides (Rengers et al., 2020). This is linked to the removal of vegetation and the loss of stabilising effects due to root mechanical reinforcement (Gehring et al., 2019) and hydrological reinforcement due to root water uptake. However, most of previous research does not consider the effect of the superficial layer of wooden ember cover (hereafter WEC) on soil-atmosphere interaction. The WEC thermal and hydraulic properties can induce significant variations in soil-atmosphere interactions compared to the bare soil and, hence, affect the soil moisture regime in the underlying slope layer. This paper investigates the effect of WEC on the hydrological response of a silty layer (hereafter SIL). The experimental study was carried out using a lysimeter (Rianna et al., 2014a) consisting of wooden tank (~1 m³) filled with SIL and exposed to natural weather conditions for several years to study the soil-atmosphere interaction. In the first four years, the experiment was conducted by keeping the layer surface under bare conditions (Rianna et al., 2014b), while in the subsequent five years the SIL surface was vegetated with grass (Pagano et al., 2019). Finally, the vegetation was removed and a 5 cm WEC was placed at the top of the SIL to study the effect of the WEC on the hydrological response of the SIL. The SIL hydrological response in the presence of the WEC was then compared with the previous observation (bare and vegetated SIL). The WEC was placed at ambient temperature; therefore, the effect of high temperature on the response of the SIL was not investigated. This is supposed to reduce soil aggregate stability and induce, enhance or destroy soil water repellency (Leighton-Boyce et al., 2007). The paper presents the physical model, the properties of the materials forming the two layers (WEC and SIL), and shows the evolution of volumetric water content and temperature within the SIL layer in response to soil-

atmosphere interaction. The comparison of the WEC-covered SIL with the bare and vegetated SIL allowed examining the thermo-hydraulic effects of the WEC.

The physical model

The physical model consists of a wooden tank, filled with a 0.75 m thick SIL of volcanic origin. The layer was covered by a 0.05 m thick WEC obtained by burning a chestnut wood (widely present on slopes of Lattari Mountains). The SIL was the same soil forming the slope subjected to rainfall induced instability in the town of Nocera Inferiore on 4 March 2005. The SIL was emplaced by pluvial deposition technique to reproduce the high porosity (about 70%) measured in the field. The WEC was simply dumped on the SIL surface to form a layer 5-cm thick.

The tank base is perforated to allow water drainage. A geotextile is interposed between the SIL and the tank base to prevent internal erosion and generate a hydraulic boundary condition that simulates a capillary barrier. Three load cells support the tank to quantify the evolution of water storage in turn controlled by infiltrating rainwater and actual evaporation. The SIL was monitored with matric suction (Jetfill tensiometer), volumetric water content (TDR), and temperature (thermistor) sensors installed at four different depths. A weather station was also installed to measure meteorological variables.

Material properties

Figure 1 shows the grain size distribution of SIL and WEC materials. The SIL is made of a volcanic sandy silt (silt fraction=50%), while the WEC is characterised by a grain-size distribution equivalent to gravelly-silty-sand (silt fraction=20%). Both materials showed no plasticity.

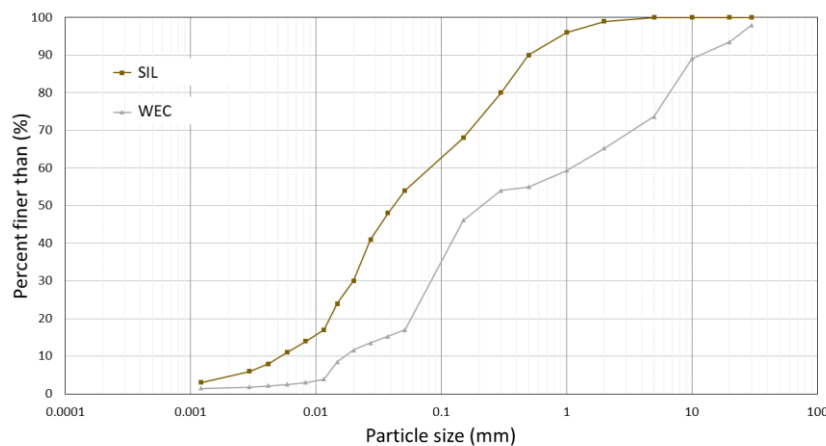


Fig. 1 SIL and WEC grain size distribution.

Hydraulic (soil-water retention and hydraulic conductivity functions) and thermal (volumetric specific heat and thermal conductivity functions) properties are plotted in figure 2 for SIL and WEC respectively. Consistently with its coarser grain size distribution, WEC shows lower entry value (4 kPa against 12 kPa for the SIL) and residual water content value (0% against 10% for the SIL). Saturated hydraulic conductivity for WEC material is one order of magnitude higher than the SIL material (10^{-5} m/s for WEC against 10^{-6} m/s for SIL). Thermal conductivity and volumetric specific heat for the WEC material are also higher than the SIL material.

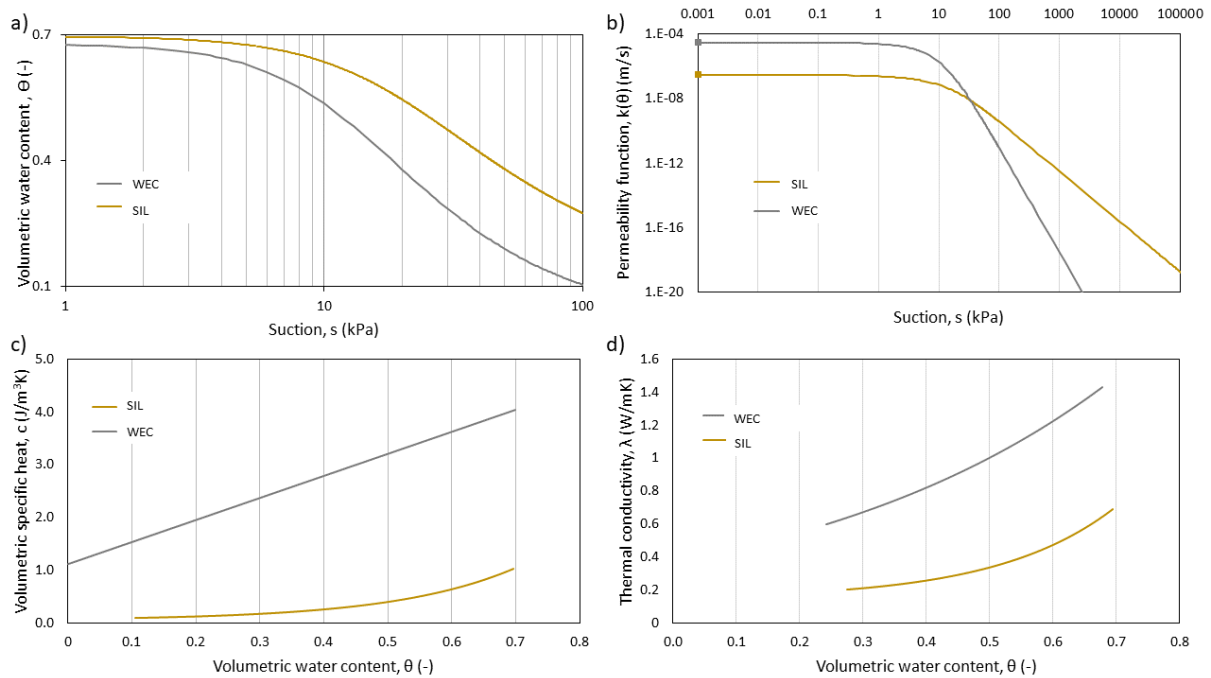


Fig. 2 (a) soil water retention curve, (b) permeability function, (c) volumetric specific heat, (d) thermal conductivity function, for WEC and SIL materials.

Temperature variations within the layer

Figure 3 shows the evolution of the temperature of air and SIL layer at the depth of 5 cm from the SIL-WEC interface, during the warmer months of years 2°, 6°, and 11° associated with bare, vegetated, and wooden ember-covered SIL respectively. Daily fluctuations in the SIL layer are considerably reduced in year 11° compared to years 2° and 6°. The reduced temperature fluctuations indicate a reduction of the incoming heat fluxes and, as a result, a reduction in the evaporative fluxes (due to the reduction in latent heat).

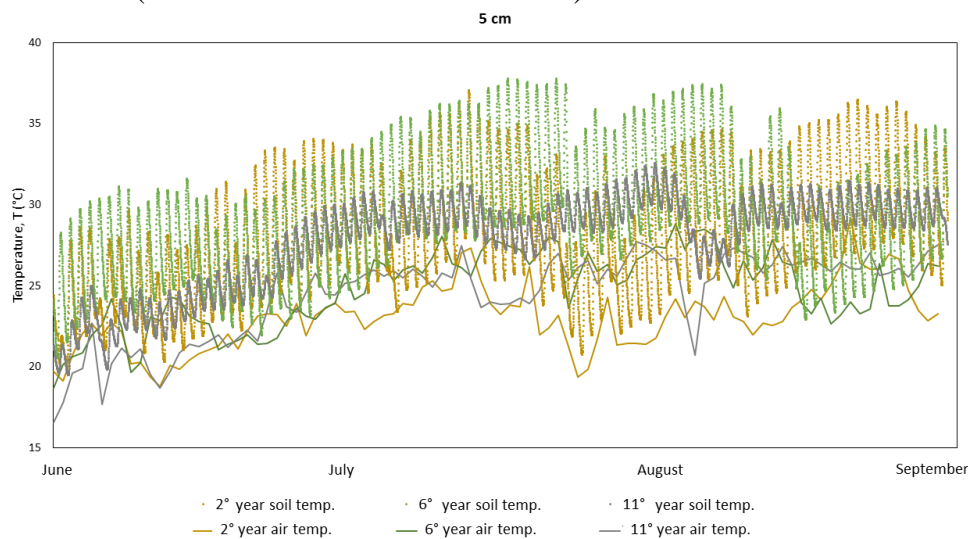


Fig. 3 Evolution of soil temperature recorded during year 2 (brown line, bare SIL conditions); year 6 (green line, vegetated SIL condition) and year 11 (grey line, WEC conditions).

Water content variations within the layer

Figure 4 shows the yearly evolution of the volumetric water content (VWC) recorded during three different hydrological years (the third, the sixth and the eleventh year) by the three load cells supporting the lysimeter. The maximum value of VWC recorded during the wet period is very similar for the three conditions ($VWC \cong 0.65$). During the dry period, VWC stabilises at about 0.30 for WEC condition (year 11°), 0.25 for bare condition (year 3°) and 0.10 for the vegetated condition (year 6°). The higher values of 'residual' VWC for WEC condition suggests a remarkable reduction in evaporative fluxes during the dry period.

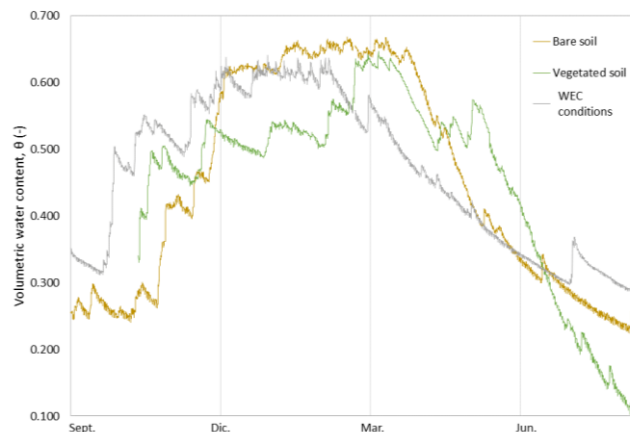


Fig. 4 Evolution of volumetric water content recorded during year 3 (brown line, bare SIL conditions); year 6 (green line, vegetated SIL condition) and year 11 (grey line, WEC conditions).

Discussion and conclusion

A silty layer covered by a thin wooden ember cover was placed in a lysimeter (Rianna et al., 2014a) and exposed to the atmosphere to investigate the effect of wooden ember cover on hydrological behaviour of the underlying silty layer. The response of the wooden ember-covered silt layer was benchmarked against the response of the same silt layer under bare and vegetated conditions. The comparison of the response of the silt layer in terms of volumetric water content and temperature has shown negligible differences to rainwater infiltration (inward water flux) and a relevant reduction in evaporative fluxes (outward water flux). The thin wooden ember cover therefore appears to act as an evaporative thermo-hydraulic barrier.

References

- Gehring, E., Conedera, M., Maringer, J., Giadrossich, F., Guastini, E., & Schwarz, M. (2019). Shallow landslide disposition in burnt European beech (*Fagus sylvatica* L.) forests. *Scientific reports*, 9(1), 1-11.
- Leighton-Boyce, G., Doerr, S. H., Shakesby, R. A., & Walsh, R. P. D. (2007). Quantifying the impact of soil water repellency on overland flow generation and erosion: a new approach using rainfall simulation and wetting agent on in situ soil. *Hydrological Processes: An International Journal*, 21(17), 2337-2345.
- Pagano, L., Reder, A., & Rianna, G. (2019). Effects of vegetation on hydrological response of silty volcanic covers. *Canadian Geotechnical Journal*, 56(9), 1261-1277.
- Rengers, F. K., McGuire, L. A., Oakley, N. S., Kean, J. W., Staley, D. M., & Tang, H. (2020). Landslides after wildfire: Initiation, magnitude, and mobility. *Landslides*, 17(11), 2631-2641.
- Rianna G, Pagano L, Urciuoli G (2014a). Rainfall patterns triggering flowslides in pyroclastic soils. *Engineering Geology*, 174: 22-35
- Rianna, G., Pagano, L., & Urciuoli, G. (2014b). Investigation of soil-atmosphere interaction in pyroclastic soils. *Journal of hydrology*, 510, 480-492.

Alaska's Unstable Slopes: A Look at Three Examples of Increasing Instability with a Warming Climate

Margaret M. Darrow¹, Denny M. Capps², Ronald P. Daanen³

¹ University of Alaska Fairbanks, Fairbanks, Alaska, U.S.A.

² Denali National Park and Preserve, Denali Park, Alaska, U.S.A.

³ Alaska Division of Geological & Geophysical Surveys, Fairbanks, Alaska, U.S.A.

SUMMARY: Like much of the Arctic and sub-Arctic, Alaska is experiencing increased air temperatures and precipitation, resulting in permafrost destabilization, glacial retreat, and a greater number and intensity of major storm events. Alaska's slopes are responding, with an increasing number of failures. Here, we present three examples of landslides that span Alaska, including: 1) frozen debris lobes in continuous permafrost that demonstrate continually-increasing movement rates; 2) destabilization of a rock glacier in discontinuous permafrost; and 3) a disastrous landslide along the glacially-sculpted coast caused by an extreme weather event. All of these landslides impacted critical infrastructure or caused fatalities, and may represent the future increase in slope failure magnitude and frequency with increased precipitation and temperature. Recognizing the potential impacts to safety and infrastructure in Alaska by increased mass movement events, we can reduce risk by identifying landslide-susceptible areas, monitoring and modeling critical unstable slopes, and raising landslide awareness in our communities.

Keywords: Landslide, frozen debris lobe, rock glacier, rain-on-snow event, Alaska

Introduction

Increasing air temperature and precipitation in the Arctic and sub-Arctic are resulting in increased slope instabilities. Alaska, for example, is currently experiencing warming; since 1950, mean annual air temperatures (MAAT) have increased by approximately 2°C, with winters experiencing 4.1°C warming over the same period (Walsh & Brettschneider 2019). The increased winter temperatures and associated precipitation not only affect permafrost stability, but may increase the number and intensity of atmospheric river (AR) and rain-on-snow (ROS) events, broadly impacting Alaska. In response to the changing climate, we already observe increased frequency and magnitude of slope movement in areas underlain by permafrost, and significant mass movement occurrences associated with major storm events. Here, we present three examples of landslides spanning across Alaska from the Brooks Range in the north, Denali National Park in Alaska's Interior, and from a rugged coastal area in Southeast Alaska (Fig. 1). All of these landslides are strongly correlated to a warming climate, and have either impacted critical infrastructure or caused fatalities.

Frozen Debris Lobes, Brooks Range

Frozen debris lobes (FDLs) are landslides in permafrost-affected terrain, many of which occur in continuous permafrost throughout the Brooks Range. Since 2013, we have monitored eight FDLs to assess their geohazard potential. All investigated FDLs consist of a soil matrix composed of silty sand with gravel, with platy rock fragments that reflect the geology of the

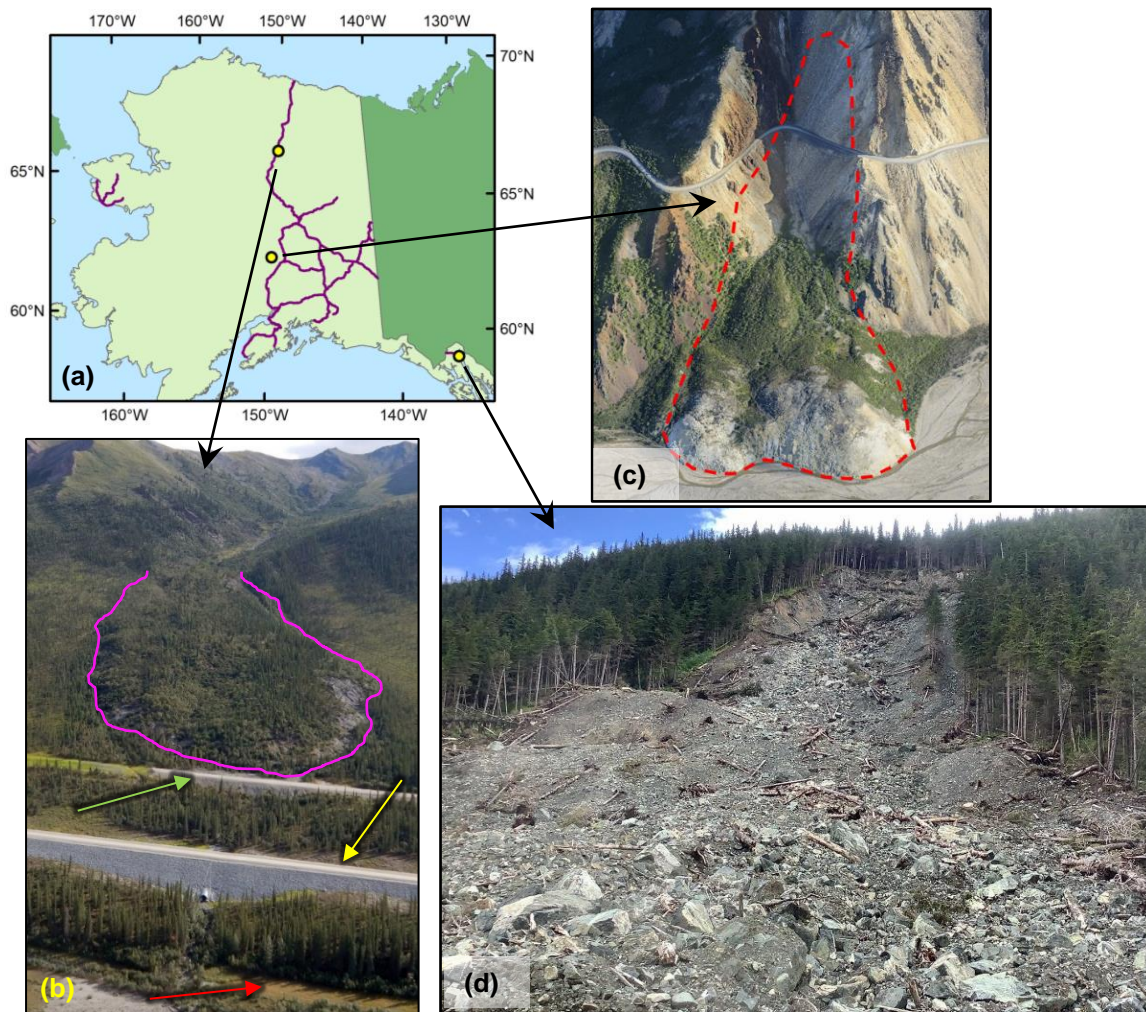


Fig 1. Location map (a) of landslide examples around Alaska; (b) view of FDL-A (outlined in pink) taken in August 2019 with old (green arrow) and new (yellow arrow) Dalton Highway alignments and Trans Alaska Pipeline System (red arrow) alignment; (c) Pretty Rocks landslide (delineated in red dashed line); (d) Beach Road landslide.

associated catchments (Darrow et al. 2016). All monitored FDLs have demonstrated increased rates of movement over the observation period, with movement rates as high as 24 m/yr. Because of its proximity to infrastructure, we focus on FDL-A (Fig. 1b). Long-term movement rates from analysis of aerial and satellite imagery dating from 1950 indicated a steady linear increase in the rate of motion for FDL-A (Darrow et al. 2016); however, our recent measurements of FDL-A's surface indicate that it is experiencing an exponential increase in movement, doubling from 5 to over 10 m/yr in less than five years. Measured temperatures within FDL-A indicated uniform temperatures of -0.85°C below the depth of zero annual amplitude, whereas temperatures measured in the adjacent undisturbed permafrost were -2.1°C . Analysis of data from subsurface instrumentation indicates that FDL-A's movement rate is sensitive to temperature and water (Darrow et al. 2017). On-going movement causes cracks that damage surface vegetation and expose mineral soil. Thermal modeling of FDL-A with a bare mineral surface and current air temperatures indicates that a through-talik forms under the exposed mineral surface within 50 years, resulting in unsustainable permafrost conditions (Darrow et al. 2019). These conditions may result in destabilization and rapid downslope movement. Understanding the risk, the Alaska Department of Transportation and Public Facilities realigned the Dalton Highway in 2018 (Fig. 1b). We continue to monitor FDL

movement, conduct subsurface investigations, and perform modeling to inform mitigation strategies along this critical infrastructure corridor in Alaska.

Pretty Rocks Rock Glacier, Denali National Park, Interior Alaska

The Pretty Rocks rock glacier (Fig. 1c), located in discontinuous permafrost in Interior Alaska, displaces 90 m of the full width of the Denali Park Road near its midpoint at km 73 (Stanczyk 2022). This dead-end road is critical park infrastructure and a major economic engine for Alaska (NPS 2021). In recent years the rock glacier has evolved from a minor maintenance concern to a long-term road closure with plans for an approximately \$53,000,000 USD effort to bridge it (NPS 2022a). Before 2014, the movement only caused small cracks in the road surface and required moderate maintenance every few years; however, road maintenance crews noticed a substantial increase in motion in 2014, which was an usually warm year. By 2016, after several consecutive years of warm weather, movement increased further, necessitating a monitoring program. The rate of road movement across the rock glacier evolved from 10's of mm/yr prior to 2014, to 10's of mm/mo in 2017, 10's of mm/wk in 2018, 10's of mm/day in 2019, and up to 16 mm/hr in 2021 (NPS 2022b). Between 1950 and 2010, Denali National Park experienced a temperature increase of $4.3^{\circ}\text{C} \pm 1.1^{\circ}\text{C}$ per century, the highest of all national parks (Gonzales et al. 2018). A recent shift in mean annual temperatures to nearly 0°C (Swanson et al. 2021), combined with heavy rainfall events, is attributed as one cause for thawing permafrost, resulting in the recent acceleration of many landslides and rock glaciers in Denali. Temperature and precipitation increases are likely to continue, and the rate may worsen over the coming decades. While these changes were predicted by Rupp and Loya (2009), the rate of the change has been greater than expected. For example, some areas have already reached MAATs predicted for the 2040s (Sousanes 2020), which has serious consequences for permafrost, ground stability, and critical infrastructure.

Beach Road Landslide, Southeast Alaska

In December 2020, an AR and ROS event with a 500-year return interval hit Southeast Alaska, significantly impacting the community of Haines. More than 50 landslides occurred as a result of this record-breaking precipitation event. The largest landslide occurred along Beach Road (Fig. 1d), which destroyed four structures and unfortunately took the lives of two people. The landslide also destroyed the local infrastructure, leaving local residents without access or power to their properties for months. The likely cause of the Beach Road landslide was the tremendous rainfall and snowmelt brought on by this mid-winter AR (Darrow et al. 2022). Climate modeling for Southeast Alaska projects a 1° - 3°C temperature increase in the next decade with increased precipitation in fall and winter (Lader et al. 2020), which may increase ROS events.

Other related concerns for Southeast and South-Central Alaska are rapidly-retreating glaciers that expose steep slopes previously supported by glacial ice. These slopes often release large volumes of debris directly into adjacent fjords, producing deadly tsunamis such as the Lituya Bay event (Miller 1961). A currently-monitored incipient landslide capable of producing such a tsunami is located in Alaska's Prince William Sound in Barry Arm (Coe et al. 2021).

Conclusions

These examples illustrate the breadth of impact from a warming climate on Alaska's slopes, and indicate that we can expect increased slope failure magnitude and frequency with increased

precipitation and higher temperatures. As a result, we must plan for these changes with existing and future infrastructure throughout Alaska by improving safety and resiliency. These improvements will vary according to specifics of the setting and situation; however, there are shared steps that we can take in many situations, such as: 1) identifying and reducing risk before damaging events occur; 2) updating and improving monitoring and modeling for unstable slopes and infrastructure; and 3) raising awareness of these risks in our communities through education and outreach (Capps, *in press*). Finally, although we can reduce risk, we never can fully eliminate it in highly dynamic environments and times; however, when risk reduction combined with enhanced emergency preparedness is executed well, it improves safety and resiliency and has a favourable benefit-cost ratio (Capps, *in press*).

References

- Capps DM (*in press*) Degradation of mountain permafrost in Alaskan national parks. In *Safeguarding Mountain Social-ecological Systems; a Global Challenge*. United Nations University.
- Coe JA, Wolken GJ, Daanen RP, Schmitt, RG (2021) Map of landslide structures and kinematic elements at Barry Arm, Alaska in the summer of 2020. *U.S. Geological Survey data release*, <https://doi.org/10.5066/P9EUCGJQ>
- Darrow MM, Daanen RP, Gong W (2017) Predicting movement using internal deformation dynamics of a landslide in permafrost. *Cold Regions Science and Technology* 143, 93-104.
- Darrow MM, Freeman AE, Daanen RP (2019) Exploring subsurface temperature dynamics of frozen debris lobes through thermal modeling. *Proc., 18th International Conference on Cold Regions Engineering/8th Canadian Permafrost Conference*, August 18-22, 2019, Québec City, Québec, Canada, 10 p.
- Darrow MM, Gyswyt NL, Simpson JM, Daanen RP, Hubbard TD (2016) Frozen debris lobe morphology and movement: an overview of eight dynamic features, southern Brooks Range, Alaska. *The Cryosphere* 10, 977-993.
- Darrow MM, Nelson VA, Grilliot M, Wartman J, Jacobs A, Baichtal JF, Buxton C (2022) Geomorphology and initiation mechanisms of the 2020 Haines, Alaska landslide. *Landslides* doi 10.1007/s10346-022-01899-3.
- National Park Service (NPS) (2021) Park Statistics. Retrieved from <https://www.nps.gov/dena/learn/management/statistics.htm>
- NPS (2022a) Pretty Rocks Landslide. Retrieved from <https://www.nps.gov/dena/learn/nature/pretty-rocks.htm>
- NPS (2022b) Polychrome Area Plan. Retrieved from <https://www.nps.gov/dena/getinvolved/polychrome-plan.htm>
- Gonzalez P, Wang F, Notaro M, Vimont DJ, Williams JW (2018) Disproportionate magnitude of climate change in United States national parks. *Environmental Research Letters* 13, 12.
- Lader R, Bidlack A, Walsh JE, Bhatt US, Bieniek PA (2020) Dynamical downscaling for Southeast Alaska: historical climate and future projections. *Journal of Applied Meteorology and Climatology* 59(10), 1607-1623, doi:10.1175/JAMC-D-20-0076.1.
- Miller DJ (1961) *Giant Waves in Lituya Bay, Alaska*: US Geological Survey Professional Paper 354, 51-86.
- Rupp S, Loya W (2009) Projected climate change scenarios for Denali National Park & Preserve. *Climate Change Summary Reports of National Parks, Preserves and Monuments*: University of Alaska Fairbanks.
- Sousanes, P (2020) Analysis of temperatures from the two stations in Denali National Park and Preserve that best characterize the Pretty Rocks location along the Denali Park Road. Fairbanks, Alaska: National Park Service, unpublished.
- Stanczyk A, Capps, D, Anderson, DA (2022) A geotechnical investigation of Pretty Rocks Landslide, mile 45.4, Denali Park Road, Denali National Park, Alaska. Natural Resource Report. NPS/DENA/NRR—2022/2365. National Park Service. Fort Collins, Colorado. <https://doi.org/10.36967/nrr-2288333>
- Swanson DK, Sousanes PJ, Hill K (2021) Increased mean annual temperatures in 2014-2019 indicate permafrost thaw in Alaskan national parks. *Arctic, Antarctic, and Alpine Research* 53, 19.
- Walsh JE, Bretschneider B (2019) Attribution of recent warming in Alaska. *Polar Science* 21, 101-109.

In Situ and Satellite Monitoring of a Landslide and of a Drainage System

J. De Rosa¹, C. Di Maio¹, R. Vassallo¹, G. Cutrera², R. Murtas², G.V. Pandiscia³, F. Trillo³,
B. Lacovara⁴

¹ University of Basilicata, Potenza, Italy

² Rete Ferroviaria Italiana (Ferrovie dello Stato Italiane Group), Bari, Italy

³ E-GEOS S.p.A., Matera, Italy

⁴ GEOCART S.p.A., Potenza, Italy

SUMMARY: A very complex landslide system in Miocene formations affects the national railway in the territory of Calciano, southern Italian Apennines. The analysis of inclinometer data provided the landslide depth and mechanism of movements, and allowed the interpretation of satellite Envisat, COSMO-SkyMed (CSK) and Sentinel-1 data. A long time series (~20 years) of displacements was thus obtained for the slow part of the landslide; the series was also used to evaluate the effectiveness of deep drainage systems built to reduce the landslide risk for the national railroad. DinSAR data show a decrease in the landslide displacement rates after the construction, in 2016-2017, of a new drainage well system. A numerical model constructed by the FD MODFLOW 3D code shows that the deceleration is consistent with the progressive decrease in pore water pressures in the landslide body and in the slip zone recorded by the piezometers installed in the zone.

Keywords: landslide, drainage, inclinometer, piezometer, DInSAR.

Introduction

In the territory of Calciano, in the southern Italian Apennines, the national railroad is affected by an active landslide system occurring in the structurally complex Miocene formations of the Numidian Flysch and Serra Palazzo, which are respectively constituted by layers and banks of quartzarenites/clays/marls and marls/clays/limestones. The material in the landslide body is very inhomogeneous, with clay, silt, gravel and block fractions much variable from site to site. The landslide has an elongated irregular shape; it extends for about 1400 m length, from 410 m to 240 m a.s.l., reaching the alluvial plain of the Basento river (Fig. 1a-c).

In order to reduce the risk for the national railway, two drainage systems were constructed (Fig.1c): the former (years 1993-1994) constituted by three wells (W01-W03) downstream of the railroad, the latter (2016-2017) upstream of it, constituted by five wells (W1-W5), both with 3 levels of 30 m long sub-horizontal drains. In order to reach a deeper insight in the landslide behaviour, inclinometer, piezometer, LiDAR and DinSAR data were analyzed, following Di Maio et al. (2018; 2021) and Vassallo et al. (2021).

Landslide displacements: inclinometer and DInSAR data

The irregular morphology of the landslide was analyzed by means of a digital terrain model (DTM) created with 1 m spatial resolution by processing LiDAR point clouds acquired in April 2022. The analysis allowed to identify three main sectors of the landslide (sectors I, II and III

in Fig. 1a) which can undergo differential movements. Recently, in July 2022, three new inclinometers have been installed in sector I that already allowed to hypothesize the shape and depth of an active slip surface (Fig. 1d). At the moment, the recorded basal displacement rates are less than 1 mm/month. Actually, since 1993, several inclinometer tubes have been installed, however data are discontinuous. Figure 2a reports the basal displacements against time for some old inclinometers, showing that the displacement rates ranged between a few cm/year and more than 10 cm/year. The inclinometer profiles show that the tube deformations were concentrated in narrow shear bands. Only in a few verticals, superficial soils exhibited a flow-like movement (Fig.3a). Consequently, superficial displacements can be considered representative of the landslide movement. So, to analyze with continuity the displacement evolution over the period 2011-2022, DinSAR data relating to COSMO-SkyMED (CSK), Sentinel-1 and Envisat constellations were analyzed. Figure 3b compares the time trend of CSK and Sentinel-1 horizontal displacements obtained for well W01; Figure 3c shows the 20 years series obtained for the same well considering CSK and Envisat data. Both figures show a decrease in the displacement rate of the 1st drainage system after the construction of the 2nd drainage system. The wells W02 and W03 exhibit lower displacement rates than W01 and similar rate decrease.

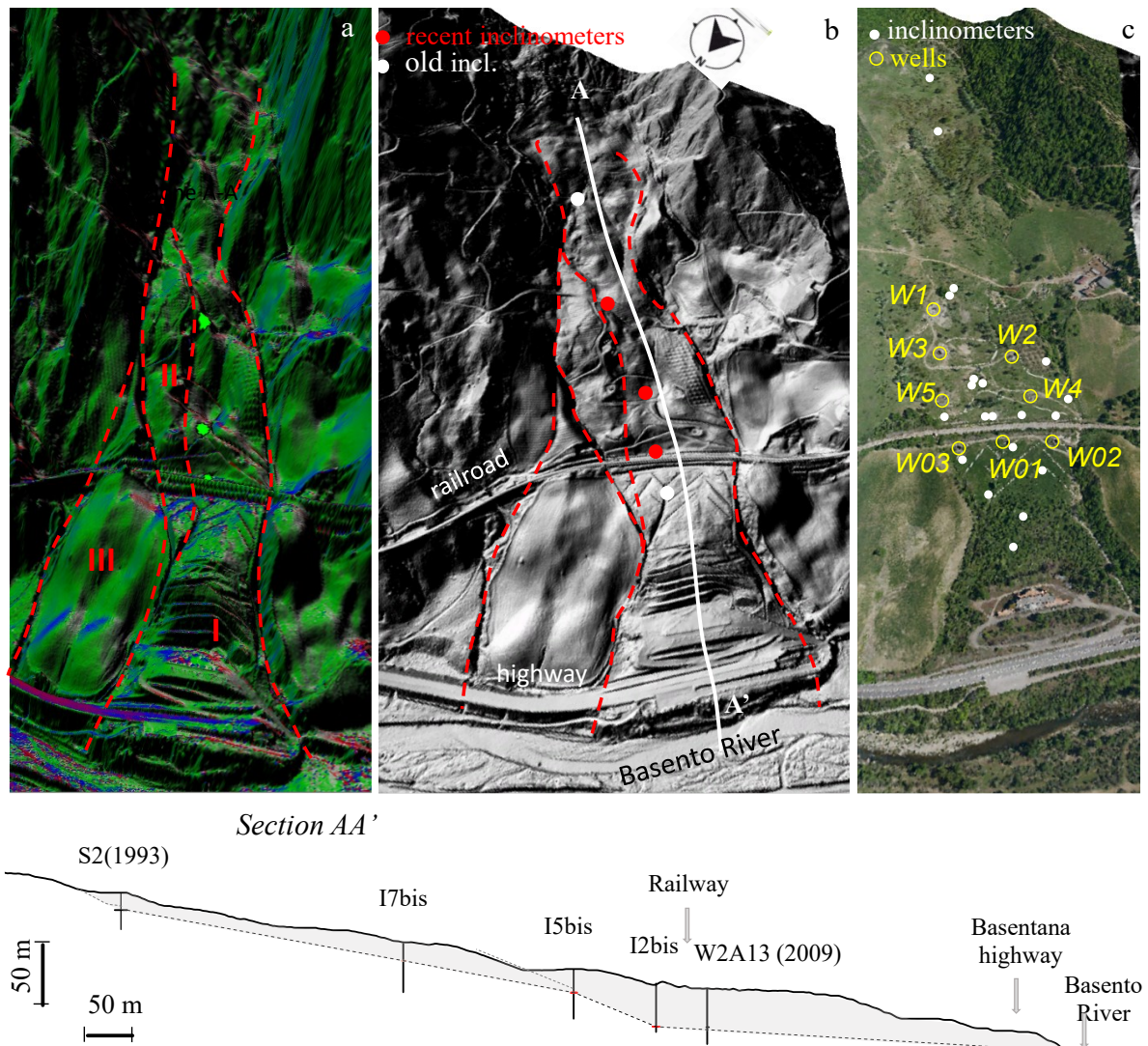


Fig. 1 Main landslide bodies: DTM with slope direction (a) and curvature (b) shades; drainage wells and inclinometers (c); section AA' with slip surfaces based on inclinometer profiles (d).

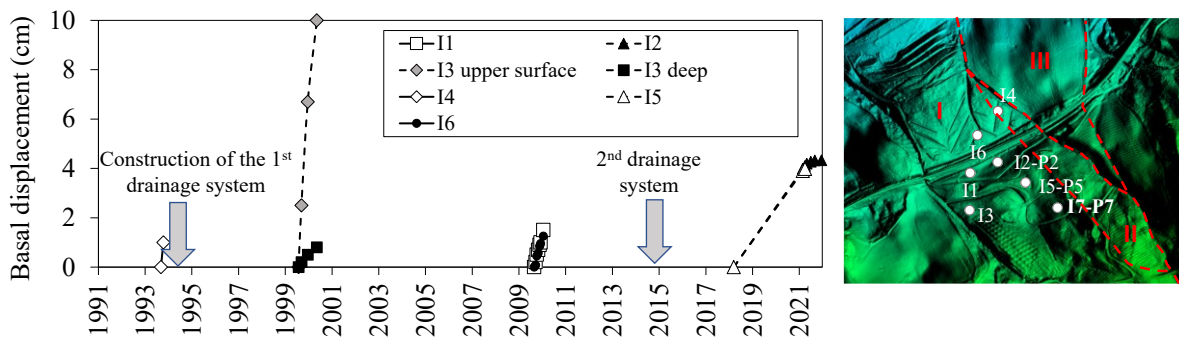


Fig. 2 Basal displacements and location of inclinometers I and piezometers P.

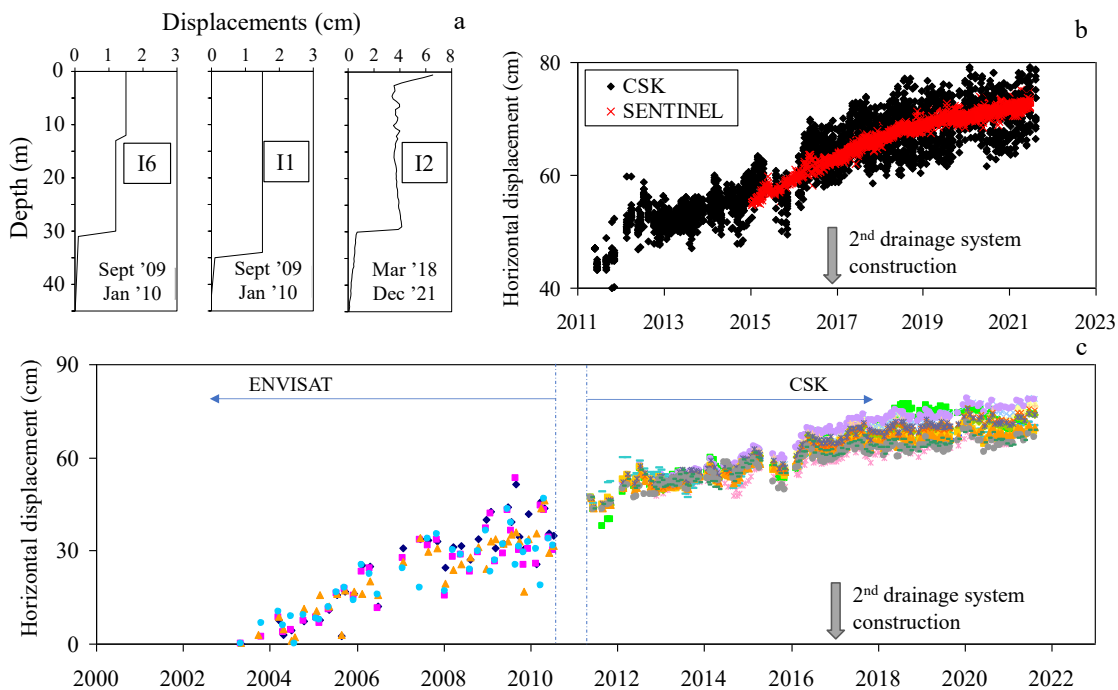


Fig. 3 Examples of old inclinometer profiles (a), time trend of horizontal displacements derived by Sentinel-1 and CSK images for well W01 (b); ENVISAT and CSK data for drainage well W01 (c).

Drainage systems and pore water pressures

The drainage systems constructed in 1993-1994 and 2016-2017 consist of three and five wells respectively, 7.5 m diameter and 15 m depth. The wells have not a structural function and they generally do not reach the slip surfaces. Three levels of sub-horizontal drains spread out 30 m from the wells. In the positions indicated in Fig. 2, three systems of Casagrande piezometers (P2, P5, P7) were installed in 2018. In each system, three piezometers at 10 m, 20 m and 30 m from the ground surface were installed. Figure 4 shows a slow but clear decrease of pore water pressures in all the piezometers. The data allow to evaluate the effects of the 2nd drainage system on pore water pressures, and thus on effective stresses and shear strength. To this aim, a 3D model of water flow in the landslide was used. The soil hydraulic conductivity was determined by means of falling head tests carried out in the piezometers P2, P5 and P7. Values ranging between 10^{-7} m/s and 10^{-5} m/s were obtained in the landslide, whereas values lower than 10^{-9} m/s were evaluated in the stable formation. Two limit cases were modelled by the FD code MODFLOW 3D, corresponding to two values of hydraulic conductivity in the landslide: a) k_1

= 10^{-6} m/s, and b) $k_1 = 10^{-9}$ m/s. For the stable soil, $k = 10^{-9}$ m/s was considered in both cases. The results relative to stationary conditions under continuous rain with high intensity (higher than the soil permeability) show that, for $k_1 = k = 10^{-9}$ m/s, drainage makes pore water pressure heights decrease of about 5 m in correspondence of the piezometers P2, P5 and P7. In the case of $k_1 = 10^{-6}$ m/s, the drain system is less effective, causing a reduction of 1 ÷ 2 m in water pressure heights, consistently with the experimental reduction recorded by the piezometers (Fig.4). It is worth noting that the water level in the piezometers is still showing a tendency to decrease, as clearly shown by Fig.4.

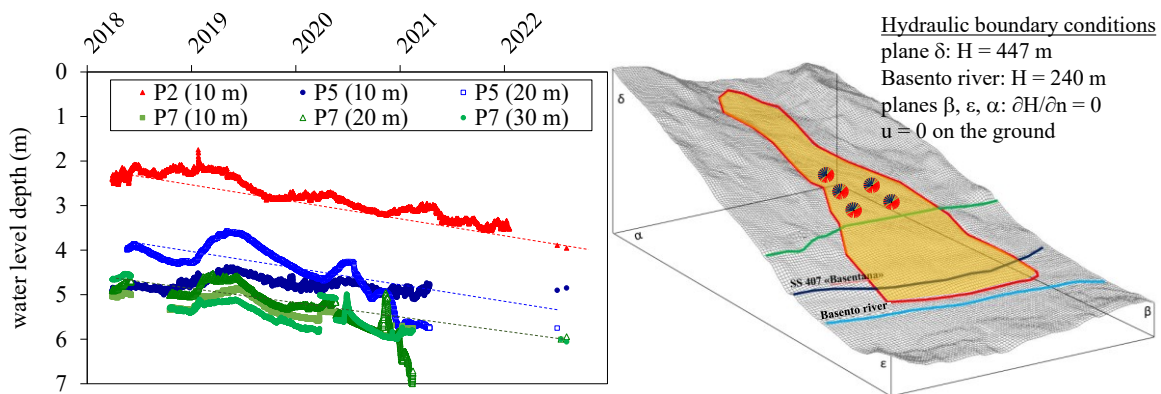


Fig. 4 Water level depth in the piezometers; flow domain and boundary conditions used in MODFLOW-3D.

Conclusions

This paper shows first results of the study of a large landslide system in structurally complex formations of the southern Italian Apennine chain, in which two deep drainage systems were built in different times. The analysis of the displacements of the landslide body and of the wells is based on available inclinometer data and DInSAR data. The displacement series show how the wells built in 1993-1994 move with the landslide. They also show that, after the construction of the second drainage system, the displacement rates of the old wells decreased from about 2 cm/year to less than 1 cm/year. The piezometric measurements show that, in the same period, water pressure progressively decreased in the well zone; the numerical 3D model suggests that the decrease can be the effect of the 2016-2017 drainage system. Continuous monitoring by new inclinometers and existing piezometers will allow the analysis of pore water pressure evolution and its influence on the landslide displacements.

Acknowledgments: This research is supported by MIUR PON R&I 2014-2020 Program (project MITIGO, ARS01_00964) and by R.F.I. Rete Ferroviaria Italiana.

References

- Di Maio C, Fornaro G, Gioia D, Reale D, Schiattarella M & Vassallo R (2018). In situ and satellite long-term monitoring of the Latronico landslide, Italy: displacement evolution, damage to buildings, and effectiveness of remedial works. *Engineering Geology* 245, pp. 218-235.
- Di Maio C, De Rosa J & Vassallo R (2021). Pore water pressures and hydraulic conductivity in the slip zone of a clayey earthflow: experimentation and modelling. *Engineering Geology*, vol. 292, <https://doi.org/10.1016/j.enggeo.2021.106263>.
- Vassallo R, De Rosa J, Di Maio C, Reale D, Verde S, Fornaro G (2021). In situ and satellite long-term monitoring of slow clayey landslides and of the structures built on them. *RIG (Italian Geotechnical Journal)*, year LV, 4, 77-95.

Including the impact of climate change in quantitative risk analysis: an example from Kaikōura, New Zealand

Saskia de Vilder¹, Chris Massey¹, Marc Andre Brideau², Biljana Lukovic¹, Regine Morgenstern¹, Dougal Townsend¹, Brenda Rosser¹

¹ GNS Science, Lower Hutt, Wellington, New Zealand

²BGC Ltd, Victoria, British Columbia, Canada

SUMMARY: We present an example of a quantitative risk analysis (QRA) of landslide hazards at a regional scale for Kaikōura, New Zealand, which has been used to inform land use planning policy. We estimated life risk from debris avalanches, rock avalanches and debris flows within the Kaikōura region from earthquake and rainfall triggers. We utilized regional scale tools, including empirical runout models and susceptibility models, to give an estimate of the number of landslides generated for a particular triggering event, the size of the landslide and runout impact area. Our results indicate that rainfall induced landslides dominate the risk profile over earthquake induced landslides, due to rainfall events occurring more frequently and wetter rainfall debris travelling further. This also emphasises the need to account for climate change scenarios.

Keywords: QRA, Climate Change, Rainfall induced landslides, Earthquake Induced Landslides

Introduction

There is a increasing need for spatial information and maps of landslide hazard and risk that can be used to inform risk management, in particular, land use planning (Corominas *et al.*, 2014). We present an example from Kaikōura, New Zealand of a quantitative risk analysis (QRA) of landslide hazards at a regional scale, which has been used to inform land use planning policy (Massey *et al.*, 2022a). We account for earthquake induced landslides and rainfall induced landslides. Additionally, as climate change is expected to change the intensity and frequency of landsliding (Gariano and Guzzetti, 2016), we include climate change scenarios within the risk analysis process. The use of multiple risk scenarios allows us to understand the impact of changing input parameters, including climate change, on present and future landslide risk.

Methodology

We estimated life risk from debris avalanches, rock avalanches and debris flows within the Kaikōura region from earthquake and rainfall triggers (Fig 1). We estimated the local personal risk (LPR), which represents the annual probability of death for a hypothetical person present at a particular location for 100% of the time (24 hours a day for 365 days a year), and the annual individual fatality risk (AIFR), which represents the annual probability of death for a hypothetical person present at a particular location for 66% of the time. We firstly undertook landslide susceptibility mapping, where we determined the maximum credible source volume that could occur from a slope using local slope relief metrics and area to volume scaling

relationships (see Brideau et al., 2020 for more information). From these identified source areas, we used empirical relationships between landslide volume and Fahrböschung angles to determine landslide runout area for various landslides volumes up to 10 M m³. For each landslide source area and volume, we modelled two runout extents that represented the 50% (mean - σ) probability of exceedance and 16% ($\sigma + 1$ standard deviation SD) probability of exceedance.

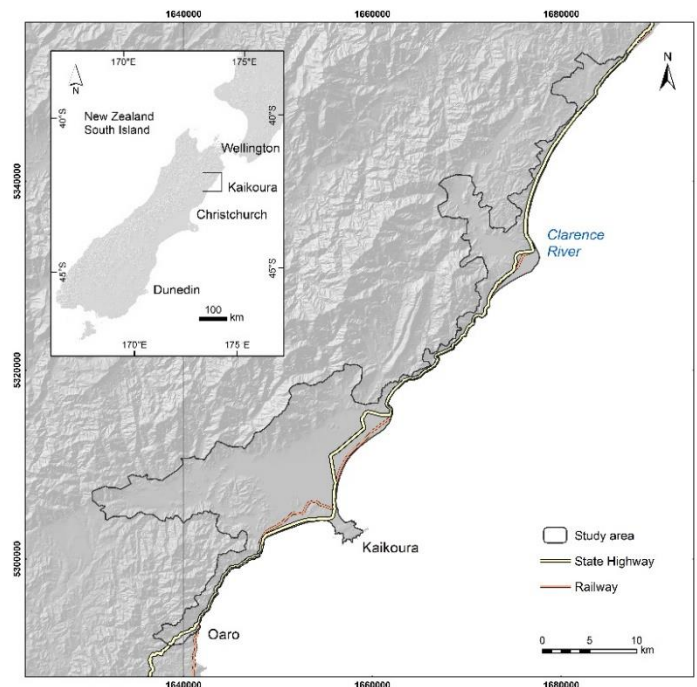


Fig. 1 Study area location, displaying the extent of the regional quantitative risk analysis (QRA).

Secondly, we used an earthquake induced landslide (EIL) probability model (see Massey et al, 2022b for more information) and a rainfall induced landslide (RIL) probability model (see Massey et al, 2022a for more information) to determine the number of landslides that could occur for a particular trigger event. For both the EIL and RIL probability model, the forecast number of landslides matches the cumulative number of observed landslides in the training datasets, and therefore the sum of the probabilities for each model will derive an estimate of the number of landslides produced for a particular triggering event. We forecast the number of landslides for four earthquake scenarios with annual return intervals of 100 years, 250 years, 500 years and 1000 years with the ground motion inputs for each of the return intervals derived from the national seismic hazard model (Stirling *et al.*, 2012). Similarly, we forecast the number of landslides for three rainfall scenarios with annual return intervals of 50 years, 100 years, and 250 years with the rainfall inputs derived from the national high intensity rainfall design system model (HIRDS: Carey-Smith et al., 2018). The HIRDS model can also output rainfall forecasts for different climate change scenarios, and we forecast the number of landslides for each of the three return intervals using an RCP 8.5 scenario. We used area-frequency relationships specific to earthquake induced landslides (Massey et al., 2020) and rainfall induced landslides (Massey et al., 2022a) to proportion the number of landslides into different landslide volume bins. From this, we calculated the probability of inundation using the probability of a landslide of a particular volume occurring and linking this through the probability of exceedance of landslide runout. We linked vulnerability to different landslide volume classes and probability of

exceedance zones (source, 50%, and 16%) based on changes in debris height (Pollock and Wartman, 2020).

Results

Our analysis of the risk maps shows that the risk from landslide hazards depends on the proximity from a person or dwelling to the steeper slopes and/or whether they are on debris flow fan. The main contributor to risk is from rainfall induced landslides, not considering climate change scenarios, with a factor of eight increase between the earthquake induced and rainfall induced risk model results. This is due to the more frequent nature of rainfall events compared with strong earthquakes, although the probability of a landslide occurring are higher for an earthquake than for a rainfall event with the same annual frequency. The risk from earthquake induced landslides also tends to decrease rapidly with increased distance from the toe of the steeper slopes, as the debris from earthquake induced landslide is assumed to be drier and therefore not travel as far as wetter rainfall induced landslide debris. Changes in landslide runout length and associated probability of exceedance for each Fahrböschung angle has the potential to alter the risk results and represents an important uncertainty. The risk from rainfall induced landslides increases to the north of the study area (Fig 1) due to increases in the rainfall intensity outputs from the HIRDS model and changes in geological materials, which are accounted for within the RIL probability model. The risk from earthquake induced landslides is highest along the steep coastal sections of the study area, and close to the highest mountain ranges in the study area (Fig 1). Fig 2 displays example outputs from the risk analysis. Increases in exposure from the AIFR with a person assumed to be present 66% of the time (Fig 2a) to LPR with a person assumed to be present a 100% of the time (Fig 2b) increases the risk by an order of magnitude with the buildings at the base of the slope shifting from 10^5 to 10^4 risk band to a 10^4 to 10^3 risk band. Similarly, accounting for the RCP 8.5 climate change scenario (Fig 2c) also results in an order of magnitude change in risk in the source regions of the slope. Changing the vulnerability value to a constant of 1 shifts the high-risk values (10^2 to 10^3 risk band) downslope (Fig 2d) and given the constant exposure and vulnerability values displays the risk of being affected by a landslide. Key uncertainties in the model are therefore changes in exposure, the impact of climate change on increasing rainfall frequency and the number of landslides generated from the RIL model.

Conclusion

We presented a regional scale quantitative risk analysis for Kaikōura, New Zealand. We utilized regional scale tools, including empirical runout models and susceptibility models, to give an estimate of the number of landslides generated for a particular triggering event, the size of the landslide and runout impact area. We estimated the risk for four different earthquake annual frequencies and three different rainfall annual frequencies. We modelled the impact of an RCP 8.5 climate change scenario within our rainfall risk models. Our results indicate that rainfall induced landslides dominate the risk profile over earthquake induced landslides, highlighting the importance of considering climate change scenarios which may alter the frequency and intensity of landsliding. The relative higher risk level associated with rainfall induced landslides was also a function of the wetter landslide debris runout travelling further than assumed drier landslide debris. Key uncertainties in our model are therefore the number of landslides generated by rainfall events, the frequency of rainfall events, changes in landslide travel distance, as well as the exposure and vulnerability of an individual to landslide hazards.

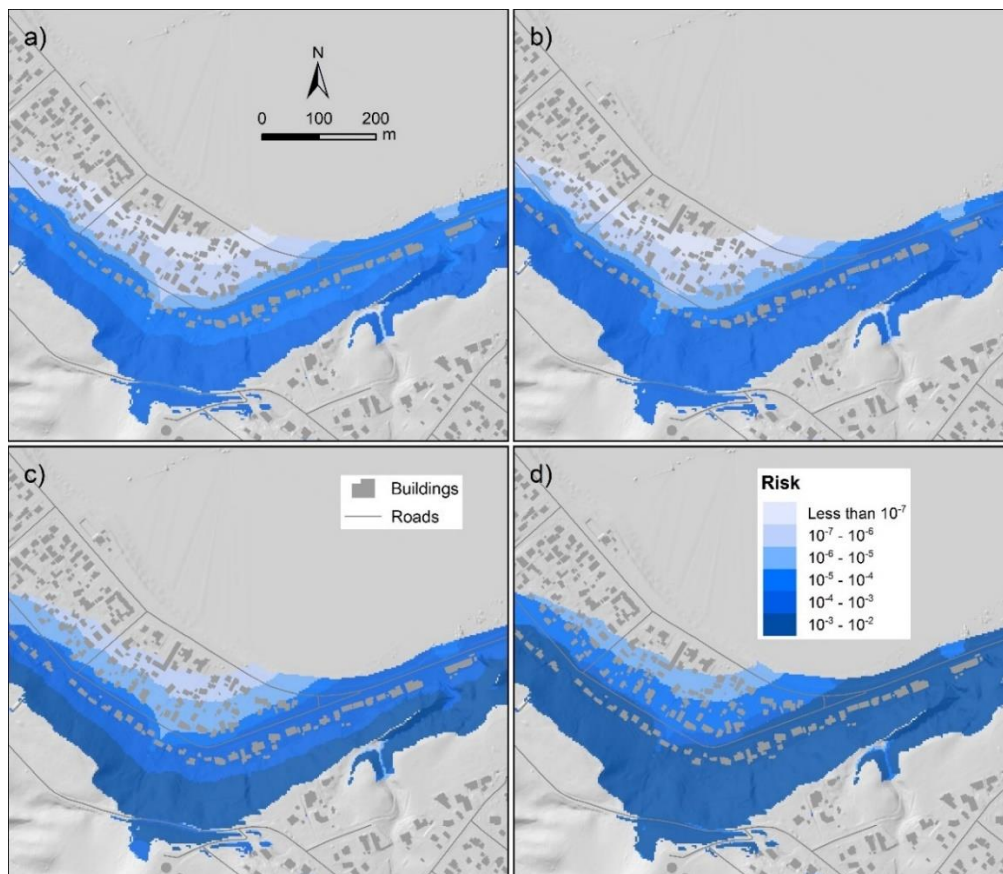


Fig. 2 Risk results from the central scenario, where a) displays annual individual fatality risk (AIFR) assuming a person is present in a building for 66% of the time, b) displays local personal risk (LPR) assuming a person is present in a building 100% of the time, c) displays LPR with an RCP 8.5 rainfall scenario, and d) displays LPR with an RCP 8.5 rainfall scenario and a vulnerability constant of 1.

References

- Brideau M-A, Massey CI, Lukovic B, Morgenstern R. (2020) Deterministic mapping of potential landslide debris inundation in the Kaikoura District. Lower Hutt (NZ): GNS Science. 37 p. *Consultancy Report 2019/102*. Prepared for Canterbury Regional Council. <https://www.kaikoura.govt.nz/assets/Uploads/CR2019-102-Deterministic-mapping-of-potential-landslide-debris-inundation-FINAL.pdf>
- Carey-Smith T, Henderson R, Singh S. (2018) High Intensity Rainfall Design System: version 4. Wellington (NZ): National Institute of Water & Atmospheric Research Ltd. 73 p. *Client Report 2018022CH*. Prepared for Envirolink.
- Corominas, J. *et al.* (2014) 'Recommendations for the quantitative analysis of landslide risk', *Bulletin of Engineering Geology and the Environment*, 73(2), pp. 209–263. doi: 10.1007/s10064-013-0538-8.
- Gariano, S. L. and Guzzetti, F. (2016) 'Landslides in a changing climate', *Earth-Science Reviews*. The Authors, 162, pp. 227–252. doi: 10.1016/j.earscirev.2016.08.011.
- Massey CI, Townsend DT, Lukovic B, Morgenstern R, Jones K, Rosser B, de Vilder S. (2020) Landslides triggered by the Mw7.8 14 November 2016 Kaikōura earthquake: an update. *Landslides*. 17(10):2401–2408. doi:10.1007/s10346-020-01439-x.
- Massey CI, Lukovic B, Huso R, Buxton R, Potter SH. (2022b) Earthquake-induced landslide forecast tool for New Zealand: version 2.0. Lower Hutt (NZ): GNS Science. (GNS Science report; 2018/08).
- Massey CI, de Vilder SJ, Lukovic B, Townsend DB, Rosser BJ. (2022a). District-scale landslide risk analysis of debris inundation for the Kaikōura District. Lower Hutt (NZ): GNS Science. 117p Consultancy report 2021/189. <https://www.kaikoura.govt.nz/assets/Uploads/Final-GNS-CR2021-89-Kaik-333-ura-Debris-Inundation-Risk-Analysis-FINA.pdf>
- Pollock W, Wartman J. (2020). Human vulnerability to landslides. *GeoHealth*. 4(10):e2020GH000287.
- Stirling, M. *et al.* (2012) 'National seismic hazard model for New Zealand: 2010 update', *Bulletin of the Seismological Society of America*, 102(4), pp. 1514–1542. doi: 10.1785/0120110170.

Time-dependent Shallow Landslide Hazard Mapping Using an Event-based Machine Learning Approach

Ann-Kathrin Edrich (edrich@mbd.rwth-aachen.de)^{1,2}, Anil Yildiz¹, Ribana Roscher³,
Julia Kowalski¹

¹ Methods for Model-based Development in Computational Engineering, RWTH Aachen University, Aachen, Germany

² AICES Graduate School, RWTH Aachen University, Aachen, Germany

³ Institute of Geodesy and Geoinformation, University of Bonn, Bonn, Germany

Current shallow landslide hazard maps are mostly static, meaning that they provide information about the general spatial risk of occurrence, yet do not necessarily represent the acute hazard in response to the predicted intensity of the triggering event such as extreme precipitation. Utilizing recent advances in forecasting and nowcasting extreme precipitation events is a natural next step to establishing time-dependent shallow landslide hazard mapping. Here, we suggest a generic shallow landslide hazard mapping workflow using an event-based machine learning algorithm which provides the option to generate time-dependent hazard maps. For its development, we are investigating the rainfall-triggered shallow landslide hazard in Switzerland as a test case scenario.

Keywords: shallow landslides, Random Forest, hazard mapping, time-dependence

Introduction

A single shallow landslide's damage potential and impact is often limited due to its localized spatial extent compared to deep-seated slope failures. Often, however, a single triggering event such as intense precipitation, may result in a large number of spatio-temporally correlated shallow landslides that in sum pose significant risks for population, infrastructure, and the environment. A hypothesized increase in extreme precipitation events due to global warming will further amplify those risks in many areas of the world. The spatial landslide hazard can be effectively communicated through hazard maps. Commonly, probabilistic hazard maps displaying the probability of occurrence are used (Regmi et al., 2014). Highly elaborate shallow landslide susceptibility and hazard mapping approaches have been produced in the last decades with the advancement of machine learning models and various computational tools. These approaches are generally derived, validated, and tested location-specific using datasets of regional or national importance. The challenge is to establish robust, reproducible workflows, which are a reliable fundament for model-based decision-support and allow tracking and managing of uncertainties. We contribute to the community through the description of a generalized workflow comprising the main steps of every shallow landslide hazard mapping study using machine learning: (1) conceptualization, (2) data preparation, and (3) the hazard map generation. Each step is accompanied, if applicable, by validation of its products and results. A particular focus will be on (1) flexibility of research question and data, (2) transparency of the mapping and validation, and (3) temporal dynamics meaning the option to generate time-dependent hazard maps. First results have been presented in Edrich et al. (2022). The workflow is set up in the process of working on the test case scenario of rainfall-triggered shallow landslide hazard in Switzerland. Switzerland was chosen as area of interest due to its alpine setting and the wide range of available open-access geodata.

Event-based machine learning for hazard mapping

Machine learning-based prediction is successfully applied in various research fields to investigate a wide range of research questions from regional to global scale (e.g. Betancourt et al., 2022). It has also taken a more prominent role in hazard mapping over the last years due to the increase in computational capability as well as publicly-available data.

Event-based approaches towards hazard mapping assume that future landslides will occur under similar conditions as past landslides (Merghadi et al., 2020). Using machine learning, patterns in the conditions of past events can be identified. These conditions comprise mostly static, meaning time-independent but also time-dependent features. The area of interest is then investigated for the occurrence of these patterns. In the case of a binary hazard map, i.e., hazard / no hazard, derived from only static features D , the prediction process can be described as:

$$f(D, A) \rightarrow \begin{cases} 0 & \equiv 0\% \text{ landslide hazard predicted} \\ 1 & \equiv > 0\% \text{ landslide hazard predicted} \end{cases}$$

where f is the mapping function, a Random Forest (RF) classifier in the present study, and A is the area of interest. Static binary hazard maps represent the susceptibility of the occurrence of landslides. RF is a machine learning algorithm that can account for complex interactions and non-linearities between the input variables making it ideal for complex, multi-feature problems such as hazard mapping (Taalab et al., 2018).

Equivalent descriptions can be made when integrating time-dependent parameters. The resulting hazard maps are valid as long as all included features do not change.

Training and prediction dataset

Training data for the RF model consists of a combination of features for historic landslide (presence) and absence locations. Absence data are non-landslide events sampled at locations where no documented landslides exist. For every presence and absence site, the prevailing environmental conditions are gathered and integrated into the training dataset as a set of features. The historic landslide database used in the regarded test case scenario is the *hangmuren database* by the Swiss Federal Institute for Forest, Snow and Landscape Research WSL (Eidg. Forschungsanstalt WSL, n.d.). From this dataset, 476 entries recorded on 12 different dates between 2002 and 2014 were extracted (see Figure 1 (b)).

Previous studies have proposed different approaches towards absence location sampling. One of the most common approaches for determining absence locations is random sampling among locations fulfilling set requirements (e.g. Taalab et al., 2018; Zhu et al., 2018). For this study, locations were sampled (1) with a slope angle of 20-50°, (2) outside of water bodies and impervious areas, and (3) away from presence locations. These requirements are based on expert knowledge. Before sampling, the number of absence locations with respect to the available number of presence data should be carefully considered as this decision might inherently transmit a probability of the occurrence. In the present study, a ratio of 1:1 was chosen. Figure 1 shows the locations of the sampled absence and presence locations.

Most studies use static features from the areas of topography, land cover, slope hydrology, and soil properties in landslide hazard mapping depending on the area of interest, availability as

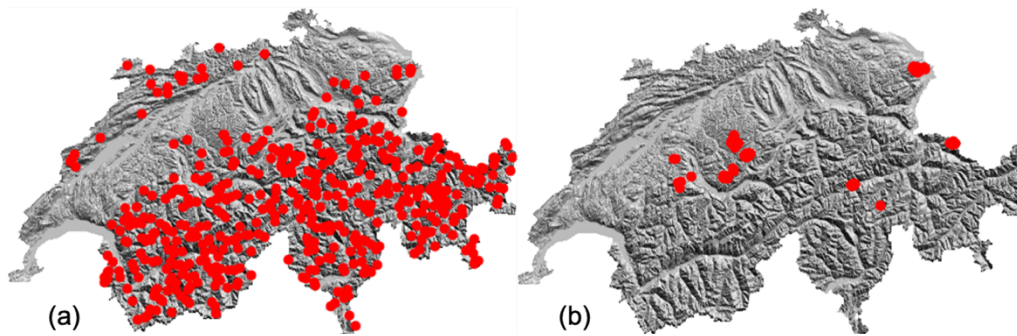


Fig. 1: (a) Sampled absence locations, (b) Presence data taken from the WSL landslide database

well as the quality of the datasets (e.g. Dang et al., 2019; Liu et al., 2021; Wang et al., 2020). This study includes the following static features: altitude, slope, aspect, USDA classes, sand, silt, clay content, coarse fragments, bulk density, land cover, tree cover density, max. precipitation in 20 years, and the parameters of the soil moisture retention curve.

Time-dependent features

Strong infiltration of water into the ground especially regarded over the course of several days can increase the probability of the occurrence of shallow landslides (Wang et al., 2020). Precipitation is therefore an important factor and allows the generation of time-dependent hazard maps that can account for changes in the spatial distribution of the hazard due to the precipitation forecast. Generally, two possible ways of incorporating precipitation into the workflow can be distinguished: (1) as a true time-dependent feature or (2) as a static feature representing precipitation characteristics (e.g. maximum observed precipitation). The definition of a time-dependent precipitation metric is not straightforward as it needs to preserve the data's time-dependency and has to be available for both absence and presence locations. If included at all, previous studies incorporated precipitation data through precipitation thresholds (see Caine, 1980), randomly sampled precipitation values for the absence locations (e.g. Stanley et al., 2021), or as a static parameter (e.g. Dang et al., 2019). In this study, we exploit the availability of long-term precipitation time series to define a suitable metric. The combination of rainfall patterns with the observed rainfall amounts at the time of landslide occurrences in the database allows the definition of probability thresholds that can also be applied to other locations in the area of interest. Further investigations are currently conducted to assess the predictive capabilities of different metrics.

Preliminary result

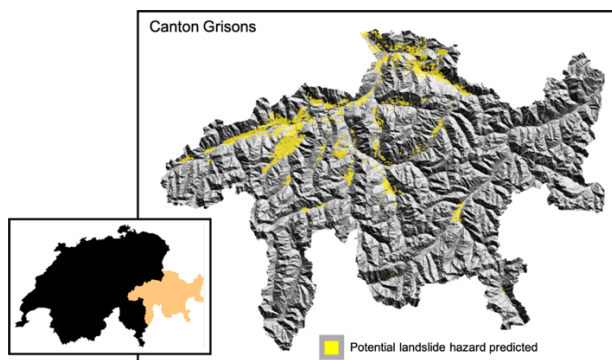


Fig. 2: Shallow landslide hazard map of Grisons

Figure 2 shows the preliminary prediction result for the Swiss canton Grisons derived using the described methodology. The resolution of the final hazard map is 25m. It can be seen that landslide hazard is mainly predicted in the north of Grisons. The total area with predicted landslide hazard is 383km².

Validation

Validation shall be conducted throughout every step of the mapping process, starting with the assessment of the quality of the input datasets, followed by a validation of the model and the final hazard map. Both the quality of the model and the resulting hazard map can be assessed by considering a confusion matrix containing the four possible outcomes of the validation process: True Positive (TP), False Positive (FP), True Negative (TN), and False Negative (FN). TP and TN indicate correct predictions, whereas FP and FN form incorrect predictions. The quality of the model is most commonly assessed through the evaluation of the validation dataset (e.g. Liu et al., 2021). For the present study, this results in an MAE of 0.05.

Furthermore, the feature importance that the RF provides after training the model (see e.g. Taalab et al., 2018) can be used to identify missing scientific consistency of the model. For the prediction shown in Figure 2 the five most important features emphasize the importance of slope hydrology and topography through altitude, bulk density, maximum precipitation, and the parameters α and n of the soil moisture retention curve.

Conclusion

The basic structure for a workflow for event-based shallow landslide hazard mapping using an RF machine learning algorithm has been set up, allowing the generation of time-dependent hazard maps. Further work will be put into the refinement and supplementation of the workflow and its technical implementation with the aim of publishing the result as an open-access package.

References

- Regmi, N. R., Giardino, J. R., McDonald, E. V., & Vitek, J. D. (2014). A comparison of logistic regression-based models of susceptibility to landslides in western Colorado, USA. *Landslides*, 11 (2), 247–262.
- Edrich, A.-K., Yildiz, A., Roscher, R., & Kowalski, J. (2022). A modular and scalable workflow for data-driven modelling of shallow landslide susceptibility, EGU General Assembly 2022, Vienna, Austria, 23–27 May 2022, EGU22-4900, <https://doi.org/10.5194/egusphere-egu22-4900>.
- Betancourt, C., Stomberg, T. T., Edrich, A. K., Patnala, A., Schultz, M. G., Roscher, R., ... & Stadler, S. (2022). Global, high-resolution mapping of tropospheric ozone—explainable machine learning and impact of uncertainties. *Geoscientific Model Development*, 15(11), 4331–4354.
- Merghadi, A., Yunus, A. P., Dou, J., Whiteley, J., ThaiPham, B., Bui, D. T., ... & Abderrahmane, B. (2020). Machine learning methods for landslide susceptibility studies: A comparative overview of algorithm performance. *Earth-Science Reviews*, 207, 103225.
- Taalab, K., Cheng, T., & Zhang, Y. (2018). Mapping landslide susceptibility and types using Random Forest. *Big Earth Data*, 2 (2), 159–178.
- Eidg. Forschungsanstalt WSL, Forschungseinheit Gebirgshydrologie & Massenbewegungen. (n.d.). Datenquelle Hangmuren-Datenbank [Accessed: 2021-03-08]. <https://hangmuren.wsl.ch/>
- Zhu, A.-X., Miao, Y., Yang, L., Bai, S., Liu, J., & Hong, H. (2018). Comparison of the presence-only method and presence-absence method in landslide susceptibility mapping. *Catena*, 171, 222–233.
- Dang, V.-H., Dieu, T. B., Tran, X.-L., & Hoang, N.-D. (2019). Enhancing the accuracy of rainfall-induced landslide prediction along mountain roads with a gis-based random forest classifier. *Bulletin of Engineering Geology and the Environment*, 78 (4), 2835–2849.
- Liu, Z., Gilbert, G., Cepeda, J. M., Lysdahl, A. O. K., Piciullo, L., Hefre, H., & Lacasse, S. (2021). Modelling of shallow landslides with machine learning algorithms. *Geoscience Frontiers*, 12 (1), 385–393.
- Wang, Z., Liu, Q., & Liu, Y. (2020). Mapping landslide susceptibility using machine learning algorithms and gis: a case study in Shexian county, Anhui province, China. *Symmetry*, 12 (12), 1954.
- Caine, N. (1980). The rainfall intensity-duration control of shallow landslides and debris flows. *Geografiska annaler: series A, physical geography*, 62 (1-2), 23–27.
- Stanley, T. A., Kirschbaum, D. B., Benz, G., Emberson, R. A., Amatya, P. M., Medwedeff, W., & Clark, M. K. (2021). Data-driven landslide nowcasting at the global scale. *Frontiers in Earth Science*, 9, 378.

Probabilistic Analysis of the Performance of a Road Network Affected by Slow-Moving Landslides

S. Ferlisi¹, A. Marchese², D. Peduto¹, P. Gehl³

¹ University of Salerno, Fisciano, Italy

² Minister of sustainable infrastructures and mobility, Potenza, Italy

³ BRGM, Orléans, France

SUMMARY: This extended abstract presents the results of a study aimed at predicting the direct and indirect slow-moving landslide-induced damage to an undamaged road network by way of performance indicators and Monte-Carlo simulations. The probabilistic analyses are conceived to enhance the combined use of available remote-sensing (DInSAR) data and empirical fragility curves generated for Quantitative Risk Analysis (QRA) purposes.

Keywords: slow-moving landslides, damage, performance indicators, Monte Carlo.

Introduction

A landslide affecting an infrastructure may cause large detrimental effects in social and economic terms. Indeed, an event causing a direct damage on a small portion of a road, but requiring the closure of the road itself to the vehicular traffic, might induce indirect damages (e.g., increasing travelling time or reducing business activities) on a wider geographical area.

Referring to a case study of the Campania region (southern Italy), this extended abstract focuses on the prediction of direct and indirect damage to an undamaged road network induced by slow-moving landslides by way of performance indicators and Monte Carlo simulations.

Procedure and performance indicators

The proposed probabilistic procedure (Fig. 1) aims at analysing the performance of a slow-moving landslide affected road network – in terms of both (length of) severely damaged road stretches and (reduction of) travel time along a given path – by enhancing the combined use of remote-sensing (DInSAR) data and empirical fragility curves generated for Quantitative Risk Analysis (QRA) purposes. The latter provide the probability of reaching or exceeding a given damage severity level (D_i , $i = 1, 2, 3$), for instance according to the classification system given by Ferlisi et al. (2021), for a certain value of the considered slow-moving landslide Intensity Measure (IM). The procedure is comprised of sequential steps (Fig. 1) and makes use of the following indicators:

- Path Damage Extent (*PDE*), which is a measure of the damage – of either D_2 (from moderate to severe) or D_3 (very severe)

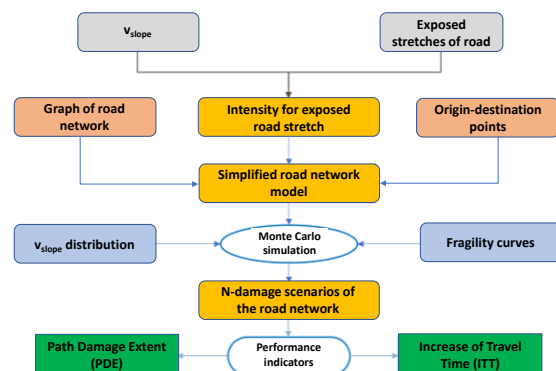


Fig. 1 Flowchart of activities to predict the direct and the indirect slow-moving landslide-induced damage to an undamaged road network (Marchese, 2020).

severity level – sustained by a road along the shortest path included between a given origin-destination pair of points. This indicator is computed as:

$$PDE = \frac{L_{AVE}}{L_0} \cdot 100 \quad [\%] \quad (1)$$

where L_{AVE} is the average length of the D₂/D₃ damaged portion of the above shortest path, whereas L_0 is the length of the shortest path.

- Increase of Travel Time (ITT), which is a measure of the increase of travel time between a given origin-destination pair of points (considering the shortest path) with respect to normal (i.e., undamaged) conditions due to the slow-moving landslide-induced road damage. This indicator is computed as (adapted from Gehl et al., 2017):

$$ITT = \frac{TT_{AVE} - TT_0}{TT_0} \cdot 100 \quad [\%] \quad (2)$$

where TT_{AVE} is the average travel time in damaged conditions, whereas TT_0 is the travel time in undamaged conditions.

Case study

The analysed road network develops within a territory extending for about 1600 km² and located within the national park of “Cilento, Vallo di Diano and Alburni” (south-western part of the Campania region, southern Italy); globally, it counts 59 municipalities.

The available slow-moving landslide inventory map at 1:5000 scale (Fig. 2a) comes from the results of activities carried out in 2012 by the former “Sinistra Sele” River Basin Authority within the Hydrogeological Setting Plan – Landslide Risk excerpt (Italian Law 365/2000). The inventoried landslides (summing up to 14,843) can be distinguished among rotational/translational slides, lateral spreads, (earth) flows, deep-seated gravitational slope deformations (DGSD), and creep phenomena. As for the road network, it mainly consists of urban roads and suburban secondary roads composed by single carriageways with two lanes, one per each travelling direction (Fig. 2b). Finally, the available dataset of DInSAR data is provided by the Italian “Ministry of the Environment and Protection of the Territory and the Sea”. It results from the Permanent Scatterer Interferometry (PSI) processing (Ferretti et al., 2001) of images acquired by COSMO-SkyMed (very high-resolution) radar sensors on both ascending (42 images from May 2011 to March 2014) and descending (42 images from October 2011 to December 2013) orbits. For further details the reader can refer to Ferlisi et al. (2021).

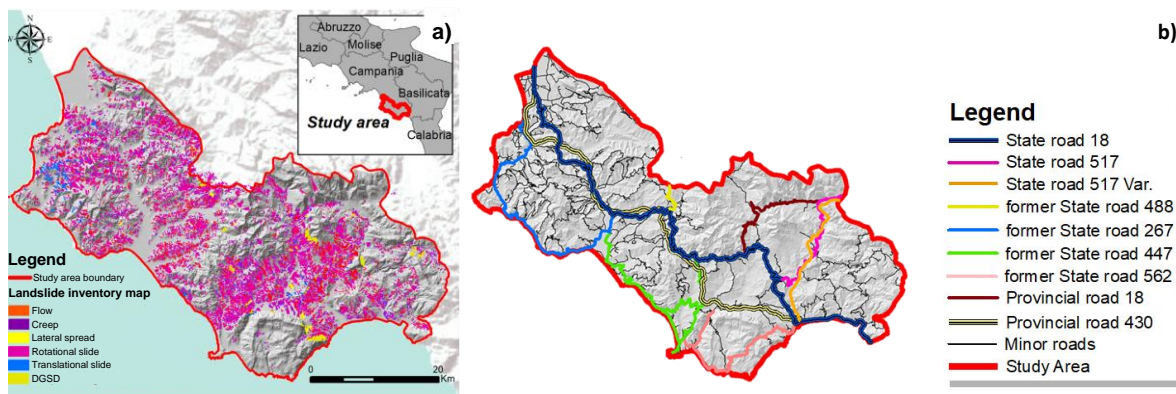


Fig. 2 a) Slow-moving landslide inventory map; b) analysed road network.

Results

The procedure shown in Fig. 1 was applied to both urban and suburban roads composing the network in the study area. First, by overlapping the landslide inventory map (Fig. 2a) to the road network (Fig. 2b) in a GIS environment, the exposed road stretches were identified. For those covered by COSMO-SkyMed PSI data, the values of the corresponding representative velocity along the steepest slope direction (v_{slope} , chosen as IM) were computed according to Ferlisi et al. (2021). Then, the road network was vectorized. The obtained computational net (Fig. 3) is composed of straight lines connected by nodes, each of them being associated with relevant information. The latter consists of: *i*) the administrative classification of involved road and the related free-flow travel speed (in undamaged conditions), *ii*) the interacting slow-moving landslide type and related IM value (if any), and *iii*) its original length (which relates to a real – not rectilinear – shape of the stretch). Out of 6,509 straight lines, 3,242 are exposed to slow-moving landslides and, therefore, affect the performance of the real road network. For probabilistic analysis purposes, 58 (out of 6,168) nodes were considered as “origin” points; they correspond to the centres of 58 urbanized municipal territories. To estimate the performance indicators by Eqs. (1) and (2), a “destination” node was selected. This corresponds to the centre of the municipality of Vallo della Lucania where the only Hospital of the study area is located.

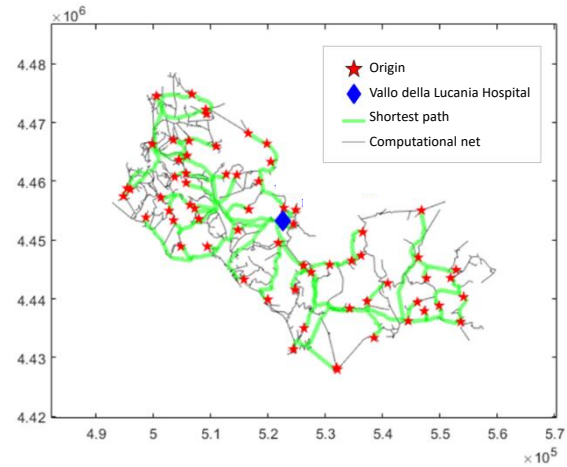


Fig. 3 Computational net and shortest paths between each origin-destination pair of points (Marchese, 2020).

Then, by using an ad-hoc algorithm implemented in the MATLAB® code, the shortest path – in terms of travel time (TT_0) – between each origin-destination (pairs of) points was retrieved. On the other hand, based on the available COSMO-SkyMed PSI data, 1,351 out of 3,242 exposed lines were not covered by remote sensing-derived information. For the latter, two work hypotheses were introduced to overcome the lack of information about the IM: stable conditions (i.e., $IM = v_{slope} = 0$ mm/year) or $v_{slope} = 16.6$ mm/y, which represents the 95% of probability of IM being at or below the selected threshold.

According to Fig. 1, empirical fragility curves generated for QRA purposes with reference to the same case study (Ferlisi et al., 2021) were used to determine the probability of reaching or exceeding a damage severity level (D_i , $i = 1, 2, 3$) for each of the exposed lines, given an IM value equalling the measured v_{slope} for PSI covered lines or, alternatively, the fixed $v_{slope} = 0$ or 16.6 mm/year for PSI not covered lines. Accordingly, two intensity scenarios were generated.

Based on Monte Carlo simulations, for each run (out of $N = 1000$) a damage severity level to be reached or exceeded by each exposed line was obtained by comparing a realization of the random variable (whose probabilistic distribution was assumed as uniform) with the probabilities retrieved – for a given intensity scenario – by way of the fragility curves. The obtained results were collected in a $[3,242 \times 1,000]$ damage matrix useful for the quantification of the performance indicators. In particular, for each run of the Monte-Carlo simulations, the direct damage was predicted for each shortest path between a given origin-destination pair of

points along with the corresponding D_2/D_3 damaged length. Finally, the Path Damage Extent (PDE) indicator was computed based on Eq. (1).

For each run of the Monte-Carlo simulations and taking account of functionality losses in terms of speed reduction – if applicable (Marchese, 2020) – the travel time (TT) was estimated for each shortest path between a given origin-destination pair of points. An example of the obtained results is shown in Figs. 4a and 4b for the shortest path having San Giovanni a Piro as origin point, considering the two intensity scenarios. Finally, the Increase of Travel Time (ITT) indicator was computed based on Eq. (2). It is worth observing that the cumulative distributions of data summarized in Figs. 4a and 4b are not coincident but enclose a narrow area (Fig. 4c) due to the lack of information about the v_{slope} values for some exposed lines. In the same Fig. 4c, the travel time in undamaged conditions ($TTO = 32.4$ minutes) is represented to highlight the increase of travel time due to D_2/D_3 road damage in the two intensity scenarios.

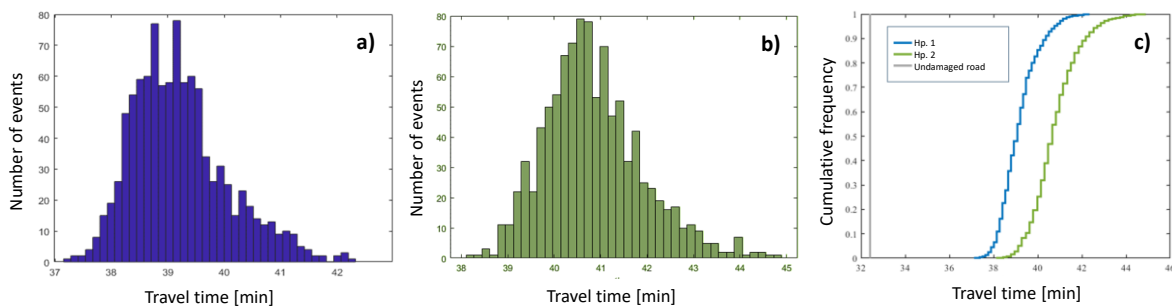


Fig. 4 a Number of events vs. travel time classes referred to the shortest path between San Giovanni a Piro and Vallo della Lucania Hospital obtained for the 1,000 runs of Monte-Carlo simulation and considering, as work hypotheses for not PSI covered exposed lines, $v_{slope} = 0$ mm/year (Hp. 1) and $v_{slope} = 16.6$ mm/year (Hp. 2); c relative cumulative frequency curves of the travel times retrieved for the same shortest path (Marchese, 2020).

Conclusions

This extended abstract showed the results of a probabilistic study – which made use of Monte Carlo simulations – aimed at analysing the performance of a road network in terms of (reduction of) travel time and (length of) severely damaged road stretches along a given path (i.e. the shortest). The knowledge of values pertaining to the performance indicators considered in the probabilistic analysis – which can be achieved at more affordable costs than those associated with the use of conventional monitoring techniques – allows for *i*) a proper understanding on whether a given road network would perform adequately during and after the occurrence of a given dangerous event and *ii*) the easy identification of the (most vulnerable) paths requiring mitigation measures, with a proper allocation of economic resources.

References

- Ferlisi S, Marchese A, Peduto D (2021) Quantitative analysis of the risk to road networks exposed to slow-moving landslides: a case study in the Campania region (southern Italy). *Landslides* 18(1), 303-319
- Ferretti A, Prati C, Rocca F (2001) Permanent scatterers in SAR interferometry. *IEEE Transactions on Geoscience and Remote Sensing* 39(1), 8-20.
- Gehl P, Cavalieri F, Franchin P, Negulescu C (2017) Robustness of a hybrid simulation-based/Bayesian approach for the risk assessment of a real-world road network. *Proceedings of the 12th International Conference on Structural Safety and Reliability*. 6-10 August 2017, Vienna, Austria, pp. 6-10.
- Marchese A (2020) Quantitative analysis of slow-moving land-slide risk to road networks. PhD Thesis, University of Salerno, Italy.

Effects of Soil Burn Temperature and Organic Content on Post-wildfire Debris Flow Mobility

Feihong Gao¹, Clarence E. Choi^{1*}

¹ Department of Civil Engineering, The University of Hong Kong, HKSAR, China
Correspondence (email: cechoi@hku.hk)

SUMMARY: Wildfires alter soil properties and generate runoff-triggered debris flows. To gain insight into the travel extent of post-wildfire debris flows, relevant rheological models must be selected. In this study, a series of experiments were conducted to investigate the effects of burn severity and organic content on the rheology of post-fire debris flow. In the experiments, kaolin clay with/without organic matter was burnt at temperatures of 400°C and 700°C. The burnt soil was then mixed with water to form debris flow mixtures. The rheologies of these mixtures were then measured using a rheometer. Test results reveal profound effects caused by the burning temperature and organic content on the rheology of post-fire debris flows. Consequently, these factors should be considered when carrying out routine hazard assessments to predict the mobility of post-fire debris flows.

Keywords: wildfire, debris flow, rheology, burn severity

Introduction

The frequency and intensity of wildfires have increased in recent years. These changes are strongly related to rises in global temperature and abnormally long drought periods (Sullivan *et al.* 2022). Consequently, a great deal of unexpected disasters linked to wildfires may occur, including post-fire debris flows, which are the mixtures of water, and burnt soil and organics, that surge downslope under the influence of gravity. Unlike debris flows in unburnt watersheds, debris flows in burnt watersheds are easily generated with little to no antecedent rainfall (Raymond *et al.* 2020). This is because wildfires combust organics and cause complex meso- and micro-scale changes to the soil, which makes them water-repellent (Alessio *et al.* 2021). Therefore, rainfall infiltration into slopes is reduced, while runoff increases to pick up burnt soil and organics to bulk into a debris flow (Rengers & McGuire 2021).

Current field studies of post-fire debris flow mainly focus on forecasting the frequency and magnitude of events based on burn severity and rainfall intensity-duration (Kean *et al.* 2021). Hoch *et al.* (2021) back-analyzed field data of soil-infiltration capacity, vegetation cover, runoff, and debris-flow behavior to reveal rainfall intensity thresholds for revealing the initiation of post-fire debris flows. Alessio *et al.* (2021) mapped the distribution of rills and measured their cross-sectional geometries to quantify the influences of runoff, lithology, and hillslope characteristics on the sediment volumes released by post-fire rill erosion. However, the existing research outcomes are catchment specific. More importantly, no research has been done to provide guidance to select an appropriate rheology to model post-fire debris flows resulting from different burn severity and organic content.

The rheology of post-fire debris flows is expected to be strongly influenced by burn severity, which changes the physical and hydraulic properties of the geomaterial involved (Sarro *et al.*

2021). Research has shown that the yield stress and rheology are strongly affected by these changes (Torrance 1999). Wildfires also consume organic matter, which alters the rheology of a soil suspension. Carotenuto *et al.* (2015) investigated the effect of the soil organic carbon content on the rheology of a concentrated natural slurry and reported that the yield stress and viscosity decreased with organic content.

In this extended abstract, experiments that simulate post-fire debris flows and their rheological characteristics are carried out. The soil comprising the debris flow mixtures are burnt at different temperatures and the burnt organic content is varied. Details of the experimental setup and some preliminary results are presented.

Methodology

The burning effect of wildfires on soils is modelled with an ashing furnace (Fig. 1), which has a maximum operating temperature of 1100°C. Since burning silica-based sand and gravel have minimal effects on their properties, only kaolin clay with and without organic content is burnt. The temperatures reached in soils during natural wildfires can be up to 700°C where high loads of heavy fuels are present (Mataix-Solera *et al.* 2011). Therefore, the burning temperature of 400°C and 700°C were tested. An organic content of 10% (Maro *et al.* 1993) is compared to debris mixtures without organic content. The organic content consist of leaves from local vegetation.



Fig.1 Ashing Furnace used for experiments.

Before burning, each clay sample is placed in a quartz-based ceramic tray, which can endure temperatures of up to 1500°C. Once the furnace temperature reaches the preset temperature, a soil sample is placed inside the furnace and the heating time is recorded. The burning duration is for one hour, which is widely used in the experimental studies on wildfires (Moody *et al.* 2005). After burning, each clay sample is cooled to room temperature and passed through a 35-um sieve to ensure that the particle size is suitable for rheological testing. The clay is then mixed with 60% water volumetrically. The rheometer used to measure the rheology of mixture samples is shown in Fig.2.



Fig.2 Rheometer used for experiments.

Test results and discussion

Fig.3 shows a comparison of the rheological measurements resulting from soil burnt at 400°C and 700°C, and with (10% by weight) and without organic content. The ordinate and abscissa show the shear rate $\dot{\gamma}$ (s^{-1}) and shear stress τ (Pa), respectively. The slope of these curves represents the viscosity. The intercept of the rheological curve along the ordinate represents the yield stress, which is a fundamental rheological property to describe whether a debris mixture will flow or come to rest.

Results exhibit a significant shift in rheology caused by burn temperature. At 400°C, the flow exhibits shear-thinning rheology. At 700°C, the flow behaves as Bingham fluid. Furthermore, organic content is also shown to strongly influence the rheology. Evidently, hazard assessment should consider the effects of burn severity and organic matter to improve predictions of the travel distance of post-wildfire debris flows.

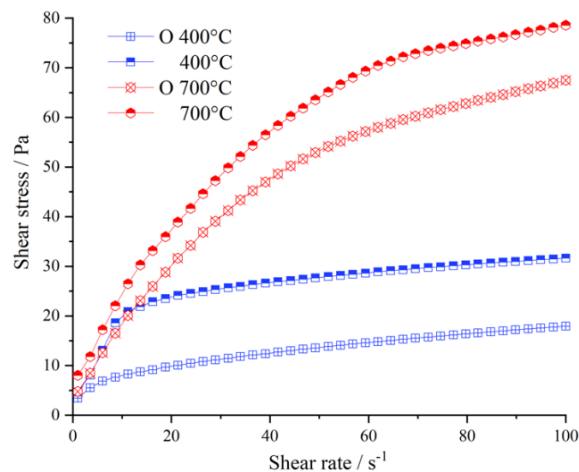


Fig. 3 Measured rheological curves for burnt debris mixtures with 40% gravimetric solid fraction.

Conclusions

The experimental procedure and some preliminary results were presented. Test results show that the burnt severity and organic content has a significant effect on the rheology of post-fire debris flow. Findings from this study are useful for advancing the knowledge base to select an appropriate rheological model to conduct hazard assessments of debris flow in burnt watersheds.

References

- Alessio P, Dunne T & Morell K (2021) Post-wildfire generation of debris-flow slurry by rill erosion on colluvial hillslopes. *Journal of Geophysical Research: Earth Surface* 126(11), e2021JF006108.
- Carotenuto C, Merola MC, Álvarez-Romero M, Coppola E & Minale M (2015) Rheology of natural slurries involved in a rapid mudflow with different soil organic carbon content. *Colloids and Surfaces A: Physicochemical and Engineering Aspects* 466, 57-65.
- Hoch OJ, McGuire LA, Youberg AM & Rengers FK (2021) Hydrogeomorphic recovery and temporal changes in rainfall thresholds for debris flows following wildfire. *Journal of Geophysical Research: Earth Surface* 126(12), e2021JF006374.
- Kean JW & Staley DM (2021) Forecasting the frequency and magnitude of postfire debris flows across southern California. *Earth's Future* 9(3), e2020EF001735.
- Maro RS, Chamshama SAO, Nsolomo VR & Maliondo SM (1993) Soil chemical characteristics in a natural forest and a Cupressus lusitanica plantation at West Kilimanjaro, Northern Tanzania. *Journal of Tropical Forest Science*, 465-472.
- Mataix-Solera J, Cerdà A, Arcenegui V, Jordán A & Zavala LM (2011) Fire effects on soil aggregation: a review. *Earth-Science Reviews* 109(1-2), 44-60.
- Moody JA, Smith JD & Ragan BW (2005) Critical shear stress for erosion of cohesive soils subjected to temperatures typical of wildfires. *Journal of Geophysical Research: Earth Surface* 110(F1).
- Raymond CA, McGuire LA, Youberg AM, Staley DM & Kean JW (2020) Thresholds for post-wildfire debris flows: Insights from the Pinal Fire, Arizona, USA. *Earth Surface Processes and Landforms* 45(6), 1349-1360.
- Rengers FK & McGuire LA (2021) Wildfire and earth surface processes. *Earth Surface Processes and Landforms* 46(6), 1099-1102.
- Sarro R, Pérez-Rey I, Tomás R, Alejano LR, Hernández-Gutiérrez LE & Mateos RM (2021) Effects of wildfire on rockfall occurrence: a review through actual cases in Spain. *Applied Sciences* 11(6), 2545.
- Sullivan A, Baker E & Kurvits T (2022) Spreading Like Wildfire: The Rising Threat of Extraordinary Landscape Fires.
- Torrance JK (1999) Physical, chemical and mineralogical influences on the rheology of remoulded low-activity sensitive marine clay. *Applied Clay Science* 14(4), 199-223.

Towards a Generic Methodology to Assess Instabilities and Retreat Rate in Flysch Seacliffs

L. Guillen¹⁻², Y. Thiery³, T. Dewez¹, C. Levy¹, P. Bourbon³, S. Caritg¹, P. Razin⁴,
L. Martins³, C. Garnier³, A. Cuccurullo², D. Gallipoli²⁻⁵

¹ BRGM, Orléans, France

² SIAME, Université de Pau et des Pays de l'Adour, Pau, France

³ BRGM, Pessac, France

⁴ École Nationale Supérieure en Environnement, Géoresources et Ingénierie du Développement Durable (ENSEGID), Bordeaux, France

⁵ Università degli Studi di Genova, Genoa, Italy

SUMMARY:

Flysch seacliffs are subject to various instability types and retreat rates. Characterizing the predisposing factors governing the erosion of these complex formations is a challenge to assess coastal landslide hazard. We propose a field observations-based generic methodology to assess the various instabilities and retreat rates of flysch seacliffs. For this purpose, we collected geomorphological and geological observations, including flysch facies, weathering, geological strength index and tectonics on two study sites of the French Basque coast. These data enabled us to build a decisional tree that we tested on other flysch seacliffs sites to assess the instability types.

Keywords: coastal erosion, seacliff, slope instabilities, flysch, generic methodology.

Abstract

Seacliffs represent 52% of the coast in the world (Young and Carilli, 2019). Seacliffs erosion by gravitational instabilities represents a risk for people and for economic activities. In order to predict these instabilities and to protect people, it is necessary to identify the types of instabilities contributing to erosion, the factors governing them and their contribution to retreat rates. In flysch seacliffs, the knowledge about variability of retreat rates (from 0.0034 to 1 m.yr⁻¹) and instability types is a challenge to assess coastal landslide hazard.

Cano and Tomás (2013) proposed a generic method for heterogeneous rocks such as flyschs, to identify their instability types and their geological and geomorphological contributing factors. This generic method gives a variety of predisposing factors combinations contributing to instability types. One theoretical advantage of the method is its applicability for different contexts, but the results are difficult to classify and to be transposed to other areas, moreover the rate erosion is not taken into account.

The aim of this work is to give a field observation-based transposable classification for flyschs seacliffs, to assess the geological and geomorphological factors conditioning their instability types and retreat rates. We believe the sedimentary facies classification of flyschs from Mutti and Ricci Lucchi (1972) could be a main predisposing factor to specific instability types. In addition, we believe that other factors such as weathering, tectonics, and strength indices may help to identify instability types and that the rate of erosion can be estimated from this information.

For this purpose we collected field observations in order to map instability types (Figure 1), geological units, geological strength index (Hoek and Brown, 1997; Marinós and Hoek, 2001), faults presence and the geometrical relationship between stratification and main slope (Cano and Tomás, 2013; Trenhaile, 1999). Geological field data are integrated into a 3D geological model based on GeoModeller (Calcagno et al., 2008)(Figure 2), in order to assess the influence of lithology and structures on landslide susceptibility in such heterogeneous contexts. This is synthesised within local conceptual sketches of instabilities (Figure 3) that enabled us to understand better the contributing factors to coastal cliffs evolution. In this way, this data enable us to: (i) test the method of Cano and Tomás (2013) on French Basque coast test sites, (ii) propose an improved instability types classification flow-chart based on a decisional tree integrating geological and geomorphological factors, including flysch facies, (iii) test this new method on other local and foreign flysch seacliffs. These various results will be confronted to retreat rates. The discussion will consider the variability of climatic and oceanic contexts and the possibility to adapt and to test the method on other flysch facies types.

The generic methodology developed here for flysch seacliffs aims to enable to characterize coastal instability types and retreat rates by field observations and simple indices. This method tested and validated for different flysch facies might be used in other geological contexts.



Figure 1: Itxas Gaïna compound landslide at Bidart, with rock block slide in marls and landslide in upper alluviums – Photography by CombyAVM 2018

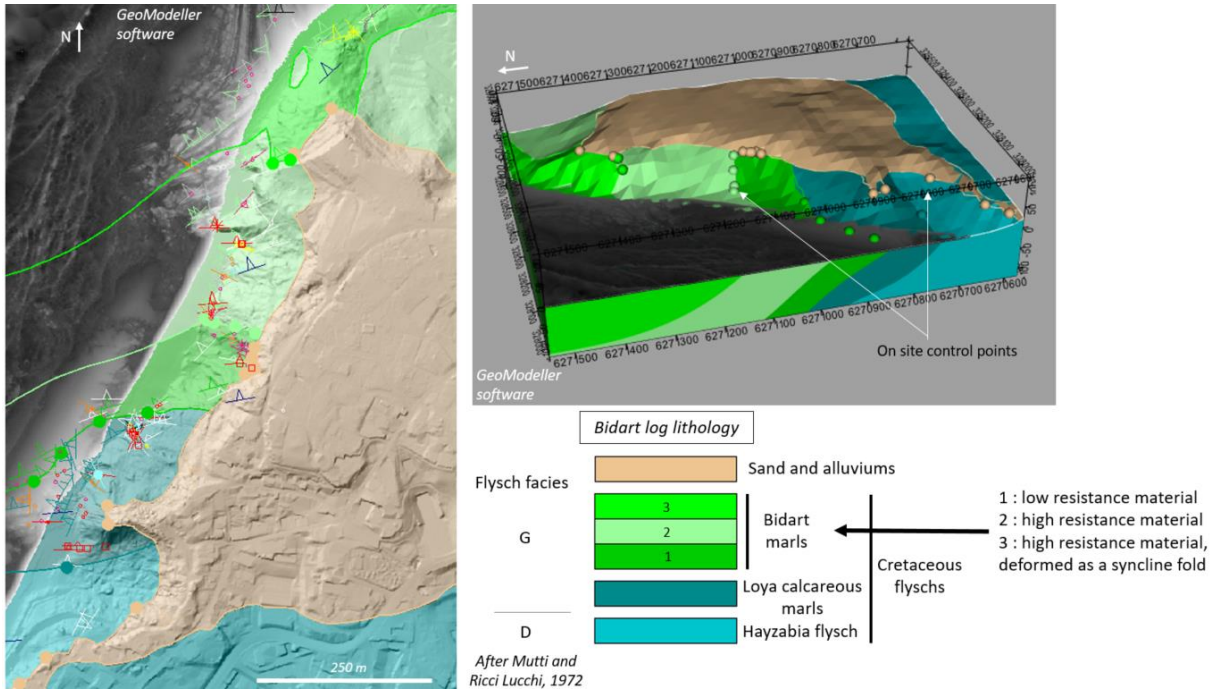


Figure 2: 3D geological model of Bidart flyschs and alluvium cover – GeoModeller (BRGM)

Conceptual sketch

of "la Corniche" Bidart cliff erosion

In facies G flysch composed of weakly resistant marls

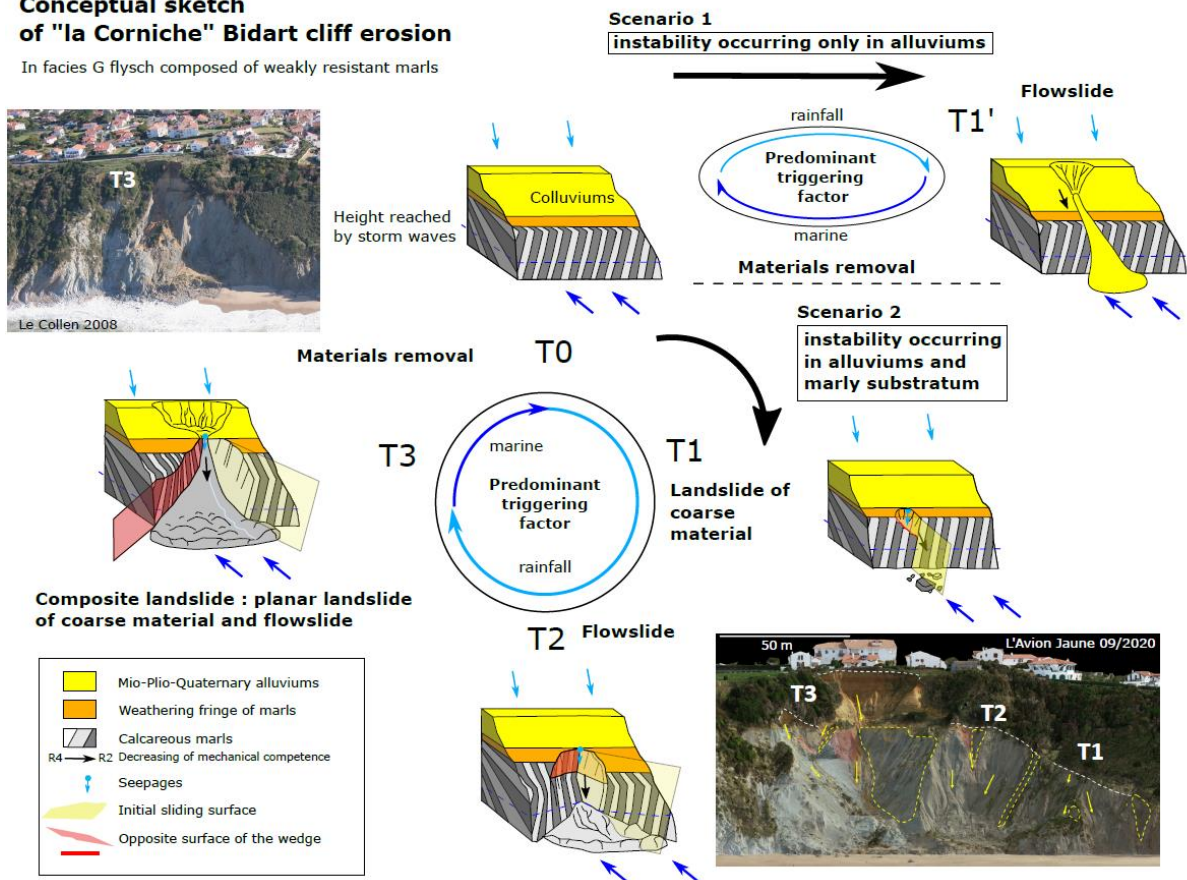


Figure 3: Conceptual sketch of “La Corniche” cliff erosion, in flyschs and alluviums, according to two different scenarii

References

- Young, A.P., Carilli, J.E., 2019. Global distribution of coastal cliffs. *Earth Surface Processes and Landforms* 44, 1309–1316. <https://doi.org/10.1002/esp.4574>
- Cano, M., Tomás, R., 2013. Characterization of the instability mechanisms affecting slopes on carbonatic Flysch: Alicante (SE Spain), case study. *Engineering Geology* 156, 68–91. <https://doi.org/10.1016/j.enggeo.2013.01.009>
- Mutti, E., Ricci Lucchi, F., 1972. Turbidites of the northern Apennines: introduction to facies analysis. *International Geology Review* 20, 125–166. <https://doi.org/10.1080/00206817809471524>
- Hoek, E., Brown, E.T., 1997. Practical Estimates of Rock Mass Strength. *International Journal of Rock Mechanics and Mining Sciences* 34, 1165–1186. [https://doi.org/S1365-1609\(97\)80069-X](https://doi.org/S1365-1609(97)80069-X)
- Marinos, P., Hoek, E., 2001. Estimating the geotechnical properties of heterogeneous rock masses such as flysch. *Bull Eng Geol Environ* 60, 85–92. <https://doi.org/10.1007/s100640000090>
- Trenhaile, A.S., 1999. The Width of Shore Platforms in Britain, Canada, and Japan. *Journal of Coastal Research* 15, 355–364.
- Calcagno, P., Chilès, J.P., Courrioux, G., Guillen, A., 2008. Geological modelling from field data and geological knowledge. *Physics of the Earth and Planetary Interiors* 171, 147–157. <https://doi.org/10.1016/j.pepi.2008.06.013>

A Massive Rockslide and Debris Flow Linked to Climate Change

Marte Gutierrez

Colorado School of Mines, Golden, CO 80401, USA

SUMMARY: On February 17, 2006, a massive rockslide followed by an extensive debris flow occurred in Guinsaugon on Leyte Island, the Philippines. The rockslide and debris flow followed several days of extensive rain, which was unusual and attributable to climate change. The rockslide created a large scarp on the 800-m high Mt. Canabac and generated a large volume of debris consisting of mud and boulders. The debris flow resulting from the slide completely inundated the village of Guinsaugon, located at the foot of Mt. Canabac, and killed about 1,328 inhabitants. Numerical modeling shows the potential link of the rockslide and debris flow with climate change.

Keywords: rockslide, debris flow, distinct element modeling, climate change

The Rockslide

On February 17, 2006, a large-scale landslide (see Fig. 1) occurred in the province of Leyte, an island in the central part of the Philippines. The slide originated on the eastern side of the steep rock slope of Mt. Canabac and buried almost the entire village of Guinsaugon, St. Bernard town, resulting in the loss of life of 1,328 people, including 248 children who were in school at the time of the slide.



Fig. 1 View of the large-scale landslide in Southern Leyte.

The Leyte rockslide generated about 25 million m³ of debris consisting of mud and boulders, which were as thick as 30 m in some areas. The debris run-off distance was as much as 3.9 km. The houses along the debris path were believed to have been carried to distances as far as 550-600 m downstream from their original positions. The village's more than 300 houses and buildings, including an elementary school and a church, were destroyed. Most were completely buried under the debris. The 2006 Leyte rockslide is the most catastrophic single landslide event recorded in the Philippines and the first major landslide to occur in the 21st century.

The Guinsaugon landslide involved the movement of an extremely large piece of rock on the eastern face of the 800-m high Mt. Canabac, part of the mountain chain that sits on a geologic fault running north-south throughout the province. The scarp created by the slide is about 600 m high, 200 m at its deepest part, and about 600 m wide at its base. Reconnaissance surveys were conducted by a combined US-Philippine team led by the Author to characterize and understand the nature of the slide and the resulting debris flow (Gutierrez 2009). The reconnaissance studies involved LIDAR imaging, photography, compass orientation measurements and fault surface profilometry of the scarp failure surfaces, and interview of survivors who witnessed how the slide unfolded. Numerical modeling of the slide using the Distinct Element Method (DEM) was carried out using data from the field reconnaissance surveys to confirm the field observations and understand the rockslide's triggering and its potential linkage to climate change.

Triggering of the Rockslide and Link to Climate Change

The rockslide followed extensive continuous rain, which fell on the area from January 1 to February 17, 2006. The amount of rain is much higher than normal due to the weather phenomenon in the Pacific Ocean known as La Niña, which causes the cooling of the water surface temperature in the Pacific Ocean as opposed to the warming of water surface temperature during El Niño years. This weather pattern had significantly enhanced rainfall across the West Pacific region. El Niño and La Niña, or the El Niño-Southern Oscillation (ENSO), have become more frequent and intense due to climate change. The increase in the occurrence of ENSO and its intensity have been shown to correlate with the global temperature rise (Cai et al., 2015).

Based on the rainfall records obtained by PAGASA (Philippine Atmospheric Geophysical and Astronomical Services Administration) from 1980-2005 in the Otikon rainfall station, located in Libagon town about 7 km southwest of Guinsaugon and on the other side of the ridge, the average monthly rainfall during the typhoon season (November to January) in the vicinity of the slide is about 350 mm. For February, the average rainfall has been 275 mm since 1980. The nine-day rainfall (from February 8 to 16, 2006) before the landslide of 687.8 mm (Fig. 2) is more than 2.5 times the monthly average. In fact, the rainfall intensity registered for the whole month of February 2006 was 970.8 mm as shown in Fig. 2, the highest monthly rainfall ever recorded since 1980, including the typhoon season.

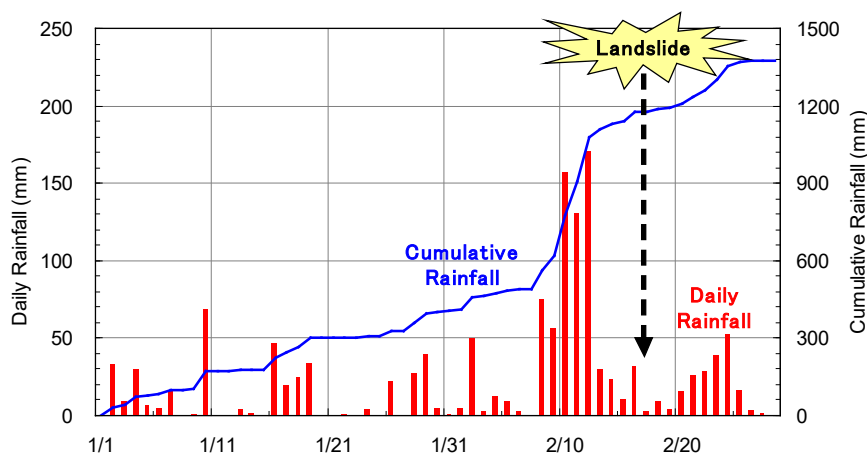


Fig. 2 Daily rainfall from January 1 to February 28, 2006, recorded near the rockslide site (Orense & Gutierrez, 2009).

During the reconnaissance survey of the slide, three major slide surfaces were identified on the scarp, which formed a complicated wedge structure. The fault, which forms the main part of the landslide scarp, is almost parallel to and is a splay of the PFZ (Philippine Fault Zone). It has not been previously identified as it had no visible exposure on the surface overgrown with vegetation, banana, and coconut trees. The primary slide surface is slickenside, as evidenced by its very smooth surface, which tends to shine like a mirror and reflect the sunlight when viewed at a distance. Initially, the rockslide was thought to have created the slickenside, as evidenced by vertical streaks running from the top to the bottom of the surface. However, a closer investigation of the surface and its morphology revealed that the vertical streaks are formed by fine materials sliding on the face of the slide. Also, the surface is smoother along the horizontal direction and undulated along the vertical direction. Thus, the surface was eventually identified as an existing fault, and the undulated surface was deemed to have been formed by gouging due to lateral movement along the fault. As verified by Schmidt hammer rebound tests, the fault surface was very hard from calcite mineralization.

Having recognized that the main failure surface is an existing fault, it is very likely that the slide was initiated along the fault. The rock mass then slid along the dip of the existing fault and failed by shear on the vertical surface on one of the faces of the scarp. Once the rock mass started to move, a third slide surface appeared at the bottom of the scarp, possibly along the bedding planes. However, the full extent and geometry of the failure surfaces and the scarp and the size of the initial sliding block cannot be completely ascertained as part of the scarp is partially filled with debris. Once the overhanging rock mass started to move, it cut through the two small hills at the foot of the mountain, creating a valley by which debris materials were transported.

Using 3DEC (Three-Dimensional Distinct Element Code) developed by Itasca (2008), DEM modeling was employed to simulate the initiation of the rockslide and the initial movement and breakage of the detached falling block. Using a Digital Element Model of the terrain before the slide and the scarp described above, a discontinuum model of the sliding block and scarp surfaces was created. The possible precursor event that was considered to have caused the triggering of the Guinsaugon rockslide was the continuous and unusually heavy rainfall up to the morning of February 17, 2006. The heavy rainfall is simulated by hydraulic pressurization and stepwise filling of the main fault with water. Water pressure increases linearly from the top of the rising water level in the fault. 3DEC is then used to determine whether the overhanging block will move against its own weight due to the increased fluid pressure along the fault. Under these conditions, the results should show the lateral-downwards movement of the overhanging block as an indication of rockslide triggering.

Simulations were carried out where the level of water in the fault was increased in stages by 25, 50, 75 and 100% of the fault height. At 50% and 75% water filling of the main fault, the displacement vectors are very small and mainly in the direction normal to the fault indicating hydraulic parting or opening of the fractures. The maximum displacements or degree of fracture opening are 0.04 mm and 0.15 mm for the fault's 50% and 75% filling. The overhanging block has not separated from the mountain even after 75% of the full fault height is filled.

At 100% water filling of the main fault, the overhanging block has started to move laterally and downwards, as was seen by the change in the directions of displacement vectors. Note that the triggering of the slide happened even though conservatively high values of shear strength

parameters in the Barton-Bandis joint model (Barton et al., 1985) were used for the scarp surfaces. Length-scale effects on shear strength, as prescribed in Barton & Bandis (1980), were not applied for the main fault, resulting in too high friction angles. The maximum displacement at this point is only 0.15 cm. Reduction of the friction angles to residual values will cause the slide to continue (Fig. 3a). The change in the direction of movement of the overhanging block for 100% pressurization was clearly seen in the tracking of the displacement history of a point on the surface of the overhanging block.

Once the slide was triggered, the falling block moved along the fault dip direction nearly as a rigid body by several meters along the main fault. As closer inspection shows, the overhanging block moved from its original position with a predominant mode of failure slipping along the scarp surfaces. This mode of failure is consistent with a witness account of the slide. The vectors of block displacements show that initially, the slide occurred downwards along the fault dip direction. The detached block continued to move downwards and started to break into blocks initiating the debris flow (Fig. 3b). It can be concluded that climate change directly contributed to the tragic event, having shown the unusual amount of rain before the slide pressurized and triggered the main fault.

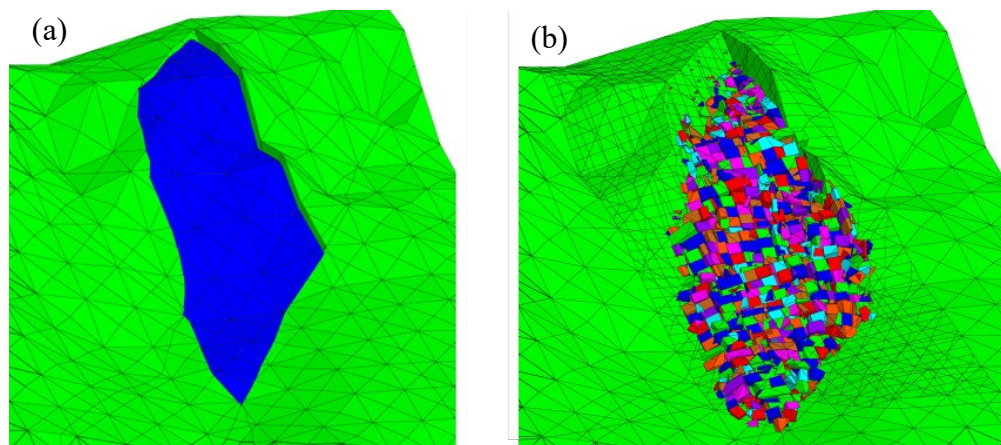


Fig. 3 (a) Initiation of the rockslide by the detachment of the main falling block, and (b) breakage of the main rockfall into smaller blocks initiating the debris flow.

References

- Barton N, Bandis S & Bakhtar K (1985) Strength, deformation and conductivity coupling of rock joints. *International Journal of Rock Mechanics & Mining Science & Geomechanics Abstracts*, 22(3), 121-140.
- Barton N & Bandis S (1980) Some effects of scale on the shear strength of joints *International Journal of Rock Mechanics & Mining Science & Geomechanics Abstracts*, 17, 69-73
- Cai, W., Santoso, A., Wang, G. et al. (2015) ENSO and greenhouse warming. *Nature Climate Change* 5, 849–859.
- Gutierrez, M. (2009) Use of LIDAR and DEM in the study of the massive February 17, 2006, Leyte, Philippines rockslide, *Proceedings of the International Symposium on Prediction Simulation Methods for Geohazards Mitigation*, Kyoto, Japan, Sept. 25-27, pp. 73-28.
- Itasca (2008) *3DEC: Three-dimensional distinct element code – Users' manual*, Itasca Consulting Group, Minneapolis, MN.
- Orense, R & Gutierrez, M (2009) The 2006 large-scale rockslide-bebris Avalanche in Leyte Island, Philippines, *Earthquake Geotechnical Case Histories for Performance-Based Design*, T. Kokusho (ed.), Chapter 2, 31-45.9

Negative Poisson's Ratio Auxetic Structures to Arrest Geophysical Granular Flows: Experimental Insights

Taikun Han¹, Jiaqi Zhang¹, Clarence E. Choi^{1*}

¹ Department of Civil Engineering, The University of Hong Kong, HKSAR, China

*Correspondence (email: cechoi@hku.hk)

SUMMARY: Geophysical granular flows, such as rock avalanches and debris flows, threaten human lives and infrastructure in mountainous regions globally. In recent years, flexible barriers have been proven to be an effective mitigation structure against geophysical granular flows. One of the practical limitations involved with flexible barriers is that they require cleaning after they are filled. To tackle this problem, 3D printing technology is used to develop negative Poisson's ratio auxetic structures (NPRAS), which can be used to form a flexible barrier net that can arrest the peak discharge of geophysical granular flows, while regulating the discharge of debris through it. In effect, NPRAS nets can achieve a self-cleaning function. To evaluate the performance of the newly-developed NPRAS, a new vertical chute experimental setup was designed. Details of the 3D printing process and experimental setup are described in this extended abstract.

Keywords: geophysical granular flows; self-cleaning flexible barrier, negative Poisson's ratio auxetic structures; 3D printing

Introduction:

Geophysical granular flows, such as rock avalanches and debris flows, threaten infrastructure in mountainous regions globally (Pudasaini & Hutter, 2007). In recent years, flexible barriers have proven to be effective countermeasures against geophysical granular flow hazards (Ashwood & Hungr, 2016; Ng et al. 2017). Compared to rigid barriers, flexible barriers are easy to install, cost-effective, and blend in well with the natural environment (Koo et al. 2017). However, flexible barriers need to be cleaned frequently to maintain their retention capacity and functionality to dissipate flow kinetic energy (Tan et al. 2019). Cleaning barriers may be difficult, especially if they are installed in catchments with high sediment loads or where access to the barrier is poor.

Designing flexible barriers that can regulate discharge through it while reducing the peak impact load remains an engineering challenge. Conventionally, a flexible barrier net, which is made using positive Poisson's ratio materials, elongates in the longitudinal direction by tension and contracts in the transverse direction when it is impacted. In turn, this reduces the porous area of the net and then the debris is trapped behind the barrier. In contrast, negative Poisson's ratio material can stretch in both the transverse and longitudinal directions upon impact, increasing the porous area for debris to pass through the net. Negative Poisson's ratio nets appear to be a promising technology to be adopted to progress towards self-cleaning flexible barriers. In this study, we propose to develop a self-cleaning barrier net by using negative Poisson's ratio structures. More specifically, 3D printing is used to manufacture flexible barriers consisting of unit cells of negative Poisson's ratio auxetic structures (NPRAS). The

performance of the printed nets is then evaluated by using a vertical chute experimental setup to impact the net with granular material.

Design and development of NPRAS net

To achieve a macroscopic negative Poisson's ratio, unit cells in a regular pattern are used to form a net. A simple re-entrant hexagonal cell is adopted (Thomas et al. 2013). Re-entrant means “inward” or with a negative angle. The geometry of the unit cell is shown in Fig. 1.

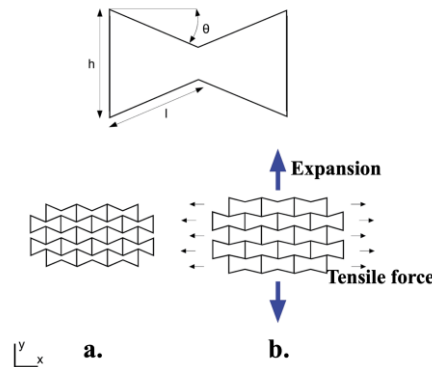


Fig. 1. Schematic diagram of a re-entrant hexagonal. The net structure can be obtained by arranging these unit cells. θ is the re-entrant angle, and h/l is the cell rib length ratio. **a.** The original shape of the net; **b.** The net is stretched in the longitudinal direction (i.e., x direction) and expands in the transverse (i.e., y direction) at the same time.

Before printing the net, the 3D model was rendered using Autodesk Inventor (2021) and exported to STL format to process for slicing. Slicing is the step of automatically dividing the 3d model into several layers according to predefined parameters. Supports are also added to the bottom of the model to prop the model up from the printer platform during printing. The processes of slicing and adding supports are shown in Fig.2.

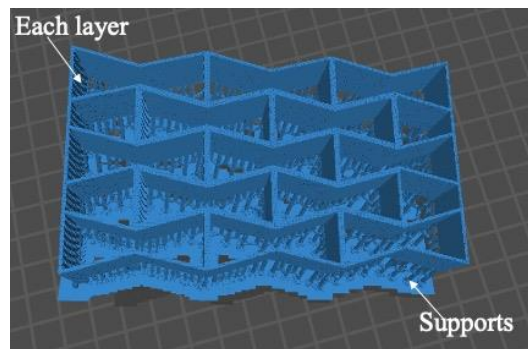


Fig. 2. 3D Model after processing (i.e., image is generated by slicing software Chitubox v.1.8.1 basic)

Printing input parameters, such as layer thickness and curing time, strongly affect the printing failure rate, printing time, and printing performance (Wang et al. 2017). The accuracy of the printer used in this study is 0.05 mm. Generally, the smaller the thickness of the single layer, the higher the printing accuracy, but at the cost of reduced printing speed (Liu et al. 2017). In this study, the model is not complex so there is no requirement for high accuracy. Therefore,

the layer thickness adopted is 0.07 mm. After determining the size of the model and the thickness of a single layer, the software automatically calculates the total number of layers required. The printing parameters used in this study are summarized in Table 1.

Table. 1 Printing parameters

Technical Parameters	Value
Layer thickness	0.07 mm
Curing time per layer	8 s
Total amount of layers	544

After the processed model is ready, it needs to be inputted into the 3D printer to print the NPRAS net. The material used is flexible photosensitive resin. Material properties are given in Table 2.

Table. 2 Material properties

Mechanical properties	Value (units)
Tensile stress	8.9 (Mpa)
Stress at 100% elongation	6.3 (Mpa)
Shore hardness	80 A
Tear strength	24 (kN/m)
Ross flex Fatigue	>200,000 (cycles)

After printing is finished, the printed NPRAS net needs to be cleaned with 95% alcohol to completely clear the uncured photosensitive resin from the model. The printed model is shown in Fig. 3.

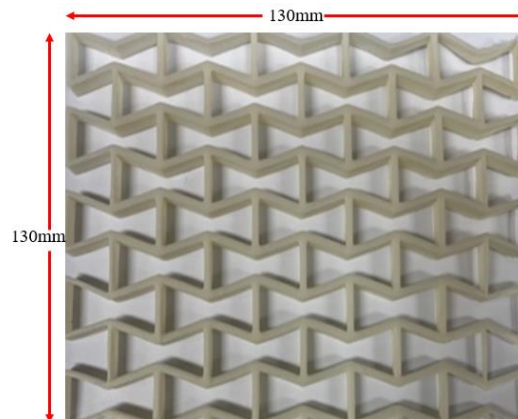


Fig. 3 3D-printed negative Poisson's ratio structure (NPRAS) net

To evaluate the performance of the NPRAS net, an experimental setup that can release granular material to impact the NPRAS net is required (Fig.4).

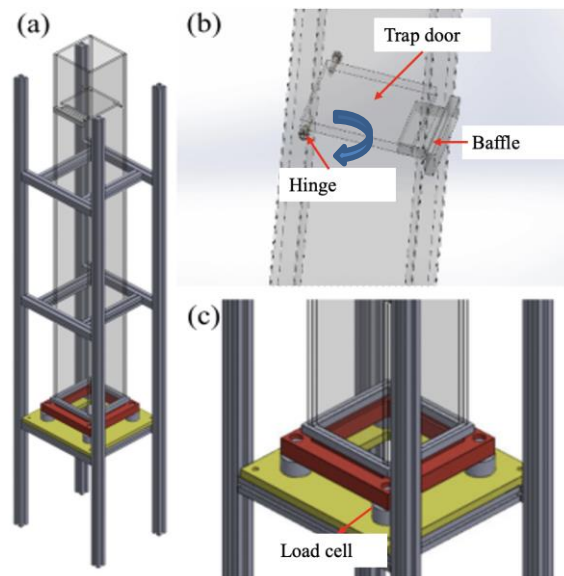


Fig. 4 Schematic of the experimental setup. **a.** Overview of the vertical chute; **b.** Schematic showing the working principle of the trap door; **c.** Enlarged view of the frame for mounting the net.

The experimental setup comprises a vertical chute, trap door, and frame to mount the net. The chute is made of acrylic walls to enable the kinematics to be observed and captured during the experiments. The chute has a total height of 1400 mm and a nominal cross-section length of 140 mm. The upper portion of the chute comprise the storage area for the granular materials, which are retained by using a trap door attached to a hinge. The door is released using the pin mechanism. A steel frame is fixed at the bottom of the chute to clamp and mount the NPRAS net in place. A load cell (max. 500N) is sandwiched at each corner between the frame and experimental setup to measure the total load exerted by the free-falling granular material.

Summary

Flexible nets with macroscopic negative Poisson's ratio were manufactured by using a 3D printer. A newly-designed vertical chute experimental setup was developed to verify the performance of the net. In future research, chute experiments will be conducted to evaluate the applicability of the self-cleaning flexible barrier under a wide range of impact conditions and granular flows with different particle sizes. It is expected that findings will be used to progress towards the development of a prototype self-cleaning flexible barriers using 3D steel printers.

Acknowledgement

This work was supported by the Research Grants Council of Hong Kong (AoE/E-603/18).

References

- Ashwood, W. and Hungr, O. (2016). Estimating total resisting force in flexible barrier impacted by a granular avalanche using physical and numerical modeling. *Canadian Geotechnical Journal*, 53(10), 1700-1717.
- Chitubox, Zhongcheng Future Industrial Park, Hangcheng Avenue, Baoan District, Shenzhen, Guangdong, China 518128
- Koo, R.C., Kwan, J.S., Lam, C., Ng, C.W.W., Yiu, J., Choi, C.E., Ng, A.K., Ho, K.K., and Pun, W.K. (2017). Dynamic response of flexible rockfall barriers under different loading geometries. *Landslides*, 14(3), 905-916.
- Kolken, H.M. and Zadpoor, A.A. (2017). Auxetic mechanical metamaterials. *RSC advances*, 7(9), 5111-5129.

- Liu, Z., Zhang, M., Bhandari, B., and Wang, Y. (2017). 3D printing: Printing precision and application in food sector. *Trends in Food Science & Technology*, 69, 83-94.
- Ng, C. W. W., Song, D., Choi, C. E., Koo, R. C. H., and Kwan, J. S. H. (2016). A novel flexible barrier for landslide impact in centrifuge. *Géotechnique Letters*, 6(3), 221-225
- Ng, C.W.W., Song, D., Choi, C.E., Liu, L.H.D., Kwan, J.S.H., Koo, R.C.H., and Pun, W.K. (2017). Impact mechanisms of granular and viscous flows on rigid and flexible barriers. *Canadian Geotechnical Journal*, 54(2),188-206.
- Pudasaini, S.P. and Hutter, K. (2007). *Avalanche dynamics: dynamics of rapid flows of dense granular avalanches*. Springer Science & Business Media.
- Thomas, C. C. and Durian, D. J. (2013). Geometry dependence of the clogging transition in tilted hoppers. *Physical Review E*, 87(5), 052201.
- Tan, D., Yin, J., Qin, J., Zhu, Z., and Feng, W. (2020). Experimental study on impact and deposition behaviours of multiple surges of channelized debris flow on a flexible barrier. *Landslides*, 17(7), 1577-1589.
- Wang, X., Jiang, M., Zhou, Z., Gou, J., and Hui, D. (2017). 3D printing of polymer matrix composites: A review. and prospective. *Composites Part B: Engineering*, 110, 442-458.

Rainfall-induced Landslides and subsequent Debris Flows in Regional-scale Areas

Sangseom Jeong¹, Moonhyun Hong²

¹ Yonsei University, Seoul, Republic of Korea

² Korea Forest Conservation Association, Daejeon, Republic of Korea

SUMMARY: This study describes a prediction method for rainfall-induced landslides and subsequent debris flows in regional scale areas. Special attention is given to the calculation of the propagation of debris flows by considering rainfall infiltration into soil slopes and soil entrainments by debris flows. A susceptibility assessment of landslides and debris flows in Umyeonsan (Mt.), South Korea was conducted as a case study by using a combined method for rainfall-induced landslides and debris flows. It is shown that the result of the analysis has a good agreement with historical landslides and debris flows. Based on the case studies, failure behaviors of landslides and debris flows are well predicted by the method described in this study. This procedure can be applied to the prediction of landslides and debris flows of another study area.

Keywords: Rainfall-induced landslide, Debris flow, Regional scale, Soil entrainment, Umyeonsan (Mt.) landslide

1 Introduction

Large-mass and high-velocity debris flows can be fatal to human society and infrastructures. Solving these dynamic problems with extremely large deformations over a short event time are slightly different from traditional problems in geotechnical engineering. It is highly difficult to reproduce debris flows in the field, so lab- or large-scale experiments or numerical simulations are usually carried out to better understand the mechanisms and assess the risks (Chen, H., & Lee, C. F., 2000).

This paper presents a simplified depth-averaged debris flow model for tracking density evolution. The developed model uses Hershel-Buckley rheology in internal and basal frictions and considers complex terrains and entrainments. In particular, the interaction between solid-fluid phases in the mixture is ignored. A proposed model is presented with relevant numerical schemes to obtain stable and accurate solutions. This work then validates some field case studies and multiple debris flow simulations.

2 Methodology

The governing equations derived by depth-averaging the Navier-Stokes equations can facilitate debris flow simulations at a large scale by reducing the computational cost compared to full-scale 3D simulations. The continuity equations for the mixture and solid phases and the momentum equations of the mixture phase are applied. More information on this model is presented in the previous research (Kang D., *et al*, 2020).

3. Modeling of debris flows

3.1 Study area description

The study area of Umyeonsan (Mt.) is located in the south-east of Seoul, Korea with a total area of 418 ha and an altitude ranging from 50 to 312 m. Between 8:30 to 8:50 a.m. on July 27, 2011, landslides and debris flows occurred simultaneously in the study area. A total of 151 landslides and 33 debris flows expanded from one or more landslides were reported (Jeong, S., *et al*, 2015). Figure 1 shows the location of the landslides and traces of the debris flows in the satellite image. In this study, simulation of the Umyeonsan (Mt.) landslides and debris flows was conducted based on the observed rainfall information at the time of the landslide occurrence, the site investigation results, and the simulation results were compared with the measured data.

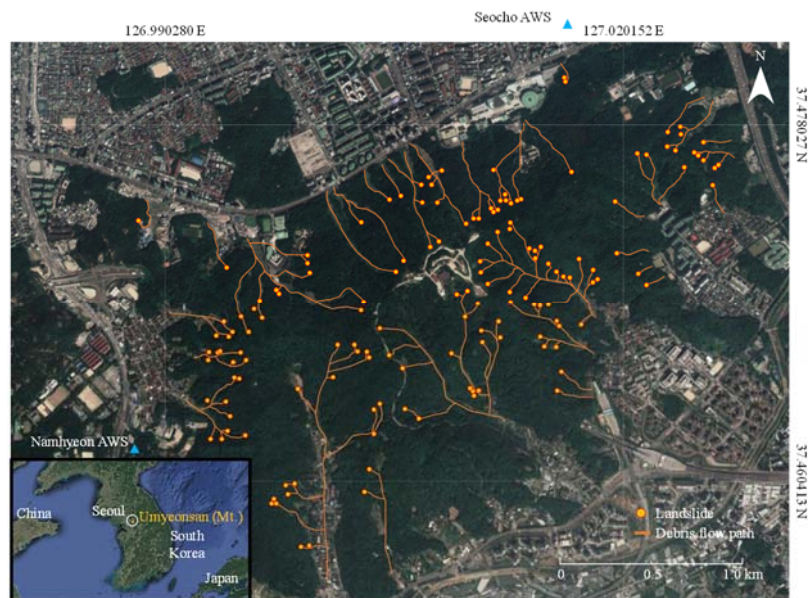


Fig. 1 Umyeonsan (Mt.) landslides and traces of the debris flows in the satellite image.

3.2 Modeling and input parameters

Two automatic weather stations are located near the study area: one is Seocho station and the other is Namhyun station (Fig. 1). The landslides occurred on the morning of July 27, and the hourly rainfall recorded ranged from 70 to 85 mm/h maximum. The cumulative rainfall was recorded as 424.5 mm at Namhyun station and 364.5 mm at Seocho station. These rainfall records were applied as rainfall input data for the rainfall-infiltration analysis and slope stability analysis.

Quercus mongolica was the most distributed species (43 %) and had a diameter at breast height of 23.1 cm and an average height of 10.7 m. From these investigations, the representative additional shear strength at the roots of the tree was determined as 1.0 kPa, and the uniform load by tree was estimated as 0.253 kPa (Kim J., *et al*, 2017).

Ground investigation was also conducted to determine the geotechnical and hydrological properties of the study area. Seven boreholes were drilled and in situ tests were conducted, including borehole shear tests. A series of laboratory tests including the soil water characteristic curve (SWCC) tests, direct shear tests and density tests were conducted to estimate the geotechnical and hydrological properties of the colluvium soil of the study (Kim J., *et al*, 2017).

Table 1 summarizes the input parameters applied to the landslide and debris flow simulations determined from the field and laboratory test results.

Table 1. Input parameters for the numerical simulation of Umyeonsan (Mt.) area.

Parameters	Values
Permeability (m/s)	8×10^{-6}
Initial water content	0.3
Deficit water content	0.2
Matric suction head (m)	0.83
Soil cohesion (kPa)	6.9-18.5 (11.7)
Soil internal friction angle (°)	21.7-32.1 (25.3)
Total unit weight of soil (kN/m ³)	18
Additional strength by roots of tree (kPa)	1.0
Additional load by tree (kPa)	0.253

3.3 Results and discussion

Fig. 2 shows the debris flow propagations of the entire study area after the landslide initiation ($t = 0$). The debris flow from the upstream to the middle of the mountain reaches the downstream after approximately 20 seconds. The sporadic landslides merge into the valley and flow downstream, and the thickness of the debris flow increases due to entrainment with time. A regional-scale analysis of rainfall-induced landslide and debris flows was conducted, and it confirmed that the proposed numerical method can offer meaningful prediction of rainfall-induced landslide and debris flows.

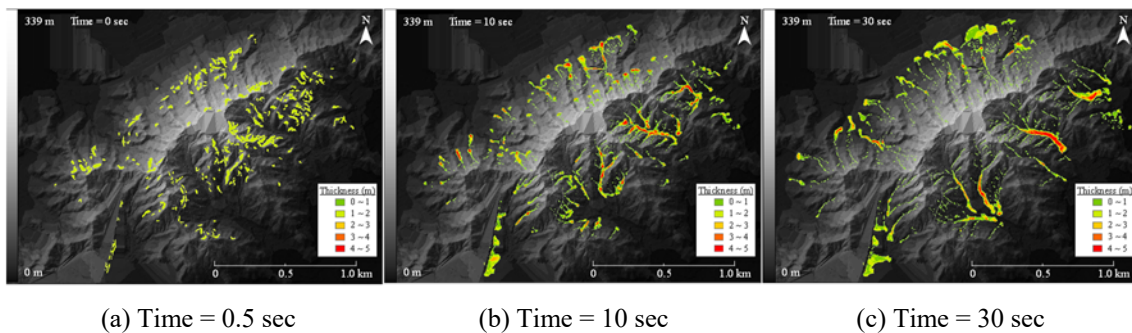


Fig. 2. Debris flow propagations from the numerical simulation

4. Conclusions

This work developed a simplified debris flow model with Hershel-Buckley rheology for tracking density evolution. By using the model developed in this study, it is possible to simulate not only reverse analysis after events but also the expandable debris flow induced by the input rainfall applied in engineering practice.

References

- Chen, H., & Lee, C. F. (2000). Numerical simulation of debris flows. *Canadian Geotechnical Journal*, 37(1), 146-160.
- Jeong, S., Kim, Y., Lee, J. K., & Kim, J. (2015). The 27 July 2011 debris flows at Umyeonsan, Seoul, Korea. *Landslides*, 12(4), 799-813.
- Kang D., Hong M., Jeong S. (2020). A simplified depth-averaged debris flow model with Herschel-Bulkley rheology for tracking density evolution:a finite volume formulation. *Bulletin of Engineering Geology and the Environment*, Vol. 80(7), pp 5331-5346.
- Kim J., Kim Y., Jeong S., Hong,M. (2017). Rainfall-induced landslides by deficit field matric suction in unsaturated soil slopes. *Environmental Earth Sciences*, Vol. 76(23), pp 808.

Earthquake Loading on Submarine Slopes Preconditioned by Marine Gas: Estimating the Triggering Potential Based on Stability Analyses

Pauline Kaminski¹, Jürgen Grabe¹

¹ Institute of Geotechnical Engineering and Construction Management, Hamburg University of Technology (TUHH), Hamburg, Germany

SUMMARY: The potential of preconditioning by gas under earthquake loading is investigated in this study. For this purpose, finite element limit analyses (FELA) were performed. In order to consider the negative influence of the gas in the analyses, further simulations with the constitutive model of Sultan and Garziglia (2014) were conducted. Stability analyses of a variety of possible slope geometries were performed and evaluated for the minimum earthquake load required to trigger failure. In conclusion, it can be stated that the slope geometries prevailing in reality have comparatively high stability reserves. In particular, steep slopes and large sliding bodies favour failure at even low earthquake loads.

Keywords: submarine landslides, gassy soil, earthquake, slope stability analyses

Introduction

Submarine landslides have been identified as a major geohazard to coastal communities and offshore infrastructure as they can initiate tsunamis and highly mobile turbidity currents. Thereby, they hold a substantial destructive potential. Nonetheless, the trigger mechanisms of submarine slide events remain uncertain for a variety of boundary conditions at the continental slopes worldwide. Recently, the occurrence of marine gases and the impact of enclosed gas bubbles on the soil's structure and shear strength has been investigated more closely from the perspective of triggering mechanisms (Berndt et al., 2012; Elger et al., 2018). However, marine gas occurrence was identified rather as preconditioning factor than a trigger mechanism for the largely prevailing slope geometries at continental slopes (Kaminski et al., 2021). Due to the scarcity of conclusive data on various influencing factors over geological timescales (such as the presence of gas) and their highly dynamic force, earthquakes are often considered as a possible failure initiator (ten Brink et al., 2009). Nevertheless, a generalized relation between seismic loading and slope failure has not been definitely established (Scholz et al., 2016). The complex mechanical behaviour of gas enclosed in the soil causes, depending on the properties of the gas deposit, an increasing or decreasing effect on the stability in case of additional earthquake impact. Free gas has a known mitigation effect regarding pore pressure build up under dynamic loading and thus prolongs a liquefaction failure. The extend of this effect depends, among other things, on the prevailing degrees of saturation as well as on the characteristics of the soil and loading (Grozic et al., 2000, Pietruszczak et al., 2003). This is contrasted with the scenario of a re-saturated soil, which exhibits a disturbed soil structure with large water-saturated cavities due to past gas release, e.g. from past periods with low sea levels. Such disturbed samples usually show lower shear strengths (Sultan et al., 2012), and thus it can be assumed that there is also a lower resistance to seismic loading. In this study, the latter scenario was investigated by applying the methodology presented in Kaminski et al. (2021). In order to make application possible in specific individual cases, the relationship between horizontal acceleration and earthquake magnitude is also addressed.

Stability Analyses of Submarine Slopes Under Earthquake Loading

The stability analyses presented herein are a further development of the simulations presented in Kaminski et al. (2021) and are therefore based on the same data set. For a more detailed description of the underlying laboratory tests and modelling, reference is therefore made to the methodology outlined therein. A fundamental difficulty in the study of submarine landslides is the lack of data on the slope geometry prior to the slide event. Therefore, a total of 1520 generic slopes with slope gradients between 0.5° to 20° (0.5° increments) and 1 m to 20,000 m slope length (logarithmic increments) were considered in the framework of this study. The assessment of the bearing capacity reserve of these generic submarine slopes under earthquake loading was carried out with the help of FELA using a shear dissipation controlled adaptive mesh with the commercial software Optum G2. The failure criterion was defined by the Generalized Tresca formulation. The seismic load is implemented as a horizontal acceleration in the direction of the slope acting in addition to gravity. Within the limit analysis the load is increased until failure of the slope. The result of the analysis is given as the relation $k_c = g_h / g_v$ where g_v corresponds to gravity. Accordingly, the failure-critical horizontal acceleration g_h can be expressed by means of k_c , which is equivalent to the gravitational acceleration percentage. The implemented soil conditions refer to laboratory testing which was conducted on a gravity core from 492 m water depth, south-west Mallorca, western Mediterranean Sea. The clayey silt contains low amounts of biogenic fine sand and shows an effective cohesion c' of 12.6 kPa along with an effective friction angle φ' of 32.7°. In order to be able to quantify the described effects of a cohesive soil that has been disturbed by previous gas exsolution, a constitutive model based on the critical state framework has been developed by Sultan & Garziglia (2014). This model was employed to simulate depth gradients of undrained shear strengths for different gas contents (hence damage levels) using the model parameters derived from the core described above. The simulations were conducted for 1 – 4 % of gas ($S_r = 0.99 - 0.96$) and the results were then implemented in the FELA model. Thus, all 1520 generic slopes could be modelled with five degrees of saturation each – four gassy scenarios and one fully saturated scenario. The results of the stability calculations are shown in fig. 1 for all geometry scenarios for full saturation ($S_r = 1.0$) as well as for a gas content of 4 % ($S_r = 0.96$).

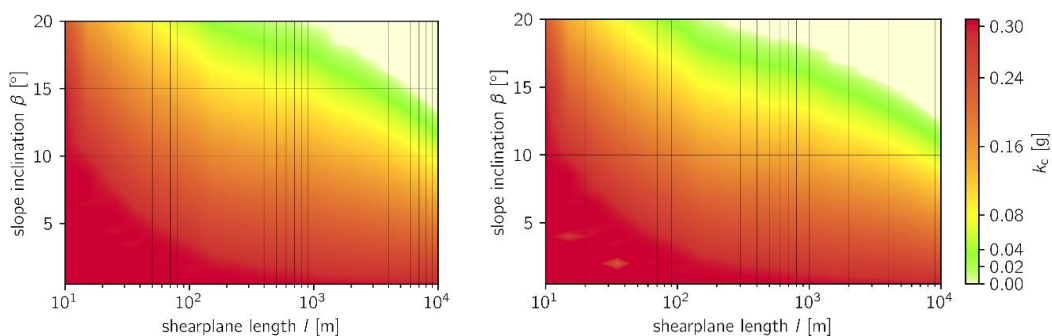


Fig. 1 horizontal acceleration required to induce slope failure depending on the slope’s geometry – left: in a soil with full saturation ($S_r = 1.00$), right: in a disturbed soil by previous gas exsolution ($S_r = 0.96$).

The colour scale describes the intensity of the seismic load resulting in a slope failure, as a percentage of the acceleration due to gravity. This can be interpreted in a wider scope as the peak ground acceleration (PGA) of a possible earthquake event. The beige coloured geometry scenarios ($k_c = 0$) are unstable even under static loads. The results show that the reduced shear strengths due to gas release generally lead to decreased critical seismic loads, but only to a limited extent. The number of slopes already unstable in the static state increases. Nevertheless,

especially the slope geometries with up to 2° inclination that are typical for large submarine landslide events still require high horizontal accelerations to fail.

The employed analysis approach only represents a very simple assessment of the situation and therefore only allows for a broad feasibility study. For a more specific interpretation of an earthquake's trigger potential, dynamic analyses and an evaluation of the earthquake duration and frequency are required. However, the reproduction of the gas influence on the soil mechanics has not yet been examined for this type of analysis, which therefore bears drawbacks as well.

Seismicity in the Western Mediterranean

In order to make the results of the stability calculations applicable in a specific case, a comparison of the prevailing seismicity in the area under consideration is necessary. However, due to the difficulties associated with local parameters such as PGA, earthquake intensities are often represented by global parameters such as magnitudes and location of the epicentre. The basic assumption when considering past earthquake events in this study is that today's earthquake-prone areas have also experienced increased earthquakes over geological time periods due to their tectonic position. Then, databases and hazard models were analysed. The data base of USGS (2021) does not contain registered offshore earthquake events from 1975 until today on the Balearic Promontory that exceed a magnitude of 5 on any magnitude scale. The mean magnitude of the 244 documented earthquake events is 2.85. All recorded events exhibit a shallow source. Numerous approaches exist to bring together global and local indicators for earthquake intensities in the form of ground motion prediction equations. However, due to their dependence on soil properties, these are strongly linked to the respective locations. For the Iberian Peninsula, reference is made to, among others, the approaches of Kotha et al. (2020) and Mezcua et al. (2008). In the following, the approach of Mezcua et al. (2008), developed for the Spanish mainland, is applied with the site classifications for stiff soil. The magnitude is expressed as moment magnitude M_w and is transposed into a PGA as a function of the distance to the hypocentre r_{hyp} (see fig. 3). The resulting PGA decrease significantly with increasing distance from the source and, especially at low magnitudes, hardly any noteworthy ground accelerations occur. Since it is the distance from the hypocentre, a very shallow source is therefore necessary to achieve significant PGA values at the surface. At this point, the influence of the magnitude scale and the location must be pointed out again, which can lead to a bias in the values, but which is considered acceptable for a basic estimation of the damage potential.

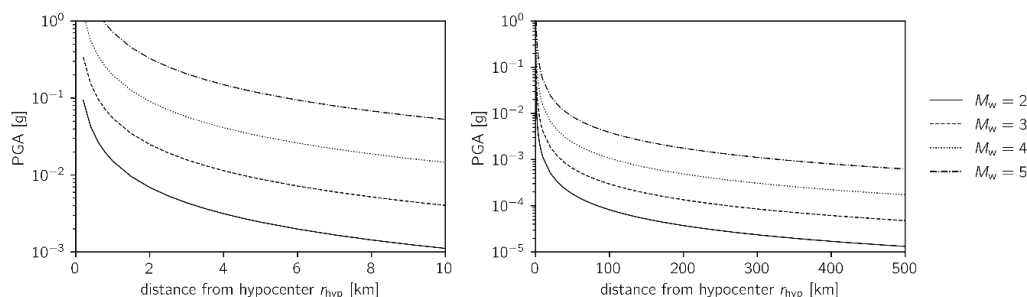


Fig. 3 resulting PGA from earthquake events with the moment magnitudes M_w of 2, 3, 4, and 5 depending on the distance from the hypocentre r_{hyp} according to Mezcua et al. (2008).

Conclusions

Despite the simplicity of the pseudo-static approach, the results allow a classification of the failure potential of submarine slopes preconditioned by gas on the Balearic Promontory. It is

evident that the gas-induced disturbances of the soil structure have a negative influence on the slope's bearing capacity reserve, but are only marginally reflected in the PGA required for a trigger event.

The exemplary data repositories consulted show that earthquake events of shallow depth with magnitudes of up to a maximum of 5 (USGS, 2021) or PGA of a maximum of 0.16 g (Jimenez et al., 2003) have recurrence intervals of around 50 years in the area of the Balearic Promontory. The magnitude to PGA conversion shows that an earthquake event only leads to relevant ground accelerations in the immediate vicinity of the source. Altered attenuation and other influencing factors of the submarine environment were not considered initially in the context of this study. In summary, only earthquakes with magnitudes greater than 4 with the hypocentre in the immediate vicinity are capable of generating ground accelerations relevant for submarine slope stability. Based on the available data, this is considered very unlikely on the Balearic Promontory, but cannot be ruled out over geological time scales.

Acknowledgements

The analyses were conducted as part of a DFG-funded, cooperative research project (GR 1024/35-1 & UR 226/3-1) with M. Urlaub and T. Sager (GEOMAR Helmholtz Centre for Ocean Research Kiel), to whom we are grateful for the good collaboration, and within the scope of the student thesis by A. Scholz, who we thank for providing her data base.

References

- Berndt, C., Costa, S., Canals, M., Camerlenghi, A., de Mol, B. and Saunders, M. 2012. Repeated slope failure linked to fluid migration: The Ana submarine landslide complex, Eivissa Channel, Western Mediterranean Sea. *Earth and Planetary Science Letters* 319-320, 65-74. doi: 10.1016/j.epsl.2011.11.045
- Elger, J., Berndt, C., Rüpke, L., Krastel, S. Gross, F. and Geissler W. H. 2018. Submarine slope failures due to pipe structure formation. *Nature communications* 9:715, doi: 10.1038/s41467-018-03176-1
- Grozic, J. L. H., Robertson, P. K. and Morgenstern, N. R. 2000. Cyclic liquefaction of loose gassy sand. *Canadian Geotechnical Journal* 37(4), 843-856. doi: 10.1139/t00-008
- Jimenez, M.-J., Giardini, D. and Grünthal, G. 2003. The ESC-SESAME Unified Hazard Model for the Europeans Mediterranean region. *EMSC/CSME Newsletter*, 19, 2-4.
- Kaminski, P., Sager, T., Grabe, J. and Urlaub, M. 2021. A new methodology to assess the potential of conjectural trigger mechanisms of submarine landslides exemplified by marine gas occurrence on the Balearic Promontory. *Engineering Geology* 295, 106446, doi: 10.1016/j.enggeo.2021.106446
- Kotha, S. R., Weatherill, G., Bindi, D. and Cotton, F. 2020. A regionally-adaptable ground-motion model for shallow crustal earthquakes in Europe. *Bulletin of Earthquake Engineering* 18, 4091–4125. doi: 10.1007/s10518-020-00869-1
- Mezcua, J., García Blanco, R. M. and Rueda, J. 2008. On the Strong Ground Motion Attenuation in Spain. *Bulletin of the Seismological Society of America* 98(3), 1343–1353. doi: 10.1785/0120070169
- Pietruszczak, P., Pande, G. N. and Oulapour, M. 2003. A hypothesis for mitigation of risk of liquefaction. *Géotechnique* 53(9), 833-838. doi: 10.1680/geot.2003.53.9.833
- Scholz, N. A., Riedel, M., Urlaub, M., Spence, G. D. and Hyndman, R. D. 2016. Submarine landslides offshore Vancouver Island along the northern Cascadia margin, British Columbia: why preconditioning is likely required to trigger slope failure. *Geo-Marine Letters* 36, 323-337. doi: 10.1007/s00367-016-0452-8
- Sultan, N., de Gennaro, V. and Puech, A. 2012. Mechanical behaviour of gas-charged marine plastic sediments. *Géotechnique* 62(9), 751-766, doi: 10.1680/geot.12.OG.002
- Sultan, N. and Garziglia, S. 2014. Mechanical behaviour of gas-charged fine sediments: model formulation and calibration. *Géotechnique* 64(11), 851-864. doi: 10.1680/geot.13.P.125
- ten Brink, U. S., Lee, H. J., Geist, E. L. and Twichell, D. 2009. Assessment of tsunami hazard to the U.S. East Coast using relationships between submarine landslides and earthquakes. *Marine Geology* 264, 65-73, doi: 10.1016/j.margeo.2008.05.011
- USGS 2021. U.S. Geological Survey Earthquake Hazards. www.usgs.gov/natural-hazards/earthquake-hazards/earthquakes. last accessed on 02.12.2021

Water Input Changes in the Kulcs Landslide Area

Cs. Király¹, Gy. Varga¹, D. Cseresznyés², G. Jakab¹, T. Földes³, N. Magyar⁴, Z. Szalai¹,

¹ Geographical Institute, Research Centre for Astronomy and Earth Sciences, Budapest, Hungary

² Lithosphere Research Group, Eötvös University, Budapest, Hungary

³ Tomogeo, Szolnok, Hungary

⁴ Department of Methodology for Business Analyses, Faculty of Commerce, Hospitality and Tourism, Budapest Business School, Budapest, Hungary

SUMMARY: Urbanization has led to extensive built-up zones, causing many formerly open fields with paleosol-loess layers to seal. Such areas are prone to mass movements due to the formation of sliding surfaces in the paleosol or red clay layers (as found in Kulcs, Hungary). For this reason, in this study not just the time series of the water level and amount of rain were analyzed, but chemical and physical analyses of clayey layers were carried out, as these are essential to determine the physical and chemical properties that may have affected or may still affect the movement of clayey layers.

Keywords: landslide, effect of water, granulometry, CIA

Introduction

Paleosol-loess layers are frequent in Hungary; furthermore, these layers occur along the banks of the Danube. Landslides occur in these bluffs. Because such locations are attractive locations, especially with their views, many holiday homes, and later family houses have been built there, and this is the case in Kulcs. For this reason, any mass movements may cause a great deal of economic damage. In this study the question of how water affects landslides is analyzed. One key finding is that the stability of loess decreases with the water content, while the degree of chemical weathering also has a relationship with water content.

Study area

The area examined is the village of Kulcs, located in Hungary, Central Europe. As a result of the westward erosional activity of the river, the east bank is characterized by eroded, sandy valleys, while the west bank is made of steep, almost vertical bluffs (Rónai & Bartha, 1965; Scheuer, 1979). Quaternary formations (Pleistocene loess and loess-like sediments) overlying the Upper Miocene and Pliocene clay layers can be found on the plateau sections, with thicknesses varying between approximately 40 and 50 m. Sand layers of varying thicknesses and in varying quantities are located within the Miocene layers (Rónai & Bartha, 1965). These beds are widely studied along the banks of the Danube (Pécsi 1994). The bluffs on the right bank of the River Danube has been experiencing landslides, slow surface creeps, and rotational slides for the last few decades. The recurring mass movements in 1964, 1966, 1977, 2006, 2011 and 2013 have ensured that the landslides of Kulcs are a relevant research topic (Farkas 2011; Fodor et al. 1983; Scheuer, 1979, Hydrogeological Diary of Kulcs and Rácalmás).

Samples and Methods

Time series analyses

The studied time series covered 1960-2020, because in this period there were more mass movement in this area. The last significant mass movement was in 2013. Water level data on the Danube in Budapest originates from the hydrogeological database, and on the amount of rainfall from the OMSZ (met.hu). Diagrams were made using the Origin program. The dates of the main mass movements at Kulcs are shown.

The studied samples originated from Kulcs. The analyzed samples can be divided into three groups, that we can see what is it different among the actual mass movements samples (and its environment) and other samples from the layer of the sliding (transect. where water come out, bank of the Danube).

The modal composition and main element composition was determined using XRD and ICP-OES. The chemical weathering index (CIA) was calculated from the main element composition according to the method of Nesbitt and Young (1982) and McLennan (1993). These properties help to understand the results of the chemical weathering processes.

The petrographical properties and texture of the sliding surface were analyzed using SEM and CT. These results assist in the understanding of the sequence of chemical and physical processes (the diagenetic sequence, weathering processes, mass movements).

Granulometric (grain size and morphology) properties may also signal the reworking and weathering processes.

Results and discussion

Earlier studies had suggested that mass movements take place in relation to the water level of Danube and amount of rain (Scheuer, 1979, Farkas, 1985). However, the present analysis shows that water level and amount of rain alone/taken in isolation do not provide a clear explanation. For example, the first noted mass movement was in March of 1964, though the water level of the Danube was actually higher in 1965-1967 (Fig. 1.). The next mass movement was in 1977; however, neither the amount of rain nor the water level was exceptional. It is, however, worth noting that building on the landslide area started in 1964 (after the mass movement, during the reclamation). The last mass movement was 2013-2014. In 2013 a high reclamation project was begun after the last landslide. In this project, for example, in order to correct/enhance drainage from the loess layer, layers were made more open with gravel (Oszvald, 2014). The channeling started in 2018.

For this reason, we studied the different red clay samples, the material which is the most significant sliding surface in Kulcs. The results show that on the sliding surface calcite agglomerates had been precipitated, which deformed during the sliding. The size of agglomerates was very variable (1 mm-2 cm), but the calcite crystals in every agglomerate were of the order of 1-2 μm . Swelling clay minerals also increased around the sliding surface, and were formed from feldspars. The most withered sample, however, originated from a transect (where water also came out) (Fig. 2.), and which is not a current sliding surface. The grain size distribution shows that the transect samples are the most reworked sample, and the clay fraction is also higher than in the other samples. The grain morphology also changed as a result of chemical weathering (Fig. 3.).

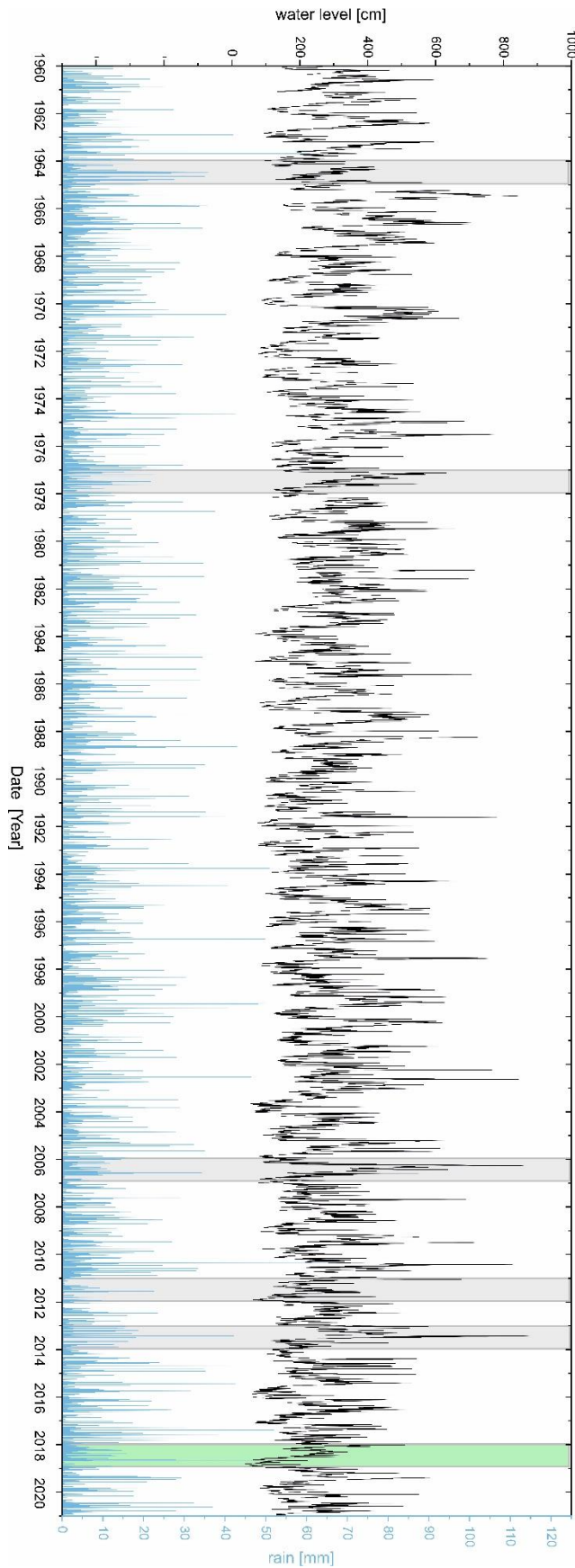


Fig. 1. Water level and amount of rain data from 1960 to 2020. The grey areas show the years of the important landslide events. The green area shows the date of channelling.

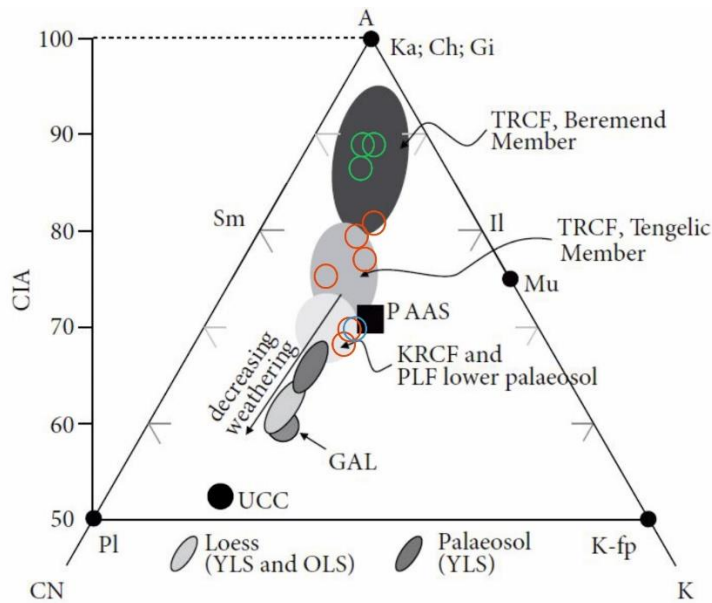


Fig. 2. Weathering conditions illustrated by an A-CN-K diagram (modified after Kovács et al., 2013), red circles are samples from the transect, green are from the environment of the sliding surface and blue is the sample from the riverside.

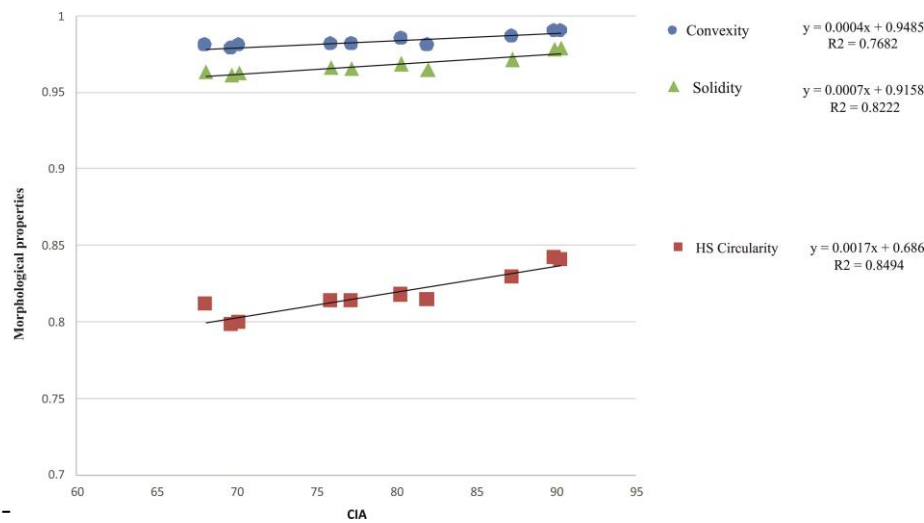


Fig. 3. Relation between morphological parameters and weathering index (CIA).

Conclusions

Our results show that increased water input is not enough to facilitate/set off/initiate/cause/precipitate a mass movement. Chemical weathering is also a very important process in mass movements where paleosol (red clay) is a sliding surface. Chemical processes affected the amount of clay minerals and secondary calcite, elements which may also facilitate/precipitate landslides.

We are grateful to NKFIH project No. FK128230.

References

- Farkas J (1985) A csapadék- illetve a víztartalomnövekedés szerepe a felszínmozgások kialakulásában 8, 343–349. HUN
- Farkas J (2011) Szakértői vélemény Kulcs felszínmozgásos területeinek vizsgálatáról. (Report about landslide prone areas of Kulcs, in Hungarian). Budapest, HUN.
- Fodor Tamásné, Horváth Zs, Scheur Gy (1983) A Rácalmás — kulcsi magaspartok mérnökgeológiai térképezése. Bull. Hungarian Geol. Soc. 113, 313–332. HUN
- Kovács J, Raucsik B, Varga A, Újvári G, Varga G, Ottner F (2013). Clay mineralogy of red clay deposits from the central Carpathian Basin (Hungary): Implications for Plio-Pleistocene chemical weathering and palaeoclimate. Turkish J. Earth Sci. 22, 414–426.
- McLennan SM (1993): Weathering and global denudation. Journal of Geology 101, 295-303.
- Nesbitt HW & Young GM, (1982) Early Proterozoic climates and plate motions inferred from major element chemistry of lutites. Nature 299, 715–717.
- Oszvald T (2014) Partfal stabilizási munkák Kulcson. Geotechnika Konferencia kiadvány, Ráckeve, 2014. 13-15 October, ISBN 978-615-800-062-8, 1-6. HUN
- Pécsi M (1994) A landslide type occurring frequently along the loess bluff in the Hungarian Danube Section. Quaternary International 24, 31-33.
- Rónai A & Bartha F (1965) A kulcsi löszfeltárás szelvénye. (Geological profile of the loess at Kulcs, in Hungarian). Budapest, HUN.
- Scheuer G (1979) A dunai magaspartok mérnökgeológiai vizsgálata. Bull. Hungarian Geol. Soc. 109, 230–254. HUN

Risk Before Failure for the Alta and Gjerdrum Landslides in Norway

Jean-Sébastien L'Heureux¹, Suzanne Lacasse¹ and Zhongqiang Liu¹

¹ NGI, Oslo, Norway

Summary: Society and standards require "risk-informed" decisions and sustainable, holistic solutions. The risk for two quick clay landslides, Alta and Gjerdrum in Norway, is discussed, using one of the simplest of risk assessment methods, a risk matrix. A framework for improved landslide risk assessment and management is proposed, with focus on risk as it changes with time.

Keywords: landslide, quick clay, hazard, consequence, risk

Risk assessment

Risk is a measure of the probability and severity of an adverse effect on life, health, property, and/or the environment. From an engineer's standpoint, risk (R) is the product of hazard (H) and consequence (C), where H is the likelihood or probability of an event occurring over a period of time, and C includes all elements at risk, their exposure, vulnerability and utility (or value of associated loss). ISO 31000:2018 defined risk as the "effect (positive or negative) of uncertainties on the objectives", emphasizing the importance of the uncertainties on risk.

There are two approaches to assessing the safety of a slope: (1) the conventional, standard-based approach with a global safety factor; and (2) the "risk-informed decision-making" (RIDM) approach (ISO 2394:2015). The safety factor is not a sufficient indicator of safety because it does not account for the different uncertainties in an analysis (Lacasse *et al.* 2022). RIDM, on the other hand, encourages a proactive mindset in identifying potential problem areas and requiring justified reasoning for the choices in the analysis. RIDM recognizes that human judgment plays an important role in decisions, and that technical information cannot be the only basis for decision-making, as gaps in knowledge are unavoidable. There exist a number of risk assessment methods. The simplest of methods, a qualitative risk matrix (which is coded in EXCEL for easy implementation), will be used herein to illustrate the change in risk with time for two landslides.

Impact of climate change on landslides in Norway

About 5,000 km² of Norway are covered by soft marine deposits, whereof 20% consist of highly sensitive or quick clay. The landslide database shows that over 85% of the quick clay landslides since 2000 were triggered by human activity, Figure 1 shows the frequency of large (volume > 50,000 m³) quick clay landslides (QCL) since 1970 in Norway. Even though quick clays are well-known to the stakeholders in the building, construction and transportation sectors in Norway, the frequency of large quick clay landslides doubled over the last two decades in Norway. The reasons for this increase are: i) new infrastructure development, ii) worsening slope stability over time due to natural processes such as erosion, snowmelt, rainfall and floods, iii) possibly a misunderstanding of the existing hazard and risk maps. In Norway, political agendas and human actions are so far more instrumental for triggering quick clay landslides than climate change. Nevertheless, climate change also plays a part. The expected deterioration in aggravating factors for landslides in Norway (in all types of soils) by year 2100 due to climate change is summarized in Table 1.

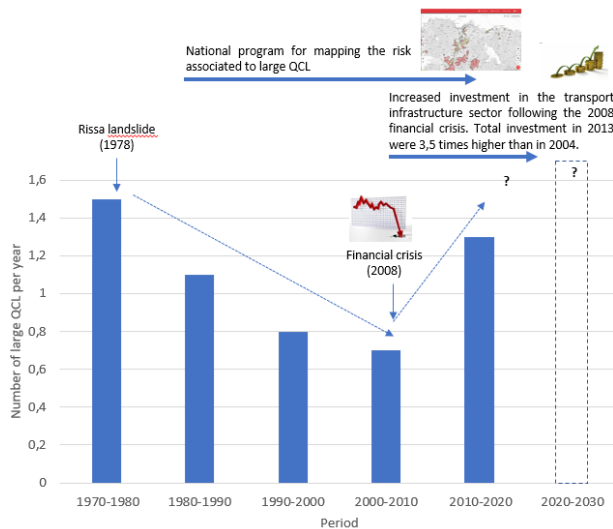


Figure 1. Annual frequency of recent large quick clay landslides (QCL) in Norway (after L'Heureux et al., 2018)

Aggravating factor	Expected change by year 2100
Temperature	Increase of 4.5°C in mean temperature
Rainfall	Increase in winter, less in summer: 18% increase in precipitation over country
Torrential rain episodes	Increase in both number and intensity of torrential rain events.
Floods	Intensity and frequency increase
Sea level rise	15 - 55 cm, depending on location.

Table 1. Impact of climate change on landslide aggravating factors by 2100 (Hansen *et al.*, 2017).

The Auditor General in Norway concluded that more frequent and more intense rainfalls (and floods) will lead to increased erosion, which can trigger more frequent landslides than today (Riksrevisjonen, 2021).

The 2020 Alta landslide

On June 3rd 2020, a 900,000 m³ quick clay landslide in Alta swept eight buildings into the sea and caused substantial damage. The landslide did not cause any loss of life. The landmasses slowly started moving as a large flake. The landslide scarp was 956 m long and nearly 20 m high. Residents had observed a 30-40 m long tension crack in the terrain and parallel to the shoreline the day before the landslide. To shed light on the cause(s) of the landslide, assessments of the geological, hydrogeological, meteorological and geomechanical conditions were investigated (NVE, 2020). Soil investigations revealed quick clay from a depth of 10 m below terrain. The 24 m thick clay deposit with interbedded layers of silt and sand, made the slope sensitive to groundwater flow. No precipitation was registered the days before the landslide, but snowmelt from a snow-rich winter, though not extreme, was at its peak. Snowmelt alone could not explain the landslide. LIDAR data revealed a 2-m thick fill over 600 m², linked to groundwork for a new house in 2015. The small fill reduced the factor of safety by 7%, yet not enough to fail the slope. The snowmelt in June 2020 likely exposed the "new" slope with the fill from 2015 to its highest porewater pressure so far.

The impact of fill placement, new house and persons exposed, and snowmelt on the landslide risk at Alta is illustrated on the matrix in Figure 2. The potential for a landslide at Alta was always present due to (1) the presence of quick clay, (2) the high slope, and (3) a stratigraphy making the slope sensitive to groundwater porewater pressure changes. The fill placed in 2015 increased the likelihood of a landslide. The new house increased the number of people in the area and therefore the impact of a potential landslide. The risk changed from medium to high.

The 2020 Gjerdrum landslide

On Dec. 30th 2020, the catastrophic landslide in Gjerdrum caused 11 fatalities, destroyed 31 houses, and required the evacuation of over 1600 residents, and led to chaos in services, infrastructure, and ecosystem. The volume of the landslide was estimated at 1.2 million m³, the distance of retrogression about 630 m and the length of the final scar about 1250 m.

Downstream, the landslide debris flowed nearly 2 km in the ravine system. The soil consists of thick deposits of marine clay. Witness observations combined with physical evidence and slope stability analyses confirmed that the landslide started on a slope in Holmen, outside the fatality area, where the 25 m high slopes had been subjected to significant erosion over the last decades. Hydrological calculations showed that erosion had been exacerbated by changes in land use in the catchment area. Urbanization and removal of vegetation led to increased runoff. Agricultural planning in the 1980s laid parts of the creek at the bottom of the slope in pipes. It was concluded that several human influences had acted in the same direction and contributed to increased erosion at the foot of the slope and the start of the landslide.

The entire area around Holmen was farmland until the late 1990s. Even though it was "likely" that a landslide could occur (Fig. 3), the risk was low as the landslide would have impacted only farmland. Urbanization in the early 2000s increased the risk of a landslide from low to medium. Urbanization increased the likelihood of a landslide because of its impact on the runoff and subsequent erosion in the creek after 2007. Dwellings were constructed and a large contingent of people moved into the area. Stabilization was done as part of the new construction, but those measures did not improve the conditions at Holmen. Consequently, the risk increased significantly landslide over a long period of time.

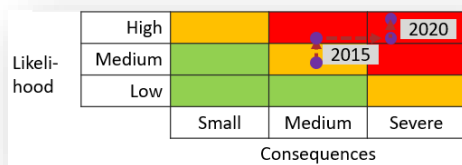


Figure 2. Change in risk with time at Alta

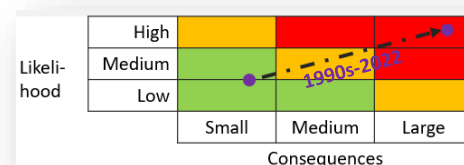


Figure 3. Change in risk with time at Gjerdrum

(high risk in red; medium risk in yellow; low risk in green)

Lessons learned

Important lessons learned from the two landslides include:

- Even small changes in loads or toe conditions can have disastrous consequences.
- The methodology to assess risk in quick clay areas in Norway is too qualitative and static in time. A design should consider changes in erosion over time, climatic impacts, land-use and urbanisation changes, as well as surrounding areas that may present hazards.
- One should use innovative and state-of-the-art remote sensing in landslide risk management.
- Landslides may occur following a long history of erosion and/or human activity.
- There is a need for strict restrictions on construction activities; monitoring of erosion and other terrain changes; a clear division of responsibilities for developer, landowner, municipality, state etc; and measures to enhance competence and education on quick clays, the danger they represent and simple mitigation measures (NoU, 2022).

Proposed integrated risk management framework

Figure 4 proposes an integrated risk management framework for risk-informed decision-making on landslide risk. The framework includes hazard and consequence analysis and the treatment of the risk. The framework integrates four parts: (1) assembling the knowledge required for both deterministic and probabilistic hazard assessment and for a consequence

analysis (green zone); (2) risk assessment, either qualitative or quantitative (yellow zone); (3) decision-making and risk reduction (blue zone); and (4) loop of regular and frequent re-assessments of landslides risk (grey zone), or if inspections reveal changed conditions.

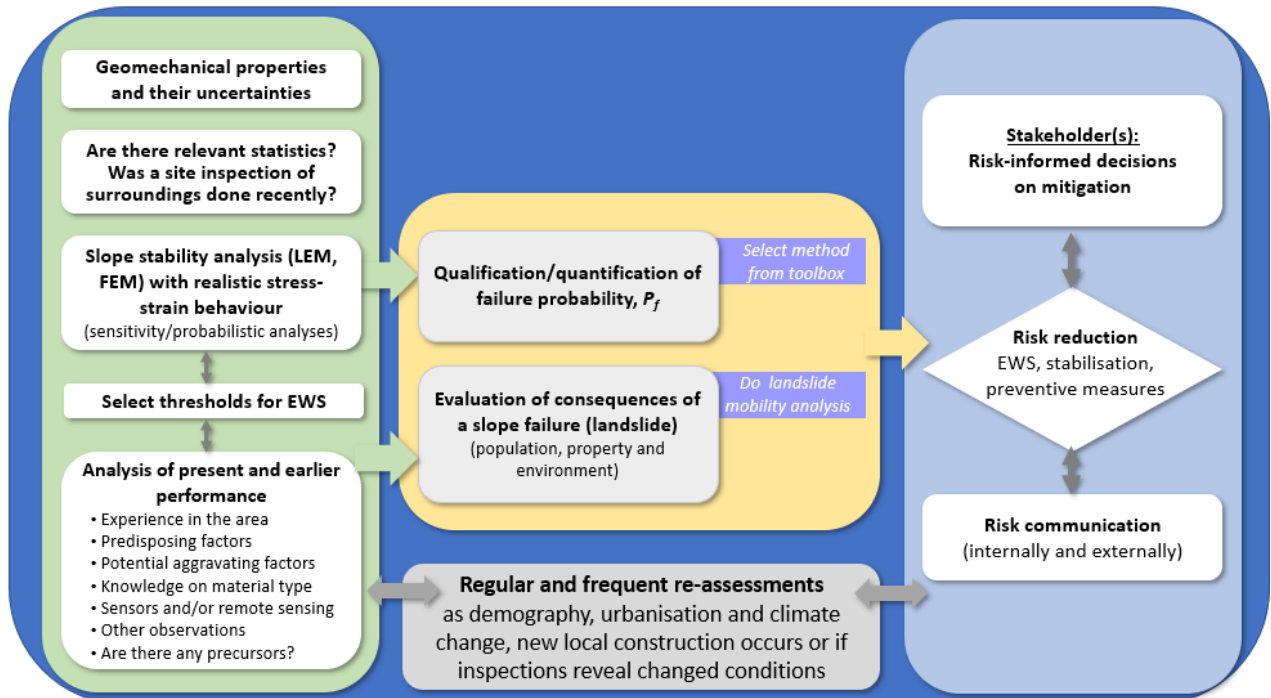


Figure 4. Proposed integrated framework for risk-informed management of landslides (Lacasse *et al.*, 2022) (LEM = Limiting Equilibrium Method, FEM = Finite Element method, EWS = Early Warning System)

References

- Expert Panel (2021). Causes of the 2020 quick clay landslide at Gjerdrum. Report from the expert commission. Publ. by the Norwegian Oil and Energy Ministry (in Norwegian). 172 pp.
- Hanssen-Bauer, I., Førland, E.J., Haddeland, I. et al. (2017). Climate in Norway 2100 – a knowledge base for climate adaptation. NCCS Report no. 1/2017.
- ISO 2394:2015. (International Standard Organization). ISO Standard: General principles on reliability for structures. ISO/TC 98/SC 2. 111 pp.
- ISO 31000:2018. (International Standard Organisation). Risk management - Principles and guidelines. 2nd ed, ICS: 03.100.01. 16 pp.
- L'Heureux, J.S., Høydal, O.A., Paniagua-Lopez, A.P. and Lacasse, S. (2018). Impact of climate change and human activity on quick clay landslide occurrence in Norway. 2nd JTC1 Workshop. Hong Kong. 12pp.
- Lacasse, S., L'Heureux, and Liu, Z.Q. (2022). Reducing landslide risk - Emerging challenges and novel technologies. Keynote Lecture Geohazards 8. Québec (June 2022).
- NoU (2022). På trygg grunn. Bedre håndtering av kvikkleirerisiko. Norges offentlige utredning 2022:3. Olje og energidept. 29 March 2022. 207 pp. (in Norwegian.)
- NVE (2020). Årsaksvurdering – Kvikkleireskredet ved Kråknes i Alta 3. juni 2020. 10220443-RIG-RAP-001. NVE Ekstern rapport 2021:4. https://publikasjoner.nve.no/eksternrapport/2021/eksternrapport2021_04.pdf (in Norwegian).
- Riskrevisjonen (2021). The Office of the Auditor General's investigation of the management and review of the national follow-up of the sustainable development goals Doc.3:3(2020–2021).93pp. <https://www.riksrevisjonen.no/rapporter-mappe/no-2021-2022/undersokelse-av-myndighetenes-arbeid-med-klimatilpasning-av-bebyggelse-og-infrastruktur/>.

Calibration of Coupled Finite Element Analyses for Early Warning System: the Case of an Unsaturated Slope in Norway

V. Mangraviti¹, V. Capobianco², L. Piciullo², J. Dijkstra¹

¹ Chalmers University of Technology, Gothenburg, Sweden

² Norwegian Geotechnical Institute, Oslo, Norway

SUMMARY: In the upcoming years, extreme meteorological events due to climate change are expected to increase the occurrence of landslides in unsaturated slopes and the related hazard posed to linear infrastructures. As a result, a better understanding of the stability conditions and efficient use of real-time monitoring data are required. The aim of this study is to couple predictive numerical models with monitoring data for slopes along infrastructures. A finite element numerical model simulating the mechanical response of a well-monitored slope, adjacent to a railway line, is calibrated. The calibration against in-situ measurements of the model carried out in Plaxis 2D will be discussed with the final goal of running fully-coupled unsaturated analyses for different rainfall scenarios.

Keywords: slope stability, fully-coupled, Plaxis, rainfall, unsaturated

Case study

The site study is an slope in Norway, 25-30 m high, with an inclination of about 45° in the upper part. At the toe of the slope is located a railway line and, an additional line is currently under construction. The slope, whose failure may hazardously involve the railway lines, has not exhibited any significant deformation so far. However, a slope failure due to heavy rainfall has occurred in a close area. In addition, a cultural heritage area, with an old church from the 12th century and its graveyard, is located at the top of the case study, making impossible the realization of physical slope stability measures on top of the slope. Therefore, the slope was instrumented with several sensors to keep monitored several hydrological parameters.

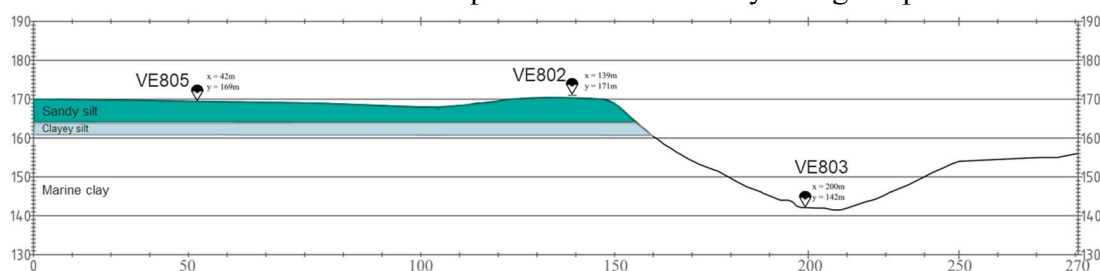


Fig. 1 Slope cross section and location of piezometers.

Volumetric water content (VWC) and pore-water pressure (PWP) sensors were installed in late spring/early summer of 2016 to monitor the hydrological conditions (Heyerdahl et al., 2018). Three boreholes are located in the studied area (Fig. 1) and piezometers are installed as in Tab. 1. The same boreholes were used to collect samples at different depths for standard lab tests (CRS, CK₀U triaxial).

Tab. 1 Depth of piezometers for each borehole.

Borehole	Depth (m)
VE805	10
	20
VE802	5
	9
	15
	23
VE803	5
	12

The slope has been schematized with the following layering: a sand/silt layer of about 6 m, a thinner layer of clayey silt (about 3 m thick), a firm marine clay layer to large depths (Fig. 1). At the top of the slope, the unsaturated zone is 6-7 meter deep depending on the water table fluctuation. The slope is saturated at the toe.

Numerical model calibration

In order to reduce the calculation time, the cross section in Fig. 2 was considered, assuming nil normal displacements at the boundaries. The spatial discretization was optimized by reducing the element size where more deformations are expected.

The hydraulic head was imposed at the boundaries according to piezometric data (Fig. 3). Since the measurements were not updated continuously since 2016, the numerical model was calibrated when data from all the sensors were available (Feb-Mar 2017, red dashed lines in Fig. 3). The hydraulic load for calibration has been chosen from boreholes VE805 and VE803 for left and right boundary, respectively. An average value during a period of no rainfall (1-15 Feb 2017) has been considered.

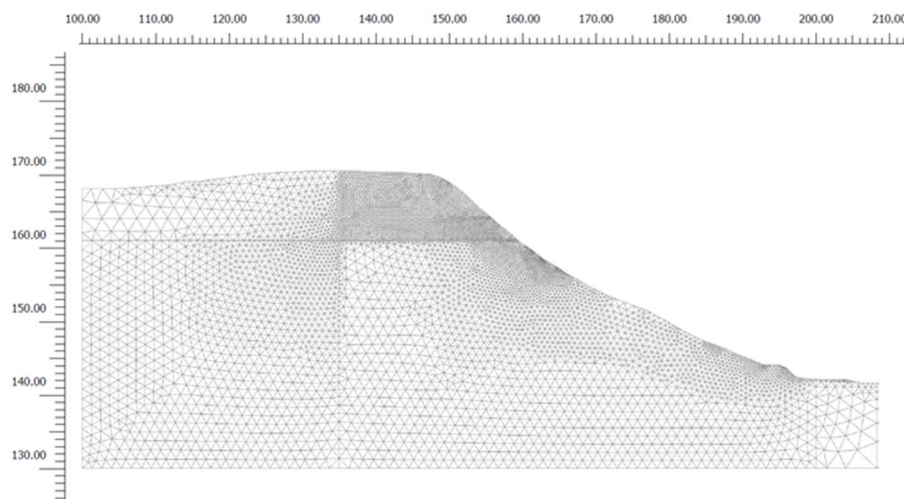


Fig. 2 Spatial discretization of the numerical model in Plaxis 2D.

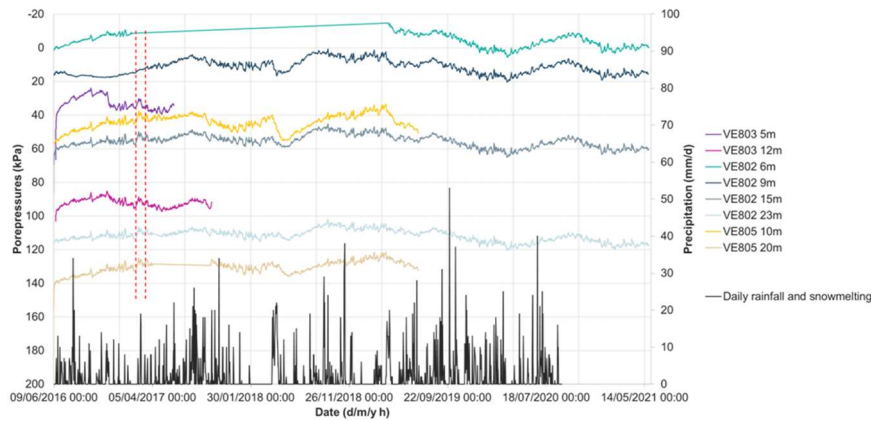


Fig. 3 Piezometers measurements and rainfall and snowmelting data.

Firstly, a stability analysis with simple elastic perfectly plastic constitutive models with Mohr-Coulomb (MC) failure criterion were chosen for all the materials, as in Piciullo et al. (2022). Unsaturated behavior of both the sandy silt and the silty sand layers was modelled with the van Genuchten model, whose parameters were calibrated on pressure plate tests from Heyerdahl et al. (2018), and are the same used in Piciullo et al. (2022). However, the stability analysis carried out by using the Gravity Increase Method (Chen and Mizuno, 1990; Hu et al., 2019) resulted in a factor of safety smaller than one. Since the slope was in equilibrium so far, the constitutive modeling was considered unrealistic. To increase the realness of the mechanical behavior of the slope, the overconsolidation of the clay was modelled by choosing a Modified Cam-clay (MCC) constitutive model, and by calibrating the parameters on lab tests (Tab. 2).

To be on safe side, zero cohesion was considered for the top layers. The stability analysis resulted, for both drained and undrained conditions, in a factor of safety greater than 1.3. The results on the most critical failure surface of the slope are not in the scope of this study and are omitted for the sake of brevity. However, some information about the stability analysis of this slope are reported in Piciullo et al. (2022).

Tab. 2 Materials constitutive models and mechanical properties.

Layer	Constitutive model	Unit weight (kN/m ³)	Young Modulus (MPa)	Poisson ratio (-)	Cohesion (kPa)	Friction angle (°)	Dilatancy (°)	Permeability (m/d)	MCC parameters: λ, κ, M (-)
Sandy silt	MC	18	15	0.3	0	36	8	0.2074	-
Silty sand	MC	18	15	0.3	0	32	8	8.6e-3	-
Clay	MCC	20	-	0.2	-	-	-	0.054e-3	0.058, 0.018, 1.2

Results and discussion

With the final goal of modelling the slope mechanical response (including a solution for both the hydraulic problem and the equilibrium) when subjected to rainfall, a fully coupled stage was run. Rainfall was modelled as seepage face imposed on all the boundaries representing the ground surface. The results in terms of both pore pressures and degree of saturation, are compared against average values of measurements, during a period of no rainfall and snowmelting, in terms of both pore pressures (Fig. 4 a) and saturation (Fig. 4 b) in the borehole more close to the slope edge. The results in terms of pore pressures for depth (z) less than 10 m are very similar to the measurements, whereas the model tends to overestimate pore pressures

when $z > 10$ m. This overestimation is due to the presence of a more permeable material below the marine clay layer that was disregarded for simplicity (so to have a constant hydraulic head imposed at the boundaries), giving a safe side estimation of stability. The agreement of the results with measurements in terms of saturation within the unsaturated soil layers is very good (Fig. 4 b).

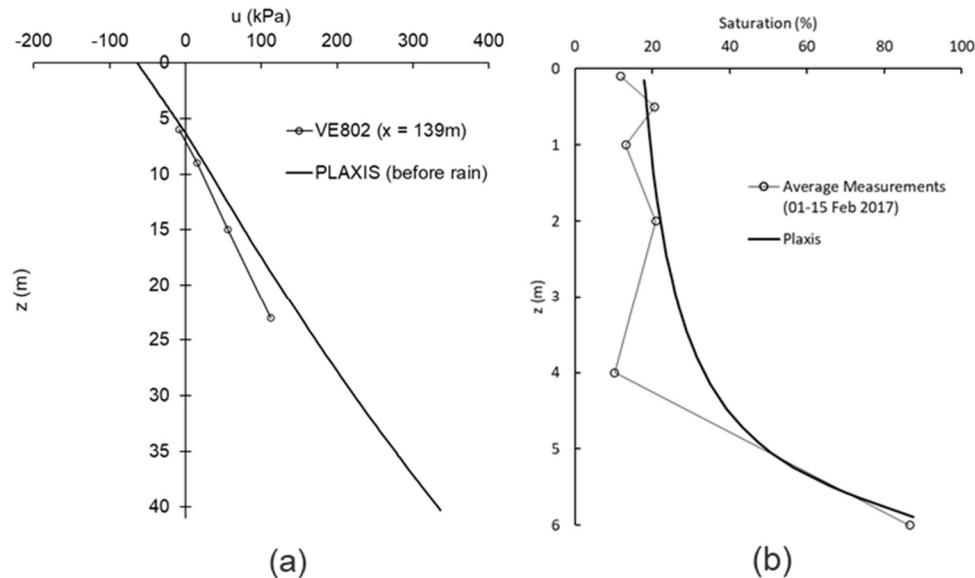


Fig. 4 Comparison between field measurements average values during a period of no rainfall and numerical results after fully coupled analysis: (a) pore pressure in borehole VE802 and (b) saturation close to the slope edge.

Conclusions

In this study, a sophisticated finite element model was developed and calibrated against both field measurements and lab tests, with the final goal of simulating the hydro-mechanical response of a Norwegian slope under different rainfall scenarios. The good agreement of the results with the available field data makes this model suitable to be used as a tool to define triggering conditions of failure for future studies on the impact of climate change.

References

- Chen, W.F., Mizuno, E., 1990. Nonlinear analysis in soil mechanics: theory and implementation. Nonlinear Anal. soil Mech. theory Implement.
- Heyerdahl, H., Høydal, Ø.A., Gisnås, K.G., Kvistedal, Y., Carotenuto, P., 2018. Slope instrumentation and unsaturated stability evaluation for steep natural slope close to railway line. In: UNSAT 2018: The 7th International Conference on Unsaturated Soils. pp. 1–6.
- Hu, C. ming, Yuan, Y. li, Mei, Y., Wang, X. yan, Liu, Z., 2019. Modification of the gravity increase method in slope stability analysis. Bull. Eng. Geol. Environ. 78.
- Piciullo, L., Capobianco, V., Heyerdahl, H., 2022. A first step towards a IoT-based local early warning system for an unsaturated slope in Norway. Nat. Hazards 114, 3377–3407.

Acknowledgment

The authors acknowledge the financial support from Nordforsk (project #98335 NordicLink).

An Efficient Reliability-based Design Approach to Reduce Rockfall Risk Below a Target Threshold

M. Marchelli¹, V. De Biagi¹

¹ Politecnico di Torino, Turin, Italy

Rockfalls are expected to increase due to global warming and extreme events induced by climate change. An accurate quantification of the risk is fundamental for Administrations to predispose effective risk mitigation plans. Risk value should account for all the possible events that can occur in a specific time, i.e. for a magnitude (block volume) frequency relationship. Among structural protective measures, rockfall barriers are widely selected. Despite their design method has been almost defined, even not standardized, the widely adopted safety factors approach with fixed factors does not allow obtaining a specific probability of failure. Moreover, the event magnitude-frequency relationship is not accounted. A novel time-independent reliability-based approach has been recently conceived by the Authors, allowing obtaining the design values for a specific failure probability. The method accounts for all the possible events, integrating them in time with their probability. In this way, an increase of rockfall events can be accurately considered. The obtained barrier failure probability can be used to compute the risk reduction in a given time or, conversely, to define the maximum failure probability of a barrier that could be accepted.

Keywords: rockfall risk, reliability design, magnitude-frequency, risk analysis

Introduction

Climate change and environmental degradation are existing threats to Europe and worldwide, and adaptation to climate change is becoming crucial in the next future. Permafrost and rock degradation, and massive glaciers retreat by global warming effects of climate change have a direct impact on mountain areas, with a significant increase of rockfall phenomena (Knoflach *et al.*, 2021). Rockfall occurrence has increased its frequency, and climate trends indicate that rockfall events are expected to rise throughout the foreseeable future (Hartmeyer *et al.*, 2020). The growing number of people and infrastructure in mountain regions increment the vulnerability of high-mountain areas, underlining the urgency for both an accurate rockfall risk assessment and effective risk mitigation strategies. A quantification of the risk is often required by Authorities to manage the risk predisposing effective mitigation plans, meaning that accurate hazard and consequences analyses have to be performed. The analysis starts from the identification and characterization of the possible initiating events, defining one or more realistic scenarios, from which propagation analyses have to be performed. As for other natural hazards, events differing for magnitudes, i.e. for rockfall the block volume, can occur with different probabilities. Even difficult, a method to estimate the return period of each possible volume has been proposed (De Biagi *et al.*, 2017; Moos *et al.*, 2022), and the profitability of rock-face monitoring systems has been widely assessed (Giacomini *et al.*, 2020). Propagation analyses and hazard computation have to be performed for each possible volume, which is characterized by a specific frequency (Lari *et al.*, 2014; Farvacque *et al.*, 2021). For each event, given the element at risk, the consequences have to be computed to obtain the risk value. When this value is higher than an acceptable threshold, mitigation measures have to be adopted. Among structural mitigation measures, and particularly among protective ones, net

fences (i.e. flexible rockfall barriers) are about the most effective for high energy events. The design of these barriers is still under debate and a standardized procedure is not yet available, even though nowadays, following the CE marking procedure, and some National Standards (i.e. UNI11211-4) the current design practice is oriented towards evaluation of the required performances of a barrier in terms of energy absorption capacity and height. On the base of the propagation analyses, the designer selects a suitable commercial product for which it can be checked that block impact energy and passing height are smaller than its performances, considered as the reference value obtained through impacts following the European guidelines (EAD 340059-00-0106, 2018). A partial safety factor approach is generally adopted. Nevertheless, the partial safety factors proposed by the National Standards are fixed values, and thus, neglecting the intrinsic variability and the site specificity of rockfall problems, their adoption inevitably leads to design structures with different failure probabilities (Marchelli *et al.* 2020). Moreover, despite probabilistic trajectory models are adopted, a unique initial scenario in terms of initial volume is generally considered for evaluating the actions.

A time-integrated reliability based design approach has been recently proposed by the Authors (De Biagi *et al.*, 2020, Marchelli *et al.* 2020, Marchelli *et al.* 2021a). The reliability calculation accounts for the variability in magnitude of the events, their occurrence probability, and for the intrinsic variability of the actions, with non-fixed probability distributions.

In the following, the mathematical framework of both time-integrated quantitative risk analysis and reliability based design approach are defined, together with their coupling. This last allows to quantify the risk reduction when protective measures are installed.

Time-integrated quantitative risk assessment

Rockfall can be considered a Poisson point process phenomenon: events are independent and have an average frequency of occurrence. From an engineering point of view, the parameter of interest is the frequency of the events reaching the areas where the elements at risk are located, only. The risk calculation should account both for this variability in magnitude, and for the discrete temporal nature of the phenomenon, aspects that have to be considered in mitigation measures design, too. Considering that the exposed area consists of q elements at risk and p rock block volumes that can detach, the risk R has to be computed as (Marchelli *et al.*, 2021b):

$$R = \sum_{l=1}^p \sum_{m=1}^q (P_T^l P_S^{l,m} E^m V^{l,m} W^m) \quad (1)$$

where P_T^l is the temporal probability, which can be associated to the frequency in a given period of time, associated to each possible released volume, $P_S^{l,m}$ is the spatial probability that this block reaches the m th element at risk, and E^m , $V^{l,m}$ and W^m are the exposure, the vulnerability and the value, respectively. As the vulnerability is function not only of the characteristics of the elements at risk but also of the intensity of the phenomenon, for each block volume, and thus for each kinetic energy at the element at risk location, the damages have to be computed.

Reliability based design method for net fences

Considering net fences, the possible failure of these structures can be simplified into a failure mode related to the exceeding height when the block is not intercepted, and one related to the exceeding kinetic energy, when the absorption capacity of the system is smaller than block translational energy. A failure probability is associated to each of them, F_h and F_k , respectively, and, finally, these two are combined into a unique failure probability, named p_f . In a specific period of time τ , this can be computed as (De Biagi *et al.*, 2020, Marchelli *et al.* 2020, Marchelli *et al.* 2021a):

$$p_f(\tau) = F_h(\tau) + F_k(\tau) = 2 - e^{-\nu\tau p_{fa,h}} - e^{-\nu\tau p_{fa,k}} \quad (2)$$

being ν the mean expected annual frequency of a rockfall event (of any intensity), and $p_{fa,h}$ and $p_{fa,k}$ the probability of failure for the two failure modes, respectively, considering the occurrence of an event as certain. These probabilities are calculated integrating all the possible block volumes and their occurrence probability (see the referenced papers for details). Provided that distributions of block (i) velocities, (ii) passing heights, (iii) volumes at the impact are provided, together with their probability density functions, a total value of failure probability in the period τ , i.e. $p_f(\tau)$, can be defined for installing a specific product in a specific site.

Coupling the approaches

The introduction of mitigation measures varies the spatial and temporal probability that a block reaches the element at risk. Since $p_f(\tau)$ is calculated with a time-integration for all the possible block volumes, considering τ equal to one year and in the hypothesis that the designed mitigation measures protect all the q elements at risk, Eq. (1) becomes:

$$R_{new} \approx p_f(1 \text{ yr}) \sum_{m=1}^q (E^m V^{p,m} W^m), \quad (3)$$

assuming that the failure of the measure refers to the largest volume, i.e. p volume, whose temporal probability is in the term $p_f(1 \text{ yr})$. In the case for which only $q_1 < q$ elements at risk are protected, Eq. (1) becomes:

$$R_{new} \approx p_f(1 \text{ yr}) \sum_{m=1}^q (E^m V^{p,m} W^m) + \sum_{l=1}^p \sum_{m=q_1+1}^q (P_T^l P_S^{l,m} E^m V^{l,m} W^m). \quad (4)$$

Example of application

A sub-vertical rock slope face insists on earth moving vehicles deposit. From a source zone at a height of about 15 m from the deposit, rockfall events different in magnitude (block volume V_b) and frequency can occur. The distribution of the volumes together with their annual release probability have been obtain through monitoring, a catalogue of past events and a survey of blocks in the surroundings. The sampled volumes are distributed according to a Pareto Type I function with threshold volume $V_{th} = 0.5 \text{ m}^3$ and whose shape parameter α is equal to 1.6. Due to the verticality of the slope, if detached, a block, in free flight, surely hits the ground, or, in this case, almost a vehicle. Provided that, according to ISO 3449:2005, each vehicle has a maximum impact resistance of 11.6 kJ and has an average value of 20000 €, the risk is calculated according to Eqn. (1). The total risk R is of 7300€/year.

To mitigate the risk, protection barriers are planned. Considering the barrier maximum elongation at the impact, the system is installed normal to the slope face at a height of about 10 m from the source zone. Despite free fall represents the most probable type of motion, trajectory analyses are performed, individuating a 95th percentiles of velocity equal to 14 m/s, with a ratio between 99th and 95th percentiles of 1.05, for all V_b . To design the barrier, $P_T^l P_S^{l,m}$ is assumed equal to the mean arrival frequency at the barrier location. A product with energy absorption capacity of 1000 kJ and 5 m high is selected. Its $p_f(1 \text{ yr})$ is computed through Eqn. (2), assuming, due to the nature of both the slope and barrier orientation, $F_h = 0$, i.e. all blocks are intercepted. It reveals $p_f(1 \text{ yr}) = 6.1 \cdot 10^{-4}$. The total risk, i.e. Eqn. (4), is $R_{new} = 24.4 \text{ €/year}$.

Table 1: Risk calculation without intervention

V_b (m ³)	P_T^l (-)	$P_S^{l,m}$ (-)	q (-)	E^m (-)	$V^{l,m}$ (-)	W^m (€)	$R^{l,m}$ (€)
< 0.03	0.5	1	1	1	0.1	20000	1000
$0.03 \leq V_b < 0.1$	0.25	1	1	1	0.3	20000	1500
$0.1 \leq V_b < 0.5$	0.15	1	1	1	0.8	20000	2400
$0.5 \leq V_b < 2$	0.1	1	1	1	1	20000	2000
≥ 2	0.01	1	2	1	1	20000	400

Conclusion

Climate change has a direct impact on mountain areas, and a significant increase of rockfall phenomena has been recorded in the last decades. Thus, an accurate quantification of the risk, accounting for a volume-frequency relationship of all the possible released block volumes, is fundamental for Administrations to manage the risk. Net fences are widely diffused as structural protective measures. The general adopted design method, with a partial safety factor approach, does not account for the volume-frequency relationship and does not allow obtaining a specific failure probability failure. To tackle these issues, a novel time-independent reliability-based design method conceived by the Authors is coupled with time-integrated quantitative risk assessment to quantify the risk reduction in a given time period. The method can thus be used to define the maximum acceptable failure probability of a net fence too.

References

- De Biagi, V., Napoli, M. L., Barbero, M., & Peila, D. (2017). Estimation of the return period of rockfall blocks according to their size. *Natural Hazards and Earth System Sciences*, 17(1), 103-113.
- De Biagi, V., Marchelli, M., & Peila, D. (2020). Reliability analysis and partial safety factors approach for rockfall protection structures. *Engineering Structures*, 213, 110553.
- EAD 340059–00-0106. Falling rock protection kits. EOTA - European Organisation for Technical Assessment; 2018.
- EN 1990:2002. Eurocode 0—Basis of Structural Design. European Committee for Standardization (CEN): Brussels, Belgium, 2002.
- Farvacque, M., Eckert, N., Bourrier, F., Corona, C., Lopez-Saez, J., & Toe, D. (2021). Quantile-based individual risk measures for rockfall-prone areas. *International Journal of Disaster Risk Reduction*, 53, 101932.
- Giacomini, A., Thoeni, K., Santise, M., Diotri, F., Booth, S., Fityus, S., & Roncella, R. (2020). Temporal-spatial frequency rockfall data from open-pit highwalls using a low-cost monitoring system. *Remote Sensing*, 12(15), 2459.
- Hartmeyer, I., Keuschnig, M., Delleske, R., Krautblatter, M., Lang, A., Schrott, L., ... & Otto, J. C. (2020). A 6-year lidar survey reveals enhanced rockwall retreat and modified rockfall magnitudes/frequencies in deglaciating cirques. *Earth Surface Dynamics*, 8(3), 753-768.
- ISO 3449:2005, Earth-moving machinery — Falling-object protective structures — Laboratory tests and performance requirements, International Organization for Standardization (ISO), Geneva, Switzerland, 2005.
- Knoflach, B., Tussetschläger, H., Sailer, R., Meißl, G., & Stötter, J. (2021). High mountain rockfall dynamics: rockfall activity and runoff assessment under the aspect of a changing cryosphere. *Geografiska Annaler: Series A, Physical Geography*, 103(1), 83-102.
- Lari, S., Frattini, P., & Crosta, G. B. (2014). A probabilistic approach for landslide hazard analysis. *Engineering geology*, 182, 3-14.
- Marchelli, M., Biagi, V. D., & Peila, D. (2020). Reliability-based design of protection net fences: influence of rockfall uncertainties through a statistical analysis. *Geosciences*, 10(8), 280.
- Marchelli, M., De Biagi, V., & Peila, D. (2021a). Reliability-based design of rockfall passive systems height. *International Journal of Rock Mechanics and Mining Sciences*, 139, 104664.
- Marchelli, M., De Biagi, V., Bertolo, D., Paganone, M., & Peila, D. (2021b). A mixed quantitative approach to evaluate rockfall risk and the maximum allowable traffic on road infrastructure. *Georisk: Assessment and Management of Risk for Engineered Systems and Geohazards*, 1-11.
- Moos, C., Bontognali, Z., Dorren, L., Jaboyedoff, M., & Hantz, D. (2022). Estimating rockfall and block volume scenarios based on a straightforward rockfall frequency model. *Engineering Geology*, 309, 106828.
- UNI 11211-4 (2018); Opere di Difesa Dalla Caduta Massi—Parte 4: Progetto Definitivo ed Esecutivo. Ente Italiano di Unificazione (UNI): Roma, Italy, 2018.

Role of Positive Temperature Variations on Rock Slopes Outcrops (a review)

Véronique MERRIEN-SOUKATCHOFF¹, Muriel Gasc-Barbier²

¹ Laboratoire Géomatique & Foncier (EA 4630), Conservatoire National des Arts et Métiers, Case courrier EPN01-C, 2, rue Conté, CEDEX 03, 75141 Paris, France; veronique.merrien@lecnam.net

² GeoCoD, Cerema, avenue Albert Einstein, CS 70499, 13593 Aix en Provence, CEDEX 03, France.

SUMMARY: The role of positive temperature fluctuations on the destabilisation or displacement of rock slopes is increasingly mentioned. The abstract identifies and classifies the related publications, involving *in situ* sites, according to observations, measurements, explaining mechanisms and outlines some challenges to be addressed in the coming years.

Keywords: rock, slope, thermomechanics fracture, *in situ*

Introduction

Thermomechanical surface effects on rock outcrops are increasingly quoted in the last twenty years. This abstract aims to list the publications around this theme, involving *in situ* sites (excluding laboratory experiments), and to and classify them according to observations, measurements and possible mechanisms, before issuing a few comments on the subject.

Observations

The direct link between positive temperature variations and rockfalls or rockslides has begun to be often quoted in the, 2000s, although since the 1930s there have been discussions among geomorphologists about the role of temperature on weathering. Gunzburger et al. (2004) and Vargas et al. (2004) were among the first authors to point the role of temperature in deep failure. Vargas et al. (2013) reported variable volume events associated with considerable daily fluctuations in maximal and minimal temperatures: small superficial volume, mainly composed of thin slab failure, but also large rock falls. Quoted thermally induced stresses failures can then be differentiated in two categories: shallow versus depth events. Superficial events, also called spalling, onionskin layers or exfoliation sheets, and which we can probably qualify as weathering, some mm³ to a m³ are described by (Vargas et al., 2004, Leith et al., 2017, Collins and Stock, 2016, Alcaïno-Olivares et al., 2021, Lamp et al., 2017) whereas important volumes (from 420 to at least 2,500 m³) of rock instability are quoted by (Vargas et al., 2013, Gischig et al., 2011a, Gischig et al., 2011b, Gunzburger et al., 2005, Gasc-Barbier and Merrien-Soukatchoff, 2019). Small events have the advantage of being recurrent and it is therefore possible to make observations and measurements where they occur, but they can rather be qualified as weathering. The large events, classified as rockfalls, are generally isolated and even if observations and instruments are placed on the site immediately, the phenomena are unlikely to recur quickly. Yet, considering the risk the latter are much more important. Due, among others, to the lack of meteorological data on the site and at the time of the failure events, it is not that easy to establish whether there is a continuum between these 2 two categories (small and large volume).

Measurements

Beside observations, *in situ* measurement are expanding. Temperature, displacement, strain or fracture opening can be measured.

Air temperature measurements are frequent, measurements in the rock itself, especially at depth, are much less numerous. Without being exhaustive, we can cite some of these measures. Coutard and Francou (1989) measure temperatures up to 48 cm deep in two alpine French sites. Messenzehl and Dikau (2017) made temperature measurement in the Swiss Alps. Gruber et al. (2004) were also interested in alpine temperature and the depth of frost. Contrariwise, Jenkins and Smith (1990) measure subsurface temperature in the Canary Islands, a much warmer environment. Molaro and McKay (2010) produce high-frequency rock subsurface temperature data from hyper-arid desert environments, an even warmer environment. They were able to detect dT/dt maximum of $137^{\circ}\text{C min}^{-1}$, but on a sampling interval of 0.375 s. In a more temperate zone, Safanda (1999) measures temperature in boreholes in Krušné Hory Mountains of Czech Republic with depth varying from 30 to 60 cm. He insists that the ground surface temperatures are strongly dependent on the slope angle and orientation. This was confirmed by Gunzburger and Merrien-Soukatchoff (2011) who show the influence of the air temperature and solar radiation on ground and depth temperature in the Valabres site. Gasc-Barbier et al. (2021) measured temperature up to 6 m depth from a cliff wall. Sometimes rock temperature at the surface is deduced from infrared thermography (Fiorucci et al., 2018). These measurements generally raise problems concerning the equipment used for the measurements: the insulation of the borehole and therefore the validity of the measurements. Spot measurements are generally insufficient; frequent and reliable measurements are needed (without drift over time) over long periods, which sets the problem of the stability of the equipment and the funds to allow this. Some in-depth measurements are combined with measurements of solar radiation (Grøneng et al., 2011) which is quite rare on the slopes.

Measurement of displacement related to temperature can be separated in measurement including the whole rock mass or displacement along fractures. Krähenbühl (2004), Gunzburger et al. (2004), Watson et al. (2004) and Gunzburger et al. (2005) quote global movement of the rock mass. The full range of surface measurements such as Lidar, infrared thermography (Guerin et al., 2020), photogrammetry, Ground-Based Radar are possibly used to look after the topographic variation, but the topographic measurement could be unable to measure the displacement in the absence of fractures involved in this movement (Gunzburger et al., 2005). Numerous authors measure of temperature variations along existing fissures associated with their aperture (Vlcko et al., 2009, Grøneng et al., 2011, Gischig et al., 2011b, Bakun-Mazor et al., 2011, Mufundirwa et al., 2011, Bakun-Mazor et al., 2013, Cloutier et al., 2015, Collins et al., 2018, Taboada et al., 2017, Gasc-Barbier et al., 2021, Marmoni et al., 2020). These measures are always superficial due to the difficulty of instrumenting deep cracks and in some of these measurements the problem of the possible drift of the instruments themselves is not clearly excluded. Measurements of angle deviation through inclinometers are also sometimes quote (Clément, 2008, Gischig et al., 2011b).

Extensometric measurements or strain gauges are less frequent but are generally associated with in-depth temperature measurement. They measure the strain on bases of a few centimetres (Clément et al., 2008) to a few metres. When the strain is measured with extensometers, they are likely to cross fractures which have an effect on the deformation but also on the field of temperature in the borehole drilling.

Many measurements are spot and superficial and raise the problem of their integration in a whole conceptual model. Only extensometers accumulate strain over a thickness and allow to the understanding of the in deep mechanism. The measurements raise the question of how these different pieces of information, rather on the surface could be combined to move on to a global mechanism in modelling. The instruments can influence how the issue is considered. Crackmeter induces discontinuous modelling whereas extensometers and inclinometers rather continuous model.

Proposed Computations, Mechanisms and Modelling

Various computations, sometimes analytical but often numerical, are proposed based on thermal or thermomechanical observation and measurements on slopes. When the models try to explain a small volume and the superficial effects, they generally consider the fracturing, whereas continuous models attempt to understand the whole slope behaviour. Some computation just explained the thermal aspects and sometimes the role of solar radiation (Gunzburger and Merrien-Soukatchoff, 2011). The thermal diffusivity can be deduced from internal temperature measurement in the rock masses. In their site (Merrien-Soukatchoff et al., 2007) mentioned that the value is twice that commonly reported in the literature, but this difference is unclearly explained.

Many thermomechanical computations (whether it concerns small or large volumes) are implemented around the idea of fracture propagation due to thermal cycles and fatigue (Clément, 2008, Vargas et al., 2009, Stock et al., 2012, Collins and Stock, 2010, Collins et al., 2018, Alcaino-Olivares et al., 2021). Eppes (2022) precise the mechanisms linked to critical or subcritical growth of fractures. She does not make any size distinction between fracture propagation, and mechanical weathering producing clastic sediments or larger volumes of rock falls. Continuous models are often used to derive a stress field that will be later used to explain fracture propagation, which can be problematic because large deep fractures involved in a large volume failure have a role in the distribution of temperatures in the rock and, moreover, the fractures modify the state of stress in the rock mass.

Discontinuous modelling is rather used to compare in situ and modelled displacement (Gunzburger et al., 2005, Bakun-Mazor et al., 2020), but this modelling raises many questions about the mechanical and thermal properties to be assigned to fractures. For example (Messenzehl and Dikau, 2017) consider that the low rock porosity and permeability in their study site may still justify using a conduction model for their study site.

Challenges and Conclusions

Numerous papers are related to thermomechanical effects of positive variation on in situ sites. Doubts still remain on the importance of these phenomena on rockfalls, and the rigorous proofs of thermomechanical failure are often difficult to establish. But we are only at the beginning of the collection of all these data. Largest inventories could highlight if the division between superficial sheets failure and larger rock falls volume involving pre-existing fractures is relevant or not. The influence of temperature on the measurements themselves are to be clearly eliminated and the insolation on rock slope is not enough registered to be taken into account. Thermal properties of fractures and, beyond, of the entire rock mass are still largely unknown. The role of fracture propagation, fatigue or potential creep must be clarified. Proof of these mechanisms is hard to find, so far, we often only demonstrate their possibility through modelling.

References

- Alcaino-Olivares, R., Leith, K., Ziegler, M. and Perras, M. (2021) 'Thermo-mechanical fatigue cracking of the bedrock on an island in the Baltic Sea', in *GEONIAGARA*, Niagara Falls, Canada, September 26-29, 2021,
- Bakun-Mazor, D., Hatzor, Y. H., Glaser, S. D. and Carlos Santamarina, J. (2013) 'Thermally vs. seismically induced block displacements in Masada rock slopes', *International Journal of Rock Mechanics and Mining Sciences*, 61(Supplement C), 196-211.
- Bakun-Mazor, D., Hatzor, Y. H., Glaser, S. D. and Santamarina, J. C. (2011) 'Climatic Effects On Key-block Motion: Evidence From the Rock Slopes of Masada World Heritage Site', in Association, A. R. M., ed. *45th U.S. Rock Mechanics / Geomechanics Symposium* San Francisco, California, June 26 - 29, 2011, American Rock Mechanics Association,

- Bakun-Mazor, D., Keissar, Y., Feldheim, A., Detournay, C. and Hatzor, Y. H. (2020) 'Thermally-Induced Wedging–Ratcheting Failure Mechanism in Rock Slopes', *Rock Mechanics and Rock Engineering*, 53(6), 2521-2538.
- Clément, C. (2008) *Auscultation d'un versant rocheux soumis aux sollicitations thermiques naturelles. Cas des Rochers de Valabres (Alpes-Maritimes)*, unpublished thesis (PhD), INPL, Ecole des Mines de Nancy.
- Clément, C., Gunzburger, Y., Merrien-Soukatchoff, V. and Dünner, C. (2008) *Monitoring of natural thermal strains using hollow cylinder strain cells: The case of a large rock slope prone to rockfalls*, translated by Chen, Z., Zhang, J., Li, Z., Wu, F. and Ho, K., Xi'an (China): Taylor and Francis Group (London), 1143-1149.
- Cloutier, C., Locat, J., Charbonneau, F. and Couture, R. (2015) 'Understanding the kinematic behavior of the active Gascons rockslide from in-situ and satellite monitoring data', *Engineering Geology*, 195, 1-15.
- Collins, B. D. and Stock, G. M. (2010) 'Quantifying thermally induced rock flexure as a potential rock-fall trigger', *Geological Society of America Abstracts with Programs*, 42.
- Collins, B. D. and Stock, G. M. (2016) 'Rockfall triggering by cyclic thermal stressing of exfoliation fractures', *Nature Geosci.*
- Collins, B. D., Stock, G. M., Eppes, M.-C., Lewis, S. W., Corbett, S. C. and Smith, J. B. (2018) 'Thermal influences on spontaneous rock dome exfoliation', *Nature Communications*, 9(1), 762.
- Coutard, J. P. and Francou, B. (1989) 'Rock temperature measurements in two alpine environments: implications for frost shattering', *Arctic & Alpine Research*, 21(4), 399-416.
- Eppes, M.-C. (2022) '3.03 - Mechanical Weathering: A Conceptual Overview' in Shroder, J. F., ed. *Treatise on Geomorphology (Second Edition)*, Oxford: Academic Press, 30-45.
- Fiorucci, M., Marmoni, G. M., Martino, S. and Mazzanti, P. (2018) 'Thermal Response of Jointed Rock Masses Inferred from Infrared Thermographic Surveying (Acuto Test-Site, Italy)', *Sensors*, 18(7), 2221.
- Gasc-Barbier, M. and Merrien-Soukatchoff, V. (2019) *Effect of natural thermal cycles on rock slopes stability-study of 2 French sites*, translated by da Fontoura, S. A. B., Rocca, R. J. and Mendoza, J. o. F. P., CRC Press.
- Gasc-Barbier, M., Merrien-Soukatchoff, V. and Virely, D. (2021) 'The role of natural thermal cycles on a limestone cliff mechanical behaviour', *Engineering Geology*, 293(106293), 8.
- Gischig, V. S., Moore, J. R., Evans, K. F., Amann, F. and Loew, S. (2011a) 'Thermomechanical forcing of deep rock slope deformation: 1. Conceptual study of a simplified slope', *Journal of Geophysical Research: Earth Surface*, 116(F4), F04010.
- Gischig, V. S., Moore, J. R., Evans, K. F., Amann, F. and Loew, S. (2011b) 'Thermomechanical forcing of deep rock slope deformation: 2. The Randa rock slope instability', *Journal of Geophysical Research: Earth Surface*, 116(F4), F04011.
- Grøneng, G., Christiansen, H. H., Nilsen, B. and Blikra, L. H. (2011) 'Meteorological effects on seasonal displacements of the Åknes rockslide, western Norway', *Landslides*, 8(1), 1-15.
- Gruber, S., Hoelzle, M. and Haeberli, W. (2004) 'Rock-wall temperatures in the Alps: Modelling their topographic distribution and regional differences', *Permafrost and Periglacial Processes*, 15(3), 299-307.
- Guerin, A., Jaboyedoff, M., Collins, B. D., Stock, G. M., Derron, M.-H., Abellán, A. and Matasci, B. (2020) 'Remote thermal detection of exfoliation sheet deformation', *Landslides*.
- Gunzburger, Y. and Merrien-Soukatchoff, V. (2011) 'Near-surface temperatures and heat balance of bare outcrops exposed to solar radiation', *Earth Surface Processes and Landforms*, 36(12), 1577-1589.
- Gunzburger, Y., Merrien-Soukatchoff, V. and Guglielmi, Y. (2005) 'Influence of daily surface temperature fluctuations on rock slope stability: case study of the Rochers de Valabres slope (France)', *International Journal of Rock Mechanics and Mining Sciences*, 42(3), 331-349.
- Gunzburger, Y., Merrien-Soukatchoff, V., Senfaute, G., Guglielmi, Y. and Piguet, J.-P. (2004) *Field investigations, monitoring and modeling in the identification of rock fall causes*, translated by Lacerda, W., Ehrlich, M., Fontoura, S. A. B. and Sayao, A. S. F., Rio de Janeiro: Taylor & Francis Group, 557-563.
- Hall, K. (1999) 'The role of thermal stress fatigue in the breakdown of rock in cold regions', *Geomorphology*, 31(1-4), 47-63.
- Hall, K. and André, M. F. (2001) 'New insights into rock weathering from high-frequency rock temperature data: an Antarctic study of weathering by thermal stress', *Geomorphology*, 41(1), 23-35.
- Jenkins, K. A. and Smith, B. J. (1990) 'Daytime rock surface temperature variability and its implications for mechanical rock weathering: Tenerife, Canary Islands', *Catena*, 17(4-5), 449-459.
- Krähenbühl, R. (2004) 'Temperatur und Kluftwasser als Ursachen von Felssturz', 9, 19-35.
- Lamp, J. L., Marchant, D. R., Mackay, S. L. and Head, J. W. (2017) 'Thermal stress weathering and the spalling of Antarctic rocks', *Journal of Geophysical Research: Earth Surface*, 122(1), 3-24.

- Leith, K., Perras, M., Siren, T., Rantanen, T., Wolter, A., Heinonen, S. and Loew, S. (2017) 'Development of a new thermally-induced fracture in a 12,000 year old bedrock surface', in Leith, K., Ziegler, M., Perras, M. and Loew, S., eds., *Progressive Rock Failure, 2017*, Ascona, Switzerland, ETH Zurich,
- Merrien-Soukatchoff, V., Clément, C., Gunzburger, Y. and Dünner, C. (2007) *Thermal effects on rock slopes: Case study of the "rochers de Valabres" slope (France)*, translated by Lisbon, Portugal.
- Messenzehl, K. and Dikau, R. (2017) 'Structural and thermal controls of rockfall frequency and magnitude within rockwall–talus systems (Swiss Alps)', *Earth Surface Processes and Landforms*, 42(13), 1963-1981.
- Molaro, J. L. and McKay, C. P. (2010) 'Processes controlling rapid temperature variations on rock surfaces', *Earth Surface Processes and Landforms*, 35(5), 501-507.
- Mufundirwa, A., Fujii, Y., Kodama, N. and Kodama, J.-i. (2011) 'Analysis of natural rock slope deformations under temperature variation: A case from a cool temperate region in Japan', *Cold Regions Science and Technology*, 65(3), 488-500.
- Safanda, J. (1999) 'Ground surface temperature as a function of slope angle and slope orientation and its effect on the subsurface temperature field', *Tectonophysics*, 306(3-4), 367-375.
- Stock, G. M., Martel, S. J., Collins, B. D. and Harp, E. L. (2012) 'Progressive failure of sheeted rock slopes: the 2009–2010 Rhombus Wall rock falls in Yosemite Valley, California, USA', *Earth Surface Processes and Landforms*, 37(5), 546-561.
- Taboada, A., Ginouvez, H., Renouf, M. and Azemard, P. (2017) 'Landsliding generated by thermomechanical interactions between rock columns and wedging blocks: Study case from the Larzac Plateau (Southern France)', *EPJ Web of Conferences*, 140, 14012.
- Vargas, E. d. A. J., Castro, J. T., Amaral, C. and Figueiredo, R. P. (2004) *On mechanisms for failure of some rock slopes in Rio de Janeiro, Brazil: Thermal fatigue?*, translated by Lacerda, W., Ehrlich, M., Fontoura, S. A. B. and Sayao, A. S. F., Rio de Janeiro: Taylor & Francis Group, 1007-1011.
- Vargas, E. d. A. J., Chavez, E., Gusmão, L. and Amaral, C. (2009) *Is thermal fatigue a possible mechanism for failures of some rock slopes in Rio de Janeiro, Brazil?*, translated by Asheville, NC.
- Vargas, E. d. A. J., Velloso, R. Q., Chávez, L. E., Gusmão, L. and Palmeiro do Amaral, C. (2013) 'On the Effect of Thermally Induced Stresses in Failures of Some Rock Slopes in Rio de Janeiro, Brazil', *Rock Mechanics and Rock Engineering*, 46(1), 123-134.
- Vlcko, J., Greif, V., Grof, V., Jezny, M., Petro, L. and Breck, M. (2009) 'Rock displacement and thermal expansion study at historic heritage sites in Slovakia', *Environmental Geology*, 58(8), 1727-1740.
- Watson, A. D., Moore, D. P. and Stewart, T. W. (2004) *Temperature influence on rock slope movements at Checkerboard Creek*, translated by W., L., M, E., S.A.B, F. and A.S.F, S., Rio de Janeiro: Taylor & Francis Group, 557-563.

Runout of Landslides in Quick Clays

Mathilde Metral¹, Alessio Ferrari², Håkon Heyerdahl³, Zhongqiang Liu³

¹ BG Ingénieurs Conseils, Lausanne, Switzerland

² EPFL, Lausanne, Switzerland

³ NGI, Oslo, Norway

SUMMARY: Landslides in sensitive clays are one of the most dangerous hazards in Norway. When shear stress in sensitive clays pass the peak strength, the clay liquefies. Flow-like landslides occur suddenly, travel far and very rapidly, and are a threat to life, property, and environment. A reliable estimate of the runout distance is needed to identify the elements at risk and to make decisions on mitigation measures. This paper applies a general methodology for back-calculation of real landslide events. The numerical model used, called BingClaw, is an extension of the Bing model in Eulerian coordinates in two-horizontal dimensions. The visco-plastic Herschel-Bulkley rheology is implemented to compute the landslide movement. The back-calculated runout was compared to the observations on two past landslides in Norway: Kattmarka (2009) and Sørnum (2016). The results show that the runout distance in sensitive clays is determined by, on the one hand, intact and remoulded yield stress and the rate of remoulding since they influence the flow behavior; on the other hand, by the initial released volume, the topography, and the interaction with water. The model gives a reasonably accurate prediction of runout distance, especially for the Kattmarka case study. However, the results are particularly sensitive to parameter changes such as the rheology parameter, and to spatial and temporal discretization of the numerical model.

Keywords: Landslides, Quick clay, Runout, BingClaw, Back calculation

Introduction

The peculiar behaviors of quick-clay landslides make them the most dangerous and damaging natural hazard in some of the Nordic countries. It then becomes essential to improve the understanding and modeling of landslide mobility. The main objective of this study is to investigate uncertainties in parameters, and their effect on runout distance of two historic landslides: Kattmarka (2009) and Sørnum (2016) landslides. The modeling is performed with BingClaw, which is one of very few models to estimate landslide mobility in sensitive clays.

Numerical model: BingClaw

Løvholt et al. (2017) and Kim et al. (2019) present in detail the governing equations and mathematical formulation applied in the numerical model. BingClaw is an extension of the Bing model in Eulerian coordinates in two horizontal dimensions (2HD) (Imran et al. 2001). Based on viscosity measurements in laboratory on Canadian (Locat and Demers, 1988) and Norwegian (Grue et. al 2017) quick clays, visco-plastic Herschel-Bulkley is the most suitable model for completely remoulded clays because the shear stress is a sub-linear function with shear rate. For simple shear conditions, the mathematical formulation is as follows:

$$\left| \frac{\dot{\gamma}}{\dot{\gamma}_r} \right| = \begin{cases} 0 & \text{if } |\tau| \leq \tau_y, \\ \text{sgn}(\dot{\gamma}) \frac{\tau}{\tau_y} - 1 & \text{if } |\tau| \geq \tau_y, \end{cases} \quad (1)$$

with τ the shear stress, τ_y the yield strength, $\dot{\gamma}$ the strain rate, $\dot{\gamma}_r$ the reference strain rate $\dot{\gamma}_r = (\tau_y/\mu)^{\frac{1}{n}}$ where μ is the specific dynamic viscosity and $n = 1$ the exponent for the Bingham fluid model.

The model considers two quick clay layers: the plug and the shear layers; the non-sensitive clay layers aren't considered. The velocity is constant in the plug layer while in the shear layer, the velocity profile follows a $n + 1$ power law. The model solves the mass balance over the entire flow depth, and the momentum balance over the plug and shear layers. Moreover, when an accelerated body is immersed in a fluid such as water, the inertia terms are multiplied by a factor $(1 + C_M \rho_w / \rho_d)$, where C_M is the added mass coefficient (Kim et al. 2019). Then, during the sliding, intact sensitive clays progressively disintegrate into a remoulded material behaving like a fluid. To characterize this remoulding process, the yield strength is reduced accordingly with the accumulated shear deformation:

$$\tau_y(\gamma) = \tau_{y,\infty} + (\tau_{y,0} - \tau_{y,\infty})e^{-\Gamma\gamma} \quad (2)$$

with $\tau_{y,0}$ being the initial yield stress, $\tau_{y,\infty}$ the remoulded yield stress and Γ an empirical coefficient describing the rate of remoulding.

The numerical implementation uses a finite volume method. At each time step, the following steps are computed:

1. The earth pressure gradient combined with gravity is compared to the yield stress at each cell. If the yield stress is larger than the driving forces in a computational cell, then this cell is stable, and no motion is imposed. If two adjacent cells are stable, there is no flux at their interface and the following steps are not necessary.
2. If at least one of the cells is unstable, the equations without friction terms are solved. At each cell interface, a Riemann problem is solved with the wave propagation algorithm of the finite volume method.
3. The friction forces are applied using a Godunov fractional step method.

Methodology

The methodology flowchart, involving sensitivity analysis of relevant parameters for runout prediction, is presented in Figure 1 and is applied to two well-documented Norwegian quick clay landslide events: Kattmarka (2009) and Sørsum (2016).

Results and discussion

Regarding the Kattmarka landslide, the best-fit of remoulded yield stress is slightly overestimated compared to field data. The model is assuming that the entire mass is made of quick clay while the soil is composed of alternating sensitive and non-sensitive materials. Thus, the predicted runout distance, equal to 207 m, is comparable to the observed one which is about 200 m (Fig. 2. (a)). Moreover, a small amount of clay is not considered remoulded in the calculation, although all the clay was evidently involved in the landslide.

About the Sørsum landslide, among the 100 simulations run, none differed significantly. Indeed, a spreading in the upward direction is always observed, debris width is way too large, and no clay is accumulated at the bottom (Fig. 2. (b)). As the choice of input parameters does not cause these observations, the topography is looked at. The digital terrain model made before the event

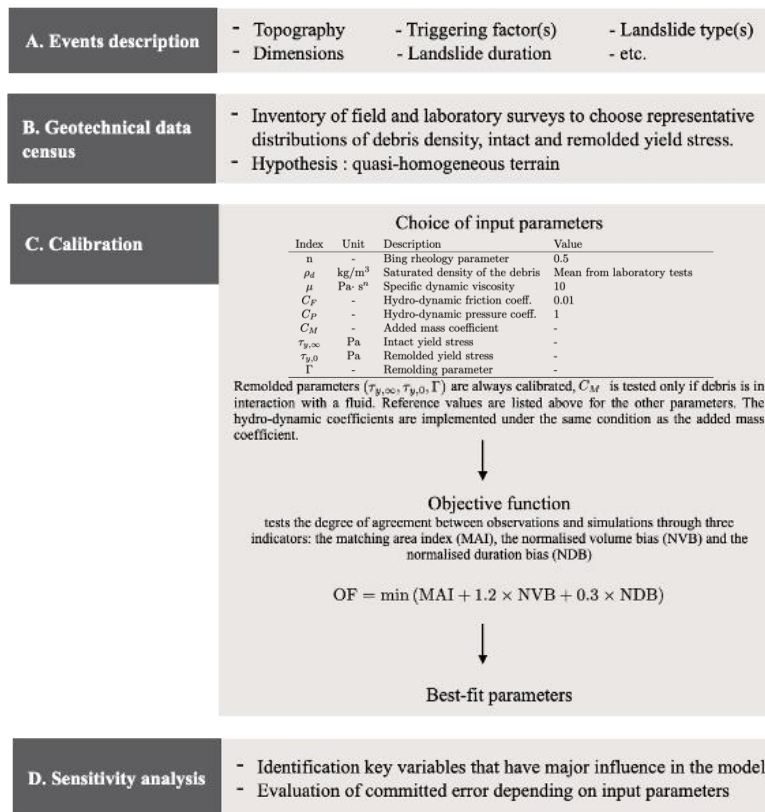


Fig. 1 Summary of the methodology for back-calculations

is used to implement both the initial release volume and initial conditions. However, multiple terrain transformations have been performed between 2013 and 2016, and any digital model was produced after 2013. Thus, the topography where the initial released mass is located does not accurately reflect the conditions just before the event, and the initial volume is also largely underestimated. Indeed, the mass has been filled up to 5 m at this location before the slide.

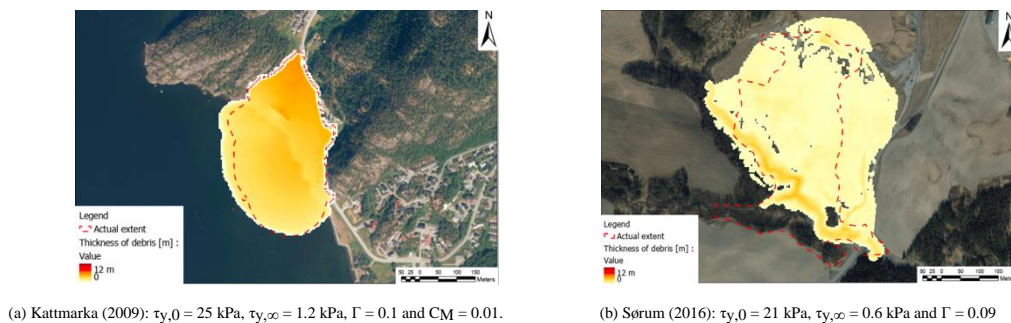


Fig. 2 Predicted average deposit height. Red dashed line represents actual landslide extent from observations.

In this sense, sensitivity analysis allows testing the robustness of the calibration results regarding the different choices that have been made. The results on Kattmarka and Sørsum case studies have shown that:

- runout distance decreased with increasing remoulded yield stress, debris height increases with increasing remoulded yield stress, maximum velocity decreases with an increase of the product $-\log(\Gamma) \times \tau_{y,0}$. The rate of remoulding and the intact yield stress also influence

the amount of remoulded clay, as they control the decrease of yield strength. These observations are in agreement with Liu et al. (2021).

- Bing rheological parameter greatly influences the landslide mobility since it governs the visco-plastic model of the fluid. The viscosity does not seem to play an inherent role in runout distance and debris thickness when it is subjected to low variations but is mainly affected by landslide velocity (Fig. 3).
- Runout distance and material height are sensitive to added mass coefficient, while maximum velocity is also affected by hydrodynamic drag. The estimation of water-interaction coefficients is delicate because they are inherently linked.
- Spatial variables are sensitive to spatial discretization while time variables are sensitive to time discretization. For Kattmarka, this effect is important and drastically changes the predicted runout distance.

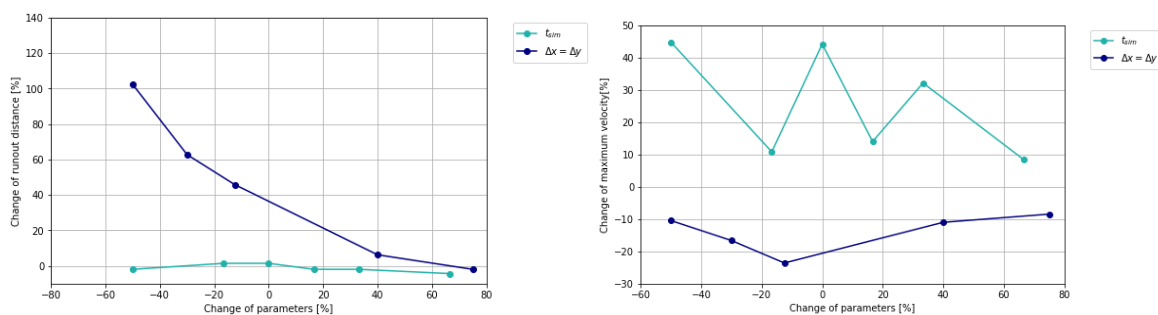


Fig. 3 Parameter sensitivity tests for spatial and temporal implementation for Kattmarka case study. Parameter changes are relative to $\Delta x = \Delta y = 4$ m, and $t_{sim} = 1200$ s.

Conclusion

This study provides the necessary steps to achieve a complete back-calculation by the definition of an objective function and by testing the robustness of the results through a sensibility analysis. The main results obtained have shown that:

- The challenge of modelling quick-clay landslides is to find representative soil parameters. Indeed, soil is seldom homogeneous, and information collected around the landslide area after an event is rarely representative of pre-slide conditions.
- Topography and bathymetric conditions play an inherent role in landslide mobility.
- Runout prediction may also be limited by the lack of witness testimony regarding retrogressive partial releases.

References

- Grue R, Issler D, L'Heureux JS & Thakur V (2017) Visco-metric tests of sensitive clay from bymeset, Norway, and fit to the Herschel-Bulkley model. *2nd Intern. Workshop Landslides Sensitive Clays* 46, 155-166.
- Imran J, Parker G, Locat J & Lee H (2001) 1d numerical model of muddy subaqueous and subaerial debris flows. *Subm. Journal Hydraulic Engineering* 127(11), 959-668.
- Kim J, Issler D, Løvholt F & Forsberg CK (2019) Landslide material control on tsunami-genesis - the Storegga Slide and tsunamis (8100 years BP). *Subm. Journal of Geophysical Research*.
- Liu, Z., L'Heureux, J.-S., Glimsdal, S., & Lacasse, S. (2021). Modelling of mobility of Rissa landslide and following tsunamis. *Computers and Geotechnics*, 140, 104388.
- Locat J & Demers D (1988) Viscosity, yield stress, remoulded strength, and liquidity index relationships for sensitive clays. *Canadian Geotechnical Journal* 25(4), 799-806.
- Løvholt F, Bondevik S, Laberg JS, Kim J & Boylan N (2017) Some giant submarine landslides do not produce large tsunamis. *Geophysical Research Letters* 44, 8463-8472.

Combining Distributed Fibre Optic Sensing With Passive Seismic Interferometry for Advanced Monitoring Applications

Susanne Ouellet^{1,2}, Jan Dettmer², Martin Karrenbach³, Gerrit Olivier⁴, Matthew Lato⁵

¹ BGC Engineering, Calgary, Canada

² University of Calgary, Calgary, Canada

³ Seismics Unusual LLC, Brea, United States

⁴ University of Tasmania, Hobart, Australia

⁵ BGC Engineering, Ottawa, Canada

Keywords: tailings dams, distributed fibre optic sensing, distributed acoustic sensing, passive seismic interferometry, ambient noise monitoring

Introduction

Distributed acoustic sensing (DAS) is a fibre optic sensing technology that relies on the backscattering of Rayleigh light waves. Perturbations to the optical fibre attributed to variations in strain or temperature, affect the phase, intensity and polarization of the backscattered light (Masoudi & Newson, 2016). As DAS can be considered as an array of seismic sensors, it is increasingly being used in place of traditional seismic sensors, installed at discrete locations, to monitor physical processes in the subsurface. DAS is unique from other types of distributed fibre optic sensing methods (e.g., Brillouin and Raman based methods to monitor strain and temperature, respectively) in its capability of monitoring tens of kilometers of fibre at kilohertz sampling rates (Muanenda, 2018). This is highly advantageous for linear assets that require real-time monitoring, such as pipelines and transportation corridors. By applying seismic interferometry, relative changes in seismic velocities (dv/v (%)) can be used to monitor structures such as landslides and dams (Mainsant et al., 2012; Planès et al., 2016). By combining dv/v monitoring with DAS, subsurface changes can be detected with unprecedented spatial and temporal resolution, showing promise for early warning applications. Here, we infer dv/v changes to monitor a tailings dam with DAS. The DAS dataset consists of data recorded from a ~120 m section of buried optical fibre recording data over spring and summer of 2021 at a tailings dam in northern Canada. The seismic velocity changes are compared with environmental site parameters including rainfall, pond levels and temperature data.

Project site and data acquisition

A telecommunications fibre optic cable was installed along ~1 m trench along the crest of multiple active and inactive tailings dams in 2020 (Figure 1). The fibre is routed along overhead lines from the location of the interrogator unit (IU) housing to the tailings dam where it is buried ~1 m below surface. There are multiple above ground splice locations that were required to reroute the cable to accommodate construction near the cable. Further details of the installation configuration are available in Forbes et al. (2021). In 2021, one of the spare optical fibres was connected to an OptaSense ODH-4 interrogator unit, collecting ~24TB of DAS data at a sampling frequency of 400Hz, over a four-month period. The raw DAS output is provided in units of optical phase change ($\Delta\phi$) which can be linearly related to a dynamic measurement of the average strain (ε) along the axis of the fibre over a distance referred to as the gauge length L_G (Lindsey et al., 2020):

$$\varepsilon = \frac{\lambda}{4\pi\xi n L_G} \Delta\phi \quad (1)$$

where n corresponds to a refractive index of 1.468 for the single mode fibre, L_g corresponds to a gauge length of 4 m, λ corresponds to the wavelength of the coherent laser pulse in a vacuum of 1550 nm and ξ corresponds to a thermal optical coefficient of 0.735, accounting for changes in the index of refraction. Separate from the gauge length, the channel spacing determines the spatial distance between each sample along the optical fibre. Selecting a channel spacing less than the L_g is akin to applying a moving average filter to the dataset. A channel spacing of 2 m was selected for the dataset, resulting in the equivalent of 5,000 sensors for 10 km of optical fibre (the total length of optical fibre is greater than the cable length as there are multiple optical fibres with a looped configuration in the cable).

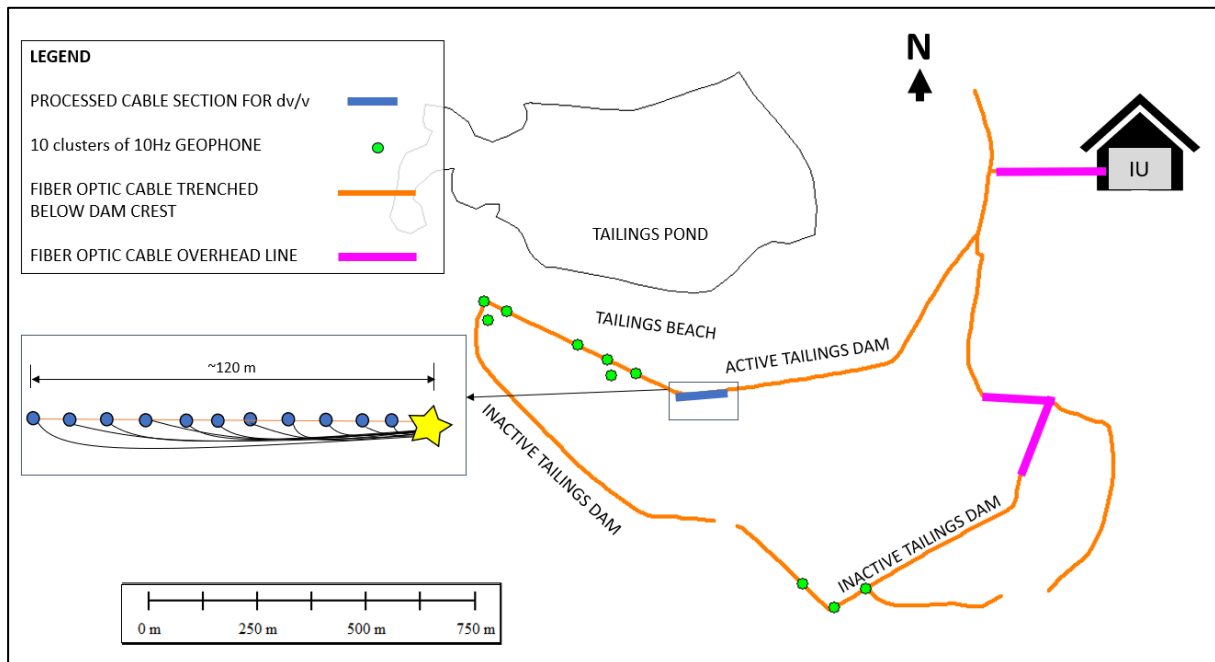


Fig. 1 General configuration of the fibre optic cable alongside the collocated geophones in relation to the tailings pond and interrogator unit (IU) housing. The cable is trenched along the extents of several active and inactive tailings dams. Inset schematic illustrating the virtual DAS channel source as a star with 11 DAS receivers.

Monitoring seismic velocity changes with DAS

Earlier work at the project site applying seismic interferometry techniques to a geophone array demonstrated an inverse correlation between tailings pond levels and seismic velocity changes (Ouellet et al., 2022). Here, we apply similar techniques to a subset of DAS channels. A total of 12 channels at 10 m spacing were selected over a 110 m segment of buried cable for processing (Fig 1). The data was decimated from 400Hz to 50Hz by subsampling. Following this, data pre-processing steps included linear detrending, bandpass filtering from 5Hz to 15Hz, one-bit normalization and spectral whitening. One-bit normalization in the time domain reduces the effect of instrumental irregularities, earthquake signals and non-stationary noise sources. Spectral whitening broadens the frequency band of ambient noise and reduces the effect of monochromatic noise sources (Bensen et al., 2007). Individual DAS channels were then cross correlated in twenty-second time windows over a twelve-hour period (18:00:00 to 06:00:00 local time). This period was chosen to minimize the effect of spurious noise sources from active traffic and construction occurring adjacent to the fibre during the day.

The easternmost DAS channel was selected as a virtual source and all other 11 DAS channels acted as virtual receivers. Cross-correlation waveforms were stacked over each day to obtain

daily cross-correlation waveforms. A reference cross-correlation waveform (required for monitoring seismic velocity changes) was obtained by computing the mean of all daily cross-correlation waveforms over the data acquisition period (~90 days). Relative changes in seismic velocities using the reference and daily cross-correlation waveforms are obtained using the ‘stretching’ method to obtain dv/v measurements. Seismic velocity changes with a correlation coefficient of less than 0.7 were removed.

Results

The results from combining DAS with seismic interferometry were compared to available environmental site data, including water levels from the nearby tailings pond, daily rainfall and air temperature. A general decrease in dv/v is observed to occur following the highest daily rainfall over the recording period. A negative correlation between the dv/v time-series data with daily resampled surface temperature data is observed, with a Pearson correlation coefficient of -0.8. To investigate the correlation with surface temperature, we model temperature at a depth of 0.85 m (corresponding to the depth of the cable) using a 1D analytical model by following a similar approach as described in van Wijk & de Vries (1963).

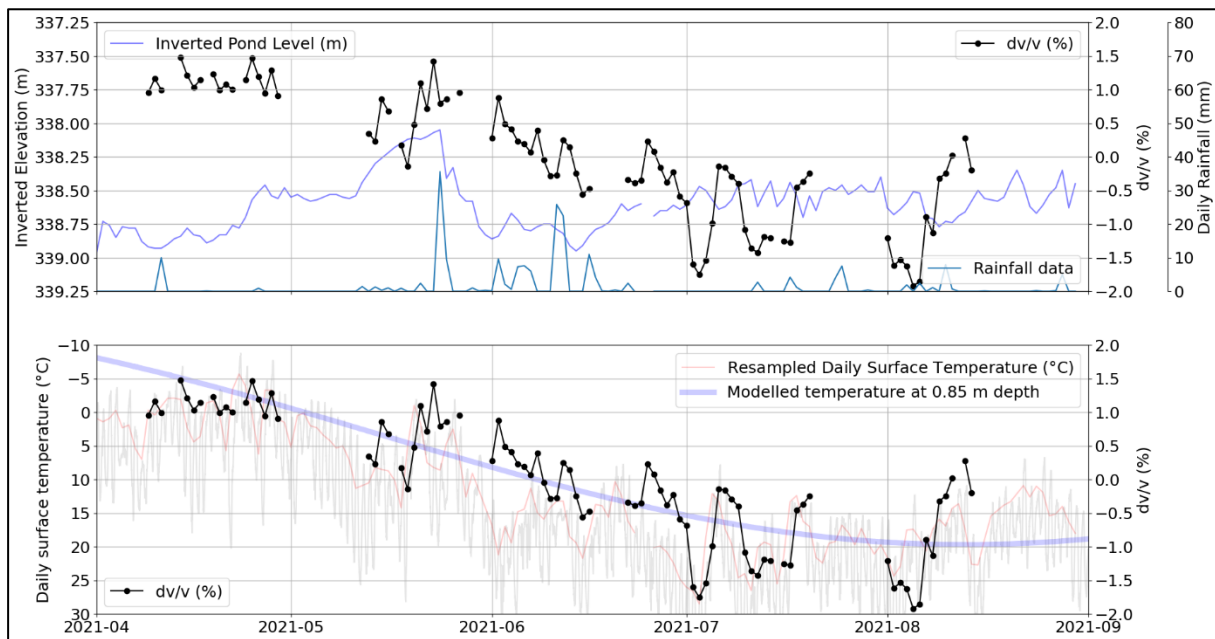


Fig. 2 Results from applying seismic interferometry to the DAS dataset, shown as dv/v (%). The upper plot compares dv/v with water levels (inverted) from the adjacent tailings pond and daily rainfall. The lower plot shows the surface temperature (daily resampled temperature in red and hourly temperature data in light grey) and dv/v for comparison. The modelled temperature at 0.85 m below surface using a 1D analytical model is plotted in blue.

Discussion and conclusions

The results from applying seismic interferometry to a DAS cable segment indicate there may be multiple physical processes contributing to the dv/v response (temperature, pond level changes, rainfall). The negative correlation with surface temperature is unlikely related to direct temperature effects on the fibre, considering the burial depth of the fibre optic cable. At a depth of 0.85 m below ground, daily temperature fluctuations are expected to be negligible based on the analytical model (van Wijk & de Vries, 1963). However, Berger (1975) demonstrated how temperature fluctuations at surface can induce earth strains. As DAS is sensitive to nano strains, we hypothesize that a component of the observed dv/v may be a result of thermally induced

strain in the overburden. Future research is planned to produce a theoretical model of strain at the cable depth to confirm.

DAS can provide continuous data streams in a broad range of frequencies, along extents ranging up to tens of kilometers. Current DAS research touches on a wide range of applications in geotechnical monitoring, including acoustic emission monitoring of slope failure (Michlmayr et al., 2017), strain changes at a landslide site (Kogure & Okuda, 2018); nonlinear earthquake response of marine sediments (Viens et al., 2022); and groundwater level changes (Rodríguez Tribaldos & Ajo-Franklin, 2021). Combining seismic interferometry with DAS is a relatively novel application that shows promise for providing crucial information on changes in soil properties, using dv/v as a proxy. Further research aims to improve understanding of the sensitivity of dv/v to different physical processes (e.g. saturation, temperature, rainfall, etc.) to support DAS monitoring with dv/v for geotechnical applications.

References

- Bensen, G. D., Ritzwoller, M. H., Barmin, M. P., Levshin, A. L., Lin, F., Moschetti, M. P., Shapiro, N. M., & Yang, Y. (2007). Processing seismic ambient noise data to obtain reliable broad-band surface wave dispersion measurements. *Geophysical Journal International*, 169(3), 1239–1260. <https://doi.org/10.1111/j.1365-246X.2007.03374.x>
- Forbes, B., Ouellet, S., Suszek, N., Lato, M., & Russell, B. (2021). Application of distributed acoustic sensing within a tailings dam warning system. *Proceedings of Tailings and Mine Waste*, 469–477. <https://www.researchgate.net/publication/357632053>
- Kogure, T., & Okuda, Y. (2018). Monitoring the Vertical Distribution of Rainfall-Induced Strain Changes in a Landslide Measured by Distributed Fiber Optic Sensing With Rayleigh Backscattering. *Geophysical Research Letters*, 45(9), 4033–4040. <https://doi.org/10.1029/2018GL077607>
- Lindsey, N. J., Rademacher, H., & Ajo-Franklin, J. B. (2020). On the Broadband Instrument Response of Fiber-Optic DAS Arrays. *Journal of Geophysical Research: Solid Earth*, 125(2). <https://doi.org/10.1029/2019JB018145>
- Mainsant, G., Larose, E., Brnimmann, C., Jongmans, D., Michoud, C., & Jaboyedoff, M. (2012). Ambient seismic noise monitoring of a clay landslide: Toward failure prediction. *Journal of Geophysical Research: Earth Surface*, 117(1). <https://doi.org/10.1029/2011JF002159>
- Masoudi, A., & Newson, T. P. (2016). Contributed Review: Distributed optical fibre dynamic strain sensing. *Review of Scientific Instruments*, 87(1). <https://doi.org/10.1063/1.4939482>
- Michlmayr, G., Chalari, A., Clarke, A., & Or, D. (2017). Fiber-optic high-resolution acoustic emission (AE) monitoring of slope failure. *Landslides*, 14(3), 1139–1146. <https://doi.org/10.1007/s10346-016-0776-5>
- Muanenda, Y. (2018). Recent Advances in Distributed Acoustic Sensing Based on Phase-Sensitive Optical Time Domain Reflectometry. In *Journal of Sensors* (Vol. 2018). Hindawi Limited. <https://doi.org/10.1155/2018/3897873>
- Ouellet, S., Dettmer, J., Olivier, G., de Wit, T., & Lato, M. (2022). Advanced monitoring of tailings dam performance using seismic noise and stress models. *Commun Earth Environ* 3, 301. <https://doi.org/10.1038/s43247-022-00629-w>
- Planès, T., Mooney, M. A., Rittgers, J. B. R., Parekh, M. L., Behm, M., & Snieder, R. (2016). Time-lapse monitoring of internal erosion in earthen dams and levees using ambient seismic noise. *Geotechnique*, 66(4), 301–312. <https://doi.org/10.1680/jgeot.14.P.268>
- Rodríguez Tribaldos, V., & Ajo-Franklin, J. B. (2021). Aquifer Monitoring Using Ambient Seismic Noise Recorded With Distributed Acoustic Sensing (DAS) Deployed on Dark Fiber. *Journal of Geophysical Research: Solid Earth*, 126(4). <https://doi.org/10.1029/2020JB021004>
- van Wijk, V. R., & de Vries, D. A. (1963). Periodic temperature variations in a homogenous soil. In *Physics of Plant Environment*. North Holland Publ. Co.
- Viens, L., Bonilla, L. F., Spica, Z. J., Nishida, K., Yamada, T., & Shinohara, M. (2022). Nonlinear Earthquake Response of Marine Sediments With Distributed Acoustic Sensing. *Geophysical Research Letters*, 49(21). <https://doi.org/10.1029/2022gl100122>

Predicting Annual Displacement Probability of Slow-Moving Landslides through Markov Chain and Monte Carlo Simulation

Michael Porter¹

¹ BGC Engineering Inc., Vancouver, Canada

SUMMARY: Normally slow-moving landslides are complex, dynamic systems. The potential variability in their velocity has important implications for risk assessment, design, monitoring, and maintenance of infrastructure. Markov Chain models offer a systematic, expert-based approach to predict landslide velocity probability distributions over the design life of existing and proposed infrastructure. In many scenarios, infrastructure condition states can be linked to cumulative and/or annual landslide displacement thresholds. Monte Carlo simulation combined with Markov model outputs can be used to estimate the annual probability of landslide displacement threshold exceedances and infrastructure condition state probabilities. In turn, these can facilitate lifecycle cost modelling and risk cost-benefit analysis of landslide stabilization and other management options.

Keywords: slow-moving landslide, displacement probability, Markov Chain

Introduction

The velocity of normally slow-moving landslides in clays and mudstones will vary seasonally and from year to year in response to numerous factors that can alter the forces resisting and promoting movement. With advances in landslide and infrastructure monitoring it is now possible to dramatically reduce the potential for some types of catastrophic loss such as life loss from train derailments, building collapse, and pipeline rupture caused by slow-moving landslides. However, landslide monitoring and response is still a relatively reactive approach that typically only manages a small fraction of the total consequence and risk. For example, Porter et al., (2019) described how normally slow-moving landslides within the Western Canada Sedimentary Basin cause damage to infrastructure with estimated economic impacts likely exceeding \$450 million per year. Most of the economic impacts were associated with infrastructure maintenance and repair effort and business interruption costs which can only be modestly reduced through monitoring.

Sometimes it will be feasible to avoid slow-moving landslides or to improve their stability to the point where they are very unlikely to move during the infrastructure design life, but in many cases neither of these options will be practical. Decisions on how best to reduce economic risk where existing or planned infrastructure crosses slow-moving landslides are ideally informed by risk cost-benefit analysis. Quantification of risk requires tools to estimate the probabilities of different landslide velocities over time horizons which may encompass several decades.

Since early 2020, the author and several colleagues have been working on methods to estimate the probabilities of landslide velocity transitions and total annual displacements using Markov Chain models which offer a systematic, expert-based approach to predict annual displacement probability distributions for certain types of landslides (Porter et al., 2022a).

Modified Landslide Velocity Classification System

The approach involves treating landslide velocity as a state variable and velocity classes as condition states. Some modifications to the Cruden and Varnes (1996) classification system are required to allow for compatibility with the modelling approach. The most significant modifications include creating a Velocity Class 0 for dormant landslides, subdivision of the Very Slow category into two classes, equating the velocity classes to expected total annual displacements (as opposed to instantaneous velocities), and assignment of an assumed left-triangular probability density function to the expected displacements associated with each velocity class range. The modified landslide velocity classification system is shown in Tab. 1, and additional detail is provided in Porter et al., (2022a).

Tab. 1 Modified Landslide Velocity Classification after Cruden and Varnes (1996)

Class	Description	Typical velocity	Annual displacement criteria (m)	Mean annual displacement based on assumed left-triangular distribution (m)
4+	Moderate	>13 m/mo	>16	64 (for the range between 16-160 m/yr)
3	Slow	>1.6 m/yr	>1.6	6.4
2b	Very slow	>160 mm/yr	>0.16	0.64
2a	Very slow	>16 mm/yr	>0.016	0.064
1	Extremely slow	<16 mm/yr	>0.0016	0.005
0	Dormant	0 mm/yr	<0.0016	0

Note: Class 4+ refers to all velocity classes Moderate or greater (i.e., Rapid, Very rapid and Extremely rapid)

Probabilities of Moderate, Rapid, Very Rapid, and Extremely Rapid velocities are not differentiated, and are lumped together in a category that includes any annual displacement exceeding 16 m (Class 4+). If such velocities are deemed credible for a specific landslide, other approaches (e.g., Glastonbury and Fell, 2008) are deployed to further estimate their conditional probabilities in the case that Class 4+ velocities are realized.

Predicting the Annual Displacement of Slow-moving Landslides

Many normally slow-moving landslides have potential to produce the annual displacements associated with Velocity Classes 0 to 4+ in Tab. 1. The challenge is to efficiently estimate the probability distribution for each landslide of interest over the design life of infrastructure or other assets of value, and with sufficient accuracy to improve decision-making. Ultimately, we aspire to develop multi-criteria, data-driven numerical and statistical models to predict landslide velocity class probabilities, but the data necessary for model training and for model application are expensive and time-consuming to generate. Until then, simplified approaches are required to inform today’s risk management decisions. To do so, we leverage the Theory of Uniformitarianism (over the long-term, future velocity distributions ought to resemble past distributions, acknowledging that climate change may challenge this assumption), and the hypothesis that current annual velocity is a useful predictor of velocity in the near-term.

Markov Chains

Markov Chains offer an approach to capture the change in our state of knowledge between a known velocity today and an assumed velocity class probability distribution many years into the future. Markov Chains are probabilistic models useful for analyzing dynamic systems

(Howard, 2007). In these models, the condition of a physical system can be described by state variables. For the physical system comprising a landslide, velocity (i.e., annual displacement) can be treated as a state variable and the velocity classes listed in Tab. 1 treated as condition states. Key elements of a Markov model can be encapsulated in a “Transition Matrix” (P) with N rows and N columns which illustrates the “ N ” possible condition states and the probabilities of transitioning between states (or remaining in the current state) during each model timestep. To predict the probabilities of being in a particular condition state after a certain number of timesteps, one needs to know the state of the system at timestep $n = 0$. This is referred to as the initial state vector. The initial state vector ($\pi(0)$) is a 1-row matrix listing the probabilities of being in each possible state at $n = 0$. The state vector at any timestep can be calculated by post-multiplying the state vector at the preceding timestep by the transition matrix P [Equation 1].

$$\pi(n+1) = \pi(n)P \tag{1}$$

After many timesteps without observation, our knowledge of the state of the system diminishes to a constant value represented by a limiting state probability vector, irrespective of the value of the initial state vector. In the case of landslide velocity, the limiting state vector can be thought of as the distribution of velocity classes that would be realized over a very long period of observation (e.g., hundreds or thousands of years). Alternatively, the observed distribution of velocity classes from a large inventory of landslides of a certain type over a period encompassing decadal-scale climate cycles also ought to resemble the limiting state vector for that type of landslide in that environment.

Example Landslide Behavior Types and Landslide Velocity Markov Models

An expert-based geomorphic assessment of the past behaviour of a landslide (e.g., its displacement over geologic time as a product of the proportion of years spent in each velocity class, and evidence of episodes of faster movement) can be used to define a subjective limiting state vector for that behaviour type. Porter et al. (2022a) proposed five different behaviour types with limiting state vectors yielding long-term average annual displacements ranging from 0.01 to 1.0 m/yr (Tab. 2). A transition matrix that would generate the desired limiting state vector was established for each landslide behaviour type (e.g., Fig. 1).

Tab. 2 Proposed landslide behaviour types and characteristics for pre-existing slow-moving landslides

Behaviour Type	Type A	Type B	Type C	Type D	Type E
Typical failure mechanism	Translational block slides and spreads	Translational block slides and spreads	Translational block slides and spreads, rotational slides	Translational and rotational slides, earth flows, complex slides	Translational and rotational slides, earth flows, complex slides
Assumed limiting state velocity class distribution					
0	70%	50%	30%	10%	0.5%
1	28.5%	45.5%	55.0%	44.9%	3.0%
2a	1.1%	3.2%	10.8%	32.4%	54%
2b	0.4%	1.1%	3.6%	10.8%	36%
3	0.06%	0.18%	0.60%	1.8%	6.0%
4+	0.005%	0.015%	0.050%	0.15%	0.50%
Mean annual displacement	0.01 m	0.03 m	0.1 m	0.3 m	1.0 m
Probability of Class 4+	1:20,000 (or not credible)	1:6,700	1:2,000	1:670	1:200

From/To	0	1	2a	2b	3	4+
0	0.99620	0.00342	0.00034	0.00003	0.000003	0.000000
1	0.00387	0.99376	0.00213	0.00021	0.00002	0.000002
2a	0.00332	0.02991	0.95320	0.01221	0.00122	0.00014
2b	0.00052	0.00467	0.04666	0.92800	0.01814	0.00202
3	0.00015	0.00134	0.01345	0.13446	0.82000	0.03060
4+	0.00007	0.00062	0.03381	0.34500	0.31050	0.31000
Target	0.50	0.455	0.032	0.011	0.0018	0.00015

Fig. 1 Velocity class transition matrix for Landslide Behaviour Type B and target limiting state vector

Asset Condition States Linked to Cumulative or Annual Landslide Displacement

The outputs of the Markov models are vectors (probability distributions) of the possible landslide velocity classes for each annual timestep. These should be treated by the practitioner as subjective probabilities that are reviewed carefully and adjusted using experience and judgment, if required. In many scenarios, infrastructure condition states can be linked to cumulative and/or annual landslide displacement thresholds. Monte Carlo simulation can be used to combine the Markov model velocity class probability distributions with the assumed left-triangular displacement probability density function for each velocity class to estimate the annual probability of landslide displacement threshold exceedances and infrastructure condition state probabilities (Porter et al., 2022b; Porter et al., 2022c). In turn, these can facilitate lifecycle cost and risk cost-benefit analysis of landslide stabilization and other management options.

Final Remarks

A Markov Chain, Monte Carlo Simulation approach has been developed to support estimates of velocity class probability distributions for normally slow-moving landslides which are useful inputs to landslide hazard and risk assessment and can inform management options. Regional landslide databases and velocity timeseries data are being assembled to improve the statistical basis for the approach. In a changing climate, the limiting state vectors of the velocity classes for different landslide types are expected to change. The approach offers the possibility of accounting for climate change by compiling limiting state vectors for similar landslide types in climatic regions that are representative of a region-of-interest’s future climate.

References

Cruden, D.M. and Varnes D.J. 1996. Landslide types and processes. In: Turner and Schuster (eds) *Landslides, investigation and mitigation, Special Report 247*, Transportation Research Board, National Research Council. National Academy Press, Washington, USA, 3: 36-75.

Glastonbury, J. and Fell, R. 2008a. A decision analysis framework for the assessment of likely post-failure velocity of translational and compound natural rock slope landslides. *Can. Geotech. J.* 45: 329-350.

Porter, M., Van Hove, J., Barlow, P., Froese, C., Bunce, C., Skirrow, R., Lewycky, D., Bobrowsky, P. 2019. The estimated economic impacts of prairie landslides in western Canada. *Proceedings of Geo St. John’s*, Canadian Geotechnical Society, St. John’s, Newfoundland, Canada.

Howard, R. 2007. *Dynamic Probabilistic Systems, Volume 1: Markov Models*. Dover Publications, New York.

Porter, M., Quinn, P., and Barlow, P. 2022a. Conceptual landslide velocity transition models for a range of landslide behaviour types. *Georisques VIII – Proceedings of the 8th Canadian Geohazards Conference*, Canadian Geotechnical Society, Quebec City, Quebec, Canada.

Porter, M., Anderson, S., Vessely, M., and Devonald, M. 2022b. Reliability models for roads crossing slow-moving landslides. *Proceedings of the 71st Highway Geology Symposium*, Asheville, NC, USA.

Porter, M., Van Hove, J., and Barlow, P. 2022c. Analysis of dynamic system risks where pipelines cross slow-moving landslides. *Proceedings of the 14th International Pipeline Conference*, Calgary, Alberta. September 26 – 30, 2022 (In Press).

A Simplified Procedure to Assess the Potential Effects of Climate Change on the Mobility of a Slow Active Earthflow in Southern Italy

Guido Rianna¹, Alfredo Reder¹, Luca Comegna², Gianfranco Urciuoli³, Luciano Picarelli¹

¹Fondazione Centro Euro-Mediterraneo sui Cambiamenti Climatici (CMCC), Caserta, Italy

²Università della Campania “Luigi Vanvitelli”, Aversa, Italy

³Università degli Studi di Napoli “Federico II”, Napoli, Italy

SUMMARY: The effects of the climate change are more and more evident. It is thus compelling to quantify their impacts to identify priorities and find effective adaptation solutions. A major issue is assessing the evolution of active landslides in unstable areas. Based on monitoring of an active earthflow in Southern Italy, the paper tries correlating the expected future precipitation-potential evapotranspiration balance and the water level fluctuations, which govern the mobility of the landslide, through a specific "vulnerability domain".

Keywords: groundwater regime, earthflow mobility, climate change, bottom-up approach, vulnerability domain

Foreword

The effects of the climate change are more and more evident. It is thus of crucial importance assessing its potential impact in order to establish proper adaptation measures. Recently, so-called “bottom-up” approaches (Johnson & Weaver 2009) are being adopted. Their starting point is the evaluation of critical aspects of the systems to protect and the establishment of suitable protection measures: climate projections are then exploited to assess how climate change can affect them and how effective the selected measures can result. The aim of this paper is just to assess if this approach would be effective in the investigation of the effects of climate change on the mobility of a slow active earthflow that threatens the serviceability of some structures and infrastructures in a small area of the Southern Italian Apennines.

The case study

Earthflows are widespread in highly fissured clay shales In Italy. In the surging "flow" stage their velocity can reach metres per hour; then, it gradually decreases while a steady-state "sliding" condition characterised by displacement rates of a few cm per year is reached. Even though the risk for human lives is low, cumulative movements can damage structures, infrastructure and lifelines.

The Masseria Marino earthflow is active since many tens of years. It consists of a softened clayey mass including rock blocks and fragments that moves over a completely remoulded shear zone up to about 1 m thick. The earthflow presents a source area, an about 200 m long and 30 m wide track, and an accumulation zone that is located in the alluvial plain of the Basento river. The average angle of the track is about 10° and its depth ranges between 5 and

6 m. Figure 1 shows a schematic section of the landslide and the boundary conditions adopted in the analysis.

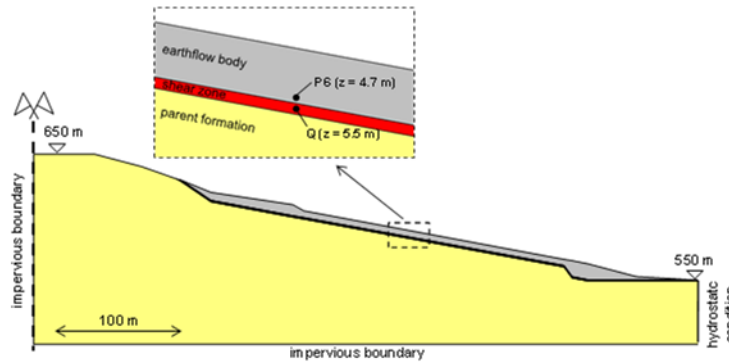


Figure 1. Schematic profile of the Masseria Marino earthflow and investigated points P6 and Q.

During the present slow “sliding” phase, landslide movements are governed by fluctuations of the water table. In particular, the water level measured from September 1992 to December 1998 at the Casagrande piezometer P6 installed in the main track at a depth of 4.7 m (Fig. 1), ranges between such a depth, i.e. $Z_{wP6} = -4.7$ m, which is the minimum value readable through the cell, and $Z_{wP6} = -0.7$ m. Based on topographic readings, the displacement rate ranges between much less than one mm/day and 5-6 mm/day. Through 2D stability analyses, Picarelli et al. (2022) back-calculated a mobilized friction angle $\phi'_{mob} = 13^\circ$.

The "vulnerability domain"

This paper focuses on the potential effects of climate change on the pore pressure fluctuations that govern landslide movement, based on a simplified approach that simulates the landslide as a 10° , 5.5 thick, infinite slope with a 1 m thick shear zone. Assuming a unit weight $\gamma_{sat} = 20$ kN/m³ and a residual friction angle $\phi'_{res} = 13^\circ$, the safety factor is equal to one as the depth of the water level on the slip surface (Point Q, Fig. 1) is $Z_{wSS} = -3$ m; any increase above such a value hence leads to landslide acceleration. To assess the future evolution of the water level, a hydrological modelling chain has been developed. The first step has been estimating through a numerical model the water level, Z_{wSS} , on the slip surface (Point Q), where piezometric data miss, using records provided by all available piezometers and all available data about soil properties. Then, based on observations over the time interval 1981-2010, a relationship has been established between Z_{wSS} and a simple climate variable allowing to cut down the computational effort. In particular, Z_{wSS} has been correlated with the potential fluxes through the ground surface that here have been assumed to be equal to the cumulative monthly values of the Climatic Water Balance, CWB, i.e. the difference between precipitation, P, and potential evapotranspiration, PE; this last has been calculated by the Hamon equation.

Such a relationship allows building a “vulnerability domain” that is represented by an abacus reporting on its axes the “anomalies” in terms of variations of yearly precipitation (P) and of yearly potential evapotranspiration (PE), for which the value of Z_{wSS} is expected to be larger than the threshold $Z_{wSS} = -3$ m. In practice, the abacus has been built by perturbing the yearly precipitation and/or the potential evapotranspiration from 0 to 200% (i.e. twice what has been provided by the baseline) and calculating the corresponding water levels Z_{wSS} . The “perturbed” yearly precipitation has been obtained by changing all the monthly cumulative values by the same fixed percentage. The same strategy has been used for potential evapotranspiration. For each combination, the mean number of months for the threshold is

exceeded has been computed. The obtained “vulnerability domain” for the Masseria Marino earthflow is shown in Figure 2. The figure also reports the effects of future climate projections, which are discussed in the next section.

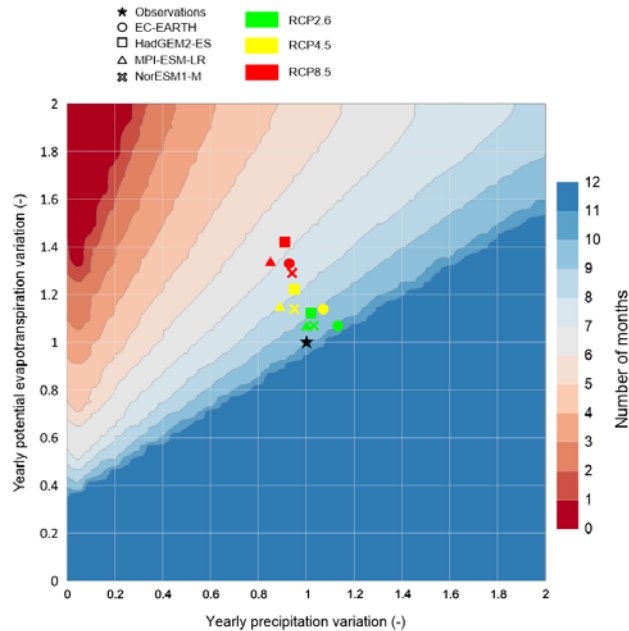


Figure 2. "Vulnerability domain" for the Masseria Marino earthflow. The symbols show the results of climate simulation chains: red symbols stand for RCP8.5, yellow ones for RCP4.5 and green ones for RCP2.6. Regarding the CSCs, circles for GCM EC-EARTH, squares for HadGEM2-ES, triangles for MPI-ESM-LR, crosses for NorESM1-M have been adopted. The black symbol refers to the calibration period 1981-2010.

Effects of future climate conditions and conclusive remarks

The future climate conditions have been obtained by exploiting a sub-set of four modelling chains driven by different Global Climate Models (GCMs) and sharing the same Regional Climate Model (RCM). The RCM outputs have been 'bias-adjusted' by the Scaled Distribution Mapping (SDM) procedure (Switanek et al 2017). In the analysis, three Representative Concentration Pathways (RCP2.6, RCP4.5, and RCP8.5), have been considered as forcing for climate projections; notice that the RCP suffix stands for the expected increase in radiative forcing compared to the preindustrial era: RCP2.6 is the most optimistic scenario; RCP8.5 is the most pessimistic one that should lead to an increment in temperature much larger than the 2°C target established in the Paris Agreement (2015).

The investigated site presents the typical weather patterns of the Mediterranean area with rainy periods concentrated in autumn, winter and early spring and potential evapotranspiration reflecting the temperature patterns. Therefore, two distinct periods, cold-wet and warm-dry respectively, can be clearly recognised, the former roughly coinciding with autumn and winter, and the latter covering the remaining part of the year. Looking at the future, in general terms, the variations in precipitation provided by the climate models span from -15% to about +15%, while the potential evapotranspiration should range from +5% and +42%. Temperature increases should then drive a growth in the evaporative demand. These values are of course a function of the time horizon and of the severity of the concentration scenario; similar tendencies, however, are shown by all climate simulation chains. Surely more complex is the evaluation of future precipitation regime with limited variations but for the RCP8.5 scenario that returns a yearly decreasing signal.

Figure 3 summarizes the results of the analyses in terms of ensemble mean (continuous line) and spread among the projections under the same forcing (RCP) and over the same period (shaded areas). Such data are reported in terms of average monthly fluctuation of the water level z_{wSS} over the hydrological year (September-August). For these analyses, the bias-adjusted monthly evolutions of precipitation and potential evapotranspiration provided by each GCM+RCM simulation chain have been adopted as input for different time horizons. The figure shows the reduction in the number of months for the threshold should be exceeded: for RCP2.6, it is limited, while for RCP4.5 and RCP8.5 it is more evident: the farther the time horizon the larger the reduction. In particular, under the more severe concentration scenario, the mean number of months during which the threshold is exceeded decreases from about 10 to 7 months with limited spread among the projections. However, the highest groundwater level ($z_{wSS} = -1.5$ m) does not seem to change significantly under the different RCPs and time horizons even though covering a shorter time span.

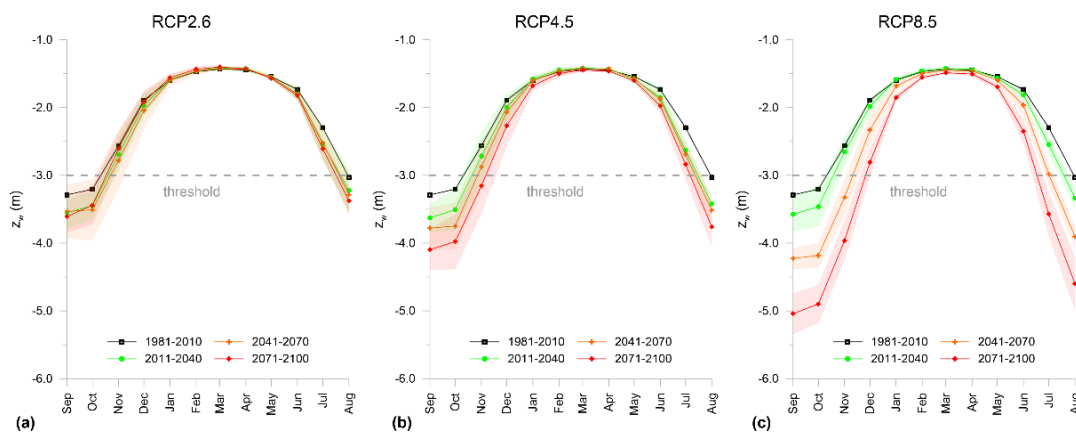


Figure 3. Mean trend of z_{wSS} . Continuous lines identify the ensemble mean computed among the projections. Four time spans are considered: 1981-2010 (black), 2011-2040 (green), 2041-2070 (orange), 2071-2100 (red).

The effects of the expected climate change have been reported through distinct symbols in Figure 2. In particular, a significant deceleration in the rate of slope movement should take place under the most severe RCP8.5 scenario. In the case at hand, the expected climate change should then cause a decrease of landslide mobility.

References

- Johnson TE & Weaver CP (2009) A framework for assessing climate change impacts on water and watershed systems. *Environ. Manag.* 43: 118–134.
- Picarelli L, Comegna L & Urciuoli G (2022). The friction angle mobilized by shallow earthflows in tectonized clay shales. *Italian Geotechnical Journal*, 56: 5-16.
- Switanek MB, Troch PA, Castro CL, Leuprecht A, Chang HI, Mukherjee R & Demaria EMC (2017). Scaled distribution mapping: a bias correction method that preserves raw climate model projected changes. *Hydrol Earth Syst Sci* 21: 2649–2666.

ACKNOWLEDGMENTS

The research has been supported by MIUR PON R&I 2014-2020 (project MITIGO). We acknowledge the World Climate Research Programme's Working Group on Regional Climate, and the Working Group on Coupled Modelling, former coordinating body of CORDEX and responsible panel for CMIP5, the climate modelling groups for producing and making available their model outputs. We also acknowledge the Earth System Grid Federation infrastructure an international effort led by the U.S. Department of Energy's Program for Climate Model Diagnosis and Intercomparison, the European Network for Earth System Modelling and other partners in the Global Organisation for Earth System Science Portals (GO-ESSP).

Adaptation to Climate Changes: a Necessary Step Towards the Improvement of Landslide Prediction Models

Ela Šegina¹, Mateja Jemec Auflič¹, Tina Peternel¹

¹ Geological Survey of Slovenia, Dimičeva 14, 1000 Ljubljana, Slovenia

SUMMARY: Validation of the Slovenian national landslide prediction model highlights the gaps and suggests some future adaptations related to the climate changes to improve the shallow landslides prediction. The analysis of weather conditions related to unpredicted landslide events that occurred between the years 2014 and 2022 in Slovenia implies five basic weather conditions that trigger the unpredicted landslides: i) intensive daily precipitation, ii) several successive days of heavy rainfall, iii) antecedent heavy precipitation, iv) antecedent intensive precipitation and v) intensive snow melting. Important factors are extreme rain events with a long return period. Recently altered weather conditions attributed to climate changes appear to greatly influence the success of the landslide prediction models and need to be considered in defining relevant triggering weather conditions and threshold values.

Keywords: landslide, prediction, model, climate changes

Introduction

The occurrence of landslides is influenced by several factors related to the stability of the slopes (Hunger et al, 2014), among which rainfall is one of the most important triggers. In a changing climate, the frequency and intensity of rainfall events are generally expected to increase (Gariano & Guzzetti, 2016). The study on the impact of climate changes on landslides in Slovenia indicates that in the mid-century (2041-2070), the frequency of heavy rainfall will be higher in the north-west, north and east of Slovenia (Jemec Auflič et al. 2021). Climate changes are presumed to considerably influence the alteration of weather conditions that are the core element of the landslide prediction systems. The scope of this research is to recognize altered weather conditions that trigger shallow landslides and remain unpredicted with current prediction models. The research aims to generate the starting points for future adaptations of landslide prediction models to climate changes that will help improve the existing landslide predictions.

Slovenian landslide prediction model (MASPREM)

The Slovenian national landslide prediction system MASPREM was launched in 2013 to inform inhabitants of an increased probability of shallow landslide occurrences as a consequence of heavy precipitations (Jemec Auflič et al., 2016; Peternel et al., 2022). It forecasts landslide probability based on a landslide susceptibility map (LSM), statistically defined rainfall threshold values and rainfall forecast models ALADIN/SI and INCA (obtained by Slovenian Environment Agency). The model operates at a national (1:250.000) and local scales (1:25.000). Model is used by the emergency service and Administration of the Republic of Slovenia for Civil Protection and Disaster Relief. Currently, the MASPREM system calculates five different landslide models in parallel. They differ in a combination of LSM, forecast models (ALADIN, INCA) and threshold values. In this paper, we analysed a model

which does not consider the antecedent rainfall. Based on the validation of the model for the period between the years 2018 and 2022, 25 % of all alarms were true positive predictions.

Analytical steps

The performance of the MASPREM prediction model was validated with the recorded landslides reported by the municipalities through the web application between the years 2014 and 2022. Dates with the unpredicted landslides were extracted from the dataset, recorded landslides were georeferenced, and the closest meteorological station (Slovenian Environmental Agency) was assigned to each landslide. Meteorological data provided by the closest station, namely the daily precipitation and the height of the snow cover for the previous month were attributed to the landslide event and analysed. Finally, archival meteorological reports for the periods of interest were reviewed and attributed to unpredicted landslide events.

Analysis of the weather conditions in the case of unpredicted landslides

In 3216 analysed days of MASPREM model performance we recorded 48 days when the model did not predict the occurred landslide events and evidenced 262 shallow landslides. The highest number of unpredicted landslides was recorded in 2014 and was related to a multiple-day long extreme rainfall event with flooding that occurred in September 2014 (Fig. 1). The event was assigned the 100-year return period and influenced the entire country (in particular the northeast); the amount of precipitation was up to 4-times above the average value.

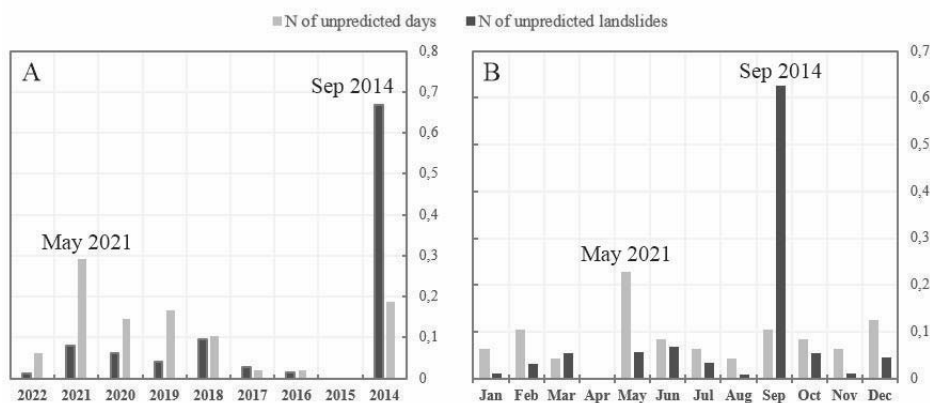


Fig. 1 Yearly (A) and monthly (B) distribution of the normalized values of all unpredicted landslide days and unpredicted landslides.

On the opposite, the highest number of unpredicted days with landslide events was recorded in 2021 and was related to another weather extreme with a 50-year return period, namely to extremely wet May 2021 when the precipitations were, particularly in the mountainous north-west of the country, up to 3-times above an average value (Fig 1).

The exclusion of extreme weather precipitation events with over 50 years of return period throws the light on other, more common weather conditions that trigger unpredicted landslides. Unpredicted days with landslides occur yearly in all seasons (Fig. 1). Detailed analysis revealed five general types of triggering weather conditions (Tab. 1).

The intensive daily precipitations triggered the highest number of unpredicted landslides, namely 139 out of 262 or 53 % of all unpredicted landslides. The majority of the landslides triggered by the daily intensive precipitations occurred related to the extreme rainfall event in September 2014. However, unpredicted landslides triggered by intensive daily precipitations occur in all seasons (Fig. 2). Excluding the extreme conditions in September 2014, the majority

of such events occurred in February and in June and July as summer storms. The intensive daily precipitations that triggered unpredicted landslides were between 55 and 127 mm/day.

Tab. 1 Weather conditions during unpredicted landslides events

Weather conditions	Detailed	N of unpredicted landslides
Intensive daily precipitation	55-127 mm/day	139
Several successive days of heavy rainfall	90 mm in 2-3 days	8
Antecedent heavy precipitation	60-150 mm/day 5-7 days before	57
Antecedent intensive precipitation	42-80 mm/day 2-10 days before	10
No significant precipitation	< 40 mm/day	48
Snow melting		15

Several successive days of heavy rainfall triggered a small number of landslides (8 landslides or 3 %). Such weather conditions encompassed 2 to 3 days of heavy rainfall when the total precipitation exceeded 90 mm. All events occurred in the wintertime (Fig. 2). Despite the very rare frequency of such weather conditions, they triggered rather many landslides (Tab. 1).

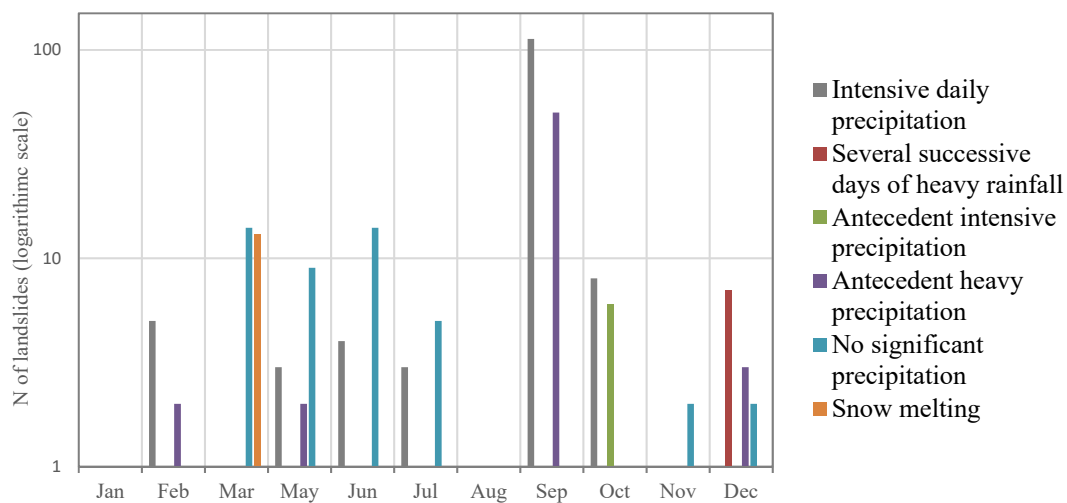


Fig. 2 Yearly distribution of landslide occurrence based on the weather conditions.

Antecedent heavy precipitation triggered 57 landslides (22 %). The total amount of the antecedent precipitation was between 60 and 150 mm, and the landslides occurred 5 to 7 days after such heavy rain. On the day of the landslide occurrence, the precipitations were negligible. Antecedent intensive precipitation triggered 10 landslides (4 %). The total amount of antecedent intensive precipitation was between 42 and 80 mm, and the landslides occurred 2 to even 10 days after such weather conditions.

The impact of snow melting was involved in 15 unpredicted landslides. The impact of snow melting could be combined with heavy, intensive, or antecedent precipitations to trigger the landslide. However, we also evidenced the occurrence of several landslides that occurred in dry

weather conditions and could be entirely attributed to the intensive snow melting. It lasted for 13 days in a row with an intensity of -10 mm/day.

48 landslides (18 %) occurred during rather dry weather conditions, indicating other than weather-related landslide triggering factors. Most landslides occurred in the spring (March to June) (Fig. 2). At the current stage, the nature of the unpredicted landslides in dry weather conditions remains unknown.

Conclusions

The analysis of weather conditions related to the landslides that remained unpredicted by the current landslide prediction model in Slovenia implies the importance of climate changes and brings about several necessary adaptations for the future improvements of such models. The frequency and impact of the individual weather condition on the success of the landslide prediction are summarized in the table (Tab. 2).

Tab. 2 Frequency and impact of different weather conditions on unpredicted landslides events

Weather condition	Frequency	Impact	Proposed threshold values
Intensive daily precipitation	high	high	55 mm/day
Several successive days of heavy rainfall	low	low	90 mm
Antecedent heavy precipitation	medium	medium	60 mm
Antecedent intensive precipitation	medium	low	40 mm
Snow melting	low	medium	-10 mm/day
Other (not weather-related) factors	high	medium	

The greatest challenge is the prediction of landslides related to the extreme precipitations with the long return period and the prediction of those triggered by intensive precipitation (summer storms and autumn-winter heavy rain). Such weather conditions trigger the highest number of events but are hard to predict due to fast evolution and spatially limited impact. Rather high frequency and impact of antecedent heavy precipitations imply the importance of antecedent precipitations in landslide prediction models. A sufficient time delay (even 7 days) needs to be considered. Fast snow melting is a triggering factor that is seldom considered in the prediction models. The results however indicate its considerable impact and suggest its implementation in future versions of the prediction models. Other triggering factors not related to the weather conditions remained unknown but their rather high impact on unpredicted landslide occurrence encourages further research on this matter.

References

- Gariano SL, Guzzetti F (2016) Landslides in a changing climate. *Earth-Science Reviews* 162, 227-52. <https://doi.org/10.1016/j.earscirev.2016.08.011>
- Hungr O, Leroueil S, Picarelli L (2014) The Varnes classification of landslide types, an update. *Landslides* 11, 167-194. <https://doi.org/10.1007/s10346-013-0436-y>
- Jemec Auflič M, Bokal G, Kumelj Š, Medved A, Dolinar M, & Jež J (2021) Impact of climate change on landslides in Slovenia in the mid-21st century. *Geologija* 64/2, 159-171. <https://doi.org/10.5474/geologija.2021.009>
- Jemec Auflič M, Šinigoj J, Krivic M, Podboj M, Peternel T, & Komac M (2016) Landslide prediction System for rainfall induced landslides in Slovenia (Masprem). *Geologija*, 59/2, 259-271. <https://doi.org/10.5474/geologija.2016.016>
- Peternel T, Šinigoj J, Jemec Auflič M, Kumelj Š, Krivic M (2022) MASPREM - Slovenian landslide forecasting and warning system. *Landslide modelling & applications: proceedings of the 5th Regional Symposium on Landslides in the Adriatic-Balkan Region*. Peranić, J (ed.). Rijeka: Faculty of Civil Engineering, University of Rijeka; Zagreb: Faculty of Mining, Geology and Petroleum Engineering, University of Zagreb.

Advantages and Challenges of Advanced Slope Stability Analyses

Carolina Sellin¹, Mats Karlsson¹, Minna Karstunen¹

¹ Chalmers University of Technology, Gothenburg, Sweden

SUMMARY: This paper studies the stability of a slope in sensitive clay by combining the rate-dependent Creep-SCLAY1S model in finite element analyses with an increase of gravity. The analyses enable us to understand the effects of unloading via erosion in arbitrary locations in a natural slope. This gives valuable insights of where to ideally perform sampling, to make sound a priori estimation of slope stability. The results are compared with stability analyses performed with Limit Equilibrium Method (LEM), Discontinuity Layout Optimization (DLO), Finite Element Limit Analysis (FELA) and Finite Element Analysis (FEA).

Keywords: slope stability, rate-dependent model, FE analysis, gravity loading

Introduction

As a result of climate change, the Nordic countries are expected to experience an increase in periods of intense precipitation and drought, respectively. This is likely to cause changes in environmental loads on slopes (Tang et al., 2018), but the effect of these single, cyclic or multiple (cascading) weather events on slope stability is, however, yet to be fully understood. This calls for further exploration of the soil-atmosphere interaction, and in particular the transient soil response. This paper discusses on the potential of applying the anisotropic, rate-dependent Creep-SCLAY1S model (Sivasithamparam, Karstunen & Bonnier, 2015; Gras, 2017; Gras, 2018) in slope stability using PLAXIS 2D FE code. By including such an advanced soil model in FE, it is not only possible to simulate the transient evolution of complex effective stress situations and the state parameters in the slope but also to see the effects of these and the rate of loading on the failure mode. A benchmark slope, with thick deposits of sensitive soil, representative for the Göta river valley in West of Sweden, is used for demonstration. In addition, the results are compared to corresponding analyses performed with Mohr-Coulomb in Limit Equilibrium Method (LEM), Discontinuity Layout Optimization (DLO) (Smith & Gilbert, 2007) and Finite Element Limit Analysis (FELA) (Sloan, 2013).

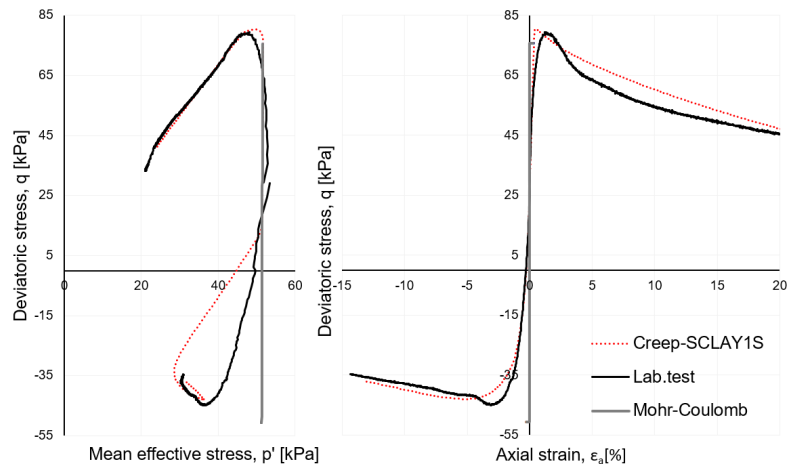
Modelling aspects

The choice of soil model

In order to subsequently include the effect of various climate scenarios, in particular the effects of changes in the porewater pressures, the soil model used needs to be based on effective stresses. Figure 1 shows simulations performed with the Creep-SCLAY1S model for anisotropically consolidated natural clay samples in undrained triaxial compression and extension tests. Black solid lines represent test results and red dashed lines are the corresponding simulation with Creep-SCLAY1S, using model parameter values derived from the site. The model gives, with the same set of parameters, a very good prediction in triaxial compression, and an acceptable prediction in extension. For comparison, an equivalent simulation with Mohr Coulomb model has been included and is as expected less satisfactory.

The calibration of the model parameters based on these triaxial tests has been validated with additional triaxial test simulations of natural clay samples from same depth at the same geological site.

Fig. 1 Experimental results and numerical simulations of undrained triaxial tests in compression and extension during shearing phase for natural clay samples from level -12, from Göta River valley.



Proposed method

The creation of natural slopes in the analyses is simplified to a linear erosion process. The final geometry is obtained by simulating a gradual erosion process, starting with a horizontal ground surface and a horizontal groundwater level 1 m below the surface. Figure 2 shows how the erosion of the slope is numerically simulated by unloading 1 m per calculation phase with a simultaneous lowering of the water table. When the water level has reached the intended final elevation, i.e. the current water level in the river, the unloading continues with no changes in the water table until the final geometry is obtained. The failure is induced by increasing the gravity in the model, similar to a centrifuge test in laboratory, until the rate of horizontal displacements at the toe of the slope start to accelerate.

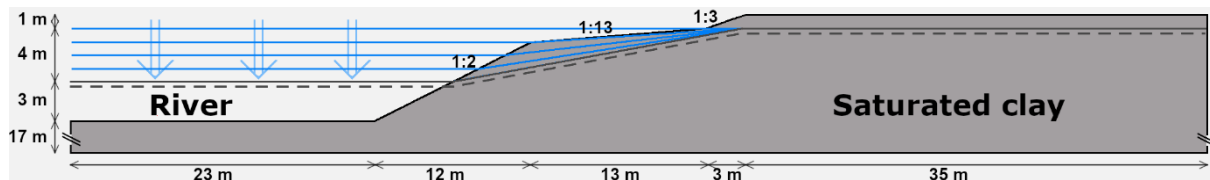


Fig. 2 Calculation phases and final geometry. Vertically cropped.

Benchmark slope

The methodology was applied to a benchmark slope in soft sensitive clay, with geometry and geotechnical properties taken from a site located approximately 12 km north of Gothenburg, in Göta River valley (Karlsson & Karstunen, 2017). The soil model, Creep-SCLAY1S (Sivasithamparam, Karstunen & Bonnier, 2015; Gras, 2017; Gras, 2018), was calibrated and validated against these soil tests, resulting in the model parameters found in Table 1 and Table 2. The values of the model parameters should ideally be calibrated against undisturbed soil samples taken at such a distance from the crest of the slope that no significant stress rotation has occurred, i.e. the right boundary in Figure 2. The chosen cross section is presented in Figure 2, with the first, horizontal, calculation phase assigned an in-situ K_0 -value of 0.6.

A reference target gravity was chosen as 2, which was linearly scaled over 24 h application time. The resulting failure surface, as presented in Fig. 3, is very similar to the one obtained via

previous calculations with Mohr-Coulomb in LEM, DLO, FELA (lower bound, LB) and FE (Strength Reduction Method, SRM) (Sellin, 2019) using total stress analyses.

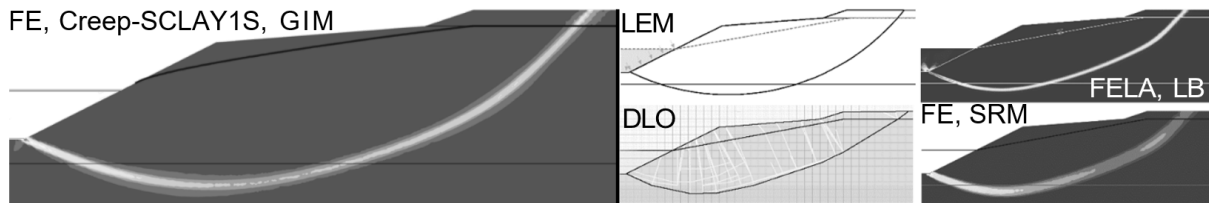


Fig. 3 Calculated critical failure surfaces.

The creation of the final slope geometry through unloading phases creates an initial stress distribution that is in equilibrium, and also affects the state of the soil, such as the size and rotation of the Normal Compression Surface (NCS) in the model. As seen in Fig. 4a, significant rotations of principal stresses are predicted to occur below the unloaded zone, which is also reflected in the predicted K_θ -value in Fig. 4b.

As a result of using an advanced soil model, it is also possible to capture the rotation of the fabric, and thus the rotation of NCS, as seen in Fig. 4c-d for two components of the deviatoric fabric tensor. Hence, the mobilised strength of the soil is also affected in these areas, and the principal stress directions no longer coincide with the principal directions of the fabric. This highlights the importance of recreating the initial conditions properly, as well as the need for choosing a representative location for soil sampling, the process of erosion is often the reason for the formation of river slopes.

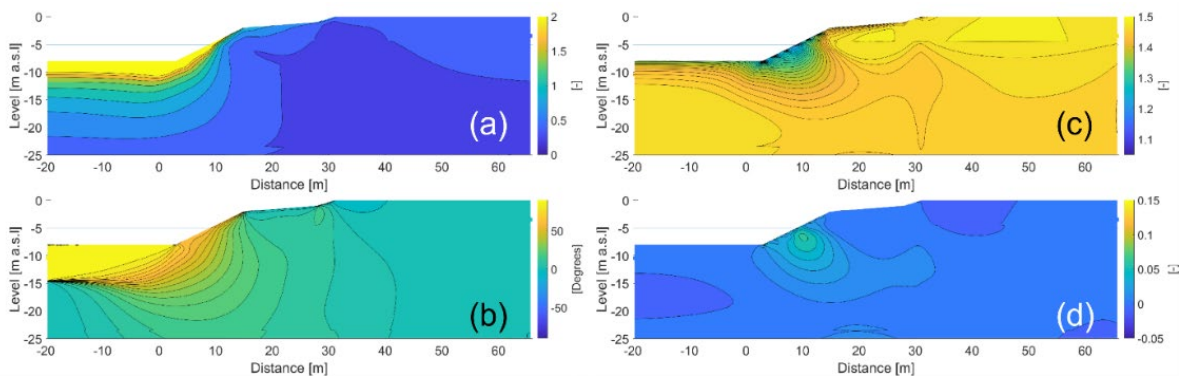


Fig. 4 Material parameters at final geometry.

(a) Rotation of principal stresses (b) K_θ and fabric rotation: (c) α_{xy} , (d) α_{yy} .

In Fig.5, the rate of application of gravity loading is changed from 1 day to 10 years, and in all cases the failure is defined as the time when the horizontal displacement at the toe of the slope (point Q) start to accelerate. In all cases the slope is predicted to fail before the target gravity of 2 is reached. Furthermore, when the rate of change of gravity is reduced, the model of failure changes from the “undrained” mode of failure (1 day) to a drained.

Conclusion

The proposed method for slope stability analyses with an advanced soil model provides a tool to understand the potential effects of unloading via erosion for a sensitive clay, in arbitrary

locations in a natural slope. This gives valuable insights of where to ideally perform sampling, and thus to make sound a priori estimation of slope stability. The observed rotation of principal stresses also highlights the importance of building a numerical model for natural slopes with gravity loading, starting from a representative K_0 -condition. The use of a rate-dependent soil model in slope stability context does however bring uncertainties of the appropriate application rate of the increasing gravity, since this highly affect the time to failure.

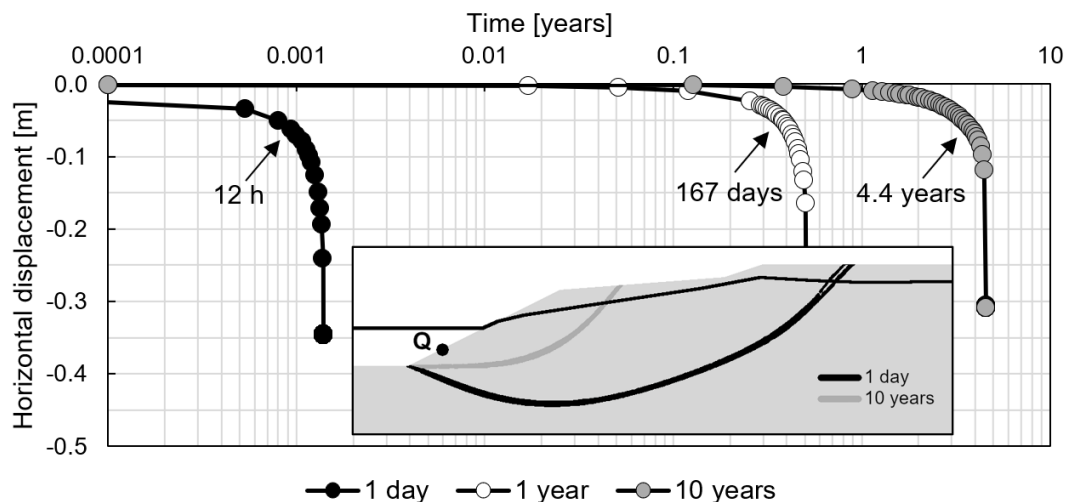


Fig. 5 Horizontal displacement during safety calculation in point Q for different application times of increased gravity, all with a target gravity of 2.

Acknowledgments

The financial support from Trafikverket in the framework of BIG (Better Interactions in Geotechnics), NordForsk (project #98335 NordicLink) and Formas (2016-00834, 2021-02400) is greatly appreciated. The work is done as part of Digital Twin Cities Centre that is supported by Sweden's Innovation Agency VINNOVA.

References

- Gras JP, Sivasithamparam N, Karstunen M & Dijkstra J (2017) Strategy for consistent model parameter calibration for soft soils using multi-objective optimization. *Computers and Geotechnics* 90, 164-175.
- Gras JP, Sivasithamparam N, Karstunen M & Dijkstra J (2018) Permissible range of model parameters for natural fine-grained materials. *Acta Geotechnica* 13, 387-398.
- Karlsson M & Karstunen M (2017) On the benefits of incorporating anisotropy in stability analyses in sensitive clays. *Landslides in Sensitive Clays: From Research to Implementation*. V. Thakur, J.-S. L'Heureux, and A. Locat (eds). Cham: Springer International Publishing, pp. 259–266.
- Sellin C (2019) On evaluating slope stability in sensitive clay -a comparison of methods through a case study. *Proceedings of the 27th European Young Geotechnical Engineers Conference*. D. Ülgen et al. (eds). Bodrum. Turkish Society for ISSMGE, pp. 249–254.
- Sivasithamparam N, Karstunen M & Bonnier P (2015) Modelling creep behaviour of anisotropic soft soils. *Computers and Geotechnics* 69, 46-57.
- Sloan SW (2013) Geotechnical stability analysis. *Géotechnique* 63, 531-572.
- Smith C & Gilbert M (2007) Application of discontinuity layout optimization to plane plasticity problems. *Proc. R. Soc. A* 463, 2461-2484.
- Tang AM, Hughes PN, Dijkstra TA, Askarinejad A, Brenčić M, Cui YJ, Diez JJ, Firgi T, et al. (2018) Atmosphere-vegetation-soil interactions in a climate change context; impact of changing conditions on engineered transport infrastructure slopes in Europe. *Quarterly Journal of Engineering Geology and Hydrogeology* 51(2), 156–168.
- Zienkiewicz OC, Humpheson C & Lewis RW (1975) Associated and non-associated visco-plasticity and plasticity in soil mechanics. *Géotechnique* 25, 671-689.

A Pilot Study in the Napf-Region (Central Switzerland) for an Upcoming National Landslide Early Warning System

Manfred Stähli¹, Tobias Halter¹, Fabian Walter¹, Adrian Wicki², Peter Lehmann³

¹ Swiss Federal Research Institute WSL, Birmensdorf, Switzerland

² Federal Office for the Environment FOEN, Bern, Switzerland

³ ETH Zurich, Zurich, Switzerland

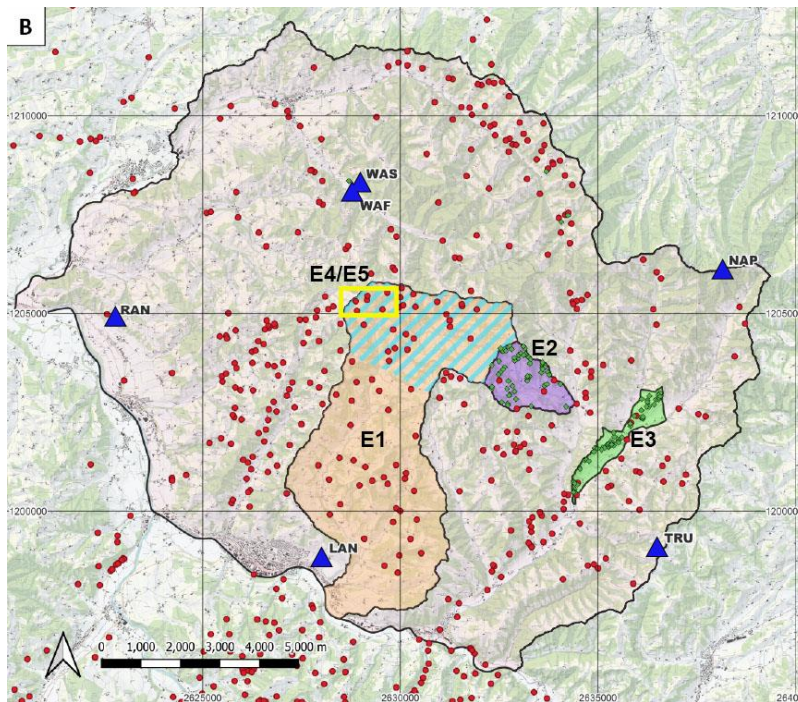
SUMMARY: In view of a national Landslide Early Warning System (LEWS) for Switzerland, a pilot study is currently running in the Napf-region (central Switzerland), a hilly semi-forested area (186 km²) with a substantial number of shallow landslide observations in the past decades. The study includes a comprehensive soil wetness monitoring, a test of a numerical model to simulate distributed landslide triggering, as well as the application of Distributed Acoustic Sensing (DAS) at the scale of a steep slope. We show that the applied tools provide a promising basis for a systematic observation, assessment and warning of critical landslide situations. At the same time, this work also suggests that the soil physical conditions can and need to be addressed in an adequate way to correctly rate the spatial and temporal criticality for landslide triggering.

Keywords: soil wetness measurements, shallow landslides, numerical model, distributed acoustic sensing

Introduction

A new official Landslide Early Warning System (LEWS) for Switzerland is under development and shall be operated by the Swiss Federal Office for the Environment from 2025. It will include a forecast system that allows for issuing warnings for shallow landslides and hillslope debris flows based primarily on precipitation thresholds (Leonarduzzi et al., 2017). Recently, work by Wicki et al. (2020, 2021) demonstrated that a similar approach using (simulated or in-situ measured) soil wetness would equally be capable to inform warning services about the probability of imminent landslides.

To further explore the importance of real-time soil moisture data for landslide warning, a pilot study was launched in a hilly semi-forested region in central Switzerland where landslides occur frequently and distributed across the entire domain (see Fig. 1). The elevation of the study area ranges from 594 m.a.s.l in the west at the river Emme to 1406 m.a.s.l. at the Napf peak in the east. The region belongs to the tectonic unit of the Molasse Basin, and the topography is



characterized by flat terrain in the valley bottoms and steep terrain on the valley sides. Forests cover approximately 44% of the area and are often located on the steep slopes.

Here we would like to give an overview of the applied methods and most important findings from this study.

Fig. 1. Map of the study area “Napf” with the sub-perimeters E1 to E5 simulated with the numerical model STEP-TRAMM. Blue triangles indicate WSL-soil wetness measurement locations, and red dots represent observed landslides.

Investigation methods

Six in-situ soil moisture measuring stations were set up between 2019 and 2021, distributed throughout the pilot study region (see Fig. 1). At all stations the volumetric water content and the soil water potential have been measured at four different depths with two sensors each. The corresponding data can be viewed (in real-time) at <https://www.wsl.ch/Napf/Bodenfeuchte/> and is available for downloading from <https://www.doi.org/10.16904/envidat.395> (including a detailed description of the installation, study site and lab-determined soil properties).



Fig. 2 a) Monitoring site Wasen i.E. with the installation of a fiber-optic cable for Distr. Acoust. Sens. (DAS) measurements; b) Set-up of the soil moisture measurements at Trub.

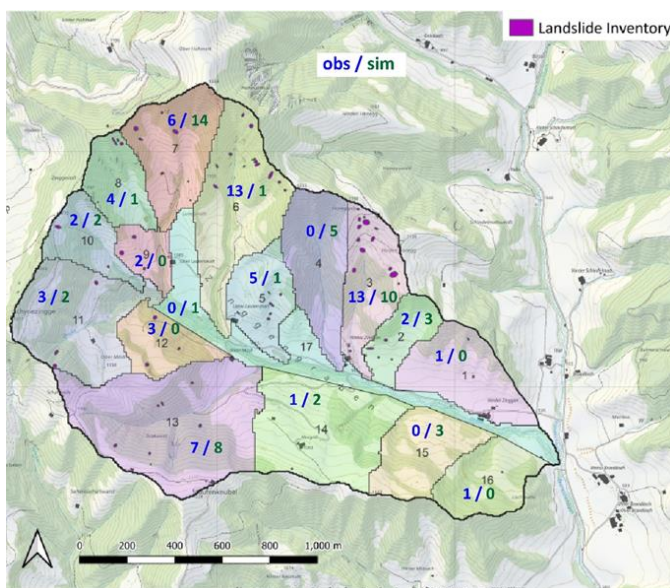
In April 2023 a fiber-optic cable was installed at one of the soil moisture monitoring sites (Wasen i.E.; see Fig. 2a) for the application of Distributed Acoustic Sensing (DAS), a novel technology to capture cracking or mini-deformations across a specific slope. The corresponding measurement campaign will take place in summer 2023.

A physically-based hydromechanical model framework (STEP-TRAMM; Lehmann et al., 2018) was set up to the entire Napf region (186 km²) as well as to specific sub-areas where dedicated landslide inventories were made after the storm events of 15-16 July, 2002 and 21-23 August, 2005 (see Fig. 1) to test the usefulness of the model in an upcoming national LEWS. The model depicts the landscape as a composite of interconnected soil columns with a hexagonal cross-section and texture-dependent soil physical properties. When exposed to heavy rainfall, individual soil columns may converge to a critical wetness state with failure of mechanical bonds between soil and bedrock, and adjacent soil columns. Such local failures destabilize adjacent soil columns and may lead to a progressive failure and eventually to a landslide release. The model and a detailed description are available at <https://emeritus.step.ethz.ch/step-tramm.html>.

Results

Based on the soil wetness measurements from two neighboring sites – one on a flat location (WAF in Fig. 1), and one on a steep slope (WAS in Fig.1) – we found that by considering relative changes and by integrating the soil water status over the entire profile, the soil wetness measurements at both sites correlated well with each other (Wicki et al., 2023). As a result, the flat and sloped monitoring site performed equally well in separating landslide triggering from non-triggering conditions. These findings encourage the use of existing soil wetness monitoring networks, that usually contain flat sites (e.g., monitoring sites of the Swiss Federal Office for Meteorology and Climatology *MeteoSwiss*). In addition to the in situ soil measurement sensors, an electrical resistivity tomography (ERT) campaign reproduced infiltration properties critical for landslide early warning reliably (Wicki et al., 2022).

Our application of the numerical model STEP-TRAMM to the entire Napf-region and to specific sub-areas demonstrated its capability of reproducing the landslide distribution that has been observed after major storm events in 2002, 2005 and 2021. Different events could be reproduced with a relatively consistent choice of parameter values and at a spatial resolution of 10 m, which allows to account for the topography in an adequate way. The sensitivity of the model to the selection of soil type and



initial (antecedent) soil saturation was relatively high and requires a more in-depth examination of the saturation and the subsequent drainage of the soil layer during heavy precipitation events.

Fig. 3 Spatial distribution of observed and simulated landslides for the storm event of 15-16 July, 2002, within sub-area E2 of Fig. 1. The spatial distribution of the simulated landslides within the entire catchment was in fair agreement with the observed landslides. For example, the model correctly reproduced the large number of landslides in sub-catchment No. 3 (13 observed, 10 simulated) and the marginal number of landslides in sub-catchments 1, 2, 9, 10, 11, 14, 16 and 17.

Conclusions and outlook

Overall, the methods tested in this pilot study have shown great potential to effectively complement a precipitation-based warning system, notably for the assessment of critical soil conditions at the local to regional scale.

The pilot study, including the Distributed Acousting Sensing of the hillslope in Wasen i.E., will continue for at least one more year. To better understand hydrologic processes and their effects on soil stability, we will compare in situ measurements of soil water potential with volumetric water content data from the study area and translate the findings into statistical landslide forecast models. We will be happy to report our experiences in future conferences (such as the World Landslide Forum *WLF6* in November 2023), but also through the international network on Landslide Early Warning Systems *LandAware* (landaware.org).

Acknowledgements

We are grateful to the Swiss National Science Foundation (project number 175785), as well as to the Federal Office for the Environment (FOEN) for their financial support. We would also like to express our sincere thanks to numerous colleagues at WSL who helped with enthusiasm to install and run the field measurements.

References

- Lehmann P, von Ruetten J & Or D (2018) How landslides become disasters. *EOS: Earth & Space Science News*, 99(12), 32-36.
- Leonarduzzi E, Molnar P & McArdeell BW (2017) Predictive performance of rainfall thresholds for shallow landslides in Switzerland from gridded daily data. *Water Resour. Res.*, 53, 6612–6625.
- Wicki A, Lehmann P, Hauck C, Seneviratne SI, Waldner P & Stähli M (2020) Assessing the potential of soil moisture measurements for regional landslide early warning. *Landslides* 17, 1881-1896.
- Wicki A, Jansson P-E, Lehmann P, Hauck C, & Stähli M (2021) Simulated or measured soil moisture: which one is adding more value to regional landslide early warning? *Hydrol. Earth Syst. Sci.*, 25, 4585–4610.
- Wicki, A, & Hauck, C (2022) Monitoring critically saturated conditions for shallow landslide occurrence using electrical resistivity tomography. *Vadose Zone Journal*, 21(4), e20204.
- Wicki A, Lehmann P, Hauck C & Stähli M (2023) Impact of topography on in situ soil wetness measurements for regional landslide early warning - a case study from the Swiss Alpine Foreland. *Nat. Hazards Earth Syst. Sci.* 23(3), 1059-1077.

Advanced Numerical Model for Landslides: From Quick Clay to Submarine Landslides

Quoc Anh Tran¹

¹ Norwegian University of Science and Technology, Trondheim, Norway

SUMMARY: In this abstract, we present recent developments in the Material Point Method applied to the simulation of landslides, focusing on practical applications rather than theoretical developments. There are a variety of applications, ranging from the 3D simulation of Gjerdrum landslides to earthquake-induced submarine landslides.

Keywords: Material Point Method, quick clay, submarine landslide

Introduction

Material Point Method (MPM) is a continuous-based method for modeling large deformations. A background mesh is used in MPM to discretize the Lagrangian particles (or integration points in FEM). As in FEM, weak differential equations are also solved on a background mesh. Unlike FEM, solutions (e.g., deformations) are updated using particles rather than meshes, and the background mesh is reset to its original configuration. Furthermore, the method is coupled with CFD to study the interaction between soil, fluid, and structure, such as earthquake-induced submarine landslides. The abstract does not present the algorithm but here we only demonstrate the application of the Material Point Method in two examples:

- (1) 3D simulation of Gjerdrum quick clay landslides.
- (2) earthquake-induced submarine landslides.

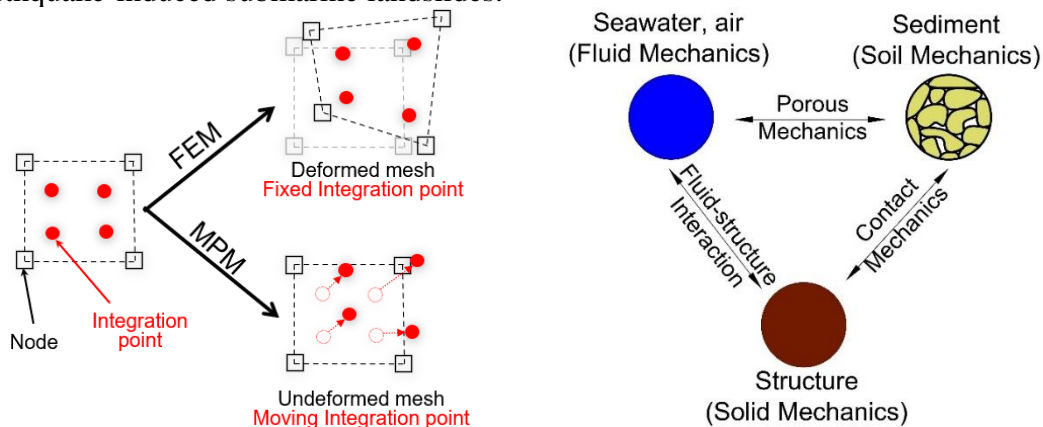


Fig. 1 Material Point method and coupled CFD-MPM for soil-fluid-interaction.

3D simulation of Gjerdrum quick clay landslide

In the first example, we perform 3D numerical analysis of the 2020 Gjerdrum quick clay landslide. The topography is obtained from the digital terrain model is interpolated from the CPTUs data. The remoulded shear strength of the quick clay is assumed to be 0.5 kPa. Fig.2 shows the elevation and the undrained shear strength of the quick clay layer in the numerical model. The quick clay layer plays important role in the simulation. In the simulation, the weak zone is not pre-defined but created under the gravity. The landslide is triggered by reducing the undrained shear strength of the weak zone according to the softening law of the constitutive soil model. Fig.3 shows the prediction of the first slide which is like the hypothesis given in the Gjerdrum report. We can also see the propagation of the shear band developed in the slope underneath the area where the erosion occurs (see Fig. 4). The progressive failure mechanism

is replicated in the numerical model. Overall, the presented model can predict satisfactory the retrogression distance of the quick clay landslide slope (red area in Fig.5) compared with the observation on the site (see red line in Fig.5).

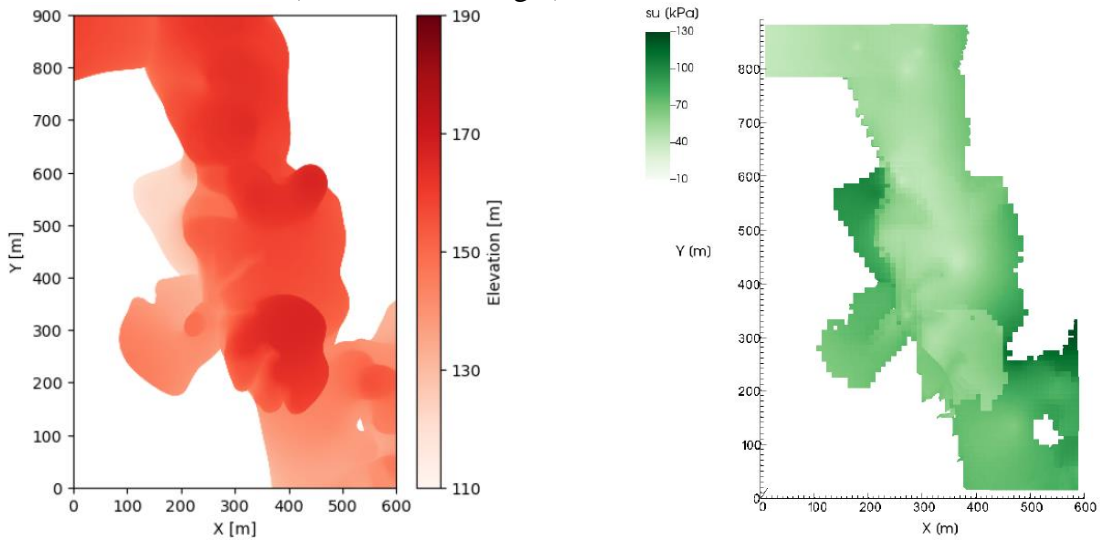


Fig. 2 Quick clay layer with the elevation (red) and the undrained shear strength (green)
Stage 1 of the slide

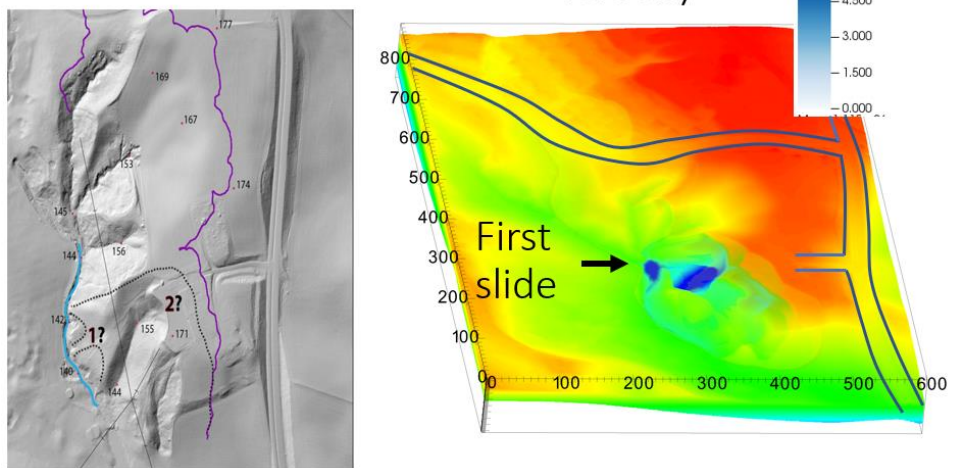


Fig. 3 Initiation of the first slide
Stage 1 of the slide

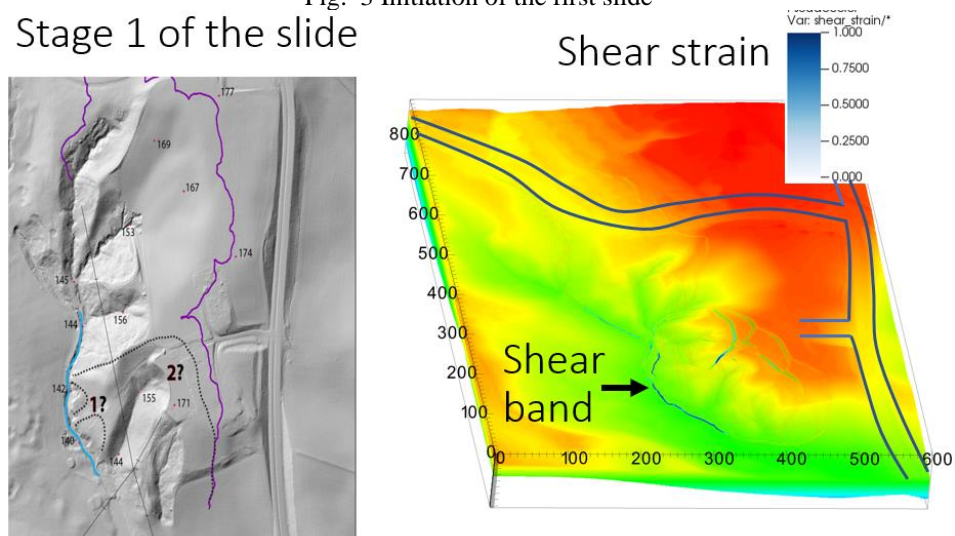


Fig. 4 Development of the shear band

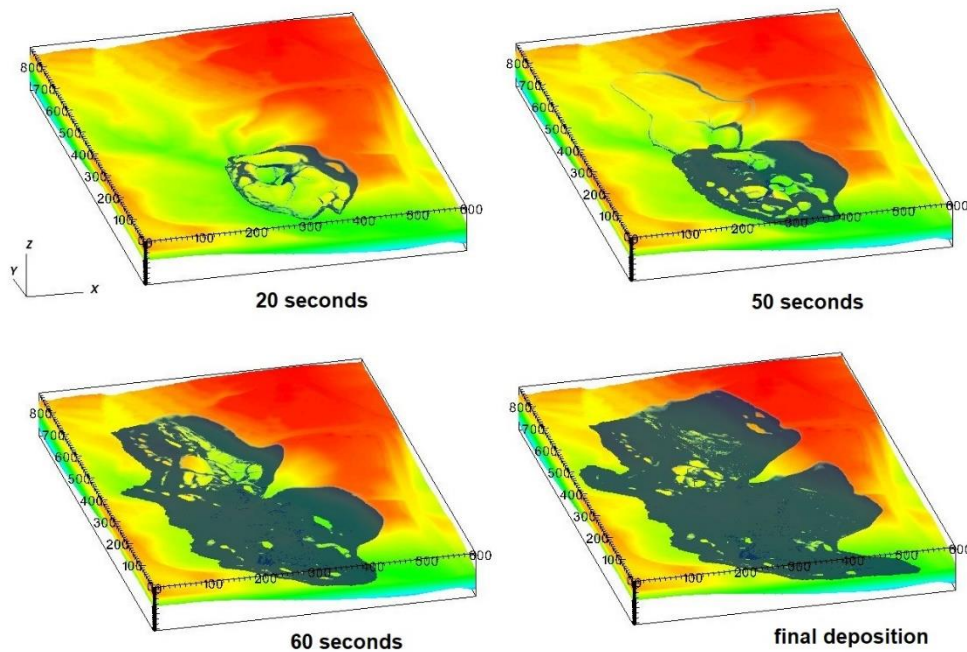


Fig. 5 Retrogression failure in the numerical model

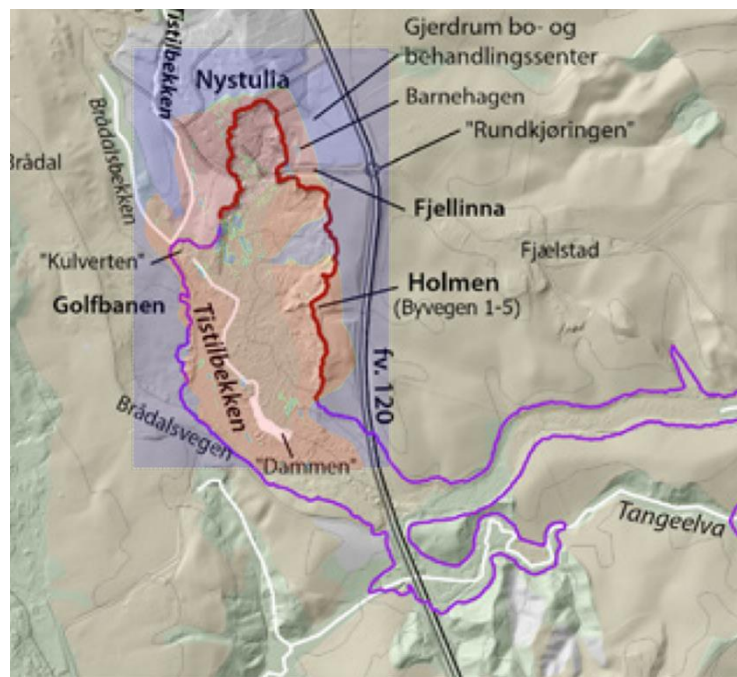


Fig. 6 Retrogression distances in the numerical model

Earthquake-induced submarine landslides

The second example is the earthquake induced submarine landslides. The earthquake is replicated by a seismic loading with the frequency of 2Hz and the peak ground acceleration of 1g. The soil is Mohr-Coulomb material model with the porosity of 0.4 and the friction angle is softening accordingly with the shear strain and the model is incorporated with the Row stress dilatancy model. Here are some numerical observations.

- (1) At the start of the earthquake, the seismic loading triggers the first slide in three seconds. The debris starts moving around 2-3 m/s at 4 seconds, with multiple shear bands developing on the slope. Waves generated from the submarine slide are around 2-3m towards the slide direction.

(2) A negative excess pore water pressure is developed along the slope when the shear band starts (like 4 seconds or 20 seconds) with a pore water pressure under 1atm. This is what happens when the soil gets sheared rapidly during an undrained event.

(3) The last shear band is mobilized when the seismic loading ends at 23 seconds, and the slope reaches the final deposition pretty fast. The slope didn't progress any further. Seawater interacts with debris flow to create turbulent flow.

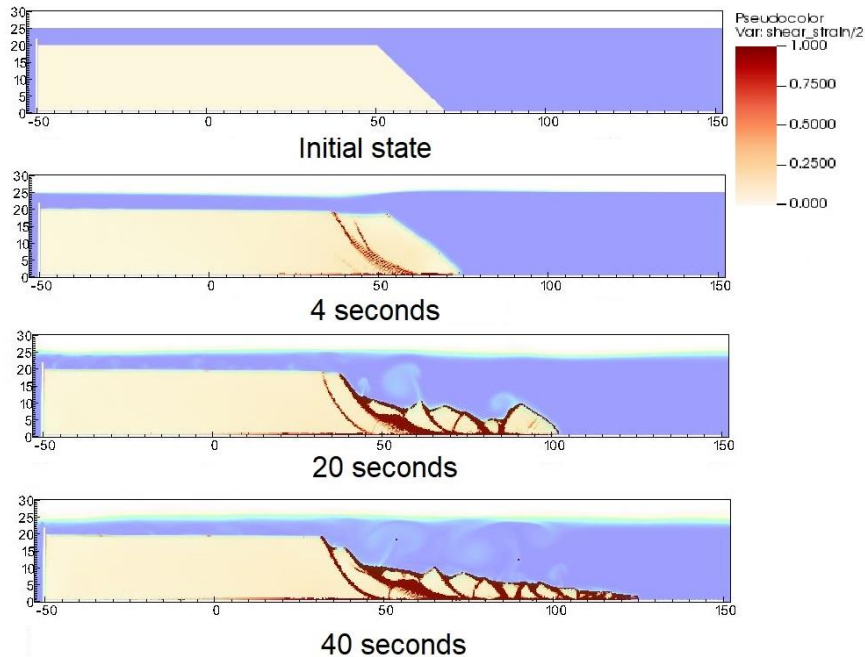


Fig. 7 Development of the shear band in the submarine landslide

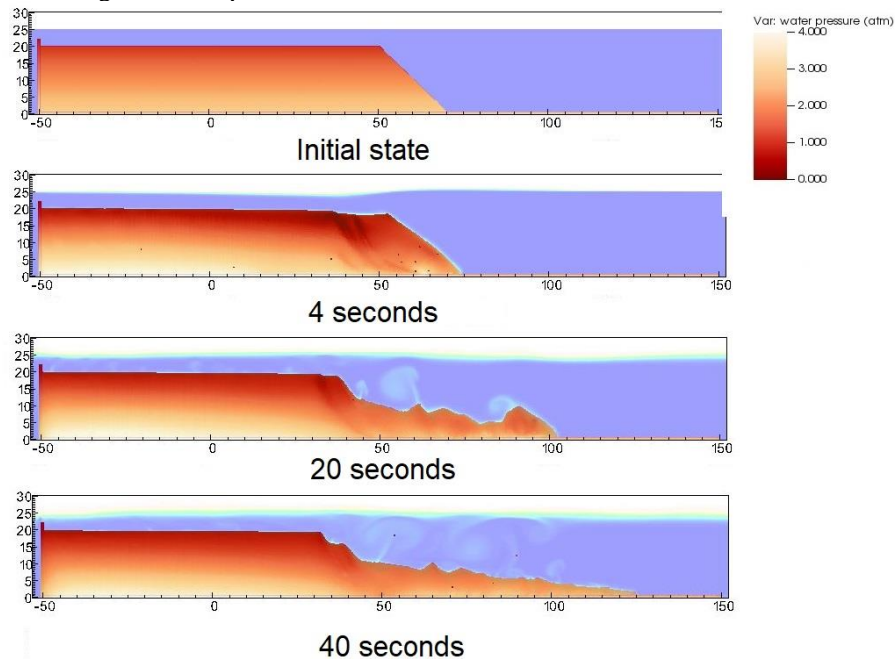


Fig. 8 Development of pore water pressure in the submarine landslide

ACKNOWLEDGEMENT: Research contributed by Gustav Grimstad, Seyed Ali Ghoreishian Amiri, Agnete Rogstad, Ivan Depina, Fabricio Fernández, Steinar Nordal. The research is supported from the European Union’s Horizon 2020 under the grant agreement 101022007. The computations were performed on resources provided by UNINETT Sigma2 - the National Infrastructure for High Performance Computing and Data Storage in Norway.

Enhanced Discontinuity Set Extractor (eDSE): An AI Tool for Classifying and Characterising Rock Discontinuities and Rock Masses from 3D Point Cloud Datasets

Dennis HY Wong¹, Stuart Millis², WK Leung³

^{1&2} Ove Arup & Partners Hong Kong Ltd, HKSAR

³ Geotechnical Engineering Office, Civil Engineering and Development Department, HKSAR

SUMMARY: The increasing ease with which point cloud datasets can be captured and generated has resulted in notable opportunities for the application of innovative approaches to geological surveying. One area in which the industry has pinned its hopes is the automated surveying and mapping of rock discontinuities, with associated rock mass assessments undertaken through AI-powered analyses of the point cloud models. Whilst a number of computerised algorithms have been successfully developed in the past, most of these only derive basic geometric information for a rock face such as discontinuity orientation, spacing, persistence, etc. The Enhanced Discontinuity Set Extractor (eDSE) has taken things a step further, adapting the open-source code developed by Riquelme et al. (2014, 2015, 2018) to provide additional functionalities that yield more comprehensive rock mass characterisations. The eDSE programme not only generates stereoplots and performs kinematic analysis from the point cloud information, but also computes advanced rock face metrics including block dimension (V_b), volumetric joint count (J_v) and Rock Quality Designation (RQD). These datasets can also be used to assist in the objective determination of input parameters for Q-value and Rock Mass Rating (RMR) computation. In addition, eDSE offers an enhanced graphical user interface (GUI) and fully integrated outputs that enable improved visualisation and easier data interrogation.

Keywords: Remote Sensing, Point Cloud, Laser Scanning, Rock Discontinuity, Rock Mass Assessment

Introduction

Discontinuities play a significant role in controlling the engineering behaviours of a rock mass, which in turn critically affects the stability of rock exposures. Accurate acquisition of rock discontinuity information is traditionally dependent on manual mapping using measuring tapes and compass clinometers to record dimensional and spatial information, supplemented with observations on surface roughness, aperture, seepage, and infilling. The process is non-reproducible and operationally demanding in terms of time and cost and can also be high-risk when safe access or proper vantage points cannot be easily gained. The increasing availability of point clouds generated from laser scanning or digital photogrammetry has promoted the development of algorithms to extract geometric properties of discontinuities from point cloud datasets using geostatistical approaches. Several classification methods have been employed for this purpose, which can be broadly categorised under approaches relating to 3D surface reconstruction (e.g. PlaneDetect by Lato and Vogé (2012)) or point cloud segmentation (e.g. Discontinuity Set Extractor (DSE) by Riquelme et al. (2014, 2015, 2018)). Considering the preservation of data integrity without the need for interpolation between points through mesh construction, as well as the robustness towards complex geometries, noise and vegetation, it is

generally agreed that point cloud segmentation provides a more reliable and accurate solution than 3D surface reconstruction, despite having a higher computational demand.

A comprehensive review has revealed that existing assessment tools only hold the capability to compute basic discontinuity information such as the discontinuity orientation (dip and dip direction), spacing and persistence, without making use of the classified point clouds to perform further kinematic analyses or to derive rock engineering parameters. To address these shortcomings and provide a greater degree of benefit to practitioners, the pre-existing DSE package has been adapted to generate the eDSE tool. This tool seeks to streamline the overall workflow for rock face assessment, integrating all resultant outputs, generating kinematic analyses, and computing key rock engineering parameters to aid engineering judgement and evaluation.

The Original Discontinuity Set Extractor

The original DSE was developed by Riquelme et al. (2014) and is driven by physical models formulated based on the definition and properties of discontinuities. The establishment of topology of the dataset and the classification of discontinuities are first carried out using a K-Nearest-Neighbours (KNN) Searching Method. The planarity of each neighbourhood is assessed with the planar inliers and outliers differentiated. Local normals are then computed using all the planar inliers and plotted on a stereoplot. The determination of major discontinuity sets is then achieved with the aid of Kernel Density Estimation (KDE). Orientation, normal set spacing, and persistence of the discontinuities are subsequently derived through Principal Component Analysis (PCA), Density-Based Spatial Clustering of Applications with Noise (DBSCAN) and Convex Hull Algorithms. Apart from the geometric information on discontinuities, the resultant outputs also include plane equations and point cloud datasets classified based on discontinuity set number. Despite the capability for generating geometric information comparable to manual mapping, further thorough review on the algorithm identified some room for improvement and notable potential for the development of additional functionality.

Proposed Enhancements and Methodology

The original DSE works as a standalone algorithm using the Matlab interface and workflows for computing orientation, spacing and persistence are fairly separated. The lack of tools for obtaining orientation information for the exposure forming face prohibits the direct integration of kinematic analyses. With due consideration to the above, the Matlab-scripted DSE was reprogrammed in C++ and integrated as a plug-in to the CloudCompare software package (CloudCompare, 2022). This is one of the most used platforms for point cloud data and benefits from a well-established GUI that provides a one-stop platform for pre-processing and viewing of resultant point clouds. The computation workflows have been streamlined to generate results in fewer clicks, with all outputs integrated into a single file for ease of interrogation. PCA is also applied to derive orientation data for the exposure forming face, thus enabling the automated generation of stereoplots for kinematic analyses.

Additionally, to fully unleash the potential of the analytical data generated new functions have been established to calculate V_b , J_v and RQD. The first step of this involves the formation of a sampling plane, either by PCA or manual definition, for the identified discontinuities to be projected on to. As illustrated in Fig. 1, circular discs are formed according to the location,

orientation and persistence of the identified discontinuities. eDSE further allows the users to adjust the sizes of the circular discs based on options for i) infinite persistence; or ii) persistence data of individual planes plus an additional length specified by users. The intersections between the circular discs and the sample plane create a flattened 2D map of discontinuities, which eliminates any non-uniform protrusions exhibited in the exposure. Making reference to a user-defined spacing parameter, horizontally and vertically evenly spaced scanlines are subsequently constructed on the 2D discontinuity map.

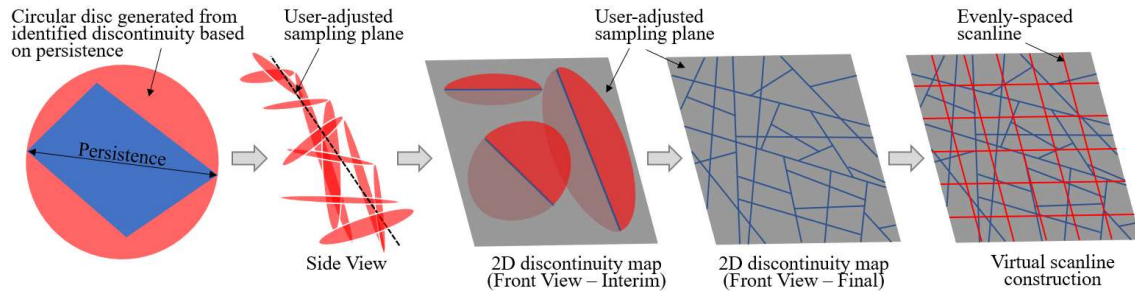


Fig. 1 Workflow on the generation of 2D discontinuity map

As presented in Fig. 2, to compute RQD scanlines are divided into shorter sections based on the intersections with the projected 2D discontinuities and sections with less than 100 mm in length are discounted from the RQD counting. This can mimic the conditions used for RQD derivation when drilling along the scanlines. Local vertical, horizontal and mean RQD values are then computed around the intersections of the scanlines, bounded by local sampling windows. This produces point data of RQD values representative of the local sampling windows at scanline intersections. In the final step, the grids are coloured based on the RQD values to produce a RQD heat map, which can be subsequently projected back to the input point cloud in CloudCompare for visualisation.

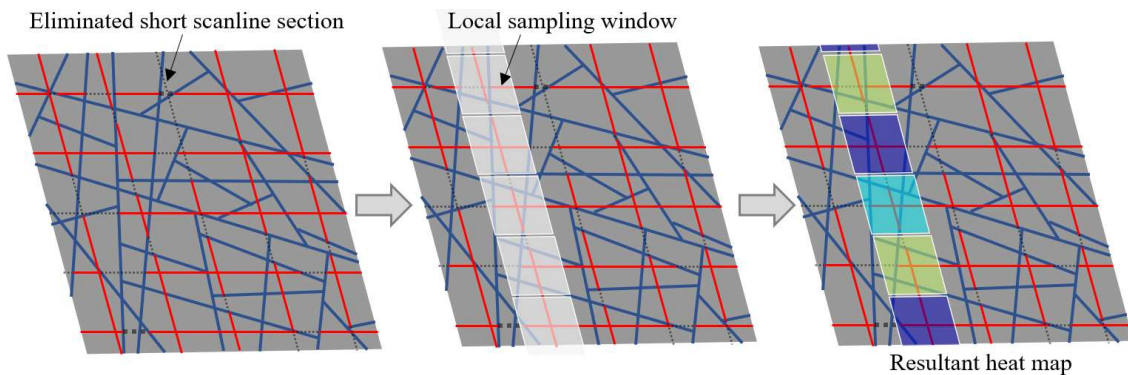


Fig. 2 Workflow on the generation of RQD heat map

J_v and V_b are calculated in a similar fashion to RQD through the use of user-defined scanlines. J_v is computed using Eq. 1, where the length of measure is taken as the scanline spacing. The computation of V_b adopts Eq. 2 by Cai et al. (2004) to test out all combinations of discontinuity spacings and angles among all the discontinuity sets falling within the same local sampling window and thus provide the maximum and minimum block volume values.

$$J_v = \sum \frac{n^\circ \text{ of discontinuities}}{\text{length of measure}} \quad (1)$$

$$V_b = \frac{s_1 s_2 s_3}{\sin \gamma_1 \sin \gamma_2 \sin \gamma_3} \quad (2)$$

Where s_i and γ_i ($i = 1, 2, 3$) are the discontinuity spacing and acute angle between discontinuity set normals respectively.

Consolidating all the geometric information extracted by eDSE and supplementing them with user-specified information on joint roughness, infilling, seepage condition, etc., the rock mass characterisation parameters of Q-value (Barton et al., 1974) and Rock Mass Rating (RMR) (Bieniawski, 1989) can also be computed in the newly developed GUI. This improves the objectivity during parameter determination.

Results

Following the enhancements implemented, eDSE provides users with a CloudCompare hosted tool that allows integrated data interrogation, kinematic analyses, and the calculation of V_b , J_v and RQD.

The heat map outputs are heavily governed by the relative distance and angles of the identified discontinuities. This means the formation of the sampling plane still relies on deductive reasoning and professional judgement from the users to produce reliable and geologically sound results. Despite the orientation and distance biases, as demonstrated in Figs 3 & 4 eDSE can easily highlight areas within rock exposures that possess denser fracture networks and poorer rock mass quality, with findings in line with direct visual observations on site. The spatial distribution of the J_v and RQD values can also be easily correlated through projection back to the source point cloud model.

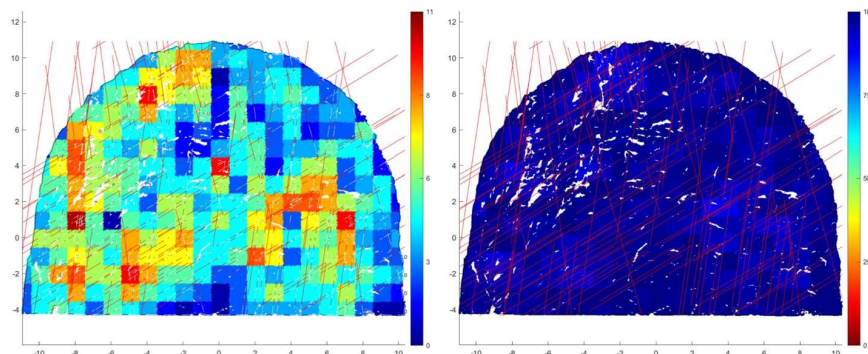


Fig. 3 J_v (left) and RQD (right) heat maps of a tunnel face generated by eDSE.

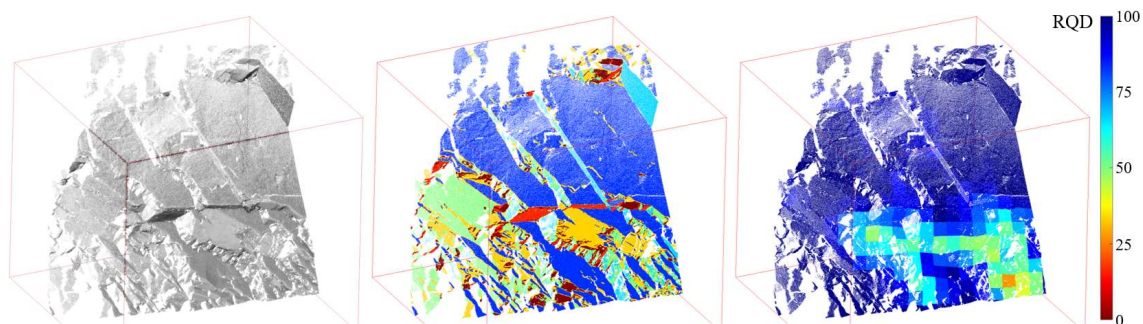


Fig. 4 Input point cloud from Rockbench repository (Lato et al., 2013) (left), point cloud coloured based on discontinuity set number (middle) and point cloud with RQD heat map projection (right).

Conclusion

The adoption of point clouds coupled with the eDSE tool provides a quicker, more robust and safer mechanism to undertake discontinuity surveys. Rock discontinuity data can now be acquired in a shorter period of time, with less labour intensity and without the need for extensive scaffold cover to access a rock face. The significant enhancements implemented to the original DSE during the development of eDSE now provide a tool that not only identifies discontinuities in a rock exposure, but also calculates additional geometric factors including V_b , J_v and RQD yielding more thorough rock mass assessment. These enhancements provide high-quality reproducible spatial and geostatistical information that facilitates informed and reliable engineering decisions.

Acknowledgement

The study was carried out under Agreement No. CE 24/2018 (GE) of the Geotechnical Engineering Office (GEO) of the Civil Engineering and Development Department (CEDD) of the Hong Kong Special Administrative Region of China. This paper is published with the permission of the Director of CEDD and the Head of the GEO.

References

- Barton N, Lien R, & Lunde J (1974) Engineering classification of rock masses for the design of tunnel support. *Rock mechanics*, 6(4), 189-236.
- Bieniawski ZT (1989) Engineering rock mass classifications: a complete manual for engineers and geologists in mining, civil, and petroleum engineering. John Wiley & Sons.
- Cai M, Kaiser PK, Uno H, Tasaka Y & Minami M (2004) Estimation of rock mass deformation modulus and strength of jointed hard rock masses using the GSI system. *Int. J. Rock Mech. Min. Sci.* 1, 3-19.
- CloudCompare (2022) 3D point cloud and mesh processing software – open-source project. CloudCompare. <http://cloudcompare.org> (Accessed August 2022).
- Lato MJ & Vöge M (2012) Automated mapping of rock discontinuities in 3D lidar and photogrammetry models. *International Journal of Rock Mechanics and Mining Sciences*, (54), 150-158.
- Lato M, Kemeny J, Harrap RM & Bevan G (2013) Rock bench: establishing a common repository and standards for assessing rockmass characteristics using LiDAR and photogrammetry. *Comput. Geosci.* 50, 106-114.
- Riquelme AJ, Abellán A, Tomás R & Jaboyedoff M (2014) A new approach for semi-automatic rock mass joints recognition from 3D point clouds. *Computers & Geosciences*, 68, 38-52.
- Riquelme AJ, Abellán A & Tomás R (2015) Discontinuity spacing analysis in rock masses using 3D point clouds. *Engineering geology*, 195, 185-195.
- Riquelme AJ, Tomás R, Cano M., Pastor JL & Abellán A (2018) Automatic mapping of discontinuity persistence on rock masses using 3D point clouds. *Rock Mechanics and Rock Engineering*, 51(10), 3005-3028.

InSARTrac as a Novel Tool for Landslide Monitoring and Failure Mechanism Assessment

Christoph Zambanini, D. Scott Kieffer

¹ Graz University of Technology, Graz, Austria

SUMMARY: InSARTrac is a hybrid monitoring system upgrading 1D line of sight interferometric synthetic aperture radars (InSAR) systems to 3D monitoring systems by using computer vision techniques. This allows the assessment of rock slope failure mechanisms by utilizing a single terrestrial InSAR combined with a single camera. This study summarizes results of InSARTrac under controlled and natural conditions revealing the high potential for landslide monitoring.

Keywords: Landslide monitoring, InSAR, Computer Vision, New technology, Remote sensing

Introduction

Terrestrial interferometric synthetic aperture radar (InSAR) is a powerful tool for real-time landslide monitoring and hazard evaluation. Because of the high measurement accuracy and spatial resolution, even the 1D line-of-sight (LOS) displacement has great utility in hazard evaluation (Fukuzono T 1985, Carlà et al. 2017). However, the LOS displacement has limited value for assessing rock slope failure mechanisms, which are often kinematically controlled by 3D discontinuity structures. InSARTrac is a novel hybrid 3D monitoring method combining computer vision methods with measurements from a single terrestrial InSAR device, and initial measurement sites indicate significant potential for enhanced landslide monitoring and mechanism assessment (Zambanini et. al. 2021, Zambanini et. al. 2022, Zambanini and Kieffer 2022).

Methods and Results

The InSARTrac method deploys a single digital camera parallel to the InSAR LOS. Time-lapse imagery is obtained, from which 2D sub-pixel shifts are quantified via feature tracking (FT). The 1D LOS InSAR measurements are then vectorially combined with the 2D FT measurements to obtain the complete 3D displacement vector. Controlled laboratory and field scale tests indicate the range (R) dependent 3D accuracy being equal to approximately $4 \times 10^{-6} R$ (figure 1) (Zambanini et. al 2021, Zambanini et. al. 2022).

This study summarizes the results of the controlled InSARtrac measurements, together with measurements of supraglacial rock debris at the Pasterze glacier in Austria from Zambanini et. al. 2021, Zambanini et. al. 202 and Zambanini and Kieffer 2022 (figure 2). The supraglacial debris has a blocky, unstratified rock structure that is considered an excellent proxy for landslide debris.

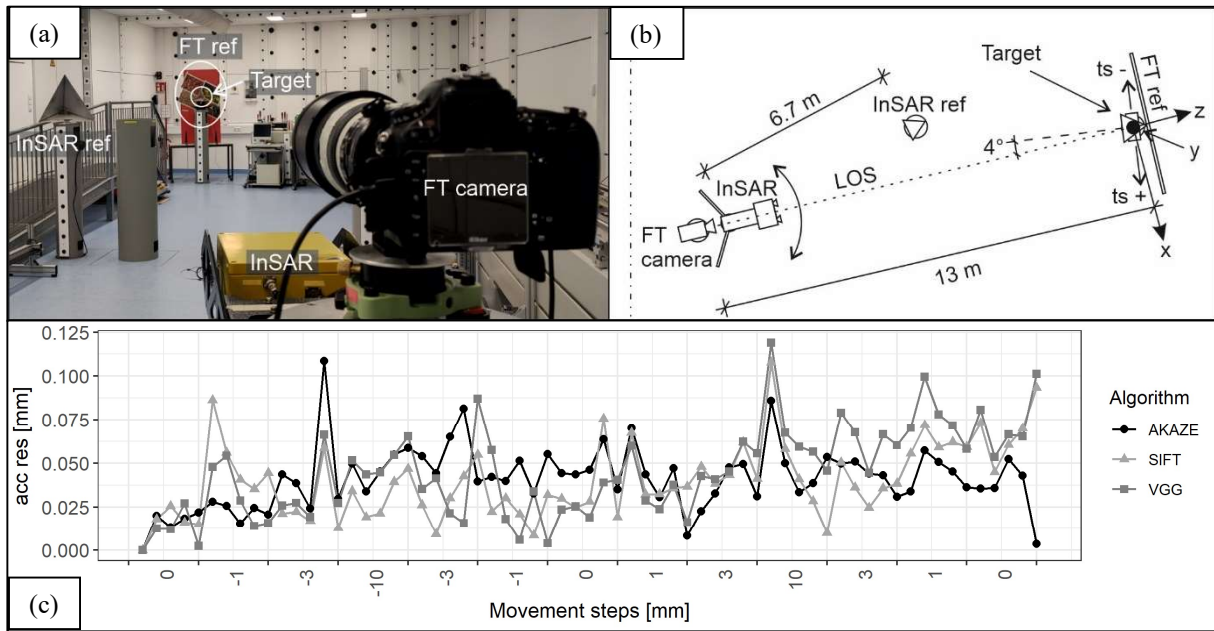


Figure 1 Controlled InSARTrac laboratory measurements at the climate-controlled Geodesy laboratory at TU Graz. (a) Monitoring perspective of measurement setup including target (mounted on micro-meter resolution translation stage), references and InSARTrac instruments. (b) Plan view of laboratory setup. Target movements were at 4 degrees to the LOS to generate displacements in and perpendicular to the LOS. (c) FT accuracy in movement direction for three different algorithms, namely accelerated KAZE, scale invariant feature transform and virtual geometry group of Oxford University (Lowe, 2004, Alcantarilla et. al. 2013, Simonyan et. al. 2014). Figures from Zambanini et. al. 2021

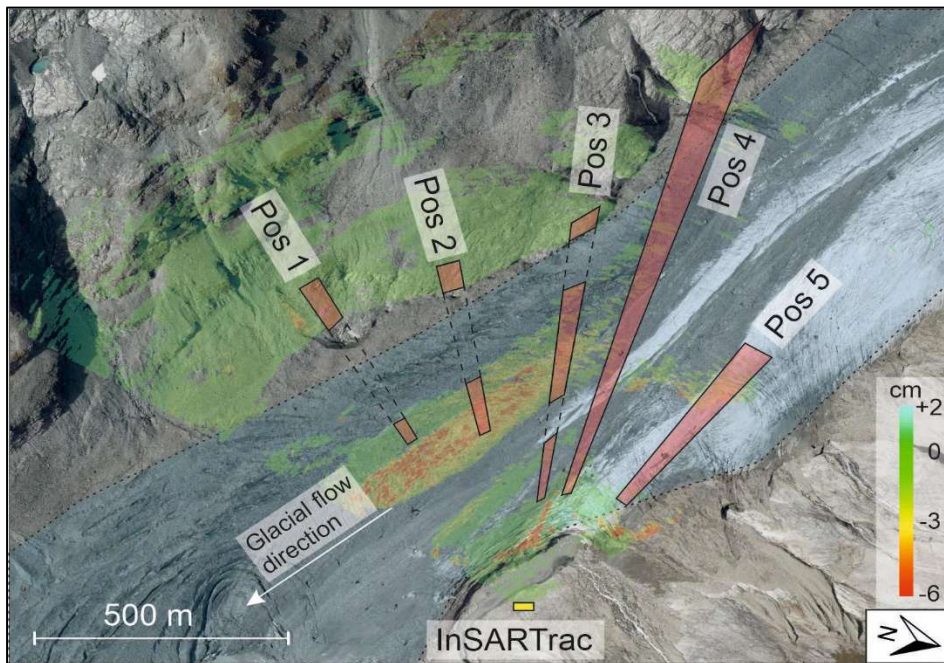


Figure 2 Plan view of the Pasterze measurement area displaying the five measurement positions (Pos 1-5) and the current glacial tongue extent (blue area). Red areas display measurement areas, dashed lines indicate obscured areas. The spectral colours indicate InSAR measurements, where blank spots correspond to not measured areas because of being obscured or having low reflectivity. Figure from Zambanini and Kieffer 2022.

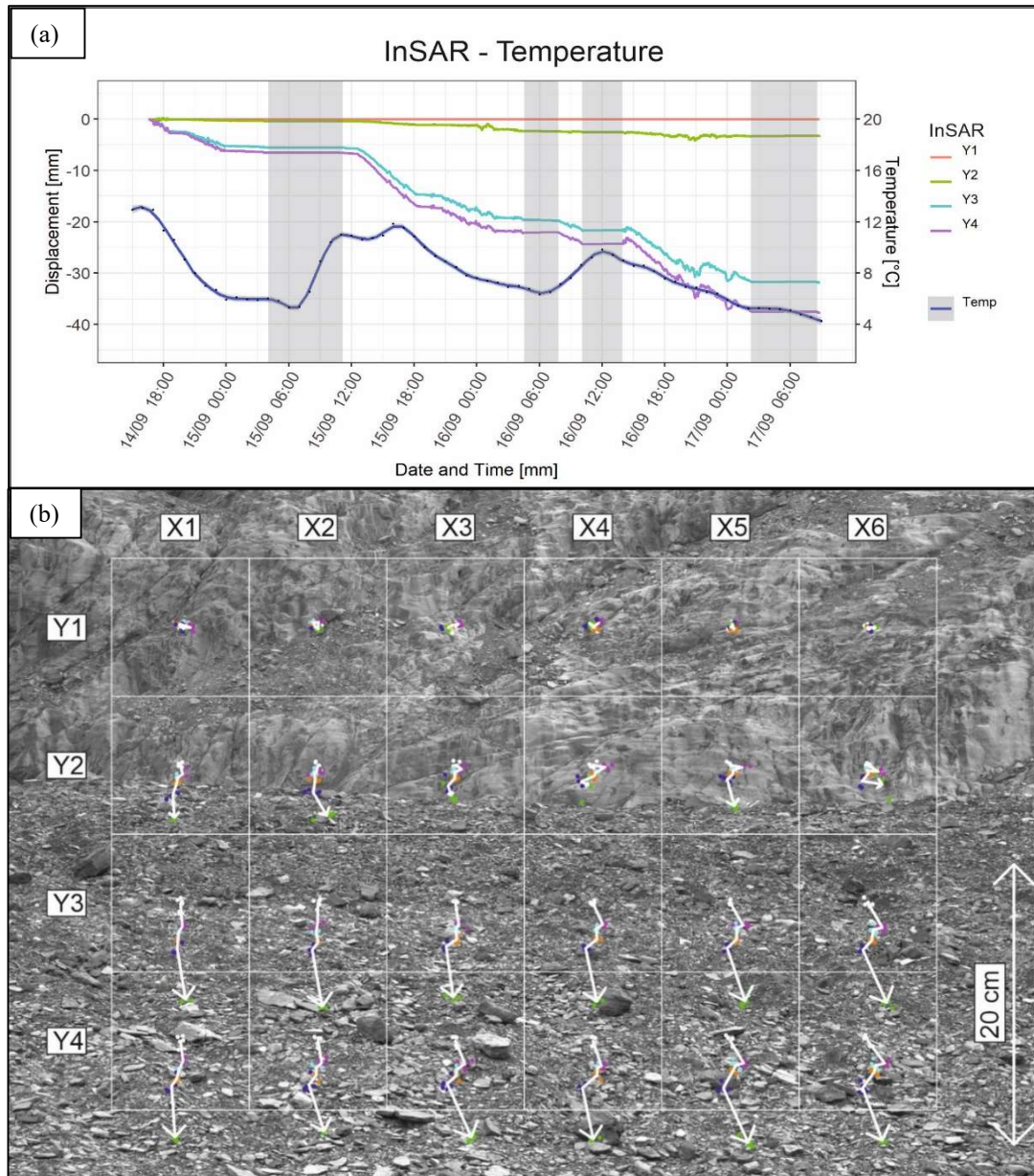


Figure 3 InSARTrac measurement results of the Pasterze (Pos 2). (a) InSAR results showing LOS displacements for the different areas indicated in (b). Additionally, the temperature profile is plotted, but no striking correlation was found (temperature data from Comprehensive Analysis (INCA) System of the Central Institute for Meteorology and Geodynamics (ZAMG) (Haiden et al. 2011)). Grey spots indicate measurement gaps. (b) FT results where dots indicate single measurements, dot colours indicate measurement intervals and arrows connect mean displacement for each measurement interval revealing. Figures from Zambanini and Kieffer 2022.

The 3D results of the Pasterze measurements where: North: 1.4 cm, East: 2.2 cm and H (height): -7.4 cm, within 2.5 days. These results were split in surface displacement and melting using a digital elevation model. These results fit well to the 2019 - 2020 monitoring results of the Pasterze by the Österreichischer Alpenverein (table 1).

Active Layer Detachment Slides, Kluane Ranges, Southwest Yukon

Crey M Ackerson¹, Brent Ward¹, Kristen Kennedy²

¹ Department of Earth Sciences – Simon Fraser University, Burnaby, Canada

² Yukon Geological Survey, Whitehorse, Canada

Abstract

Active layer detachment landslides (ALD's), where the failure plane is the contact between seasonally thawed ground and permafrost, are common in Yukon Territory. Ground disturbance associated with these slides can have a negative effect on water quality, infrastructure and human safety. The close connection between permafrost thaw and ALD's raises the possibility the frequency of these events may be increasing with anthropogenic climate change. This project aims to:

1. Determine frequency changes of ALD's through historic airphoto analysis.
2. Study the failure mechanisms of a cluster of 25 ALD's that occurred on or around August 17, 2020, associated with a large precipitation event.

The study area is the Kluane Ranges of the St. Elias Mountains, southwest Yukon. The area extends from Ä'äy Chù (Slim's River) northwest to the Donjek River and was selected based on an abundance of permafrost related landslides. Fieldwork occurred in July and August of 2020 and included field visits, unmanned aerial vehicle (UAV) based photogrammetry and low-level helicopter flights.

Changes to the frequency of ALD's will be investigated utilizing historic airphotos and satellite imagery. Time intervals of 10-20 years, beginning in 1946, will be used to generate digital elevation models (DEM's) from airphotos and satellite imagery using Structure-from-Motion photogrammetry techniques. An inventory of ALD's will be made for each time interval to determine changes in frequency.

The cluster of 25 near-synchronous ALD's have failure planes marked by the 1250 BC White River Tephra, giving them a distinctive streaky white appearance. Detailed DEM's generated from satellite imagery indicate a gentle-over-steep topography. The insulating properties and hydraulic conductivity of the tephra are likely contributing factors in the failure mechanism.

Keywords

Active layer detachments, permafrost, landslides

What Causes Creep Bursts in the Åknes Landslide, Norway

Andreas Aspaas^{1,3}, Pascal Lacroix², Lene Kristensen³, Bernd Etzelmüller² & Francois Renard^{1,2}

¹ Department of Geosciences, University of Oslo, Oslo, Norway

² ISTerre, Univ. Grenoble Alpes, Grenoble INP, Univ. Savoie Mont Blanc, CNRS, IRD, Univ. Gustave Eiffel, 38000 Grenoble, France

³ Section for Landslides and Avalanches, Norwegian Recourses and Energy Directorate, Trondheim, Norway

SUMMARY: Slow creeping landslides move at rates of millimetres to several meters per year. They can cause extensive damage to infrastructure and pose a major threat to human lives if failing catastrophically. Landslides can progressively weaken over time by rock mass damage processes that may occur by constant slow creep or sudden transient slips. Eventually, damage can lead to strain localization along the basal shear plane and catastrophic failure of the landslide. When observed, transient slip events, also called creep bursts, may induce short-term loading and hence can control landslide stability. These creep bursts correspond to short periods that can last several days where the displacement of a landslide accelerates and then decelerates. Here, we compiled and analysed extensive multi-physics data series of the Åknes landslide, Norway. This landslide is moving at a slow slip rate of 6 cm per year, and could generate a large tsunami wave in a fjord if it would rupture catastrophically. Based on time series of an array of eight seismometers, five extensometers, seven borehole inclinometers and piezometer strings, one borehole with a string of 8 seismometers, and ten continuous GPS stations, sampled with time resolutions down to 5 minutes over several years, we detected creep bursts in this landslide. These events interact with the distinct slow slip trend related to seasonal variations of rainfall and snowmelt. We analyse the creep bursts in regards to micro earthquake activity and water pressure levels, to study their origin.

Keywords: Landslides, Friction, Statistical analysis, In-situ monitoring, Micro-seismicity

Degradation of Hard Clays under Freezing and Thawing Cycles

Kateřina Bočková¹, Jean Vaunat¹, José Moya¹

¹ Department of Civil and Environmental Engineering, Universitat Politècnica de Catalunya, Barcelona, Spain

Abstract

The erosion rate in badlands seems to be mainly limited by the weathering (degradation) rate, which is controlled by freezing and thawing (F/T) cycles. This work aims to assess the thickness of the erodible layer in weathered claystones, by means of deepening the understanding of the degradation processes experienced by the material, using both field monitoring at a test site and experimental work at a laboratory.

The site is a badland area in the Vallcebre basin located in the Eastern Pyrenees, Spain. The site is a small divide on the head of a badland, with north and south facing slopes. The claystone bedrock is weathered to a depth of 250 to 350 mm; degradation is much more intense in the first 30 to 130 mm (topsoil layer). Weather and soil conditions (water content, suction, temperature, and thermal properties) are monitored in a 400 mm deep vertical soil profile on each slope. Results revealed a significant difference in the soil conditions of the two slopes. For example, no freezing occurred on the southern slope during the last (2021/2022) winter, whereas two long F/T cycles occurred in the northern one. Soil structure, density, and aggregate size distribution measurements showed a depth for the topsoil layer up to 75 mm on the southern slope and up to 130 mm on the northern one.

Field data are used to set up laboratory experiments that mimic in situ F/T cyclic conditions. Natural material is a silty clay (25% clay- and 71% of silt-sized particles) of relatively low plasticity (LL 40.3% and IP 20.6 %). Both natural clay samples and samples remolded and recompacted on the wet and dry side of Optimum Proctor ($\rho_d = 1771 \text{ kg/m}^3$ and $w = 17\%$) are tested under F/T cycles with the objective to study the degradation effect for different microstructures. Experiments consist in placing centimeters size samples in purposely designed plastic cells allowing for visual observation in a freezing bath. Vertical load is minimal. Temperature is measured using thermocouples and Micro-Electro-Mechanical System (MEMS) and displacement by LVDTs. After a minimum of 5 cycles is applied, Mercury Intrusion Porosimetry (MIP) is performed on the specimen, evaluating its microstructural degradation. In parallel, a careful calibration campaign of field sensors is performed to include the effect of soil density changes during F/T cycles in the water content measurements. Heat capacity measurement sensors have also been added to the instrumentation profile to provide additional data enabling the derivation of ice content.

Field monitoring and laboratory test setup are first presented, with emphasis on the estimation of the changes in dry density, water and ice content, suction, and aggregate size distribution curve during natural and controlled F/T cycles. MIPs information is finally used to provide insights into the mechanism of clay degradation during F/T cycles.

Keywords: Clay, Degradation, Freezing and thawing cycles, Badlands

Selection of Appropriate Landslide Mitigation Measures – LaRiMiT (Landslide Risk Mitigation Toolbox)

Vittoria Capobianco¹, Bjørn Kalsnes¹, Erlend B. Storrrøsten¹

¹ Norwegian Geotechnical Institute, Oslo, Norway

Abstract

LaRiMiT (Landslide Risk Mitigation Toolbox) is a web-based database and user portal for identifying and selecting mitigation measures for a specific landslide case, assisted by an embedded expert scoring system.

The webtool, developed within the KLIMA2050 Centre for Research-based Innovation, contains more than 80 structural landslide mitigation measures, including active (aimed at reducing the likelihood of a landslide) and passive (aimed at reducing the consequences) measures. For each mitigation measure a description, examples of application and design methods are provided, as well as references from literature or from Best Management Practices. The database of mitigation measures has open access to all users at <https://www.larimit.com/>. To help practitioners and decision makers find relevant measures for their specific case, an Analytic Hierarchy Process resident in the toolbox provides a ranked list of suitable mitigation measures based on site specific conditions and some other relevant factors such as time-related, economic or environmental constraints. The quantitative scores reflect the input relevance weights and option scores.

The first two categories are *NBS for erosion control (living approach)* and *NBS for erosion control (combined living/not living approach)*. Among the NBS measures listed, soil bioengineering techniques involving the use of live materials and vegetation for controlling surface erosion are the most common. Some examples of soil bio-engineering measures available on LaRiMiT are: turfing, bush layering, direct/pit planting, vegetation – mechanical effects, vegetation -hydraulic effects (Kalsnes & Capobianco, 2019, Capobianco et al. (2022).

Keywords: landslides, mitigation, web-based tool

References

- Capobianco, V., Uzielli, M., Kalsnes, B., Choi, J.C., Strout, J., Tann, L., Steinholt, I., Solheim, A., Nadim, F., Lacasse, S. (2022) Recent innovations in the LaRiMiT risk mitigation tool; implementing a novel methodology for expert scoring and extending the database to include nature-based solutions. *Landslides* 2022
- Kalsnes, B & Capobianco, V. (2019) Nature-Based Solutions. Landslides Safety Measures. *Klima 2050 Report* 16. ISBN : 978-82-536-1638-4

Full-Scale Slope Monitoring and Back-Analysis of a Weather-Induced Landslide with and without the Effect of Vegetation: Preliminary Insights

Donvito S.E.¹, Capobianco V.², Shin Y.³, Piciullo L.², Tagarelli V.¹

¹ DICATECh, Polytechnical University of Bari, Bari, Italy

² Natural Hazards, Norwegian Geotechnical Institute, Oslo, Norway

³ Platform Technology Geotechnics, Equinor, Oslo, Norway

Abstract

The purpose of this preliminary study was to back analyse a failure observed in a bare man-made test slope in Øysand, Trondheim, Norway. In this site, which was part of the Norwegian Geotechnical Test Sites project (NGTS), a full-scale pilot slope, scaled of 10 m height, 15 m width, and inclined 37°, was generated in a critical natural slope and the pre-existing dense vegetation cover was totally removed. Field investigations and laboratory testing were performed, and piezometers, inclinometers, and water potential sensors were installed to monitor the slope behaviour with the original aim to study the impact of freezing-thawing cycles on slope stability. A shallow failure occurred in the slope between March and April 2020 and some preliminary analyses concluded that the slope instability was most likely triggered by rainfall.

In this study, a more accurate numerical back-analysis has been carried out using the GeoStudio package, considering the real measured precipitations data. At first, a hydraulic saturated/partially saturated transient analysis with SEEP/W was conducted. Then the back-analysis of the failure was performed with SLOPE/W, assuming a critical surface consistent with what observed in the field and computing also the increase of strength due to suction.

Furthermore, in order to investigate the hazard mitigation effect on slope failures by applying Nature-based Solutions (NbS), a preliminary assessment of the role of vegetation on the slope stability was carried out quantifying how the hypothetical contribution of roots to the soil strength affects the Factor of Safety (FoS). A sensitivity analysis was performed to investigate different vegetation scenarios: the FoS was computed implementing different rooted soil thickness and different increments of the soil cohesion within the rooted area. This simple analysis shows that even small increments of strength related to vegetation can increase the FoS above the critical value and could have prevented a failure. This highlights the marginal yet important role that vegetation can have on natural slopes and embankments. Existing vegetation cover on embankments should be preserved, when possible, especially in future scenarios, when rainfall induced failures are expected to be more frequent due to climate change. Future work will be focused on a more advanced back-analysis of the slope failure and deformations with the use of finite element models also for the slope stability part.

Keywords: landslide, landslide hazard mitigation, nature-based solutions (NbS), rainfall.

Mechanism of Deep Groundwater Inflow into Landslide Mass based Ground Temperature Monitoring in the Metamorphic Area, Japan

Gen Furuya¹, Daichi Habashita², Kouta Nawa³, Akira Suemine⁴, Gonghui Wang⁵

¹ Faculty of Engineering, Toyama Prefectural University, Imizu, Japan

² Taisei Corporation, Tokyo, Japan

³ Meiko Construction Co. Ltd., Nagoya, Japan

⁴ Former Kyoto University, Kyoto, Japan

⁵ Disaster Prevention Research Institute, Kyoto University, Uji, Japan

Abstract:

We installed thermocouples at the Nishi-ikawa landslide to clarify groundwater behaviours' in the landslide mass at the metamorphic area, and carried out monitoring. The principle of this monitoring is to measure the phenomenon that ground temperature is disturbed by groundwater flowing in the slope. There were two types of ground temperature behaviour in the Nishi-ikawa landslide by the monitoring results: one was only annual change without the influence of groundwater, the other was significant temperature decreasing immediately after heavy rainfall in summer season. In the analysis, we showed sine curve of the ground temperature annual change without the influence of groundwater. Then, we calculated the difference between this curve and the data from monitoring points where a decrease in ground temperature, and extracted the time when the temperature difference was maximum. Furthermore, we investigated the correlation between the maximum decreasing temperature and the accumulated antecedent rainfall by the day from the time of this temperature. The result of investigation led that there is positive correlation between the maximum value of decreasing temperature and the 10 days antecedent rainfall at the middle part of the landslide block, the 4 days at the upper part of the block. We confirmed the increasing rate of borehole water level is faster than the infiltration rate of rainwater by the monitoring. It has been pointed out that the ground water and ground temperatures equivalent to the isothermal layer are 12.5°C, and that rainwater temperatures during heavy rainfall are around 20-22°C in summer season at this landslide (Furuya et al., 2017). From the above, we concluded that the groundwater behaviour (decreasing of ground temperature) during heavy rainfall might be not simply a rapid inflow of infiltrated water from rainwater into the existing groundwater, but also the piston flow like inflow from the deep layer.

Keywords: ground temperature disturbance, temperature difference, monitoring, borehole water level, antecedent rainfall

References

Furuya G, Suemine A & Wang G (2017) Monitoring of flowing groundwater behavior by continuous ground temperature measurement in landslide. *Proceeding of Symposium -Groundwater influences on landslide movement-*, Japan landslide society, pp. 13-16. (in Japanese with English abstract)

Preliminary Stages of a Landslide-Generated Tsunami Hazard Assessment of Glacier Bay National Park and Preserve, Alaska USA

Chad Hults¹, Jeffrey Coe², Nikita Avdievitch², Jin Woo Kim³, Zhong Lu³, Dennis Staley⁴

¹National Park Service, Anchorage, Alaska, USA

²U.S. Geological Survey, Golden, Colorado, USA

³Southern Methodist University, Dallas, Texas, USA

⁴U.S. Geological Survey, Anchorage, Alaska, USA

Abstract

Climate change is causing permafrost degradation, glacier retreat, and increasing rain events in place of snow events. These factors are decreasing the stability of rock slopes and increasing landslide hazards. The apparent and expected adverse impacts on the stability of the landscape from climate change are of acute interest and concern to Glacier Bay National Park and Preserve (GLBA), because of its historical record of very large landslide-generated tsunamis and 600,000 people visit GLBA by cruise ship, tour boat, and sea kayak every year.

On the outer coast of GLBA in Lituya Bay, on July 9, 1958, near the toe of the retreating Lituya Glacier, a 30 million cubic meter rock avalanche generated a tsunami that ran up 525 meters on the opposite fjord wall, which is the highest recorded runup of a landslide-generated tsunami. The wave sank two fishing boats, resulting in two fatalities. In upper Glacier Bay, an obvious subaerial landslide is hanging on the flank of a mountain in Tidal Inlet. GPS investigations by the U.S. Geological Survey (USGS) in the early 2000s indicated the landslide was moving a couple centimeters per year. A review of Landsat imagery for alpine areas of GLBA from 1984 to 2016 revealed an increase in the magnitude of landslides between 2012 and 2016; years coinciding with a period of record-breaking high winter and spring air temperatures.

Recent, very large landslides in coastal areas of Alaska have increased attention to climatic impacts on landslide occurrence in GLBA. In 2019, the National Park Service (NPS) and USGS partnered to conduct a park-wide landslide inventory and hazard assessment for tsunamis triggered by failure of subaerial, partially submerged, and fully submerged landslides. We used remote sensing data, including InSAR, LiDAR, and satellite imagery to map bedrock fractures, faults, scarps, and landslides and to detect landslide movement and subsidence of glacier outwash deltas. We mapped submarine landslides and modeled landslide susceptibility using available bathymetry. In 2021, we assessed rock-mass quality throughout the park and collected samples from subaerial parts of the deltas for geotechnical testing. Preliminary results indicate that the landscape of GLBA contains numerous fractures, Holocene faults, hundreds of scarps, and many landslides with tsunamigenic potential. The next steps are to combine our existing data to evaluate and map the susceptibility of GLBA to subaerial bedrock landslides, followed by modeling of potential tsunamis that could be generated from rapidly moving landslides in highly susceptible areas. While our results are specific to GLBA, our objectives, methodology, and analyses are relevant for other locales where rapid changes in climate and glacial extent result in increased risks posed by landslides and tsunamis, such as in GLBA's sister park, the West Norwegian Fjords UNESCO World Heritage Site.

Keywords: Glacier, Tsunami, Landslide, Park, Climate

A Rock Glacier Inventory Of The Central Alaska Range, Alaska

Kaytan Kelkar¹, Louise Farquharson¹, Margaret Darrow², Daniel Mann³, Simon Zwieback⁴, Denny Capps⁵

¹Geophysical Institute Permafrost Laboratory, University of Alaska, Fairbanks, USA

²Department of Civil, Geological, and Environmental Engineering, University of Alaska, Fairbanks, USA

³Department of Geosciences, University of Alaska, Fairbanks, USA

⁴Geophysical Institute, University of Alaska, Fairbanks, USA

⁵Denali National Park and Preserve, Denali Park, USA

Rock glaciers are striking periglacial landforms that consist of a perennially-frozen ice/rock matrix that gradually undergoes displacement on permafrost-affected slopes (Barsch, 1996). Ongoing warming is driving a shift in mountain permafrost thermal regimes potentially leading to accelerated rock glacier movement. As such rock glaciers in a warming climate can pose a threat to human life and vital infrastructure in mountain terrain.

Here we present a preliminary rock glacier inventory for a 150 km² subsection of the central Alaska Range, an area of discontinuous permafrost in the sub-Arctic. We build upon initial efforts by Wahrhaftig and Cox (1959) to explore what influence slope, aspect, elevation, permafrost distribution, and geology exert over rock glacier location and morphology, and movement including slope destabilization.

We manually mapped periglacial talus derived rock glaciers using medium to high resolution spectral satellite imagery in ArcGIS Pro. Each rock glacier was manually delineated and categorized into lobate, tongue-shaped, and spatulate morphology classes. Slope aspect, and elevation were derived from the 5-m resolution Arctic digital elevation model (DEM) of the study area while permafrost distribution and geology were derived from Gruber (2017) and USGS maps (Wilson and Labay, 2016), respectively. To estimate rock glacier movement and destabilization locations, we conducted InSAR analysis using 12-day temporal baselines C-band (wavelength 5.6 cm) Sentinel-1 data between January 1, 2015 to June 30, 2022.

Results from this study provide critical baseline data on rock glacier location and dynamics in the central Alaska Range that can be used to infer mountain permafrost extent and predict permafrost-affected slope failure in mountain communities.

Keywords: rock glaciers, creep rates, mountain permafrost, slope failure, remote sensing

References

- Barsch, D (1996). Rockglaciers-Indicators for Present and Former Geoecology in High Mountain Environments. *Springer Berlin Heidelberg*.
- Gruber, S (2017) Global Permafrost, [Dataset]. University of Zurich. <https://doi.org/10.7488/ds/1877>.
- Wahrhaftig, C & Cox, A (1959) Rock glaciers in the Alaska Range. *Geological Society of America Bulletin*, 70, 383-436.
- Wilson, F & Labay, K (2016) Alaska geology revealed: *U.S. Geological Survey General Information Product 168*, <https://doi.org/10.3133/gip168>.

Numerical Modelling of the Initiation of progressive failure in Eastern Canadian sensitive clay

Andries Kirstein¹, Ariane Locat¹, Gustav Grimstad², Hans Petter Jostad³

¹ Université Laval, Québec City, Canada

² NTNU, Trondheim, Norway

³ NGI, Oslo, Norway

SUMMARY:

A spread is a type of large landslide occurring in sensitive clays that involves the translation of horsts and grabens along a thin, quasi-horizontal layer of remoulded clay (Locat et al., 2013; Cruden and Varnes, 1996). It has previously been demonstrated that progressive failure due to strain-softening is a key mechanism in the propagation of spreads (e.g. Locat et al., 2013, 2015). Past numerical studies of these landslides include 1-dimensional modelling considering the bottom shear band and an elastic upper soil layer being unloaded (Locat et al., 2013; Quinn et al., 2010) and 2-dimensional, large-deformation finite element analyses using techniques such as CEL (Dey et al., 2015; Wang et al., 2021, 2022) and MPM (Tran & Solowski, 2019).

The objective of the study is to understand the mechanism of spread initiation, particularly the factors that control horizontal propagation of the shear band. With this goal, Plaxis is used to model the initiation of a progressive failure, selecting the “Updated Mesh” option and using the soil model NGI-ADPsoft. Failure is initiated by removing a toe block, simulating stream erosion. A parametric study of factors such as clay sensitivity, brittleness, elastic modulus, anisotropic strength ratios, and shear band thickness is presented. The influence of the size of the toe block removed is also studied.

Keywords: spread, sensitive clay, progressive failure, Plaxis

References

- Cruden DM, and Varnes DJ (1996) Landslides types and processes. *Landslides investigation and mitigation, Special Report 247*. Transportation Research Board, National Research Council. A.K. Turner and R.L. Schuster (eds.). National Academy Press, Washington, D.C. pp. 37–75.
- Dey R, Hawlader B, Phillips R & Soga K (2015) Large deformation finite-element modelling of progressive failure leading to spread in sensitive clay slopes. *Géotechnique* 65(8), pp. 657-668.
- Locat A, Jostad HP, Leroueil S (2013) Numerical modeling of progressive failure and its implications for spreads in sensitive clays. *Canadian Geotechnical Journal* 50, pp. 961-978.
- Locat A, Leroueil S, Fortin A, Demers D, Jostad HP (2015) The 1994 landslide at Sainte-Monique, Quebec: geotechnical investigation and application of progressive failure analysis. *Canadian Geotechnical Journal* 52, pp. 490-504.
- Tran QA & Solowski W (2019) Generalized Interpolation Material Point Method modelling of large deformation problems including strain-rate effects – Application to penetration and progressive failure problems. *Computers and Geotechnics* 106, pp. 249-265.
- Wang C, Hawlader B, Perret D & Soga K (2021) Modeling of Initial Stresses and Seepage for Large Deformation Finite-Element Simulation of Sensitive Clay Landslides. *Journal of Geotechnical and Geoenvironmental Engineering* 147(11).
- Wang C, Hawlader B, Perret D & Soga K (2022) Effects of geometry and soil properties on type and retrogression of landslides in sensitive clays. *Géotechnique* 72(4), pp. 322-336.

Seasonal and Climatic Controls on Unstable Rockslopes in Norway

L. Kristensen¹, I. Skrede¹, K. Indrevær, I¹. Penna², A. Aspaas¹, G. Pless¹

¹ NVE The Norwegian Water Resources and Energy Directorate, Oslo, Norway

² NGU Geological Survey of Norway, Trondheim, Norway

Abstract

Rock avalanches are infrequent events – in Norway 2-4 fatal events have occurred per century in historic times. Rock-slope instabilities leading to rock avalanches develop over time, with climate and meteorological events acting both as a long-term weakening mechanism, and as triggering factor. In Norway, no clear meteorological trigger has been identified in the few historic events though the largest historic rock avalanche -Tjelleskredet in 1756 – was probably triggered by very heavy rainfall.

Today several large unstable rock-slopes are monitored continuously or periodically by NVE. The monitoring data shows cases of clear seasonal or meteorological imprint on the movement. In Northern Norway, increased movement is recorded during May-July for several monitored slopes. Indre Nordnes, Revdalsfjellet and Dusnjarga moves almost exclusively in this period being stable the rest of the year. A similar pattern is seen in Jettan and Gamanjunni, though movement occurs throughout the year at these sites. The increased velocities are clearly related to snowmelt, and it is possible permafrost plays a role for some of these sites. In Western Norway Mannen also increases its movement during snowmelt. A small part of Mannen “Veslemannen” accelerated repeatedly during late summer and autumn rainfall for several years, but did not react particularly to snowmelt. However, in the weeks and months before its failure in September 2019, it accelerated independent of rainfalls. Another lower part of Mannen shows a peculiar behaviour of “rock slope breathing” with expansion during snowmelt (and once after a heavy rainfall) and subsequent retraction. This has been attributed to increased water pressure and could play a role in slope weakening. In contrast, Joasetbergi moves mainly from October to January and moves less the rest of the year.

It seems clear that periods of increased water supply (rain or snow melt) increase movement in many monitored rock slopes. The current risk classification system of unstable rock-slopes does not address driving forces. An ongoing project dating several deposits and headscarps intend to provide a better understanding of paleo-displacement rates and the frequency of rock avalanches in relation to Holocene climatic fluctuations. Climate change and more extreme weather could change the frequency of large rockslides in or outside permafrost areas, but we are unable to quantify such influence today. NVE hopes to increase the knowledge on mechanisms controlling the movement of unstable rock-slopes and determine the effects that climate change may have on the stability of unstable rock-slopes. Therefore, we present some examples of unstable rock slope behaviour under different meteorological conditions and discuss possible mechanisms controlling the observed patterns.

Keywords: Unstable rock-slopes, rock avalanche, climate, trigger, extreme weather

Study on the Potential of Nature Based Solutions for the Protection of a Rockfall site at Artouste (French Pyrenees)

Lévy Clara¹, Colas Bastien², Bernardie Séverine¹, Antonio Pignalosa³, Francesco Pugliese³, Carlo Gerundo³, José Carlos Robredo Sánchez⁴, Santiago Fàbregas⁵, Juan Antonio Ballesteros Canovas⁶

¹ BRGM, Orléans, France

² BRGM, Montpellier, France

³ UNINA, Napoli, Italy

⁴ Univ. Politecnica de Madrid, Madrid, Spain

⁵ AECT Pirineos-Pyrénées, Sallent de Gállego, Huesca, Spain

⁶ Spanish Research Council, National Museum of Natural Sciences, Madrid, Spain

SUMMARY: The H2020 PHUSICOS project aims at providing new insights into the effectiveness of Nature-based solutions (NBSs) against natural hazards in the context of climate change. One of the demonstration sites consists of a very steep slope prone to rockfalls, which overlooks a road. Here, we aimed to quantify the benefits of NBSs (forest & protection systems) on the mitigation of rockfall hazard at road level. The rockfall hazard assessment was based on field expertise as well as on the use of high-resolution airborne LIDAR, Terrestrial Laser Scanners (TLS), botanical surveys and 3D numerical-based simulations of boulder propagation. This rockfall hazard assessment was achieved according to the following steps: 1) mapping of the rockfall departure zones, 2) inventory of boulders/events and the definition of scenarios with different classes of boulder volumes and associated return periods, 3) simulations of boulders trajectories using the Rockyfor3D software, with considering the different NBSs.

Particular attention was paid to correctly map source areas and estimate input settings for simulations of boulders trajectories, by applying the method proposed by Loye et al. (2009) on morphometric analysis of DTMs, which allows defining different slope thresholds corresponding to an increasing probability for a pixel to belong to a cliff. A clustering approach was then designed to map continuous release areas. Moreover, the soil roughness was estimated based on the differences between DTMs of different cell sizes and degree of smoothing. The soil type mapping was then carried out by combining different sources of information. All these data were validated based on field data from some sample areas.

Rockfall simulations were then validated with botanical-based evidence in two selected plots. In particular, we focused on the analyses of scars on trees as they represent the potential height of boulder transport and can be dated dendrochronologically to identify temporal rockfall patterns. Moreover, a detailed forest inventory was performed in the studied site using mobile terrestrial laser scanning (MTLS) in order to detect the position of each tree and to collect characteristics of the trees. To extend the information obtained from the detailed surveys over the entire survey area, we performed and calibrated a semi-automated forest model based on a canopy height model (CHM) developed by comparing the DSM and the DTM using the Ecorisq FINT software. The considered NBSs consist of wooden rockfall barriers of 2.25 m height with absorption energy of 100 kJ. Based on the modelling outputs, no relevant improvements of rockfall hazard are noted with NBS (except locally). However, a shift of the highest values of kinetic energy and rebound height is obtained. Thus, the designed NBSs are not sufficient to significantly reduce the risk of rockfalls, but such NBSs might be considered as an additional solution for dampening the rockfall intensity limiting the sizing and, thus, the economic and environmental impacts of other interventions such as steel rockfall barriers.

Keywords: rockfall hazard ; nature based solution ;

References:

Dorren, L., 2017. FINT - Find Individual Trees User manual.

Dorren, L.K.A., 2015. Rockyfor3D (v5. 2) revealed-transparent description of the complete 3D rockfall model. EcorisQ paper (www.ecorisq.org).

Loye, A., Jaboyedoff, M., & Pedrazzini, A. (2009). Identification of potential rockfall source areas at a regional scale using a DEM-based geomorphometric analysis. *Natural Hazards and Earth System Sciences*, 9(5), 1643-1653.

Numerical Simulation for Runout Behaviour of Sensitive Clay Landslides Using the Material Point Method

Zhongqiang Liu¹, Mingliang Zhou², Meng Lu², Amanda Johansen DiBiagio¹, Håkon Heyerdahl¹

¹ Norwegian Geotechnical Institute, Oslo, Norway

² Department of geotechnical engineering, Shanghai, China

Abstract

Landslides in sensitive clays are usually triggered by natural causes (e.g. erosion in ravines, intensive rainfall) and/or human activity (e.g. construction work). The propagation of such landslides often exceeds several hundred meters. It is vital to model the complete process, including initiation and runout, of landslides in sensitive clays in order to improve the method for hazard zone mapping in use today. This study conducted material point method (MPM)-based simulations to investigate the runout behaviour of the recent sensitive clay landslide in Gjerdrum in Norway. A strain-softening Mohr-coulomb model is adopted to simulate the tendency toward progressive failure of the sensitive clay slope. The undrained shear strength of the soil block at the slope toe was significantly reduced in the simulations to imitate the slide initiation caused by erosion in the creek at the foot of the sensitive clay slope. The simulation results suggest that a throughgoing shear band is formed in the sensitive clay layer, triggering the landslide with a large extent of movement. The parametric analysis suggests that the strain-softening parameters and the increasing of undrained shear strength with depth significantly affect the runout behaviour. Overall, the proposed simulation approach can capture the slide's initiation and progressive failures in one combined analysis. In future work, an advanced sensitive clay constitutive model can be developed in the MPM-based simulation approach to facilitate improved simulation accuracy and capture the retrogressive failure process of sensitive clay landslides.

Keywords: Sensitive clay, Landslides, Strain softening, Progressive failure, Material point method

The Effect of Rock Fragmentation on Rockfall Barriers

G. Matas¹, J. Gili¹, N. Lantada¹, J. Corominas¹

¹ Civil and Environmental Engineering Department. Universitat Politècnica de Catalunya, Barcelona, Spain

Abstract

Fragmentation in rockfalls is a phenomena that has shown a significant effect in rockfall analysis and risk assessment (Corominas et al. 2019). These studies showed that when a detached rock mass fragments during its propagation several consecutive impacts may be expected on protective structures. However, as per the authors' knowledge, the consideration of fragmentation effect on protective structures remains an unexplored topic. In this contribution we tested a simple approach to consider cumulative impacts on rockfall barriers due to fragmentation of a single rockfall event. Rockfall barriers are a widely used passive countermeasure against rockfalls.

In a real scenario the selection of an appropriate barrier often consists of estimating the expected impacting energy and comparing it to the reference capacity of market available barriers. However, this reference value is obtained in very specific loading conditions and has been shown to fail to reproduce real response in some cases (Toe et al. 2018) and thus providing a non-conservative design approach. When simulating the behavior of flexible barriers for meta-modelling approaches, Lambert et al. (2021) found that a barrier can fail with impacting energies under its operational level depending on the impacting conditions and thus showed that the barrier efficiency is extremely site-dependent. When considering fragmentation, the loading conditions of a barrier can be considerably different from the conditions under which their maximum capacity is determined since several successive impacts may be expected. In this study we used a simple cumulative damage law to successively reduce the capacity of the barrier after each fragment impact in an already existing rockfall simulation model called RockGIS (Matas et al, 2020; Georisk Project, 2022). This approach allows determining whether a barrier could withstand a single detachment rockfall event that fragments during its propagation rather than checking if it is able to withstand each single individual impact. This study is a conceptual approach to discuss the relevance of considering multiple impacts due to fragmentation in rockfall barriers for future more advanced approaches

Keywords: Rockfall, fragmentation, barriers, risk assessment

References

- Corominas J., Matas G., Ruiz-Carulla R. (2019) Quantitative analysis of risk from fragmental rockfalls. *Landslides*. Volume 16, Issue 1, pp 5–21 Doi 10.1007/s10346-018-1087-9
- Gerosik Project (2022) Advances in rockfall quantitative risk analysis (QRA) incorporating developments in geomatics (Ref. PDI2019-103974RB-I00, funded by MCIN/AEI/10.13039/501100011033)
- Lambert, S., Toe, D., Mentani, A. et al. (2021) A Meta-Model-Based Procedure for Quantifying the On-Site Efficiency of Rockfall Barriers. *Rock Mech Rock Eng* 54, 487–500
- Matas G., Lantada N., Corominas J., Gili J.A., Ruiz-Carulla R., Prades A. (2020) Simulation of full-scale rockfall tests with a fragmentation model. *Geosciences*, 10 (5),168. Doi 10.3390/geosciences10050168
- Toe D, Mentani A, Govoni L, Bourrier F, Gottardi G, Lambert S (2018) Introducing meta-models for a more efficient hazard mitigation strategy with rockfall protection barriers. *Rock Mech Rock Eng* 51(4):1097–1109

Rock Avalanches in Northeastern Baffin Island: Understanding low occurrence in a region with high hazard potential

Maureen Matthew¹, John Gosse¹, Reginald Hermanns², Alexandre Normandeau³

¹ Dalhousie University, Halifax, Canada

² Geological Survey of Norway, Trondheim, Norway

³ Geological Survey of Canada (Atlantic), Dartmouth, Canada

In 2017, a coastal rock avalanche along a fjord in Western Greenland triggered a tsunami that devastated the village of Nuugatsiaq. Two years earlier, on the Alaskan Coast, a rock avalanche below the Tyndall Glacier triggered a tsunami in Taan Fjord that reached heights over 190 m above sea level. In the last century, similar disasters have been recorded in the fjords of western Norway. In a review, it was found that over 70% of recorded tsunamis with runups > 50 m were triggered by large landslides, often rock avalanches, in glaciated terrane (Higman et al., 2018).

Do these large, catastrophic, and often cascading geohazards happen in fjords of NE Canada? If they do – where and when have they occurred? What controls their recurrence? Despite the hazard potential, few studies have focused on coastal geohazards in the fjords of the eastern Canadian Arctic. Northeastern Baffin Island, between the Inuit hamlets of Clyde River and Pond Inlet, is located directly across Baffin Bay from the 2017 Greenland event, with similar fjord relief. The region is potentially vulnerable to rock avalanches given the steep coastal cliffs, active seismicity, accelerating deglaciation, and rapidly thawing permafrost. As a result, the area is well-suited to investigate current knowledge gaps around controlling mechanisms of rock avalanches in high-relief glaciated terrane.

To develop an understanding of the prevalence, location, and characteristics of rock avalanches and large-scale debris slides in the region, systematic mapping of onshore deposits was carried out using high-resolution (<0.5 m) optical satellite imagery and 2 m digital elevation models. Mapping was extended with available multibeam bathymetry throughout the study area to identify potential submarine deposits from coastal events. The results of this study suggest that rock avalanche deposits are scarce throughout the study area. Only 6 deposits have been identified through the mapping of the onshore and offshore study area (60,000 km², or 0.0001 deposits/km²) that meet the volume and mobility criteria of a rock avalanche.

We hypothesize that comparatively fewer rock avalanche deposits are observed among the fjords of Baffin Island for the following reasons: 1) some deposits remain masked underwater in very deep and steep walled fjords, 2) persistent permafrost in the region continues to act as a stabilizing factor, and 3) overall rock mass quality is high in the areas of extreme relief contrast. A comparison of global analogues is provided to further investigate these hypotheses.

Keywords: rock avalanche, fjord, Arctic, mapping, tsunami

References:

Higman, B., Shugar, D.H., Stark, C.P., et al. 2018. The 2015 landslide and tsunami in Taan Fiord, Alaska. *Nature Scientific Reports*. 8: 12993.

Geo-Infrastructure Vulnerability to Landslide Hazards and Climate Change in the UK: Predictable Consequences?

Roger Moore^{1,2} and Helen Reeves³

¹ Jacobs, Birmingham, United Kingdom

² Professor Emeritus of Applied Geomorphology, University of Sussex, Falmer, United Kingdom

³ Jacobs, Leeds, United Kingdom

Abstract

Climate change is one of the most significant issues affecting modern society. Climate models and predictions indicate global sea level rise of up to 1 metre by year 2100, with 2.5m possible under extreme scenarios. The effects on climate are equally concerning, with extreme weather events, such as heavy rainfall, storms and heat waves occurring more frequently. It is widely regarded that climate change is potentially one of the most serious threats to humanity, with far reaching and devastating impacts on coastal communities, infrastructure, natural environments, and economies. Landslides and erosion are often overshadowed by flooding in terms of profile and awareness as flooding tends to impact larger areas and hence more people. However, the impact of landslides on geo-infrastructure can have long-term disruptive and knock-on consequences to the economy and welfare of affected communities. It is clear from recent high-profile failures and accidents in the United Kingdom that geo-infrastructure owners face a huge challenge to future-proof existing assets and improve designs to ensure they are resilient to climate change. Equally, operators need to develop real-time weather forecasting and landslide response systems to ensure network safety and operational efficiency. The talk will provide a UK perspective of relevance to the theme of the JTC1 workshop; specifically whether we are capable of predicting and quantifying the expected changes in landslide hazard and risk with any reliability to guide risk management.

Keywords: Climate Change, Sea Level Rise, Landslides, Erosion, Infrastructure, Resilience

Meteorological Thresholds for Regional Scale Rockfall Early Warning in Norway

Rosa M. Palau¹, Kjersti G. Gisnås¹, Graham L. Gilbert¹, Anders Solheim¹

¹ Norwegian Geotechnical Institute, PO Box 3930 Ullevaal Stadion, N-0806 Oslo, Norway

Abstract

Current practice for risk reduction relating to rockfall hazards is almost entirely reliant on structural mitigation. Structural mitigation of rockfall hazards at regional scales is costly and impractical. Early warning systems are tools to depict the time and location of future hazard events so that emergency managers and other stakeholders can act to evacuate persons in advance. Thus, early warning systems can constitute a suitable alternative to structural interventions and mitigate risk by reducing exposure.

Existing regional-scale landslide early warning systems (LEWS) focus on shallow landslides and debris flows. These LEWS use rainfall thresholds (sometimes combined with water derived from snowmelt) to evaluate if the conditions for landslide triggering are exceeded. In comparison to shallow landslides, rockfall triggering mechanisms are more complex – involving water infiltration, temperature fluctuations, and biological activity. Most LEWS for rockfalls have been implemented at local scales based on the monitoring and analysis of seismic signals from moving rock masses or cracking of rock joints.

In Norway, rockfalls constitute a significant hazard, accounting for almost 50% of Norway's national landslide database entries. Rockfalls commonly impact the functioning of infrastructure assets such as roads and railways and occasionally damage buildings or result in fatalities. We have evaluated the relation between rockfall events and weather conditions for two regions in Norway – Trollstigen and the upper Gudbrandsdalen valley – to develop meteorological thresholds for regional scale rockfall early warning.

To develop meteorological thresholds for rockfalls, several variables, including rainfall, snowmelt, and air temperature fluctuations, have been analysed for more than 300 rockfall events. The highest frequency of rockfalls in these areas is observed in spring, during periods of freeze-thaw cycles and snowmelt. Finding correlations between weather events and rockfall events has been challenging. Our results indicate that temperature cycles play a significant role in rockfall initiation, not only during autumn, winter, and spring when freeze-thaw is the predominant process but also in summer when temperature oscillates above zero degrees. We propose that rock fall thresholds in our study regions should vary with seasons and combine temperature and water supply criteria.

Keywords Rockfall, early warning system, meteorological thresholds

Low-cost Methods For Monitoring Shallow Landslide Occurrence Along Linear Infrastructures

Margherita Pavanello¹, Massimiliano Bordoni¹, Valerio Vivaldi¹, Mauro Reguzzoni²,
Andrea Tamburini³, Fabio Villa³, Claudia Meisina¹

¹ Department of Earth and Environmental Sciences, University of Pavia, Via Ferrata 1, 27100 Pavia, Italy

² Hortus Srl (Monitoring Solutions & Software Application), Via Caboto 8/b, 20025 Legnano (MI), Italy

³ Imageo Srl, Via Pitteri 8, 20134 Milano, Italy

Abstract

Shallow landslides induced by heavy rainfall are a worldwide widespread phenomena and their related hazard is expected to increase due to more intense rainfall as a consequence of climate change (EEA Report No 15/2017). Since 2017, a decision-making tool based on Multi-Criteria Analysis (MCA) has been proposed as an objective approach to obtain landslide susceptibility maps and plan proper remedial works along linear infrastructure corridors (Tamburini et al., 2017). The study of low-cost sensors for Landslides Early Warning Systems (LEWS) as a risk mitigation tool to these phenomena along highways, railways and pipelines is here presented.

Soil hydrological conditions before a rainfall event for the estimation of trigger moments (Bordoni et al., 2019) are the starting point of a LEWS. Different sensors for the measure of these parameters, particularly soil volumetric water content, exist with different pros and cons. The aim of the research is to compare seven low-cost sensors selected by *IMAGEO Srl* company together with *HORTUS Srl*. The sensors have been engineered with a datalogging system and an automatic in-cloud transmission of the data and have been located on field at 2 different depths (-0.6 m and -1.2 m) at the test-site of Montuè in the Northern Apennines (Italy) where an Hydrometeorological Monitoring Station (*Andromeda Project*) is operating since 2012 with high-cost TDR probes present at the same depths. The comparison between the hydrological data acquired by different sensors allows to evaluate the quality and reliability of the low-cost system before its final installation along the infrastructures lines. Monitored data together with rainfall parameters provided by both in situ rain gauges and ERA5-LAND satellite-derived data are used as input for the reconstruction of soil moisture values physically based thresholds.

The near real-time access to the monitored data allows to send warning alert when the established thresholds are exceeded, resulting in a LEWS able to identify periods of imminent landslide danger and to assess security along the lines.

Keywords: shallow landslides, linear infrastructures, soil water content low-cost sensors, LEWS, physically based thresholds

References

Climate change adaptation and disaster risk reduction in Europe *EEA Report - No 15/2017*

Tamburini A., Villa F., Miceli G., Epifani F. (2017) Application of Multi-Criteria Analysis (MCA) to assess landslide hazard and plan mitigation strategies along railway corridors in Central Italy. *ARMA* 17-621

Bordoni, M., Corradini, B., Lucchelli, L., Valentino, R., Bittelli, M., Vivaldi, V., Meisina, C. (2019) Empirical and Physically Based Thresholds for the Occurrence of Shallow Landslides in a Prone Area of Northern Italian Apennines *Water* 2019, 11, 2653

A Methodology To Detect Ground Deformation Events In A-DInSAR Time Series: Application To Slow-Moving Landslides

Pedretti Laura¹, Bordoni Massimiliano¹, Vivaldi Valerio¹, Figini Silvia², Parnigoni Matteo³, Grossi Alessandra³, Lanteri Luca⁴, Tararbra Mauro⁴, Negro Nicoletta⁵, Meisina Claudia¹

¹ Department of Earth and Environmental Sciences, University of Pavia, Pavia, Italy

² Department of Political and Social Sciences, University of Pavia, Pavia, Italy

³ RIDS-RES Institute for Data Science, Pavia, Italy

⁴ ARPA Piemonte, Torino, Italy

⁵ REGIONE PIEMONTE, Torino, Italy

Abstract

A-DInSAR Time Series (TS) interpretation is advantageous to understand the relation between ground movement processes (slow-moving landslides) and triggering factors (snow, rainfall), both in areas where it is possible to compare satellite TS with in-situ monitoring systems, and in areas where in-situ instruments are scarce or absent. However, the analysis and elaborations of huge satellite dataset covering large areas could be tricky and time-consuming without a preliminary analysis to identify areas of potential interest for significant ground deformations.

This work aims to illustrate a new statistical methodology to establish the presence in satellite TS of a significant trend of ground motion measured along time; to classify the trend of each TS (linear, non-linear); to identify and quantify periods of acceleration (breaks) in non-linear TS by furnishing the descriptive parameters (beginning and end of the non-linear deformation break(s), duration of the event, cumulated displacement in mm) to characterize the magnitude and timing of changes of ground instabilities.

The methodology has been tested on two Sentinel-1 datasets available from 2014 to 2020 in Piemonte region, in northwestern Italy, an area prone to slow-moving slope instabilities. The results have been compared with in-situ monitoring systems, possible triggering factors (rainfall, snow) and documented events of the territory.

The methodology applied to Sentinel-1 will provide a new tool for both back analysis and “near-real-time” monitoring of the territory thanks to the shorter revisiting time (6-12 days) with respect to previous satellites. Moreover, it can be applied to any type of satellite datasets characterized by low or high-temporal resolution of measures and tested in areas with different geological and geomorphological setting to identify and characterised any ground instability (slow-moving landslides, subsidence) at local or regional scale.

In addition, this methodology can be helpful not only as regards the characterization and mapping of the kinematics of the ground instabilities, but also in the assessment of hazard, risk and susceptibility, becoming a supporting and integrated tool with conventional methods for planning and management of the area.

Keywords: landslides, ground motion, remote sensing, near-real time monitoring, time series

¹laura.pedretti01@universitadipavia.it;

¹massimiliano.bordoni@unipv.it;

¹valerio.vivaldi@unipv.it;

¹claudia.meisina@unipv.it; ²silvia.figini@unipv.it; ³matteo.parnigoni@res-it.com; ³alessandra.grossi@res-it.com;

⁴luca.lanteri@arpa.piemonte.it; ⁴mauro.tararbra@arpa.piemonte.it; ⁵nicoletta.negro@regione.piemonte.it

NBS Methods for Hydrological Correction in a Glacier Deposit Torrent to Avoid Recurrent Debris Flows into The Urban Area of Erill-La-Vall (Lleida Province-Spain)

Carles Raïmat¹, Jona Trujillo¹, Anders Solheim²

¹ Kuroba Quatre SL, Taüll, Spain

² NGI, Oslo, Norway

Abstract

The Erill-la-Vall basin (La Vall de Boí-Spain), is located on the southern side of the South Face Axial Zone of the Pyrenees, (Lleida province). The basin is located at a mean altitude of 1700 m.a.s.l. as a small tributary of Noguera de Tort river. The project is focused on the sub-basin called "l'Esvomegada", meaning "rocky boulder sliding basin". The basin is slightly over 90 Hect, of which the head scarp comprises 38 Hect, directly eroded in glacial sediments. The main part of the basin is covered with alpine grass, and a young pine forest grown from 1950s.

The collection of historical data from the 20th century shows a total of that 140.000 m³ of materials have been eroded and transported. This displacement of sediment, with concentration time of less than 10 minutes for each event, puts the Erill-la-Vall village, located in the alluvial fan, at risk. The same scenarios exist in 6 more UNESCO Heritage villages of the same valley with 11 active torrents affecting residential areas.

Different types of torrential or debris flow interception methods were implemented in the 1960's and 90's to reduce the risk. These were 'traditional measures' including concrete dams, big rock gabion dams, etc. These measures have however not been able to eradicate the problem.

Recent monitoring studies carried out between 2007 and 2018 have enabled the definition of the mechanisms for debris flow generation, as well as determining the relationship between the magnitude and frequency of debris flow episodes. None of the recorded events have exceeded 2500 m³ of material. However, the monitoring has made it possible to numerically and photographically document a series of minor events that can be the most important precursors for larger events.

The activities of the H2020-PHUSICOS project (<https://phusicos.eu/>) started in September 2021, with the aim of implementing NBS for debris flow mitigation at the Erill-la-Vall site. Initial activities were to obtain and analyse new and previously available data about rain (accumulated and intensity), ground piezometry, erosion (airborne lidar) and flow parameters, and through this establish technical and scientific criteria to define where and how to implement the NBSs in the most effective way, which also was practically possible. A principal goal of including local citizens was introduced from the beginning. An active living lab activity was set up, with interdisciplinary meetings based on shared data from an open data dashboard with fully available test site information including alert thresholds. This type of stakeholder involvement forms an important part of the PHUSICOS project. The designed NBSs are now implemented, and both the background monitoring data and the measures will be presented.

Keywords: debris flow, field laboratory, long term monitoring, mass movement triggering mechanisms, NBS traditional methods

Relevant reading

Hürlimann, M. et al. (2011) *Debris-flow monitoring stations in the Eastern Pyrenees. Description of instrumentation first experiences and preliminary results* - 10.4408/IJEGE.2011-03.B-061 JO - 5th International Conference on Debris-Flow Hazards Mitigation: Mechanics, Prediction and Assessment

Luis-Fonseca, R. et al. (2011) Debris-flow protection in recurrent areas of the Pyrenees. Experience of the VX systems from output results collected in the pioneer monitoring station in Spain 10.4408/IJEGE.2011-03.B-115 JO - 5th International Conference on Debris-Flow Hazards Mitigation: Mechanics, Prediction, and Assessment, Proceedings and Assessment

Raimat-Quintana, C. (2018). PhD Thesis. Dinámica y peligrosidad de las corrientes de derrubios : aplicación en el barranco de Erill, Pirineo catalán, headed by Jordi Corominas and Marcel Hürlimann.

Characteristics of Fluidized Landslides in the Niigata Area, Japan

Naoki Watanabe¹, Natsumi Aiba¹, Gen Furuya²

¹ Niigata University, Niigata, Japan

² Toyama Prefectural University, Imizu, Japan

Abstract

Fluidized landslides have often occurred in the southwestern Niigata Prefecture, Central Japan. For example, a snowmelt-induced landslide occurred in the Kurumizawa area around 10:30 p.m. on March 3, 2021. The council for landslide disaster management in Niigata Prefecture (2021) reported that the landslide mass partly changed into a mudflow which had a total volume of 90,000 m³ and that the mudflow eventually reached a small village 1,100 m downstream about 12 hours later, destroying five houses, roads and paddy fields. Triggers for the fluidized landslides are mainly heavy rainfall and rapid snowmelt. The bedrocks consist of soft sedimentary rocks, especially mudstones during the Miocene to Pliocene. Main bodies of the landslides are usually composed of weathered mudstones and soil layers. Such landslides sometimes transition into mudflows which occasionally long-travel downstream and cause serious damages to local communities. Key factors that contribute to fluidization include (1) characteristics of the bedrock geology and weathered soils such as consistency, grain size distribution, water content, shear strength and mineral composition, (2) topographical conditions such as slope angle and flow path shape, and (3) hydrological conditions such as behaviours of heavy rainfall or rapid snowmelt and catchment area of surface water and groundwater. Here we pay attention to the geological backgrounds and geotechnical properties of the fluidized landslides.

Samples of mudflow deposits as fluidized landslide-related sediments and weathered mudstones as source of mudflows were collected from five landslides for several soil tests such as consistency test, permeability test, grain size test and rotary drum type flow test.

Weathered mudstones which are the source materials of mudflows were easily fluidized under the condition of relatively low water content on the basis of their liquid limits ranging from approx. 40 to 50%. It was most difficult to separate or remove water from mudflow deposits due to their considerable low permeability ranging from approx. 5×10^{-9} to 4×10^{-8} m/s. The weathered mudstones including water were also easily broken into finer fragments during flow processes as the result of rotary drum type flow test. For the above reasons, the mudflows transferred from the fluidized mudstones was retaining liquid property for a considerable time and finally long-travelled downstream.

Keywords: landslide, mudflow, fluidization, particle crushing, weathering

References

Council for landslide disaster management in Niigata Prefecture (2021) Prompt report on the snowmelt-induced landslide in Kurumisawa, Itoigawa City, Niigata Prefecture on March 3, 2021. *Journal of Japan Landslide Society*, Vol.58, pp.135-140.

Landslides and Hydrological Environment of Sedimentary Rock Slope in north Greenland

Shintaro Yamasaki¹, Tatsuya Watanabe²

¹ Disaster Prevention Research Institute, Kyoto University, Kyoto, Japan

² Kitami Institute of Technology, Kitami, Japan

Abstract

A lot of recent studies suggest that rapid climate change in the Arctic. Chance of mass-movements is probably increasing by its related phenomena. For example, increase chances of rain events are remarkable effect to destabilize slope condition. Sedimentary rock areas in the Arctic have thick colluvium on slope, and their surface has unique structure formed by periglacial environment. However, the effect of erosion by abundant rain water and/or water flow to the slope has been little known. In Siorapaluk, the northernmost settlement of Greenland, the fjord cliff is covered with such thick colluvium. The colluvium collapsed and slid down by strong rainfalls in summers of 2016 and 2017 (Yamasaki and Watanabe, 2019; Walls et al., 2020). Those landslides are extremely large (the maximum width is 125 m, and two to three meters thick) as colluvium slope failures. To prevent landslide disasters from small settlement in the Arctic, the landslide mechanism should be clarified. The authors investigated the Siorapaluk case in 2018 and 2022. According to our investigation, thick colluvium consists of large angular boulders and sandy fragments, which are weathering products of sedimentary rocks. Sand fills the gap between the boulder, but the strength reduction by saturation could not be main factor of landsliding. Because the sand is relatively low permeability due to poor sorting. On the other hand, the basement rock exposed at the upper slope, the rock generally has numerous and wide-open cracks. Those structural characters of basement are common feature in the area. Probably repeated change of glacier stress and freeze-thaw cycle has made deep cracky zone on the basement of colluvium. At the heavy rain event, rain water penetrates from upper slope to lower part through the cracky zone, and then it enhances pore pressure behind the impermeable colluvium cover, leading to landslide. The source area of landslides tends to distribute on middle parts of slope. Water flow converges at lower parts of slope, but landslides are not likely to occur at lowest part, because the colluvium is too thick to move. Also, the distribution of landslides tends to be controlled by the basement form to receive water flow. For example, some strata on sedimentary rock surface are prominent laterally due to high resistibility against weathering. The source areas sometimes aligned along those strata.

Keywords: colluvium, periglacial, sedimentary rock, Arctic, Greenland

References

- Walls M, Hvidberg M, Kleist M, Knudsen P, Mørch P, Egede P, Taylor G, Phillips N, Yamasaki S, Watanabe T (2020) Hydrological instability and archaeological impact in Northwest Greenland: Sudden mass movement events signal new concerns for circumpolar archaeology. *Quaternary Science Reviews* 248, 106600.
- Yamasaki S, Watanabe T (2019) Landslide and flash flood caused by the 2016-17 heavy rain events in Siorapaluk, north Greenland. *Geophysical Research Abstracts* 21.